



# Durham E-Theses

---

## *Design and Application of Probes of Novel Bioactivities*

LANDRUM, MARIE

### How to cite:

---

LANDRUM, MARIE (2009) *Design and Application of Probes of Novel Bioactivities*, Durham theses, Durham University. Available at Durham E-Theses Online: <http://etheses.dur.ac.uk/28/>

### Use policy

---

The full-text may be used and/or reproduced, and given to third parties in any format or medium, without prior permission or charge, for personal research or study, educational, or not-for-profit purposes provided that:

- a full bibliographic reference is made to the original source
- a [link](#) is made to the metadata record in Durham E-Theses
- the full-text is not changed in any way

The full-text must not be sold in any format or medium without the formal permission of the copyright holders.

Please consult the [full Durham E-Theses policy](#) for further details.

# DESIGN AND APPLICATION OF PROBES OF NOVEL BIOACTIVITIES



MARIE LANDRUM

Ph.D Thesis

University of Durham

Department of Chemistry

October 2009

## **Abstract**

### **Design and application of probes of novel bioactivities**

**Marie Landrum**

**Ph.D, October 2009**

Whilst methods for the isolation and optimisation of bacterial enzymes for preparative biotransformations are well established the use of plant biocatalysts is relatively unexplored. Since the plant kingdom contains a greater diversity of potential biocatalysts this represents an untapped resource. Two simple plant enzyme systems were investigated: *AtSFGH* and *AtCXE12*. A series of profluorescent esters based on 4-methylumbelliferone and fluorescein were synthesised and used in screening experiments against these enzymes. To produce libraries of recombinant proteins molecular biology techniques such as site-directed mutagenesis and error-prone PCR were utilised and *Agrobacterium tumefaciens* infiltration methods developed to increase the levels of transformation within plant protoplasts.

In order to isolate specific enzymes probe molecules were developed in which a desired bioactivity resulted in the 'switching on' of a fluorophore during enzymatic processes. Several reactivity probes were synthesised which contained a fluorophore, a fluorescent quencher moiety and a functional group which was able to react with a specific protein target. An ester probe was developed which reacted with porcine liver esterase, with the enzymatic response causing the molecule to fragment in such a way as to release the fluorescent quencher and result in a concomitant increase in fluorescence. The modular synthesis and structure of the probe allowed for a variety of reactive groups to be introduced.

Several BODIPY analogues were synthesised that were able to exclusively target the peroxisome organelle, as demonstrated by co-localisation studies. Their proliferation in the presence of external signals, such as the drug clofibrate and biotic stress, were studied. Confocal microscopy enabled the dynamics of the peroxisome to be visualised in a variety of cell types and species, including both plant and mammalian cells. In addition to this computational studies were carried out to enable the rational design of probes based on their fluorescent properties. Systematic alteration of the probe molecule has highlighted areas of the compound which are amenable to adaptation. This includes the ability to extend the conjugation of the pyrrole functionality which enables the emission wavelength, and hence colour, to be changed.

<b>Acknowledgements .....</b>	<b>ix</b>
<b>Declaration .....</b>	<b>x</b>
<b>Copyright .....</b>	<b>x</b>
<b>Abbreviations .....</b>	<b>xi</b>
<b>1 GENERAL INTRODUCTION .....</b>	<b>1</b>
1.1 Introduction .....	1
1.2 Directed Evolution .....	2
1.2.1 Introduction .....	2
1.2.2 Polymerase Chain Reaction (PCR) .....	2
1.2.3 Site-directed Mutagenesis .....	4
1.2.4 Error-prone Polymerase Chain Reaction (epPCR) .....	5
1.2.5 DNA Shuffling .....	6
1.2.5.1 Full length parent shuffling .....	7
1.2.5.2 Single cross-over .....	9
1.2.5.3 Domain swapping .....	11
1.2.5.4 <i>In vivo</i> recombination .....	12
1.2.5.5 Synthetic shuffling .....	12
1.3 Screening and Selection Techniques .....	13
1.3.1 Introduction .....	13
1.3.2 pH-Indicators .....	13
1.3.3 Colorimetric Assay .....	14
1.3.4 Digital Imaging .....	15
1.3.5 IR Thermography .....	17
1.3.6 Yeast Two-hybrid System .....	18
1.3.7 Fluorescence Activated Cell Sorting (FACS) .....	20
1.4 Transgenic Hosts .....	22
1.4.1 Protoplasts .....	23
1.4.2 Transformation techniques .....	24
1.4.2.1 Polyethylene glycol (PEG) .....	24
1.4.2.2 Electroporation .....	25
1.4.2.3 Particle bombardment .....	25
1.4.2.4 <i>Agrobacterium tumefaciens</i> .....	26

1.5	<i>Reactivity Probes</i> .....	26
1.5.1	Introduction .....	26
1.5.2	Reactive Group .....	27
1.5.2.1	Mechanism-based reactivity probes .....	27
1.5.2.2	Suicide-based reactivity probes .....	31
1.5.2.3	Affinity-based reactivity probes .....	31
1.5.3	Linker unit .....	33
1.5.4	Isolation/identification tag .....	35
1.5.4.1	Isotope tags .....	35
1.5.4.2	Affinity tags .....	37
1.5.4.3	Fluorescent tags .....	38
1.5.5	Bio-orthogonal labelling .....	41
1.6	<i>Project Aims</i> .....	43
<b>2</b>	<b>STUDIES TOWARDS THE DIRECTED EVOLUTION OF ESTERASES.....</b>	<b>46</b>
2.1	<i>S-Formylglutathione Hydrolase</i> .....	46
2.1.1	Introduction .....	46
2.1.2	Enzymology.....	48
2.1.2.1	Characterisation of SFGH .....	48
2.1.2.2	Substrate Mapping.....	50
2.1.3	4-methylumbelliferone (4-MU) esters.....	53
2.1.3.1	Previous Results .....	53
2.1.3.2	Synthesis of 4-MU esters.....	53
2.1.3.2.1	Lithium Enolates .....	54
2.1.3.2.2	Carboxylic Acid Dianion Chemistry.....	56
2.1.3.2.3	Amino Acid Derivatives.....	57
2.1.3.3	<i>AtSFGH</i> Enzyme assays.....	61
2.1.3.4	Assays <i>In Planta</i> .....	63
2.1.3.5	Screening in protoplasts.....	67
2.1.3.5.1	Uptake of Substrates .....	67
2.1.4	Alternative Probes .....	73
2.1.5	Summary.....	74
2.2	<i>AtCXE12</i> .....	75
2.2.1	Introduction .....	75
2.2.2	Previous Research.....	75

2.2.3	Directed Evolution of AtCXE12 .....	77
2.2.3.1	Hormone Sensitive Lipase .....	77
2.2.3.2	AtCXE12 probe molecules .....	80
2.2.3.2.1	Fluorescein probes .....	80
2.2.3.2.2	AtCXE12 in vitro assays.....	81
2.2.3.2.3	Flow cytometry screening .....	81
2.2.3.3	Site directed mutagenesis .....	84
2.2.3.4	Error-prone PCR .....	86
2.2.3.4.1	epPCR methodology development.....	88
2.2.3.4.2	On-plate screening .....	93
2.2.3.5	Agrobacterium-mediated transformation.....	94
2.2.3.5.1	Cloning of AtCXE12 into binary vectors.....	95
2.2.3.5.2	Transformation and infiltration .....	99
2.2.3.5.3	BIN-STRP3-AtCXE12 recombinant library .....	100
2.2.4	Summary.....	100
2.3	Conclusions.....	101
<b>3</b>	<b>REACTIVITY PROBES.....</b>	<b>103</b>
3.1	Introduction.....	103
3.1.1	Previous research .....	103
3.1.1.1	<i>p</i> -Quinone methide systems .....	103
3.1.1.2	Fluorescently quenched reactivity probes .....	107
3.2	Probe Design.....	109
3.3	TBS probe.....	110
3.3.1	Synthesis .....	110
3.3.2	1,6-elimination analysis .....	111
3.4	Esterase Probe.....	113
3.4.1	Synthesis .....	113
3.4.2	1,6-elimination analysis .....	116
3.4.2.1	Chemical-mediated 1,6-elimination.....	116
3.4.2.2	Enzymatic-mediated 1,6-elimination .....	117
3.4.2.2.1	Porcine Liver Esterase (PLE).....	118
3.4.2.2.2	Binding studies .....	119
3.5	<i>p</i> 450 <i>O</i> -demethylation probe .....	121

3.5.1	p450 O-demethylation enzymes.....	121
3.5.2	Synthesis .....	122
3.5.3	Chemical-mediated 1,6-elimination Analysis .....	122
3.6	<i>MOM Probe</i> .....	126
3.6.1	Synthesis .....	126
3.6.2	1,6-elimination analysis .....	127
3.7	<i>Summary</i> .....	128
3.8	<i>Conclusions</i> .....	128
<b>4</b>	<b>Oxidative Cytochrome p450 .....</b>	<b>129</b>
4.1	<i>Introduction</i> .....	129
4.1.1	Mechanism of action .....	129
4.1.2	Evolution of the Enzyme .....	130
4.2	<i>Probe Design Rationale</i> .....	131
4.2.1	Synthesis .....	133
4.3	<i>BODIPY-based Probe</i> .....	134
4.3.1	Synthesis of probes.....	135
4.3.1.1	From benzaldehyde derivatives .....	135
4.3.1.2	From benzoylchloride derivatives .....	138
4.3.2	Photophysical analysis .....	140
4.3.3	Computational Studies .....	143
4.3.4	Cellular/biological Studies .....	146
4.3.4.1	Inhibition Studies .....	146
4.3.4.2	Flow cytometry analysis .....	152
4.3.4.3	Metabolite studies .....	154
4.3.4.4	Different cellular types.....	154
4.4	<i>Summary</i> .....	155
4.5	<i>Conclusions</i> .....	155
<b>5</b>	<b>BODIPY .....</b>	<b>157</b>
5.1	<i>Introduction</i> .....	157
5.2	<i>Peroxisomes</i> .....	157
5.2.1	Peroxisome Markers.....	158

5.3	<i>Cell Studies</i> .....	159
5.3.1	Probe synthesis.....	159
5.3.2	Species/cell types.....	160
5.3.3	Viability and uptake studies.....	162
5.3.4	Inhibition Studies .....	164
5.3.4.1	Brefeldin A.....	164
5.3.4.2	Wortmannin .....	165
5.3.5	Co-localisation Studies.....	165
5.4	<i>Peroxisome Proliferator-activated Receptor (PPAR) Studies</i> .....	167
5.4.1	Clofibrate .....	168
5.5	<i>Localisation Causes</i> .....	168
5.5.1	Reactive Oxygen Species.....	169
5.5.1.1	ROS Studies .....	170
5.5.1.1.1	Hydrogen peroxide .....	171
5.5.1.1.2	Hydroperoxyl and peroxy radical.....	171
5.5.1.1.3	Hydroxyl radical, $\cdot\text{OH}$ .....	172
5.5.1.1.4	Superoxide, $\text{O}_2^{\cdot-}$ .....	172
5.5.1.1.5	Singlet oxygen, $^1\text{O}_2$ .....	173
5.5.2	Phenyl substituent substitution.....	174
5.5.3	Fluorine substitution.....	175
5.5.4	Pyrrole conjugation.....	177
5.5.5	Boron substitution .....	179
5.6	<i>Mammalian Studies</i> .....	181
5.6.1	NIH 3T3 .....	181
5.6.2	MG63 osteoblasts .....	181
5.7	<i>Summary</i> .....	182
5.8	<i>Conclusions</i> .....	183
<b>6</b>	<b>CONCLUSIONS AND FUTURE WORK</b> .....	<b>185</b>
6.1	<i>Conclusions</i> .....	185
6.2	<i>Future Work</i> .....	186
<b>7</b>	<b>EXPERIMENTAL</b> .....	<b>188</b>
7.1	<i>Chemistry</i> .....	188



7.1.1	General Procedures .....	188
7.1.2	Experimental detail.....	190
7.2	<i>Biology</i> .....	224
7.2.1	General Procedures .....	224
7.2.2	Experimental detail.....	226

## Acknowledgements

I would like to thank my supervisor Dr. Patrick Steel for all the ideas and advice. To my co-supervisors Prof. Rob Edwards and Dr. Andy Beeby for help on biology and photochemistry respectively.

Dr Aileen Congreve for help with the flow cytometry, endless chats and general advice! All my friends in CG1, past and present: Victoria, Pete, Amel, Matt, Marvis, Michel, Little Lisa, Nick, Kathryn, John M, Phil, John D, Pieropaulo, Hayley, Lisa J, Pete, Ben, Kathryn, Jon and Lisa. The biology peeps upstairs – Ian for SFGH advice, Markus for help with *AtCXE12*, David for the *Agrobacterium* work, Vicky for keeping me entertained, Phil, Aggie and Melissa. A big thanks as well to Dave Hunter for the coffees and Miriam for being so wonderful.

My good friends Tom, Dave and Will – thanks for keeping me sane and the one or two laughs along the way. Will for the endless trivia and geography quizzes, Dave for the insane chat and amazing listening skills and Tom for the comedy nights out and helping me hang in there when times were tough!

Thanks to all the analytical staff, including Alan, Ian and Kathryn in NMR; Mike, Lara, Dave and Jackie in mass spec and DBS Genomics for DNA sequencing.

Dr Bernard Connolly and all his group for teaching me how to do error-prone PCR. Dr Andrei Smertenko and Prof. Patrick Hussey for all the useful discussion with Bodipy and peroxisomes and especially Andrei for the work with the confocal microscope. Dr Lars-Olof Pålsson for the lifetime measurements and Ben Coombs for helping me with the quantum yield methodology. Prof. John Murray for his diligent proof-reading.

Katherine, Charlie and Jules for being such good friends and helping me get through the hard times with lots of listening and even more wine. Daniel and Mark for the Shortridge years!

And last, but no means least, Paddy, for all the support, encouragement and being there for me all the time no matter what – I honestly couldn't have done this without you.

## **Declaration**

The work contained in this thesis was carried out in the Department of Chemistry, University of Durham between October 2004 and May 2008. All the work is my own unless otherwise indicated. It has not previously been submitted for a degree at this or any other university.

## **Copyright**

The copyright of this thesis resides with the author. No quotation may be published from it without the prior written consent and information derived from it should be acknowledged.

## Abbreviations

The following abbreviations appear in this thesis:

4-MU	4-methylumbelliferone
A	Adenine
Å	Angstrom
AAPH	2,2-Azobis(2-amidinopropane)
ABA	Abiscic acid
ABT	1-Aminobenzotriazole
AOMK	Acyloxymethyl ketone
AOS	Allene oxide synthase
Ar	Aryl group
<i>AtCXE12</i>	<i>Arabidopsis thaliana</i> carboxylesterase 12
ATP	Adenosine triphosphate
ATR	Attenuated total reflection
<i>AtSFGH</i>	<i>Arabidopsis thaliana</i> S-formyl glutathione transferase
BFAE	Brefeldin A esterase
Boc	<i>tert</i> -Butyloxycarbonyl
BODIPY	Borondipyrromethane
bp	Base pair
br	Broad
BSA	Bovine serum albumin
BY-2	Bright Yellow-2
C	Cytosine
CDNB	1-Chloro-2,4-dinitrobenzene
CLERY	Combinatorial libraries enhanced by recombination in yeast
COSY	Correlation spectroscopy
CPR	Cytochrome p450 reductase
CXE	Carboxylesterase
Cy3	Cyanine3
DAPI	4',6-Diamidino-2-phenylindole
DCF	Dichlorofluorescein
DCFDA	Dichlorofluorescein diacetate
DCM	Dichloromethane
DDQ	2,3-Dichloro-5,6-dicyanobenzoquinone

DFT	Density functional theory
dH <sub>2</sub> O	Deionised water
DIPEA	Diisopropylethylamine
DMAP	Dimethylaminopyridine
DMF	Dimethylformamide
DMPO	5,5-Dimethyl-1-pyrroline <i>N</i> -oxide
DMPU	<i>N,N'</i> -Dimethylpropyleneurea
DNA	Deoxyribonucleic acid
dNTP	Deoxyribonucleotide triphosphate
DOGS	Degenerate oligonucleotide gene shuffling
dppf	1,1'-Bis(diphenylphosphino)ferrocene
ds-DNA	Double stranded deoxyribonucleic acid
DTT	Dithiothreitol
DUB	Deubiquitinating enzyme
<i>E. coli</i>	<i>Escherichia coli</i>
ECH-1	Enoyl CoA hydratase
EDCI	1-Ethyl-3-(3'-dimethylaminopropyl)carbodiimide
EDTA	Ethylenediaminetetraacetic acid
ee	Enantiomeric excess
ELISA	Enzyme-linked immunosorbent assay
Em.	Emission
eq	Equivalent
ER	Endoplasmic reticulum
ESR	Electron spin resonance
EtOAc	Ethyl acetate
EtOH	Ethanol
eV	Electron volt
Ex.	Excitation
F*	Fluorophore
FAAH	Fatty acid amine hydrolase
FACS	Fluorescence activated cell sorting
FAD	Flavin adenine dinucleotide
FCC	Flash column chromatography
FDA	Fluorescein diacetate
fM	Femtomolar
FMDH	Formaldehyde dehydrogenase

FQ	Fluorescent quencher
FRET	Förster resonance energy transfer
FSC	Forward scatter
G	Guanine
GSH	Glutathione
GST	Glutathione S transferase
h	Hour
HA	Hemagglutinin
HMBC	Heteronuclear Multiple Bond Coherence
HMPA	Hexamethylphosphoramide
HOCl	Hypochlorous acid
HOMO	Highest occupied molecular orbital
HPLC	High performance liquid chromatography
HRMS	High resolution mass spectrometry
HSL	Hormone sensitive lipase
HSQC	Heteronuclear Single Quantum Coherence
Hz	Hertz
i.p.	Intraperitoneal
ICE	Interleukin-1 $\beta$ converting enzyme
<sup>i</sup> PrOH	Isopropanol
IPTG	Isopropyl $\beta$ -D-1-thiogalactopyranoside
IR	Infra red
ITCHY	Incremental truncation for the creation of hybrid enzymes
IVC	<i>In vitro</i> compartmentalisation
kb	Kilobase
kDa	Kilodalton
kg	Kilogram
l	Litre
LB	Luria-Bertani
LC-MS	Liquid chromatography-mass spectrometry
LDA	Lithium diisopropylamide
Lit.	Literature
LP	Longpass
LUMO	Lowest unoccupied molecular orbital
M	Molar
m.p.	Melting point

MALDI	Matrix-assisted laser desorption/ionisation
MeCN	Acetonitrile
MeOH	Methanol
mg	Milligram
min	Minute
ml	Millilitre
mM	Millimolar
mmol	Millimole
MOM	Methoxymethyl ether
MS	Mass spectroscopy
MUA	Methylumbelliferyl acetate
mw	Molecular weight
n/a	Not applicable
NA	Not assayed
NAD <sup>+</sup>	Nicotinamide adenine dinucleotide
NADPH	Nicotinamide adenine dinucleotide phosphate
NBD	Nitrobenzofurazan
NBP	4-( <i>p</i> -Nitrobenzyl)pyridine
NC	Nitrocellulose
nM	Nanomolar
nm	Nanometre
NMP	<i>N</i> -Methylpyrrolidone
NMR	Nuclear magnetic resonance
NOESY	Nuclear overhauser enhancement spectroscopy
ns	Nanosecond
NSAID	Non-steroidal anti-inflammatory drugs
Nu	Nucleophile
<i>p</i>	Para
p450	Cytochrome p450
PBO	Piperonyl butoxide
PCR	Polymerase chain reaction
PEG	Polyethylene glycol
PeT	Photoinduced electron transfer
<i>Pfu</i>	<i>Pyrococcus furiosus</i>
PI 3-kinase	Phosphoinositide 3-kinase
PLE	Porcine liver esterase

<i>p</i> NPAc	<i>para</i> -nitrophenylacetate
PPAR	Peroxisome proliferator activator receptor
ppm	Parts per million
PSI	Photosystem I
PSII	Photosystem II
PTGS	Post-transcriptional gene silencing
PTS1	Peroxisome targeting signal 1
PVPP	Polyvinylpyrrolidone
R	Rectus
RCF	Relative centrifugal force
r.f.u.	Relative fluorescent units
rac	Racemic
RACHITT	Random chimeragenesis on transient templates
ROS	Reactive oxygen species
rpm	Revolutions per minute
RPR	Random priming recombination
rt	Room temperature
RT-PCR	Reverse transcription-polymerase chain reaction
S	Sinister
s	Second
SDS	Sodium dodecyl sulfate
SDS-PAGE	Sodium dodecyl sulfate-polyacrylamide gel electrophoresis
secs	Second
SHIPREC	Sequence homology-independent protein recombination
SISDC	Sequence-independent site-directed chimeragenesis
SSC	Side scatter
StEP	Staggered extension protocol
T	Thymine
Taq	<i>Thermus aquaticus</i>
TBAF	Tetra- <i>n</i> -butylammonium fluoride
TBDMSCl	<i>tert</i> -Butyldimethylsilylchloride
TBS	<i>tert</i> -Butyldimethylsilane
TBSV	<i>Tomato bushy stunt virus</i>
T-DNA	Transfer deoxyribonucleic acid
TFA	Trifluoroacetic acid
THF	Tetrahydrofuran



TLC	Thin layer chromatography
TMEDA	Tetramethylethylenediamine
TOF	Time of flight
TR	Thioredoxin reductase
TRX	Thioredoxin
Ts	Transition
Tv	Transversion
UV	Ultra violet
UV/Vis	Ultra violet/visible
V	Volt
vol	Volume
ZnTPP	Zinc tetraphenylporphyrin
$\lambda_{em}$	Emission wavelength
$\lambda_{ex}$	Excitation wavelength
$\mu\text{L}$	Microlitre
$\mu\text{m}$	Micrometre
$\mu\text{M}$	Micromolar
$\tau$	Fluorescent lifetime
$\phi_F$	Fluorescent quantum yield

# 1 GENERAL INTRODUCTION

## 1.1 Introduction

The current state of the art for the development of new bioactivities relies on the expression of recombinant enzymes in bacterial hosts. Such an approach has limitations if the cellular environment required to support catalysis is absent in the microbial host. Recent advances in plant transformation technology potentially allow the exploitation of plant cells as a generic host for biocatalyst transgene expression. The use of plant expression systems has been limited by the relative efficiency in their transformation and their relatively short lifetime. These problems can be resolved by exploiting and enhancing the power of flow cytometry to rapidly analyse and sort large populations of plant protoplasts which have been genetically transformed to express libraries of recombinant biocatalysts. In the search for novel biocatalysts, current research is aimed towards the technique of directed evolution. Through the use of mutagenesis methods, directed evolution involves the production and selection of a variant enzyme with the desired properties.

This project is concerned with the development of methodology for the identification, isolation and optimisation of novel biocatalysts. In order to achieve this, reactivity probes are used to isolate biocatalysts and the technique of flow cytometry employed to sort arrays of mutant enzymes against profluorescent probes. New specific, more stable enzymes can be produced and these exciting techniques, along with directed evolution, are discussed further within this chapter. The importance of transgenic hosts and reactivity probes will also be considered. Further details of the enzymes *AtSFGH* and *AtCXE12*, which have been targeted as model proteins of interest, are described in Chapter 2. These enzyme systems have been of previous interest to the group. Discussion of the procedures undertaken in the design and use of fluorescent reactivity probes based on both phenylacetylene and BODIPY are given in Chapters 3 and 4. The application of studies towards the isolation of oxidative cytochrome p450 is also discussed in Chapter 4. Studies undertaken on peroxisomes are detailed in Chapter 5. All experimental procedures are documented in Chapter 6.

## **1.2 Directed Evolution**

### **1.2.1 Introduction**

In an effort to mimic natural selection, directed evolution aims to generate an enzyme with improved or new activity by screening and selecting for the desired function from a large pool of enzyme variants. Current research is aimed at the production of enzyme variants with improved stability,<sup>1</sup> specificity<sup>2</sup> and selectivity,<sup>3</sup> including enantioselectivity<sup>4</sup> and regioselectivity.<sup>5</sup> Directed evolution is a process of iterative cycles, with the mutant gene of the optimal enzyme variant subjected to several rounds of mutagenesis/expression/screening. This creates an evolutionary pressure, leading to a much improved enzyme. Mutations can be introduced at specific points using site-directed mutagenesis or throughout the gene by random mutagenesis, such as error-prone PCR and DNA shuffling. An important tool for all mutagenesis techniques is the polymerase chain reaction (PCR), which amplifies DNA.

### **1.2.2 Polymerase Chain Reaction (PCR)**

This technique allows scientists to amplify a specific DNA sequence millions of times in just a few hours. During PCR, high temperature is used to separate the DNA molecules into single strands; synthetic sequences of single-stranded DNA serve as primers. Two different primer sequences are used to bracket the target region to be amplified. One primer is complementary to one DNA strand at the beginning of the target region; a second primer is complementary to the other strand at the end of the target region (See Figure 1.1).

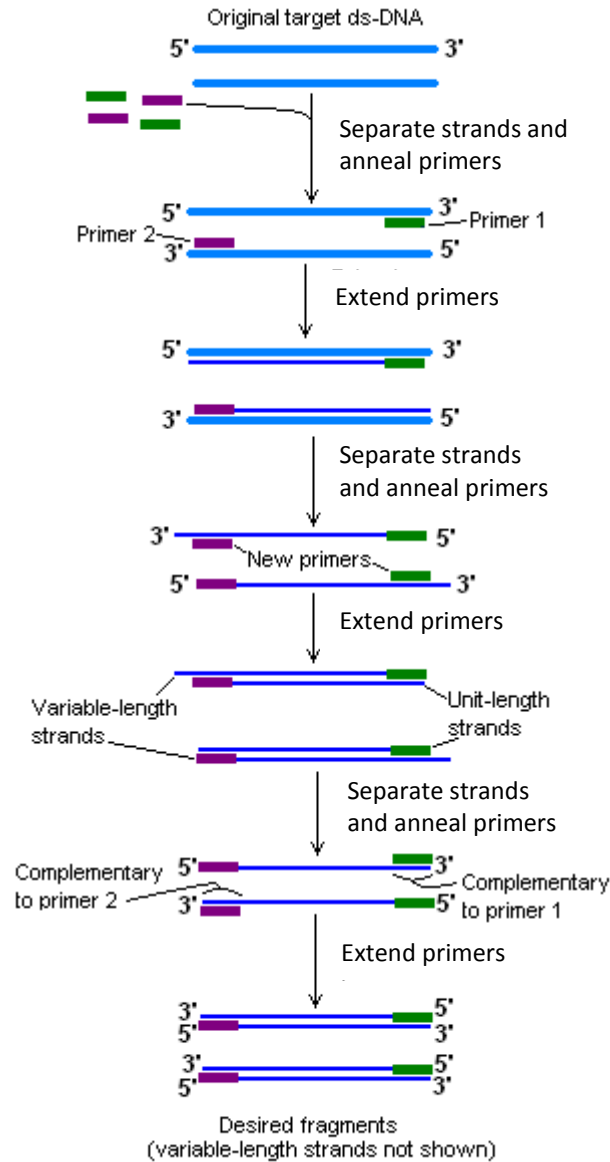


**Figure 1.1 The polymerase chain reaction (PCR)**

To perform a PCR reaction, a small quantity of the target DNA is added to a test tube with a buffered solution containing DNA polymerase, short oligonucleotide primers, the four deoxynucleotide bases of DNA and the cofactor  $MgCl_2$ . The PCR mixture is taken through replication cycles consisting of:

- 94 – 96 °C: DNA is denatured into single strands
- 50 – 65 °C: Primers anneal (hybridise) by way of hydrogen bonds to their complementary sequences on either side of the target sequence

- 72 °C: DNA polymerase binds and extends a complementary strand from each primer

Automated PCR came about through the use of *Taq* DNA polymerase which was isolated from the bacterium *Thermus aquaticus*. This enzyme is able to remain active through the heating required during the many cycles of amplification. After just 30 cycles over 1 billion copies of the target DNA sequence can be synthesised.

### 1.2.3 Site-directed Mutagenesis

Site-directed mutagenesis, a technique that relies on computational or molecular modelling to identify the amino acids involved in key interactions with the substrate, is commonly used in directed evolution studies. In general, site-directed mutagenesis requires that the wild-type gene sequence be known. An oligonucleotide with a sequence containing a desired mutation is chemically synthesised and annealed by base pair H-bonding to the complementary wild-type gene sequence. The synthetic oligonucleotide is used as a primer for the *in vitro* synthesis of a new DNA strand that is complementary to the original (template) strand. This newly synthesised strand of DNA has the primer and the desired mutation incorporated into it. By using a pair of primers and the polymerase chain reaction it is possible to amplify the newly created DNA molecule and produce enough copies to make further manipulation of the new DNA possible.

Arnold and co-workers<sup>5</sup> utilised site-directed mutagenesis in the directed evolution of the bacterial cytochrome P450 BM-3. This enzyme hydroxylates linear medium chain (C<sub>12</sub> - C<sub>18</sub>) fatty acids at the  $\omega$ -1,  $\omega$ -2 and  $\omega$ -3 positions in the presence of O<sub>2</sub>, using NADPH as a co-factor. Using the crystal structure of the enzyme active site, two key residues, alanine<sub>328</sub> and alanine<sub>82</sub>, were targeted for mutagenesis. Alanine<sub>328</sub> was converted to valine in order to reduce the volume of the active site. The variant enzyme A328V was able to hydroxylate shorter chain fatty acids (C<sub>7</sub> - C<sub>9</sub>) with a shift in the regioselectivity towards the  $\omega$ -2 position, compared with the wild-type which resulted in roughly equal hydroxylation at the  $\omega$ -2,  $\omega$ -3 and  $\omega$ -4 position. It was also shown that a second mutant A82L was able to hydroxylate propane at faster rates and with higher turnover numbers than the wild-type enzyme.

### 1.2.4 Error-prone Polymerase Chain Reaction (epPCR)

Error-prone polymerase chain reaction (epPCR) is a random mutagenesis technique used to introduce amino acid changes into proteins. Mutations are deliberately introduced during PCR through the use of error-prone DNA polymerases and varying reaction conditions. Traditional epPCR methods commonly employ *Taq* DNA polymerase as it lacks a 3' - 5' proofreading activity and is inherently error-prone.<sup>6</sup> Various conditions are employed to alter the mutation rates, which include the use of reaction buffers containing Mn<sup>2+</sup> (in place of the normal divalent ion Mg<sup>2+</sup>) and unbalanced, or unnatural,<sup>7</sup> dNTP concentrations. Commonly a low mutation rate is chosen so as to ensure an average of only one amino acid exchange per enzyme molecule. However, the use of *Taq* polymerase often gives rise to a mutational bias, favouring transversions over transitions and being 4 times more likely to mutate As and Ts than Gs and Cs.<sup>8</sup>

Various other polymerases have been used in an attempt to overcome this mutational bias. One example includes the error prone polymerase Mutazyme® II, developed by Stratagene.<sup>9</sup> This enzyme exhibits a much lower mutational bias compared to *Taq*, Figure 1.2.

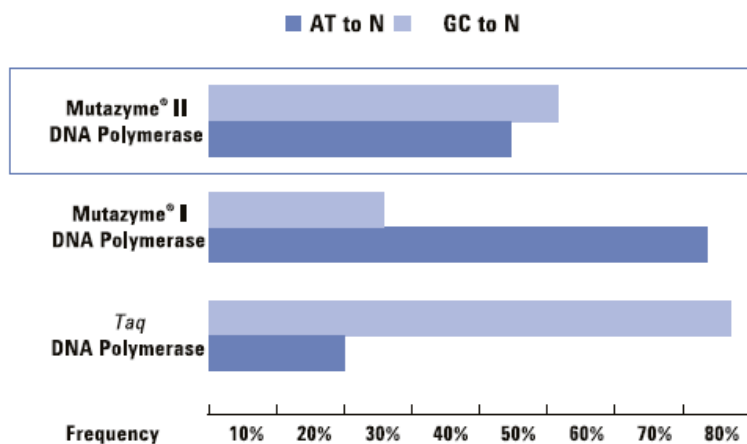
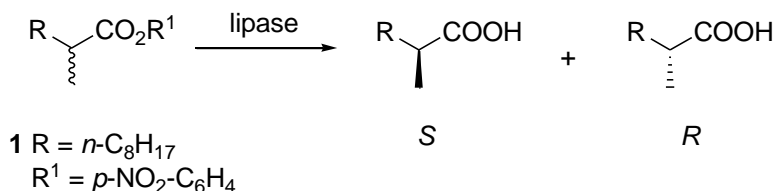


Figure 1.2 Mutazyme II DNA polymerase mutates Gs and Cs at nearly identical rates compared to As and Ts.

Reetz employed this technique to enhance the enantioselectivity of a lipase-catalysed hydrolytic kinetic resolution involving a chiral ester.<sup>10</sup> The wild-type lipase from *Pseudomonas aeruginosa*, which catalyses the hydrolysis of ester **1** with slight preference

for the *S*-acid, See Scheme 1.1, was mutated into a variant enzyme which shows high *S*-preference.



**Scheme 1.1 Lipase-catalysed hydrolysis of *p*-nitrophenol ester 1**

In an extension to this work, epPCR was again employed with a change in the conditions resulting in an increased mutation rate (2 – 3 amino acid changes, compared with 1 in the previous experiment). A library of 15,000 clones was screened which identified several *S*-selective mutants, but also two *R*-selective variants.<sup>11</sup> One of these *R*-variants was selected for further mutagenesis and after another two rounds of epPCR the *E*-value was increased from 2.0 to 7.0.

Upon inserting the mutant genes into a host such as *E. coli*, variant enzymes are expressed which are individually screened for activity in the reaction of interest. As this process can be repeated several times there is no necessity to know anything about the structure or mechanism of the enzyme, an advantage when compared with site-directed mutagenesis. This technique is discussed in more detail in section 2.2.3.4.

### 1.2.5 DNA Shuffling

More radical mutations can be achieved through recombination techniques. Stemmer was the first to report this and coined the technique DNA-shuffling.<sup>12</sup> This method takes a collection of homologous genes and fragments them into small pieces by limited digestion with DNase I. Following purification to remove undigested material the combined fragments are then reassembled in a primer-less PCR reaction in the presence of a thermostable polymerase (See Figure 1.3). Recombination arises as a result of fragments from different parent genes cross-priming to produce a hybrid DNA strand. Stemmer's group demonstrated their technique on a β-lactamase enzyme system and results showed a 32,000-fold increase in activity, compared with a 16-fold increase when utilising only cassette mutagenesis and error-prone PCR techniques.

Shao *et al*<sup>13</sup> reported the similar technique of random priming recombination (RPR), in which the gene fragments are obtained through random priming synthesis, avoiding the use of DNase I. Following template removal the fragments are used to reassemble parent sized hybrid genes as in conventional DNA shuffling.

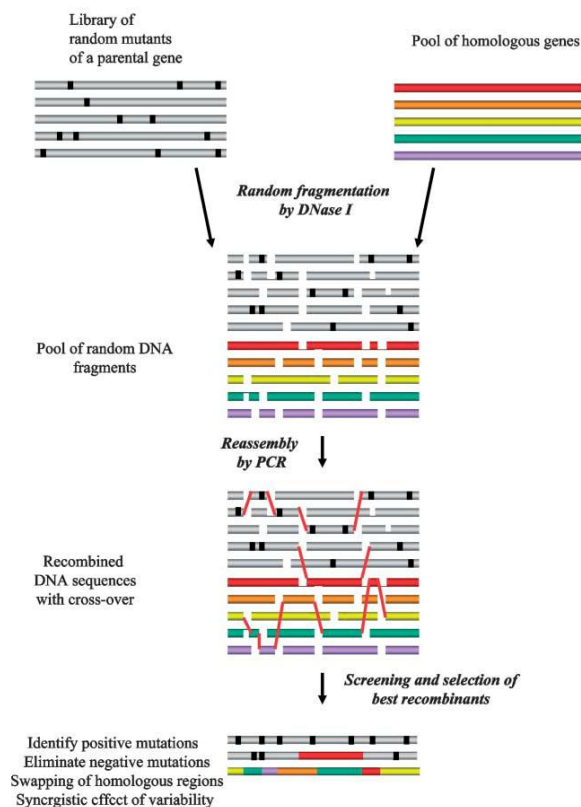


**Figure 1.3 Homologous *in vitro* recombination method (DNA shuffling) used to create hybrid gene libraries from multiple parental sequences.** *Nat. Prod. Rep.*, 2004, 21, 492 – Reproduced by permission of The Royal Society of Chemistry

A high level of recombination is important to achieve all possible combinations of mutations. As these recombinations can be biased, several methods have been developed to overcome this.<sup>14</sup> These methods can be divided into distinct groups, each having their advantages and disadvantages, which are outlined below.

### 1.2.5.1 Full length parent shuffling

The staggered extension process (StEP),<sup>15</sup> whereby the use of gene fragments is eliminated, uses template-switching as a way of building chimeric sequences from multiple parents (See Figure 1.4). The recombination of small fragments from different



origins using one or more full length strands allows a higher recombination frequency over normal DNA shuffling. However, these recombinations tend to be more elaborate.

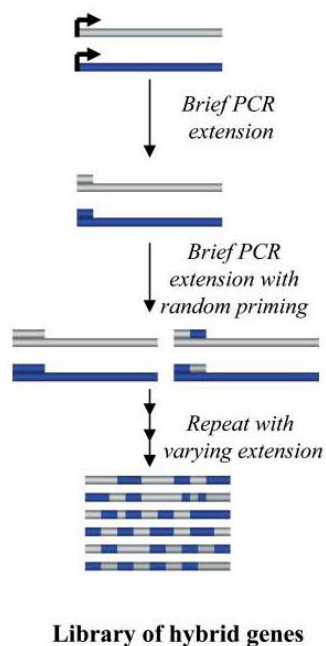


**Figure 1.4 Staggered Extension Process (StEP).** *Nat. Prod. Rep.*, 2004, **21**, 493 – Reproduced by permission of The Royal Society of Chemistry

A more recently developed technique, which combines features of both DNA shuffling and StEP, is termed random chimeragenesis on transient templates (RACHITT).<sup>16</sup> Initially parental genes are fragmented using DNase I with a uracil-containing template strand used in the direct assembly of chimeras from the fragment pool. Fragments annealed to the transient template are trimmed and joined by treatment with nuclease competent polymerases and DNA ligase. The template strand is then glycosylated by uracil-DNA-glycosylase, rendering it non-amplifiable in further PCR experiments (See Figure 1.5). This effectively eliminates the parent templates from the gene pool, a common problem encountered with other methods of homologous recombination. Although RACHITT appears to be a more demanding technique than those previously discussed, a much more diverse library is produced due to a greater number of crossovers per gene.

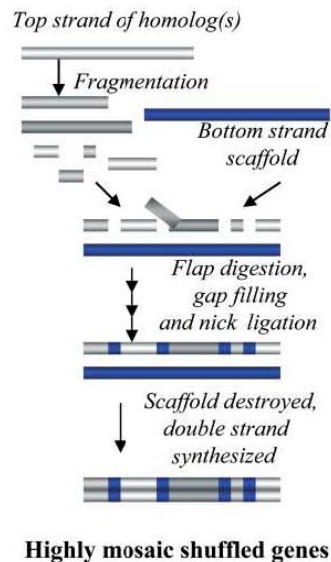


**Figure 1.5 Random Chimeragenesis on Transient Templates.** *Nat. Prod. Rep.*, 2004, 21, 493 – Reproduced by permission of The Royal Society of Chemistry

A common problem with each of the above techniques is the prerequisite of a high DNA sequence homology in order to generate hybrid crossovers. To overcome this several methods have been developed to create hybrid libraries independent of the DNA sequence homology of the parental genes. This has been achieved by eliminating the need for homologous fragment hybridisation and allows the possibility for more distantly related protein sequences to be recombined in a combinatorial technique.

### 1.2.5.2 Single cross-over

This group includes methods that involve the recombination of low or non-homologous genes by ligating the front and back of two different genes. One such technique, known as incremental truncation for the creation of hybrid enzymes (ITCHY),<sup>17</sup> involves the production of two opposing incremental truncation libraries, in which every single DNA base pair deletion is generated (See Figure 1.6). Following blunting with single-stranded nuclease, the two fragment libraries are then randomly fused head-to-tail to produce a single crossover hybrid gene library. As the ligation step is completely random hybrids of all possible lengths and reading frames are produced. The selection of variants is possible by size.

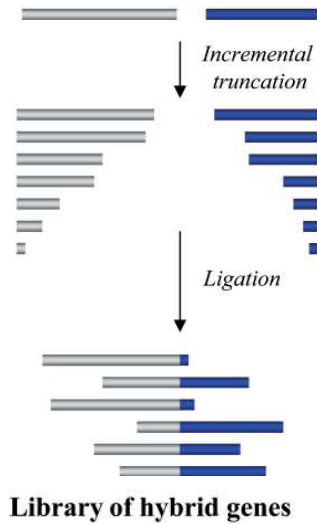


**Figure 1.6 Incremental Truncation for the Creation of Hybrid Enzymes.** *Nat. Prod. Rep.*, 2004, **21**, 493 –  
 Reproduced by permission of The Royal Society of Chemistry

Another technique within this group is termed sequence homology-independent protein recombination (SHIPREC). This involves the fusion of two parent genes to form a dimer which is then digested with DNase I to produce random length fragments. Fragments that are the same length as either of the two parent genes are isolated and the remaining ends are fused by circularisation (See Figure 1.7).

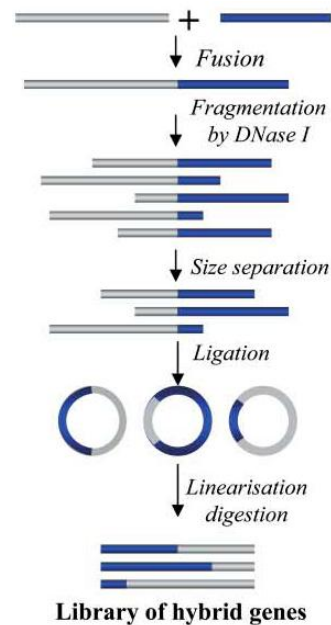


**Figure 1.7 Sequence Homology-Independent Protein Recombination.** *Nat. Prod. Rep.*, 2004, **21**, 493 –  
 Reproduced by permission of The Royal Society of Chemistry

Sieber and co-workers successfully used this method to produce interspecies hybrids of a human cytochrome P450 (1A2) and a soluble bacterium P450 (BM3). They identified two functional P450 hybrids which were more soluble in the bacterial cytoplasm than the wild-type 1A2 enzyme. Problems with the single crossover technique include the fact that only one recombination point is possible. Increasing numbers of crossovers are desirable as they have been shown to improve the evolution of proteins with appropriate characteristics.<sup>18</sup>

### 1.2.5.3 Domain swapping

Techniques within this group include exon shuffling<sup>19</sup> and degenerate oligonucleotide gene shuffling (DOGS)<sup>20</sup> and incorporate the recombination of structural, functional or less homologous parts of different family members. Bequist and co-workers developed the DOGS procedure<sup>21</sup> using degenerate primers that allowed control of the level of recombination between the genes that are shuffled and hence reduces the regeneration of unshuffled parent genes. Arnold *et al*<sup>19</sup> have developed the sequence-independent site-directed chimeragenesis (SISDC) method, which allows crossovers at multiple sites and is independent of DNA sequence identity shared by the parent genes (See Figure 1.8). They showed that the ligation of building blocks regenerated a full-length and highly recombined library of two distantly related  $\beta$ -lactamases, TEM-1 and PSE-4. It often results in more active enzymes but with only a few recombination points, which are often difficult to locate.

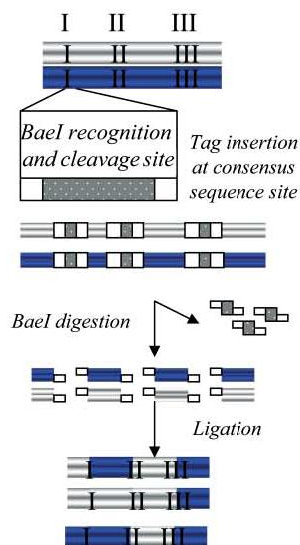


**Figure 1.8 Sequence-Independent Site-Directed Chimeragenesis.** *Nat. Prod. Rep.*, 2004, 21, 493 –  
Reproduced by permission of The Royal Society of Chemistry

#### 1.2.5.4 *In vivo* recombination

These methods involve recombination using the gap repair system of yeast or the recE/recT system of *E. coli*. Abécassis *et al*<sup>22</sup> used the combinatorial libraries enhanced by recombination in yeast (CLERY) procedure to successfully create hybridised cytochrome P450 *CYP1A1* and *CYP1A2* enzymes. This process results in a high yield as there is no ligation necessary, however, specialised vectors and multiple steps are required.

#### 1.2.5.5 Synthetic shuffling

Synthetic shuffling, which includes single step shuffling, involves the recombination of known or unknown mutations in synthetic oligonucleotides. It uses sequence length rather than sequence similarity to achieve crossovers at positions likely to be structurally related (See Figure 1.9). Developed by Ness *et al*<sup>23</sup> this method was used in the study of the serine protease subtilisin, in which a variant enzyme was generated with both improved thermostability and high pH tolerance. Two synthetic variants were found to be two- to four-fold more active at pH 10 after heat treatment at 70 °C, compared with Savinase®, the current commercial product. Synthetic shuffling allows the recombination of close mutations, but this technique is expensive and good selection is necessary.

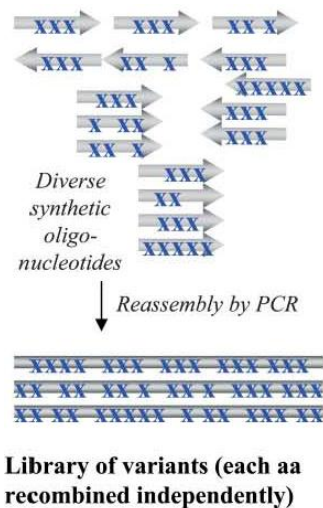


**Figure 1.9 Synthetic Shuffling.** *Nat. Prod. Rep.*, 2004, 21, 493 – Reproduced by permission of The Royal Society of Chemistry

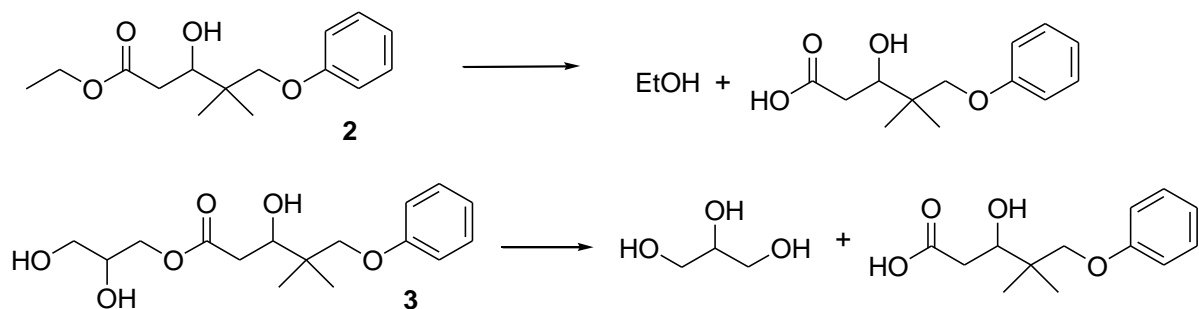
## **1.3 Screening and Selection Techniques**

### **1.3.1 Introduction**

The success of a directed evolution experiment is highly dependent on the screening method used to locate the optimum variant. Since most directed evolution experiments generate a huge mutant library, typically around 15,000 clones, a high throughput selection strategy needs to be developed to screen for different enzyme functions. These methods should be sufficiently sensitive and specific to identify positive variants.<sup>24</sup> An important point to note here is the difference between the terms selection and screening. Screening involves the assaying of all library members individually and requires an active search of all the variants produced. In selection criteria, conditions are set that allow only variants of interest to appear. This is achieved by exploiting the conditions favourable for the exclusive survival of desired variants. Some of the most commonly utilised techniques, including pH indicators, digital imaging, *in vivo* compartmentalisation and fluorescence activated cell sorting are outlined in the following section.

### **1.3.2 pH-Indicators**

pH indicators allow the screening of libraries based on the change in pH as a result of the enzyme reaction. This can be seen in the following example in which Bornscheuer *et al* produced a variant esterase enzyme library and screened for mutants on the basis of pH.<sup>25</sup> These libraries were assayed by means of agar plates in the presence of pH indicators in combination with a growth assay. Identification of the desired variants, which were required to hydrolyse the sterically hindered esters **2** and **3**, Scheme 1.2, was performed using a combination of neutral red and crystal violet indicators. The formation of a red colour, caused by a pH decrease due to the released acid, allowed the easy detection of active variants.



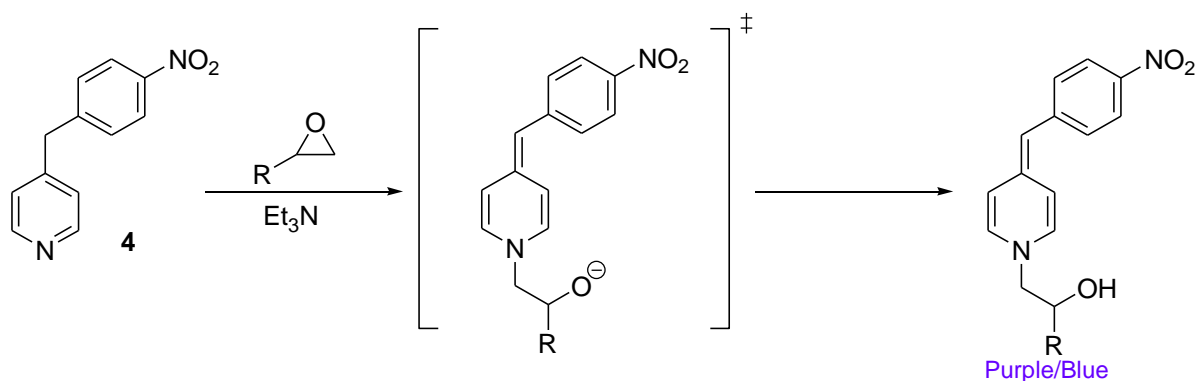
Scheme 1.2

They also introduced a selection criterion by utilising the metabolite of the glycol ester **3**, as the release of the carbon source glycerol facilitates growth on the minimal media used. Using this strategy Bornscheuer identified a double mutant which hydrolysed **3** in a stereoselective manner.

Major advantages of the use of pH indicators are that a large number of clones can be examined within a short space of time, *e.g.* 300 – 500 colonies per plate, the wide variety of pH indicators allowing the adaption of the assay to the optimum pH range of the enzyme of interest and that there is no need for special substrates.

### 1.3.3 Colorimetric Assay

UV/Vis spectrophotometry methods permit high throughput screening due to the simple and fast measurements which can be taken. Zocher *et al*<sup>26</sup> utilised UV/Vis spectrophotometry in the determination of epoxide hydrolytic activity by measuring the decrease of epoxide concentration. They used the 4-(*p*-nitrobenzyl)pyridine (NBP, **4**) test, which can determine the epoxide concentration due to alkylation of **4**, Scheme 1.3.



Scheme 1.3 Alkylation of epoxide by NBP, **4**

Various substituted epoxide substrates, such as styrene oxide, indene oxide, *n*-hexane oxide and *n*-decane oxide were used. A linear correlation between epoxide concentration and absorbance was found for all epoxides except *n*-decane oxide. A microtiter-plate assay with a robotic arm was used and showed a high sensitivity for the detection of low levels of epoxide concentration (0.1 – 1 mg/well). This method was found to be suitable for the screening of epoxide hydrolase in the presence of other enzymes such as esterases, lipases or proteases. Zocher postulates that with the use of enantiomerically pure epoxides the identification of enzyme variants with high enantioselectivity should be possible.

### 1.3.4 Digital Imaging

This technique relies on the metabolite product being coloured and/or fluorescent, allowing easy detection. A specific advantage of fluorescence-based imaging is the high degree of sensitivity, which allows the use of very dilute substrate concentrations and extremely small amounts of catalysts. Copeland *et al* have used a fluorescence-based method for assaying the activity of catalysts in acylation reactions.<sup>27</sup> They were able to determine the activity of several acylation catalysts by the use of a molecular sensor which fluoresces upon formation of the product (See Figure 1.10). In their experiments, isopropanol (**5**; R<sub>1</sub> = R<sub>2</sub> = CH<sub>3</sub>) was treated with acetic acid anhydride in the presence of the nonfluorescent chemosensor **6**. In the absence of catalysts no fluorescence was observed. Upon the addition of tetrapeptide catalysts, of which **7** is an example, fluorescence was detected using a fluorescent plate reader, monitored for 30 – 40 minutes.

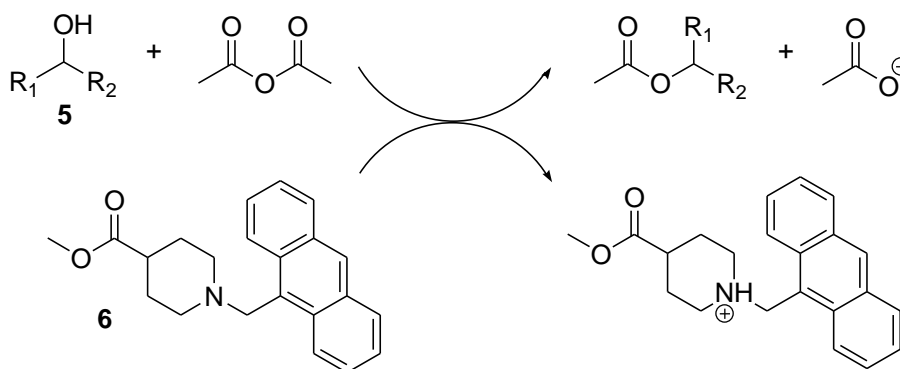
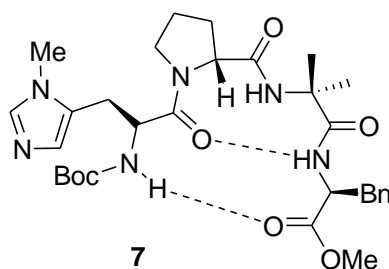
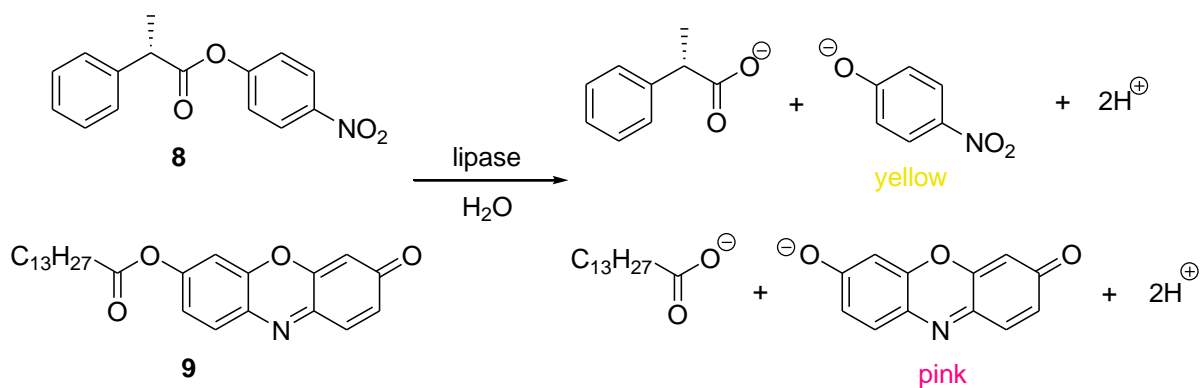


Figure 1.10





For coloured metabolites, UV/Vis spectrophotometry can be used for the screening of variant enzymes. Janes and co-workers have developed a colorimetric assay for testing the enantioselectivity of esterases in ester hydrolyses.<sup>28</sup> This assay was able to simulate the competitive conditions of an enzymatic process. A mixture of the *p*-nitrophenol ester of one enantiomeric form of a chiral ester **8** and a reference compound, the resorufin ester **9**, was subjected to enzyme-catalysed hydrolysis. Upon hydrolysis of *S*-**8** and the reference compound **9**, yellow and pink chromophores were formed. If both substrates are hydrolysed the solution turns deep orange (See Scheme 1.4).



Scheme 1.4

The two hydrolyses were monitored in the same solution by recording the UV/Vis absorption of the two products at 404 and 572 nm wavelengths. The ratio of hydrolysis of the two different compounds yielded the selectivity of the esterase for *S*-**8** over the reference, **9**. To determine the enantioselectivity of the enzyme the assay was repeated using *R*-**8** and **9**. This method is able to overcome previous limitations as in past experiments both the *R* and *S* enantiomers needed to be screened separately, therefore unable to test normal enzymatic conditions, such as competitive binding of the two enantiomers to the enzyme.

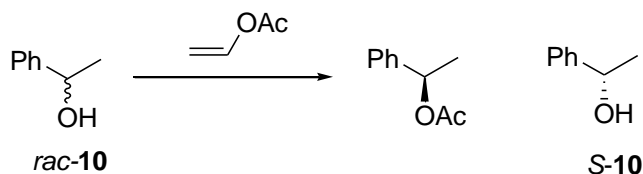
This screening technique was successfully used to identify a lipase with a much improved enantioselectivity. The wild type enzyme, with a 2% *ee*, was optimised to

yield a lipase exhibiting an 81% *ee* in only four cycles of epPCR.<sup>29</sup> One limitation that remains is that the optimisation is performed on the *p*-nitrophenol ester **8** and not on a more practical ester such as the analogous methyl ester.

### 1.3.5 IR Thermography

This screening technique uses an infrared camera to detect minute changes in temperature in the reaction vessel, with an increase relating to an increase in activity. IR radiation is actively emitted from all objects and no external light source is required for imaging. The IR image of an object is composed of emitted and reflected radiation with the relative ratio different for each surface. The different colours on these images visualise different photon intensities of detected IR radiation. From these photon intensities blackbody temperatures can be calculated by Planck's law. These blackbody temperatures can be converted to the actual surface temperature of the object only if no reflection occurs or becomes insignificant and its emissivity is known.<sup>30</sup> A PtSi-based camera was used in order to allow emissivity correction. To avoid reflections at the catalyst library, a slate plate of low reflectivity was chosen. As these two factors were controlled the heat evolution due to the catalytic activity of the enzyme was reliably detected since only temperature changes are visible. Temperature differences of 0.1 K are clearly detected.

Reetz used this technique to screen for enantioselective lipases in the acylation of 1-phenylethanol, **10**, with vinyl acetate (See Scheme 1.5).<sup>31</sup> This reaction proceeds with 99% enantioselectivity in favour of the *R*-ester in the presence of a catalytic amount of lipase. Using a microtiter plate, Reetz added vinyl acetate to separate solutions of *R*-**10**, *S*-**10** and *rac*-**10** and measured the temperature change at 5 second intervals, taking 250 recordings.



Scheme 1.5

Changes in temperature could be clearly seen, indicated by the appearance of red spots (See Figure 1.11), showing that *R*-**10** reacts preferentially over *S*-**10**. As spatial resolution

is not a problem this method lends itself towards the high-throughput screening of active enzymes.

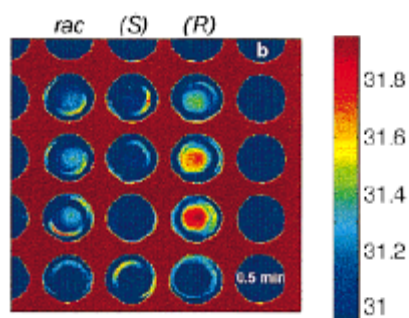


**Figure 1.11** Time-resolved IR-thermographic imaging of the lipase-catalysed enantioselective acylation of 10 after 0.5 mins. The bar on the right is the temperature/colour key of the temperature window used (°C). Reetz M.T., Becker M.H., Kühling K.M. and Holzwarth A., *Detection of Catalytic Activity in Combinatorial Libraries of Heterogeneous Catalysts by IR Thermography*, *Angew. Chim. Int. Ed.*, 1998, 37, 2647-2650. Copyright Wiley-VCH Verlag GmbH & Co. KGaA. Reproduced with permission.

### 1.3.6 Yeast Two-hybrid System

Directed evolution is generally limited to those reactions in which enzyme variants can be easily screened or selected, often restricting this to reactions in which the product is fluorescent or an essential metabolite. The yeast two-hybrid system overcomes this problem and is used to detect protein-protein interactions *in vivo*.<sup>32</sup> Advantages include the fact that it is technically straightforward and can be carried out rapidly. Furthermore, the sequence of two interacting proteins can be read off directly from the DNA sequence of the plasmids encoding them and does not depend on the identity of the interacting proteins and is therefore generally applicable.

The yeast two-hybrid system consists of two protein chimeras and a reporter gene downstream from the binding site for the transcriptional activator (See Figure 1.12). If two proteins of interest (X and Y) interact, they dimerise the DNA-binding protein chimera (DNA-binding domain, DBD-X) and the transcriptional activation protein chimera (AD-Y). This dimerisation of DBD and transcriptional AD help recruit transcription machinery to a promoter adjacent to the binding site for the transcriptional activator, therefore activating transcription of the reporter gene.

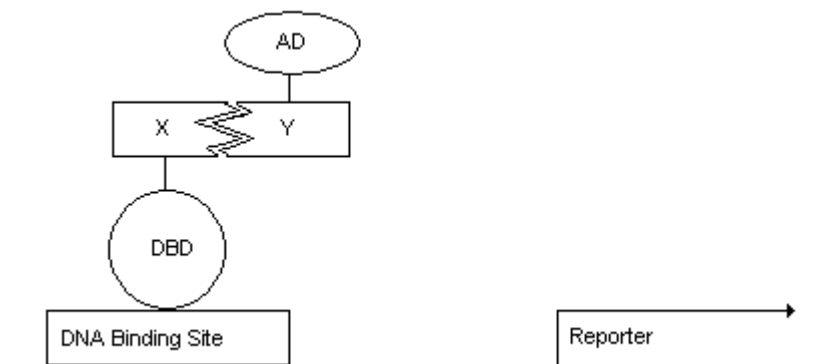


**Figure 1.12 Yeast Two-hybrid System**

This method was initially used for verifying positive protein-protein interactions but is also well suited to screening libraries of proteins to identify new activities. Cornish *et al*<sup>33</sup> have developed a high-throughput assay, which has built upon the ideas of the yeast two-hybrid system and can be applied to a wide range of chemical reactions. They termed this Chemical Complementation, a method that uses a yeast three-hybrid assay to link enzyme catalysis to reporter gene transcription *in vivo* and was successfully used to develop variants of both  $\beta$ -lactamase<sup>34</sup> and glycosynthase<sup>35</sup> enzymes.

Chemical Complementation detects enzyme catalysis of bond formation or cleavage reactions based on covalent coupling of two small molecule ligands *in vivo*. The heterodimeric small molecule reconstitutes a transcriptional activator, turning on the transcription of a downstream reporter gene. Bond formation is detected as activation of an essential reporter gene, whilst bond cleavage by repression of a toxic reporter gene (See Figure 1.13). In both enzyme systems, Cornish has utilised dexamethasone-methotrexate derivatives (Dex-Mtx) as the heterodimeric ligand.

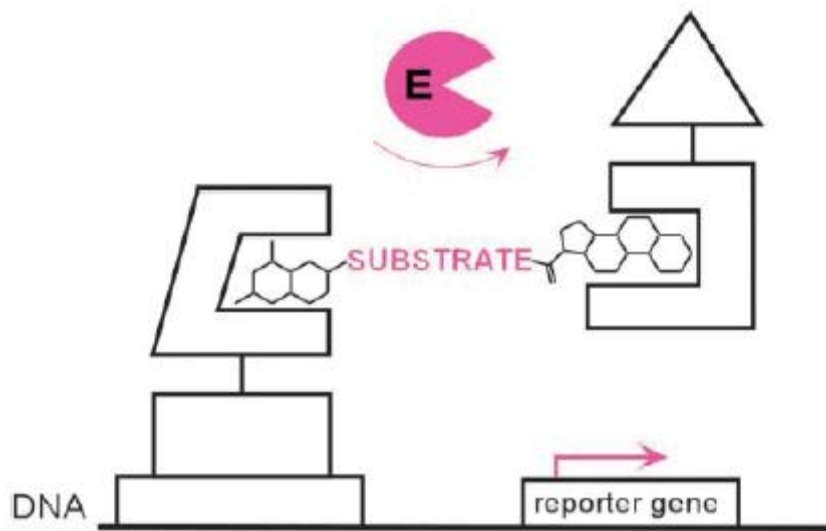


**Figure 1.13 Chemical Complementation.** A reaction-independent complementation assay for enzyme catalysis based on the yeast three-hybrid assay. Copyright (2002) © by the National Academy of Sciences

A heterodimeric small molecule bridges a DNA-binding domain-receptor fusion protein and an activation domain-receptor fusion protein, activating transcription of a downstream reporter gene *in vivo*. Enzyme catalysis of either cleavage or formation of the bond between the two small molecules can be detected as a change in transcription of the reporter gene.

The assay is high-throughput because it can be run as a growth selection where only cells containing a functional enzyme survive. The assay can be readily extended to new chemistry simply by synthesising small molecule heterodimers with different chemical linkers as the enzyme substrates.

### 1.3.7 Fluorescence Activated Cell Sorting (FACS)

Cytometry is a process for measuring the physical and chemical characteristics of biological cells. In flow cytometry, the measurements are made as cells flow through the instrument in a fluid stream. This section will detail fluorescence activated cell sorting (FACS), a technique in which cells are sorted by electrical and/or mechanical means to divert and collect cells with measured fluorescence that fall within a user-selected range of values.<sup>36</sup>

FACS has been used to screen for improved antibodies. In the directed evolution of antibodies cell-surface display techniques are used which involve the creation of large

DNA libraries encoding for randomly mutated antibodies.<sup>37</sup> These proteins are expressed and displayed on a scaffold and favourable variants are selected from the pool. Such scaffolds include bacteriophage, *E. coli* and yeast. Wittrup and co-workers engineered a fluorescein-binding single-chain Fv, achieved through four rounds of epPCR and FACS screening, with a dissociation constant ( $K_d$ ) of 48 fM.<sup>38</sup> However, limitations on the surface expression of enzymes and constraints on substrate design make this approach fairly specialised.<sup>39</sup>

To overcome these constraints a technique known as *in vitro* compartmentalisation has been developed. *In vitro* compartmentalisation (IVC) is based on water-in-oil emulsions where the water phase is dispersed in the oil phase to form microscopic aqueous compartments. Each droplet contains a single gene and serves as an artificial cell in enabling transcription, translation and the activity of the resulting proteins, to take place within the compartment. The oil phase remains largely inert and restricts the diffusion of genes and proteins between the compartments. The droplet volume enables the detection of a single enzyme molecule. The high capacity of the system ( $> 10^{10}$  in 1 ml of emulsion), the ease of preparing emulsions and their high stability over a broad range of temperatures render IVC an attractive system for high-throughput screening.

The selection of enzymatic activity requires a link between the desired reaction product and the gene. One such method is to have the substrate, and therefore the product, of the desired enzymatic activity physically linked to the gene. Active enzyme-encoding genes can then be isolated by virtue of their attachment to the product, whilst other genes that encode an inactive enzyme carry the unmodified substrate (See Figure 1.14). Sorting of these enzymes can be achieved by fluorescent activated cell sorting (FACS). This technique was used to select a bacterial phosphotriesterase which exhibited a 63-fold improved turnover number towards the substrate paraoxon compared to the wild-type.<sup>40</sup> Despite the obvious advantages, this mode of selection is restricted, as it must be performed under defined pH, buffer, ionic strength and metal ion composition.

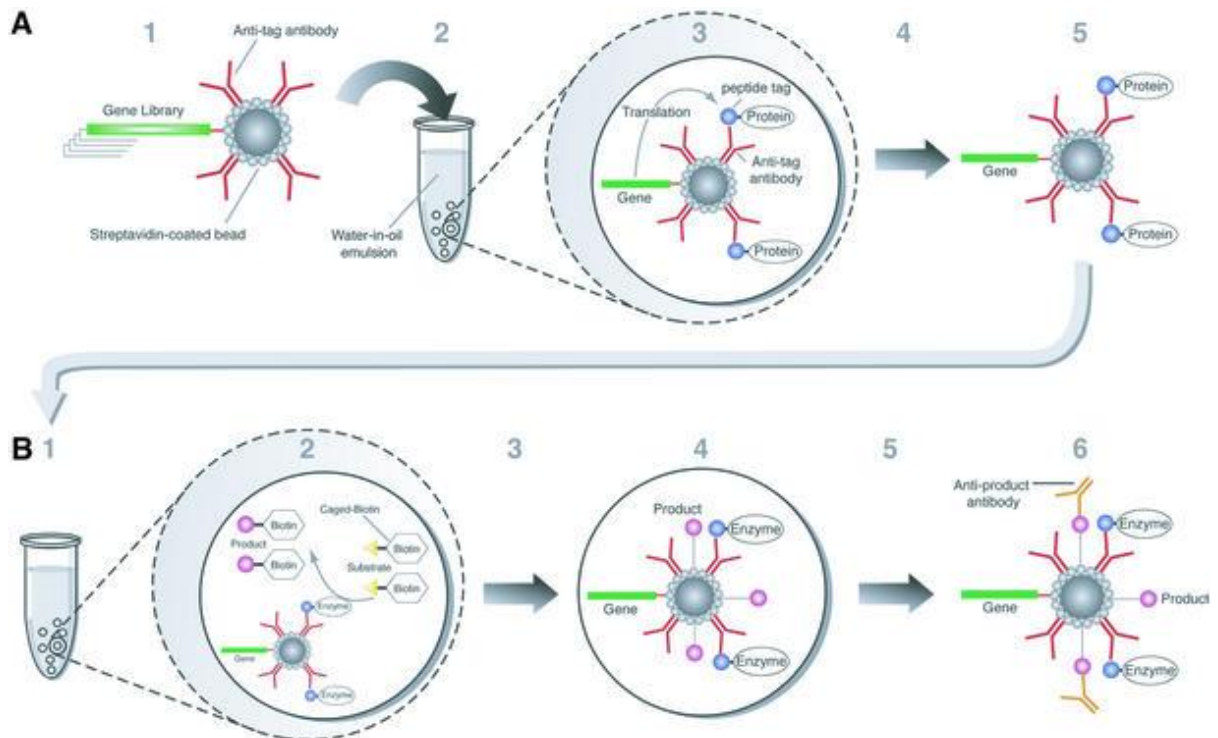


**Figure 1.14** Creation of microbead-display libraries and selection for catalysis by compartmentalisation. **A)** Creation of microbead-display libraries. Genes are linked to streptavidin coated beads (1), which are then compartmentalised in a water-in-oil emulsion to give one bead per compartment (2) and transcribed and translated *in vitro* thereby linking the gene to the protein. The emulsion is broken (4) and microbeads are isolated (5). **B)** Enzyme selection by compartmentalisation. Microbead-displays are compartmentalised (1) and a soluble substrate attached to biotin is added. This substrate is converted to the product in compartments containing active enzymes (2). The emulsion is then irradiated to uncage the biotin (3) and the product becomes attached to the gene *via* the bead (4). The emulsion is broken (5) and the beads are incubated with anti-product antibodies and a fluorescently labelled antibody (6) and enriched using flow cytometry. Reprinted by permission from Macmillan Publishers Ltd: *EMBO Journal* (22, 24-35), copyright (2003)

There are a huge number of techniques available for the screening and selection of improved biocatalysts, with each one having their own advantages and disadvantages.

### 1.4 Transgenic Hosts

Bacterial transformation is the process by which bacterial cells take up DNA molecules.<sup>41</sup> If the foreign DNA has an origin of replication recognised by the host cell DNA polymerases, the bacteria will replicate the foreign DNA along with their own DNA. When transformation is coupled with antibiotic selection techniques, bacteria can be induced to uptake certain DNA molecules, and those bacteria can be selected for. Bacteria which are able to uptake DNA are called competent and are made so by treatment with CaCl<sub>2</sub> in the early log phase of growth. The bacterial cell membrane is

permeable to chloride ions but is non-permeable to calcium ions. As the chloride ions enter the cell water molecules accompany the charged particle. This influx of water causes the cells to swell and is necessary for the uptake of DNA. The exact mechanism of this uptake is unknown. It is known, however, that the  $\text{CaCl}_2$  treatment be followed by heat. When *E. coli* are subjected to 42 °C heat, a set of genes are expressed which aid the bacteria in surviving at such temperatures. This set of genes is called the heat shock genes. The heat shock step is necessary for the uptake of DNA. At temperatures above 42 °C, the bacteria's ability to uptake DNA becomes reduced, and at extreme temperatures the bacteria will die.

Due to their ease of transformation, including high transformation efficiency, relative low cost of use and wide number of publications describing a multitude of protocols, bacteria are the most commonly used transgenic host. However, when attempting to express plant-based biocatalysts in bacteria problems can arise. This is often due to the absence of critical co-factors which are needed for catalysis to take place. Advances in plant transformation technology potentially allow protoplasts to be used as transgenic hosts.<sup>42</sup> Details regarding plant protoplasts, along with recent studies utilising these as transgene hosts are described in the following sections.

### **1.4.1 Protoplasts**

Plant protoplasts are plant cells which have had the cell wall removed by treatment with digestion enzymes, such as fungal cellulases and pectinases.<sup>43</sup> Despite the enzymatic treatment step, protoplasts maintain many of the same physiological responses and cellular activities as intact plants, such as active photosynthesis and respiration.<sup>42</sup> Since the first recorded instance of protoplast isolation,<sup>44</sup> they have been used to study a huge range of cellular mechanisms including auxin signalling,<sup>45</sup> membrane transport,<sup>46</sup> cell death<sup>47</sup> and cell wall regeneration.<sup>48</sup> Figure 1.15 shows protoplasts isolated from *Arabidopsis thaliana*. These cells are spherical, single entities, surrounded by a single membrane.



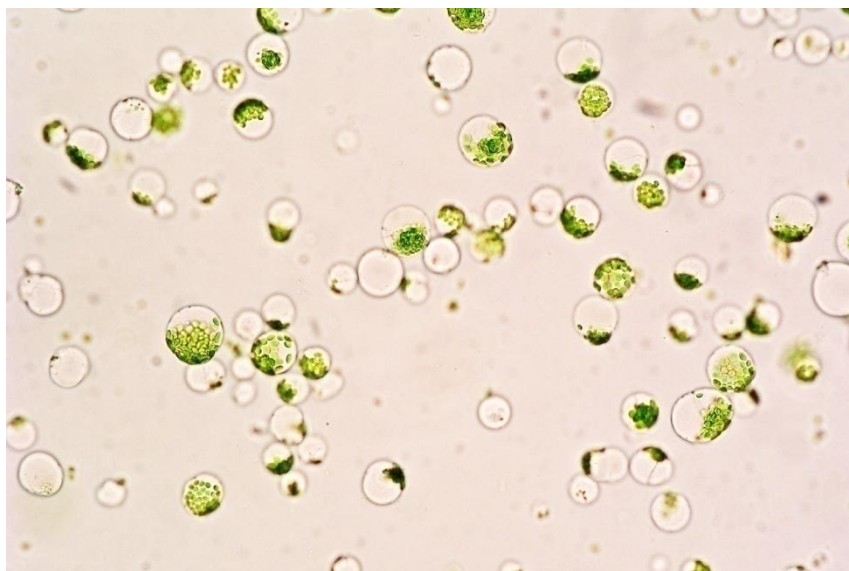


**Figure 1.15** Protoplasts isolated from *Arabidopsis thaliana*. The large, green organelles seen are chloroplasts.

## **1.4.2 Transformation techniques**

Several different techniques exist for the transformation of protoplasts including polyethylene glycol (PEG), electroporation, particle gun and *Agrobacterium tumefaciens*. The following section will describe each one in turn highlighting both the advantages and disadvantages.

### **1.4.2.1 Polyethylene glycol (PEG)**

Transformation methods using polyethylene glycol (PEG) are commonly used in combination with many other transformation techniques. Following the initial period of exposure to DNA, PEG is usually added in high concentrations, up to around 10 volumes of 40% PEG 4000.<sup>49</sup> The effect of PEG is to increase the membrane permeability to allow the uptake a large DNA molecules.<sup>50</sup> The tolerance of protoplasts against PEG is known to vary amongst species. A variety of optimum transformation yields have been reported, which include 28% in *Nicotiana tabacum*,<sup>51</sup> 20% in *Arabidopsis thaliana*<sup>52</sup> and 13% in *Brassica napus*.<sup>53</sup> PEG-mediated transformation has been used to successfully transform mesophyll protoplasts of *Brassica oleracea* with marker genes carrying resistance to kanamycin.<sup>54</sup> An optimum transformation yield of 30% was achieved using 15% PEG 4000 at 42 °C. In addition to this successful plant regeneration was seen when transformed protoplasts were grown in a kanamycin environment, Figure 1.16.

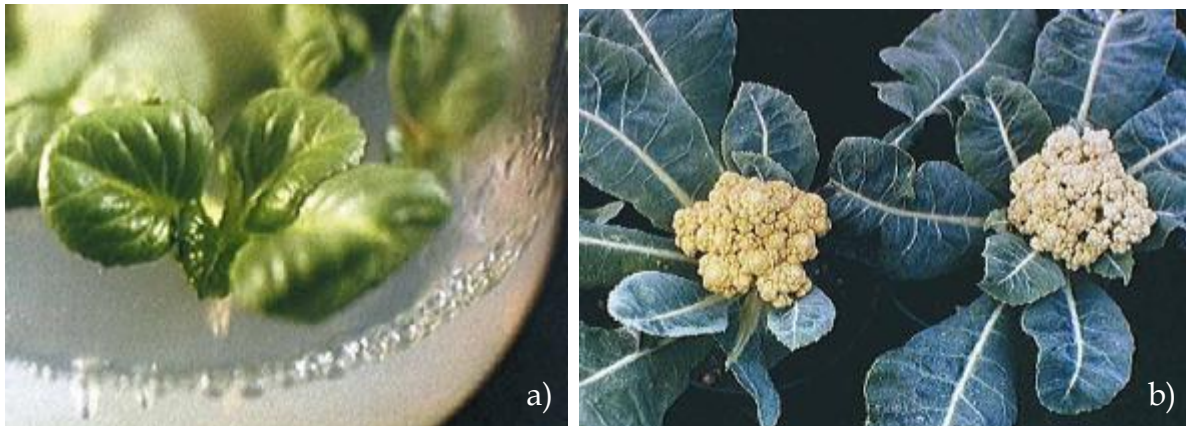


**Figure 1.16 a) Developed green plants growing on medium with 10 mg/l kanamycin for rooting; b) Following rooting the transgenic plant (right) was grown in soil in a greenhouse. The left plant is a control plant, grown directly from seeds in soil in a greenhouse.** Radchuk V.V., Ryschka U., Schumann G. and Klocke E. Genetic transformation of cauliflower (*Brassica oleracea* var. *Botrytis*) by direct DNA uptake into mesophyll protoplasts, *Physiol. Plant.*, 2002, **114**, 429-438. Copyright Wiley-Blackwell. Reproduced with permission.

Tiwari *et al* have found that transformation of protoplasts with PEG lead to their expansion in size from around 20  $\mu\text{m}$  to 80 - 120  $\mu\text{m}$ , with 10 - 20% bursting after 5 days in culture.<sup>55</sup> It has also been reported that the transformation rate is also affected by variations in the efficiency of different batches of cell wall-degrading enzymes in the preparation of protoplasts and in some cases can be too low for certain applications.<sup>56</sup>

### 1.4.2.2 Electroporation

This technique is based on the reversible permeabilisation of biological membranes induced by a short duration, high amplitude electric field. The membrane changes that occur during an electric pulse allow the uptake of DNA, which in turn can result in molecular transformation.<sup>50</sup> Electroporation of protoplasts can result in transformation yields as high as 50%. Fromm *et al* found this method to be useful in the transformation of maize protoplasts with a gene encoding for a neomycin phosphotransferase.<sup>57</sup> However, Meyer reported that electroporation was inappropriate for transforming *Aspergillus giganteus* due to the very low transformation yield.<sup>56</sup> This technique is therefore not universally applicable and can only be used for specific species.

### 1.4.2.3 Particle bombardment

This technique involves the introduction of DNA particles into intact cells through the use of high-velocity microprojectiles which are able to penetrate cell walls and membranes.<sup>58</sup> These microprojectiles are typically spherical particles, composed of high

density metals such as tungsten or gold and usually 0.4 – 2.0 µm in diameter. DNA is carried on the surface of the particles. Particle bombardment devices make use of macroprojectiles which can be accelerated to a high speed and thereby able to accelerate the microprojectile which is placed on its surface. Typically macroprojectiles are bullet-like plastic cylinders or a disk-like metallic film. Advantages of this technique include the ability to transform a wide variety of tissue types, it is a rapid and simple procedure and able to transform organelles such as chloroplasts.<sup>59</sup> However, special instrumentation is required and transformation yields are lower when compared to techniques such as electroporation, typically around 5%. For example, Christou and co-workers were able to transform soyabean plants (*Glycine max* L.) using DNA-coated gold particles with a transformation efficiency between 0.1 – 5%.<sup>60</sup>

#### **1.4.2.4 *Agrobacterium tumefaciens***

*Agrobacterium tumefaciens* is a bacteria present in soil, which is able to infect plants and cause crown gall disease.<sup>61</sup> It does this by transferring a particular DNA segment, T-DNA, of the tumour-inducing plasmid (Ti) into the nucleus of the plant cell, whereupon it is incorporated into the genome and transcribed, causing crown gall. T-DNA contains two types of genes: oncogenic genes which are responsible for the tumour formation and genes responsible for the synthesis of opines, compounds formed by the condensation of amino acids and sugars and form the carbon and nitrogen source for *A. tumefaciens*. The ability of *A. tumefaciens* to transfer its DNA into a host plant cell make it an attractive option for plant biotechnology for a number of reasons, including the T-DNA only being transcribed in plant cells not taking part in the transfer process. However, most importantly, any foreign DNA inserted into the T-DNA segment can be transferred to plant cells.<sup>62</sup> There are now a number of vector and bacterial strain systems available for plant transformation.<sup>63</sup>

### **1.5 Reactivity Probes**

#### **1.5.1 Introduction**

To be able to perform directed evolution on a protein, that protein must first be isolated from a cell or complex mixture of proteins. One technique to achieve this makes use of small molecules known as reactivity probes.<sup>64</sup> Reactivity probes consist of three distinct parts: a reactive unit for covalent attachment to the enzyme, a linker unit that may modulate the activity of the reactive group and a tag to allow identification and isolation of modified proteins (See Figure 1.17). Reactivity probes are designed to

interact with active-site residues of proteins resulting in the formation of a stable covalent bond. The following section describes recent advances in the use of reactivity probes, with specific examples highlighted.



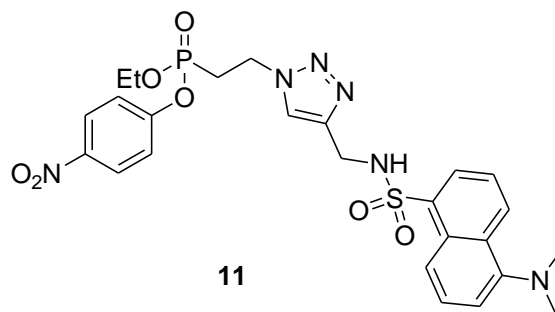
Figure 1.17 Cartoon representation of the general structure of a reactivity probe, which contains a reactive group, linker and tag.

## 1.5.2 Reactive Group

### 1.5.2.1 Mechanism-based reactivity probes

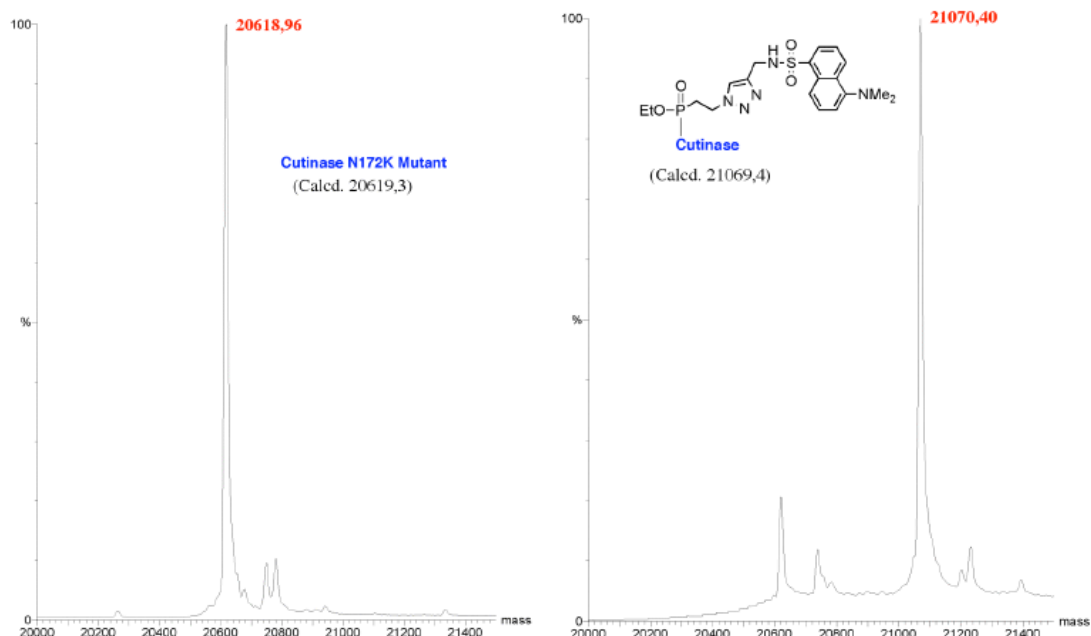
Mechanism-based reactivity probes are the most common class of probes used as the reactive group closely resembles the natural substrate or inhibitor for the enzyme, therefore allowing the synthesis of relatively simple molecules.

Dijkstra used the well known serine hydrolase inhibitor, fluorophosphonate, as the basis for the mechanism-based reactivity probe, **11**.<sup>65</sup> The fluoride leaving group was replaced with a *p*-nitrophenyl group and a dansyl fluorophore was included to allow for easy identification of labelled proteins. Upon reaction of **11** with the enzyme, a yellow colour was observed due to release of the *p*-nitrophenyl group, which allowed the inhibition times to be monitored.



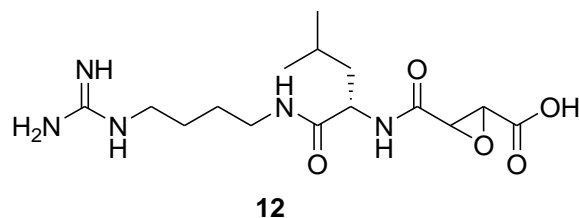
Incubation of **11** with the lipase cutinase, resulted in inhibition of the enzyme, with the rate constant calculated as  $0.13 \text{ min}^{-1}$ . After full inhibition was obtained, monitored by the release of *p*-nitrophenol, the protein-inhibitor constructs were purified and analysed

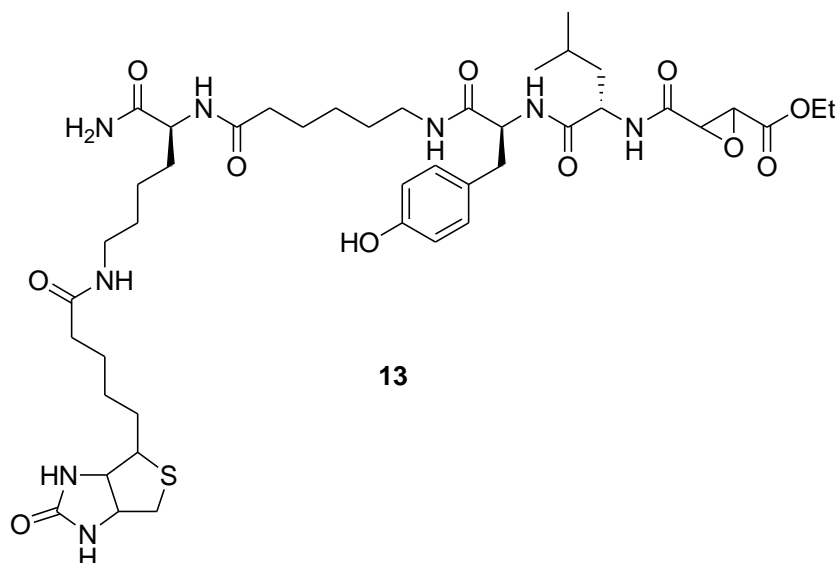
by ESI-MS. Formation of **11**-labelled proteins could be seen: mw(cutinase) = 20619 Da, mw(cutinase-**11**) = 21070 Da (See Figure 1.18).



**Figure 1.18 Formation of 11-labelled proteins: mw(cutinase) = 20619 Da, mw(cutinase-11) = 21070 Da.**  
*Org. Biol. Mol.*, 2008, 6, 523 - Reproduced by permission of The Royal Society of Chemistry

In a similar approach, Bogyo *et al* have been able to monitor cysteine protease activity in a crude protein mixture.<sup>66</sup> **12** has previously been shown to be an inhibitor of cysteine protease activity and this was used as the scaffold for the reactivity probe **13**. The peptide backbone is used as a recognition unit for the enzyme, whilst the electrophilic epoxide reacts with the thiol group of the cysteine residue resulting in a labelled, inactive protein. By making use of the biotin tag, labelled proteins can be visualised following SDS-PAGE/Western blotting with streptavidin-based antibodies.





Incubation of **13** with dendritic cell extracts successfully resulted in protein labelling, as seen by Western blotting, Figure 1.19. A pre-heating control was used and revealed non-specific labelling, with the assumption that denatured proteins modified by **13** represented non-specific modifications. All labelling of proteins in the 20 – 40 kDa region was lost upon heat denaturation, illustrating that enzymatic activity is needed for labelling to occur. This suggested that these bands correspond to major proteases within the cell extract.

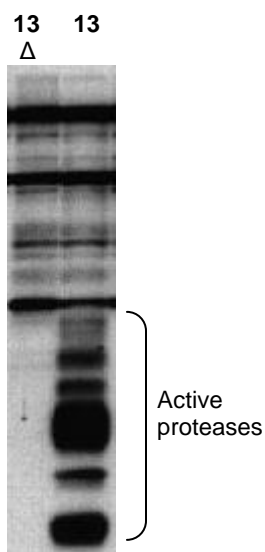
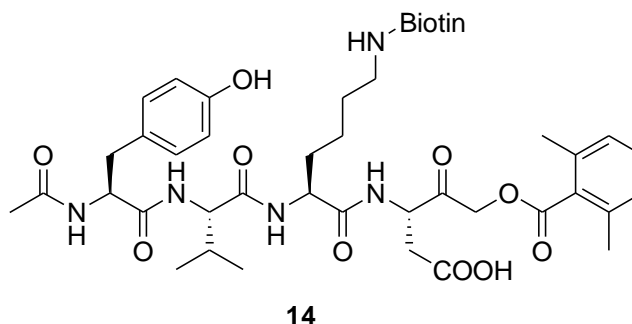


**Figure 1.19 Immunoblotting of dendritic cells incubated with 13. Labelling of active proteases can be seen (20 – 40 kDa range), which was lost upon heat inactivation.** Reprinted from *Chemistry & Biology*, vol 7, Greenbaum D., Medzihradzsky K.F., Burlingame A. and Bogoy M., *Epoxide electrophiles as activity-dependent cysteine protease profiling and discovery tools*, 569-581, Copyright (2000), with permission from Elsevier.

Interleukin-1 $\beta$  converting enzyme (ICE) is a cysteine protease that is responsible for the activation of interleukin-1 $\beta$ , an important mediator of inflammation. ICE is a unique cysteine protease, lacking sequence homology with all other known enzymes in this class. Peptide (acyloxy)methyl ketones are known potent irreversible inhibitors of ICE, with inactivation proceeding *via* expulsion of the aryl carboxylate leaving group to form a thiomethylketone with the active site cysteine. In an effort to isolate ICE, the (acyloxy)methyl ketone reactivity probe **14** was synthesised, which also contained a biotin affinity tag.<sup>67</sup>



THP.1 cells, where ICE levels were less than 0.001% of the total protein, were incubated with **14** (200 nM) for 10 minutes, followed by SDS-PAGE, Western blotting and visualisation by <sup>125</sup>I-streptavidin. Figure 1.20 shows that only one protein was labelled (lane 2), which co-migrates with the affinity-purified ICE (lane 1). Labelling could be completely prevented by including the potent aldehyde inhibitor, Ac-Tyr-Val-Ala-Asp-CHO, in the reaction mixture (lane 3), indicating that an active enzyme is needed for effective labelling to occur.

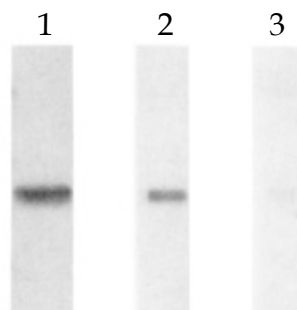
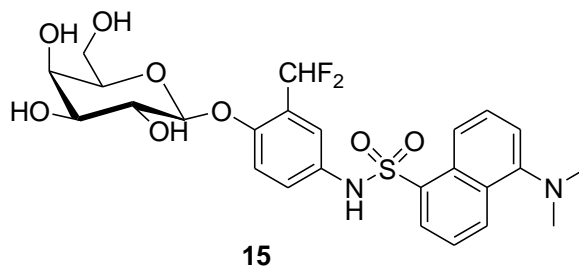


**Figure 1.20** Labelling of ICE protein visualised by <sup>125</sup>I-streptavidin. Lane 1 - purified ICE, lane 2 - ICE labelled with **14**, lane 3 - inhibition of labelling by treatment with ICE inhibitor. Reprinted with permission from *Biochemistry*, 1994, 33, 3934-3940. Copyright (1994) American Chemical Society

### 1.5.2.2 Suicide-based reactivity probes

This class of probes is similar to the mechanism-based reactivity probes in that a reaction relies on an active enzyme, which is able to react with the reactive group of the probe. However, this class contain a masked electrophile, which is only uncovered when the enzyme has reacted with a different part of the probe. One such example of a suicide-based probe is the  $\beta$ -galactosidase probe **15**.<sup>68</sup>



Upon reaction of **15** with the enzyme, the  $\beta$ -galactose unit is hydrolysed from the probe, with the postulated release of HF. The highly electrophilic intermediate then reacts with a nucleophilic residue in close proximity to the active site, yielding a fluorescently tagged protein. Isolation of the protein was achieved by initial protease digestion and subsequent elution of the peptides from an antidansyl antibody column. MALDI TOF/TOF analysis allowed the identification of the exact modified residue, which was shown to be arginine.

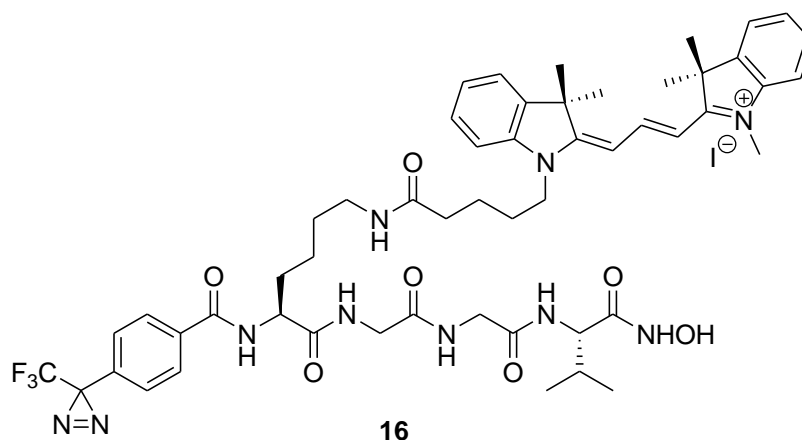
### 1.5.2.3 Affinity-based reactivity probes

A major difference between affinity-based probes and probes such as **13**, **14** and **15**, described previously, is that fact that the former do not require an active enzyme for modification. This class of probes contain a group which has a high affinity for the enzyme but is not modified by it. Subsequent cross-linking of these probes to the protein is achieved by the presence of a group which, after treatment by either chemical or photochemical means, generates a highly reactive intermediate such as a carbene or a nitrene. These species are able to react with a residue within the protein resulting in a covalent link. The reaction is relatively indiscriminate with a wide range of chemical groups and therefore able to react with a much larger number of amino acids than the electrophilic suicide labels which generally react with nucleophilic residues.

Yao *et al* have utilised this class of reactivity probes in the isolation of metalloproteases.<sup>69</sup> These enzymes are able to hydrolyse peptide bonds by the



interaction of a catalytic zinc(II) ion coordinated to three amino acid residues, usually His and Glu, and a water molecule. During hydrolysis the tetrahedral peptide intermediate formed is coordinated to the zinc but not covalently bound to the enzyme and as such no mechanism-based irreversible inhibitors are known. Consequently the development of mechanism-based reactivity probes is very challenging. By making use of the zinc binding group hydroxamic acid, the affinity-based probe **16** was designed. Diazirine was chosen as the photolabile group, which upon irradiation at 360 nm, cleaves to form a triplet carbene that is able to insert into any C-H bonds close by. In addition, the fluorophore Cy3 was used as a fluorescent tag to allow for easy identification of labelled metalloproteases.



Using thermolysin, a bacterial 35 kDa extracellular endopeptidase, as a model metalloprotease optimisation of the enzyme labelling conditions was performed. It was found that an optimum level of labelling could be achieved with 500 nM **16**. Above this concentration nonspecific labelling occurred. In addition, irradiation times were also investigated. No labelling was seen in the absence of UV, indicating that photolysis is essential for protein labelling, Figure 1.21.

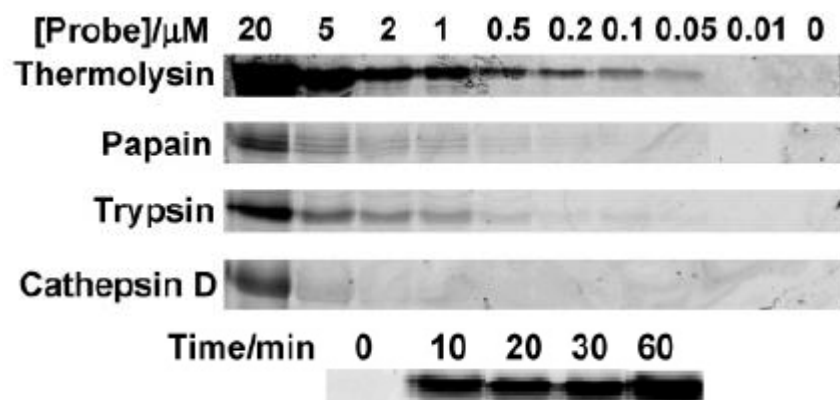


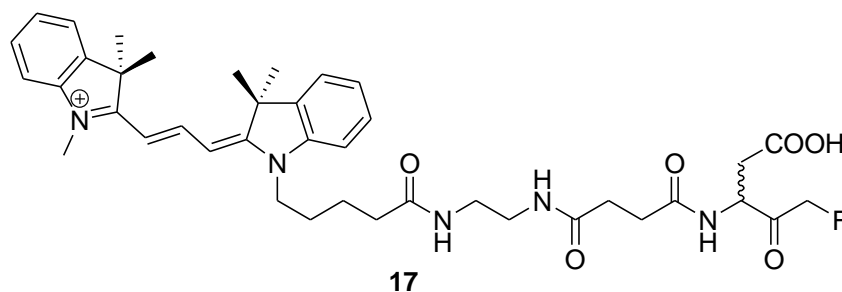
**Figure 1.21** Fluorescence image of SDS-PAGE gel showing that the optimum level of labelling of thermolysin was 500 nM. In addition, no labelling was seen in the absence of UV. Reprinted with permission from *Journal of the American Chemical Society*, 2004, 126, 14435-14446. Copyright (2004) American Chemical Society

Incubation of **16** with yeast cell lysates containing several known metalloproteases, resulted in fluorescent labelling of these proteins as visualised by SDS-PAGE analysis, highlighting the applicability of this class of probes in the isolation of metalloproteases.

### 1.5.3 Linker unit

The linker unit of the reactivity probe connects the reactive unit to the tag (See Figure 1.17) and serves several purposes in the overall probe design. In many cases, it simply provides space between the reactive unit and the tag and often takes the form of an alkyl or PEG chain. An alkyl chain brings about hydrophobicity to a probe, thereby enabling entry into a cell, whereas a PEG chain can confer solubility to hydrophobic probes in aqueous environments.<sup>70</sup>

The linker can also contain specificity elements that target the probe towards a particular class of enzymes. This is commonly seen in the form of peptide structures, particularly in probes which are designed to isolate proteases. In one such example, probe **17** was used to isolate a class of protease known as caspases.<sup>71</sup> These enzymes are involved in apoptosis pathways. Fluoromethylketone-containing peptides are known to covalently react with the active site residues of caspases and the linker unit was used to direct the specificity of the probe towards individual caspases. A linker unit consisting of a simple alkyl chain was chosen, which was approximately the length of the tripeptide sequence in a typical caspase inhibitor but at the same time will not impose any specificity upon a particular caspase. By using this simple linker unit, probe **17** was able to efficiently react with caspase enzymes, yielding a fluorescently tagged protein.



In order to test the selectivity of **17** towards caspase, three other non-caspase proteases were used as controls and analysed at the same time. Figure 1.22 shows that only caspase was labelled by **17** following incubation for 30 minutes. In addition, inactivation of caspase by heat, followed by incubation with **17** resulted in no labelled protein seen, therefore indicating that enzymatic activity is required for labelling to occur. Other linkers may be chosen when needed to fine-tune the specificity of the probes against their targeting enzymes.

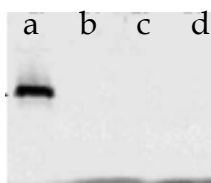
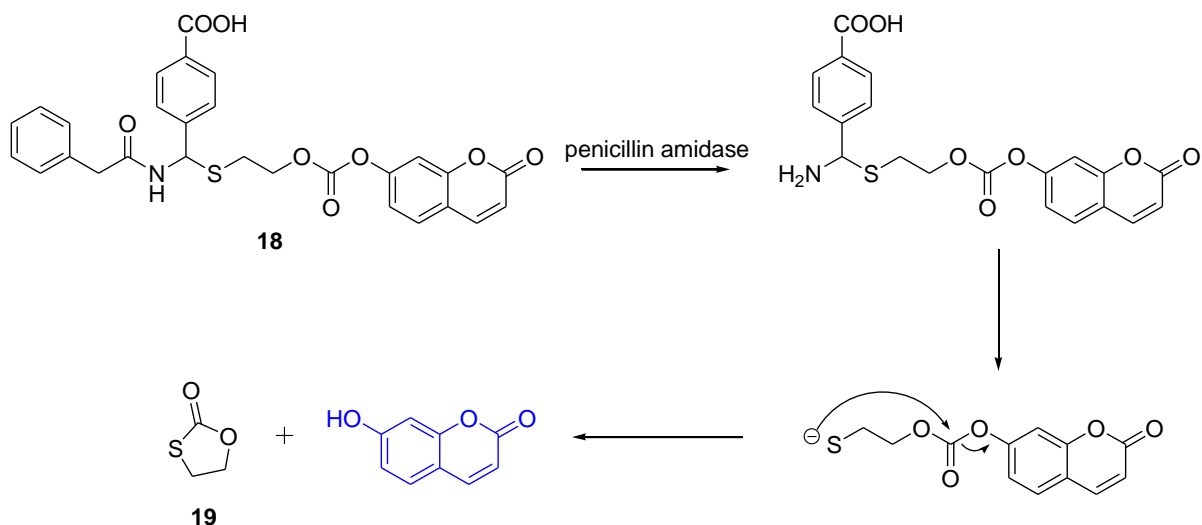


**Figure 1.22** Fluorescence image of SDS-PAGE gel showing specificity of **17** towards the caspase enzyme. a) caspase-1, b) papain, c) chymopapain, d) bromelain. Reprinted from *Tetrahedron Letters*, vol. 44, Zhu Q., Huang X., Chen G.Y.J. and Yao S.Q., *Activity-based fluorescent probes that target phosphatases*, 1043-1046, Copyright (2003), with permission from Elsevier

As well as bringing substrate specificity, linker units can also assist in the breakdown of the probe. The penicillin amidase probe, **18** contains a *N*-acylhemithioaminal linker, which upon enzymatic cleavage of the phenylacetamide moiety, self-cyclises to form **19** with concomitant release of umbelliferone, Scheme 1.6.<sup>72</sup> Incubation of **18** with penicillin G amidase resulted in an increase in fluorescence at 460 nm, indicating the cleavage of carboxamide group and generation of free umbelliferone (See Figure 1.23).



**Scheme 1.6** Upon reaction with penicillin amidase the self-immolative linker breaks down causing release of methylumbelliferone fluorophore

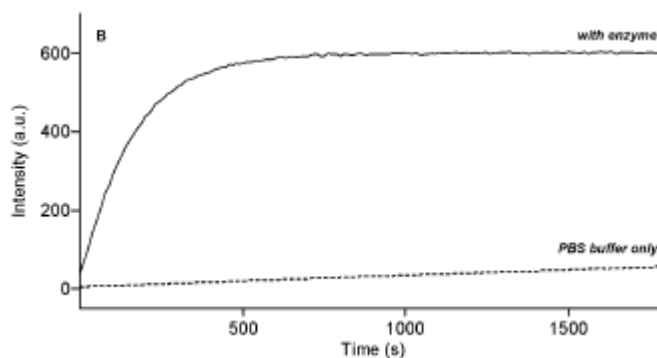


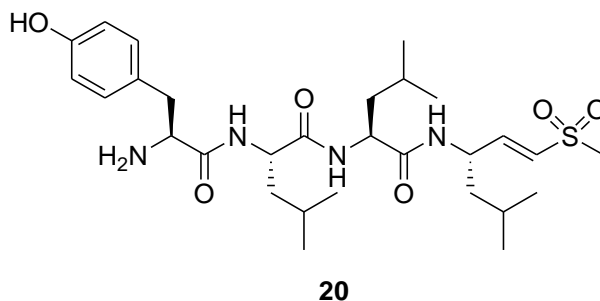
**Figure 1.23** Fluorescence emission of 18 incubated with penicillin G amidase at 460 nm. Reprinted with permission from *Organic Letters*, 2008, 10, 1517-1520. Copyright (2008) American Chemical Society

## 1.5.4 Isolation/identification tag

### 1.5.4.1 Isotope tags

Isotope tags are commonly used to monitor biological processes as they require minimal equipment for production, provide a very sensitive signal with low background and are easy to detect using simple autoradiography methods. The radioisotope  $^{125}\text{I}$  is often used due to its relatively small size, which results in minimal modification of the parent inhibitor and has been used to study proteasome activity in living cells.<sup>73</sup> Mammalian proteasomes have been shown to contain three distinct catalytic subunits ( $\beta_1$ ,  $\beta_2$  and  $\beta_5$ ). In addition to this, upon exposure to  $\gamma$ -interferon another set of catalytic subunits are expressed ( $\beta_{1i}$ ,  $\beta_{2i}$  and  $\beta_{5i}$ ). These new subunits form a new particle, the immunoproteasome. Each of these catalytic subunits has slightly

different substrate specificities, which makes activity profiling difficult to achieve. Tetrapeptide vinyl sulfones, such as **20**, are known proteasome inhibitors and studies using fluorogenic derivatives have indicated differences in the catalytic subunits. However, studies with natural protein substrates have shown a more complicated cleavage preference, with considerable overlap seen.



Using probes based on the structure of **21**, which have been extended at the N-terminus and include a  $^{125}\text{I}$  tag for identification, inhibition is enhanced. In addition to this, subunit specificity is largely unseen, which reflects the extensive overlap seen with *in vitro* protein degradation, Figure 1.24.

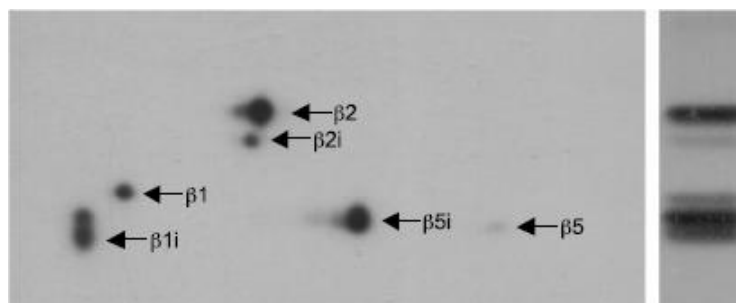
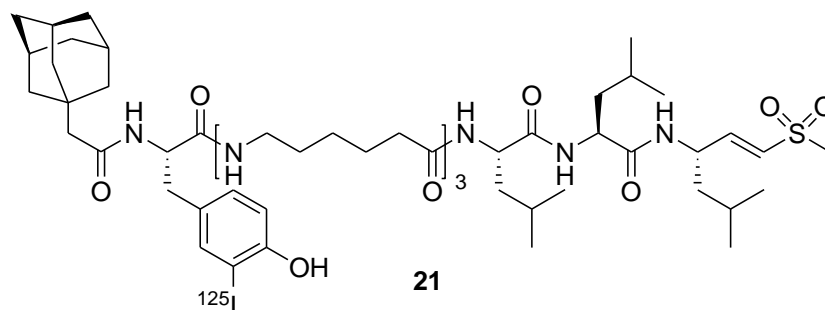


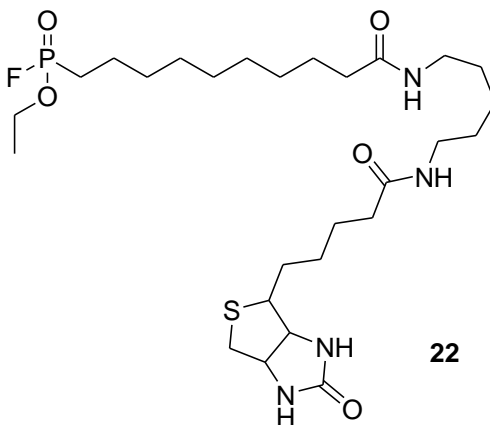
**Figure 1.24** 1D and 2D SDS-PAGE analysis of EL-4 lysate labelled with **21** showed that most proteasomal subunits were labelled equally well. Reprinted from *Chemistry & Biology*, vol. 8, Kessler B.M., Tortorella D., Altun M., Kisselev A.F., Fiebigler E., Hekking B.G. Ploegy H.L. and Overkleeft H.S., *Extended peptide-based inhibitors efficiently target the proteasome and reveal overlapping specificities of the catalytic  $\beta$ -subunits*, 913-929, Copyright (2001), with permission from Elsevier.

Although radiolabelling offers advantages there are several disadvantages associated with its use. These include the relatively short half-life of  $^{125}\text{I}$  (57.4 days<sup>74</sup>), which means probes cannot be stored for long periods of time and require more care in handling. Also, these tags offer no direct means to isolate labelled proteins and therefore most radiolabelled probes are used for profiling known protein targets.

#### 1.5.4.2 Affinity tags

In an effort to overcome the limitations of radioisotopes, affinity tags are often used as this enables the isolation of labelled proteins. Biotin is the most commonly used affinity tag in reactivity probes, with numerous publications documenting its use. Isolation of a biotin-labelled protein makes use of the strong affinity of biotin towards the protein streptavidin, having an association constant of  $\sim 10^{15}$  mol/L.<sup>75</sup> Various methods are used which include elution columns containing streptavidin-coated beads and ELISA methods.

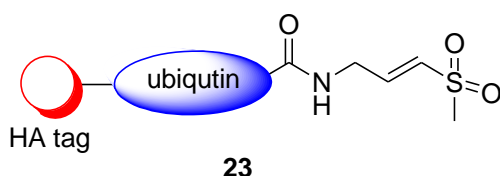
A biotinylated fluorophosphonate, **22** was used to isolate serine hydrolases from a crude protein mixture.<sup>76</sup> Soluble fractions of rat testis were incubated with **22** and following SDS-PAGE/Western blotting analysis, more than 10 labelled proteins were detected. Importantly, heating of the protein sample to 80 °C for 5 minutes before treatment with **22** blocked nearly all protein labelling, indicating that this probe reacts with serine hydrolases in an activity-dependent manner.



However, there are disadvantages to the use of biotin. It has a low cell permeability and therefore cannot be used *in vivo*, restricting its applications to *in vitro* experiments to isolate targets from cell or tissue extracts. Although, the biotin-streptavidin affinity system makes the isolation of biotin-labelled proteins relatively easy, it is often bound

so tightly that elution requires harsh conditions that release non-specific, unlabelled background proteins.

As an alternative to biotin, short peptide sequences that recognise specific antibodies can be used as an affinity tag. This form of tag was used to isolate deubiquitinating enzymes (DUBs), which form part of the ubiquitin-proteasome system.<sup>77</sup> The use of the hemagglutinin (HA) tag as part of the reactivity probe **23** allowed identification and isolation of a tagged DUB following treatment with a HA-antibody during SDS-PAGE/Western blotting techniques.



Although this technique allows for selective detection of labelled proteins, the peptide tags are often large and generally block cell permeability of the probe.

#### 1.5.4.3 Fluorescent tags

Fluorescent tags make use of small molecule fluorophores which allow for direct imaging of labelled proteins and ease of detection in gel-based analysis. There is a large diversity of commercially available fluorophores which have a wide range of structural and photophysical properties, increasing the scope for their use in reactivity probes.<sup>78</sup>

There are a huge number of examples in the literature of fluorescent reactivity probes. In an extension to the work on cysteine proteases using the biotinylated probe, **13**, several fluorescent probes, **24** - **27** were synthesised.<sup>79</sup> Following incubation of **24** - **27** with total rat liver homogenate four different cysteine proteases were labelled, as could be seen in the SDS-PAGE gels, Figure 1.25. These BODIPY based probes were shown to be cell permeable and able to selectively isolate cysteine proteases *in vivo*, which represents an advantage over the biotin-based probe **13**, Figure 1.26a and b.

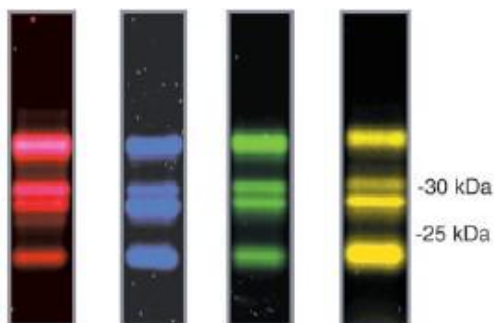
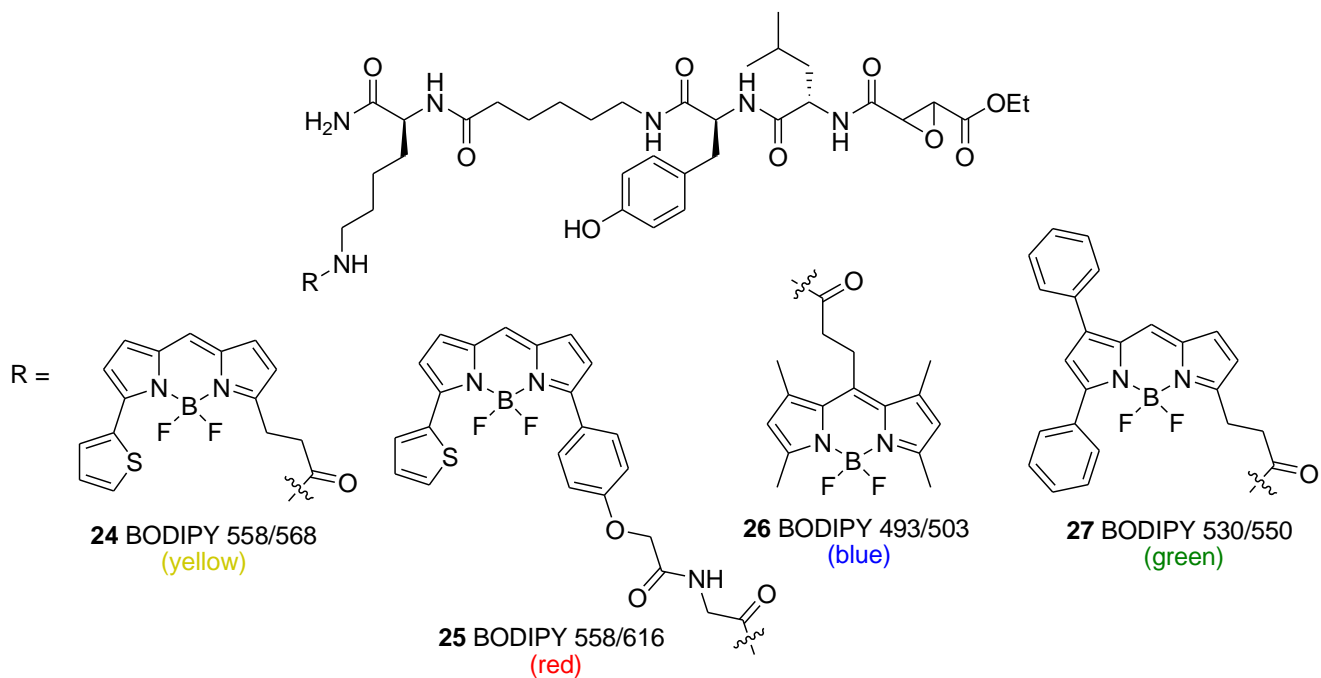


**Figure 1.25** All four BODIPY probes labelled all proteins, with only slight differences in intensity seen. Copyright © 2002, by the American Society for Biochemistry and Molecular Biology

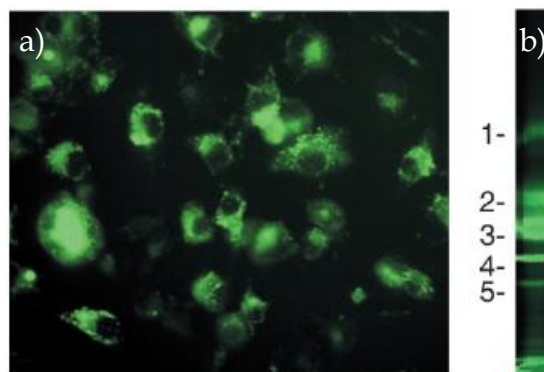


**Figure 1.26** a) shows HeLa cells incubated with 27. These cells were then homogenised and the resulting suspension was analysed using SDS-PAGE. b) The gel revealed a number of proteases had been labelled by 27, indicated by numbers 1 – 5. Copyright © 2002, by the American Society for Biochemistry and Molecular Biology



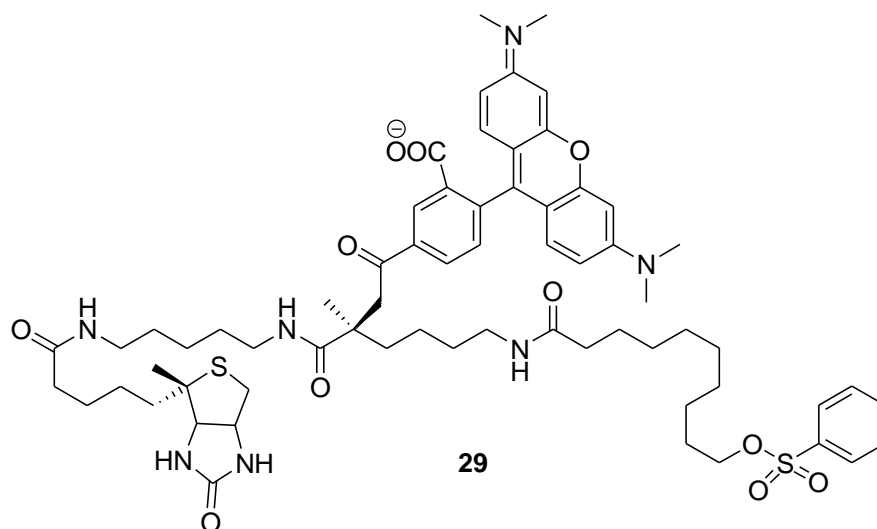
The extremely high sensitivity of fluorescent tags is exemplified by the serine hydrolase probe **28**, in which detection levels were as low as 100 attomolar.<sup>80</sup> Purified fatty acid amine hydrolase (FAAH) was incubated with **28**. Serial dilutions were performed and these were analysed using SDS-PAGE, with fluorescent bands seen at extremely low concentrations, Figure 1.27



**Figure 1.27 SDS-PAGE analysis showing the low attomolar levels of detection of FAAH using **28**.**

Patricelli M.P., Giang D.K., Stamp L.M. and Burbaum J.J. Direct visualisation of serine hydrolase activities in complex proteomes using fluorescent active site-directed probes, *Proteomics*, 2001, **1**, 1067-1071. Copyright Wiley-VCH Verlag GmbH & Co. KGaA. Reproduced with permission.

To combine the advantages of both affinity and fluorescent tags would result in a probe which, upon protein labelling, would result in a high level of detection sensitivity and ease of isolation. **29** is an example of such a probe, in which both biotin and rhodamine are used.<sup>81</sup>



This probe was utilised in the isolation of a membrane-associated protein, 3 $\beta$ -hydroxysteroid dehydrogenase/ $\Delta$ 5-isomerase-1 (3HSD1), which is an NAD<sup>+</sup> dependent integral membrane protein found predominately in the adrenal glands and gonads. Following treatment of rat testis with **29** and solubilisation using Triton X-100 the membrane proteins were separated using Q chromatography. Fluorescence imaging of the resulting gel, revealed a band at 40 kDa (See Figure 1.28). Those fractions containing this protein were pooled and enriched using a streptavidin column. MALDI mass spectrometry revealed the identity of the protein to be that of 3HSD1.



**Figure 1.28** Fluorescence image of SDS-PAGE gel showing band corresponding to 3HSD1 at 40 kDa.  
 Copyright © 2002, by the American Society for Biochemistry and Molecular Biology

### 1.5.5 Bio-orthogonal labelling

Despite the many advantages offered by both biotin and fluorophores in the detection and isolation of protein targets, there are disadvantages to their use, in particular the often large, sterically hindered molecules used. This may impede not only the cellular uptake, but also reduce their affinity for certain protein targets. In an effort to overcome these problems, strategies have been developed in which the tag of the reactivity probe has been replaced by a surrogate tag. Once protein labelling has occurred, it is then reacted with either biotin or a fluorophore by a bio-orthogonal ligation reaction, resulting in labelled protein targets that can be isolated or visualised, See Figure 1.29.

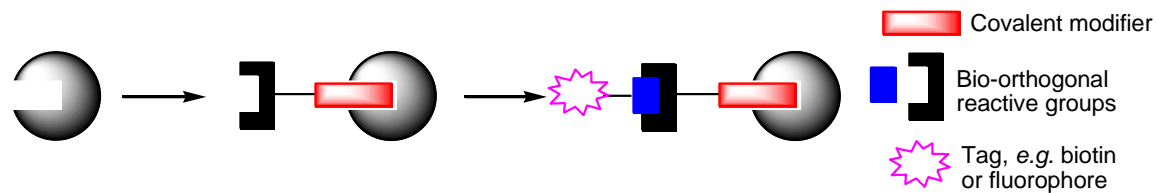


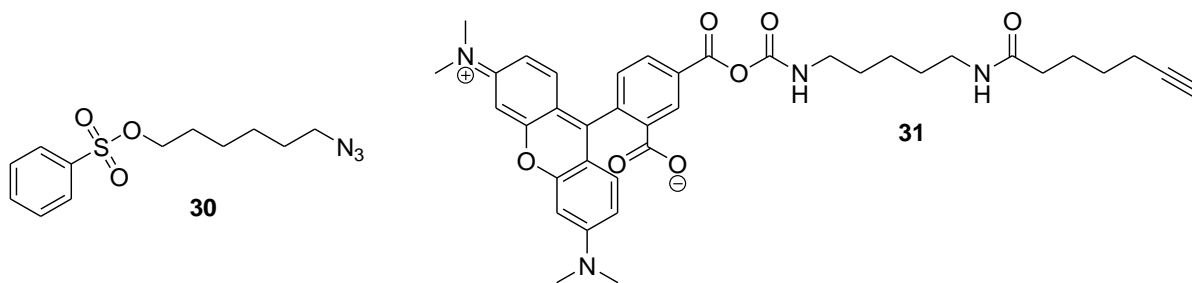
Figure 1.29 Cartoon representation of reactivity probes utilising bio-orthogonal labelling

The most commonly used bio-orthogonal labelling strategy employs the Cu-catalysed [3+2] azide-alkyne cycloaddition, which has been termed 'click chemistry'.<sup>82</sup> In this approach, the tag is replaced with either an azide or alkyne group. In the ligation step, a chemically modified tag which is coupled to either an alkyne or azide, is used to produce a 1,4-disubstituted triazole that connects the probe-labelled protein to the reporter tag. The overall reaction can be seen in Scheme 1.7.



Scheme 1.7

Bio-orthogonal click-chemistry has been used to isolate the enzyme enoyl CoA hydratase (ECH-1).<sup>83</sup> By using an azide-derivatised phenyl sulfonate, **30** and an alkyne-rhodamine tag, **31**, ECH-1 was isolated both *in vitro* and *in vivo*. See Figure 1.30. The labelling was shown to be heat sensitive, indicating that enzyme activity is vital for protein labelling. In addition, no labelling was seen in the absence of CuSO<sub>4</sub>.



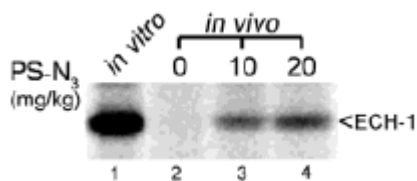
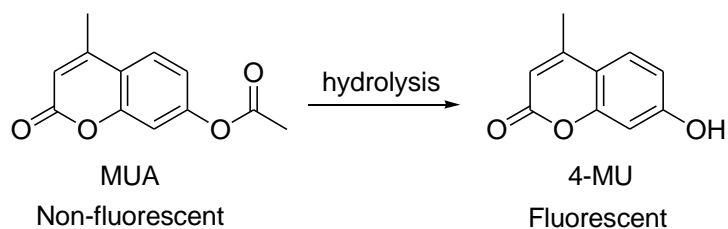


**Figure 1.30 Labelling of ECH-1 in mice.** The phenyl sulfonate-azide probe was administered to mice (0, 10, 20 mg/kg; i.p.) and after 1 hr the animals were sacrificed and heart tissue removed and analysed following reaction with the alkyne-rhodamine tag. The *in vitro* lane shows labelling of ECH-1 in mouse heart homogenate. Reprinted with permission from *Journal of the American Chemical Society*, 2003, 125, 4686-4687. Copyright (2003) American Chemical Society

## 1.6 Project Aims

Work undertaken within the group has shown that flow cytometry can be used to sort plant protoplasts performing specific biotransformations.<sup>84</sup> Using the cell viability stain methylumbelliferyl acetate (MUA), the activity of endogenous esterases was visualised through the hydrolysis of MUA to the fluorescent molecule, 4-methylumbelliferone (4-MU), Scheme 1.8.



**Scheme 1.8**

Subsequent transformation of the gene encoding for the esterase *AtSFGH* which contained a single point mutation (Cys59Ser) was attempted using PEG-mediated methods. Despite transformation levels being as low as 5%, cells remained viable and did not clump together as was seen when electroporation techniques were employed. *AtSFGH* is not inhibited by the organofluorophosphonate paraoxon<sup>85</sup> and therefore in order to abolish all background esterase activity, cells were treated with 1 mM paraoxon prior to incubation with MUA. Following this treatment, a population of 400,000 wild-type cells was spiked with 8,000 *atsfgh(C59S)*-expressing cells and the total suspension was sorted based on 4-MU fluorescence. A population which exhibited approximately 10-fold greater fluorescence was observed (Figure 1.31) and a sample of cells from populations 1 and 2 were collected.

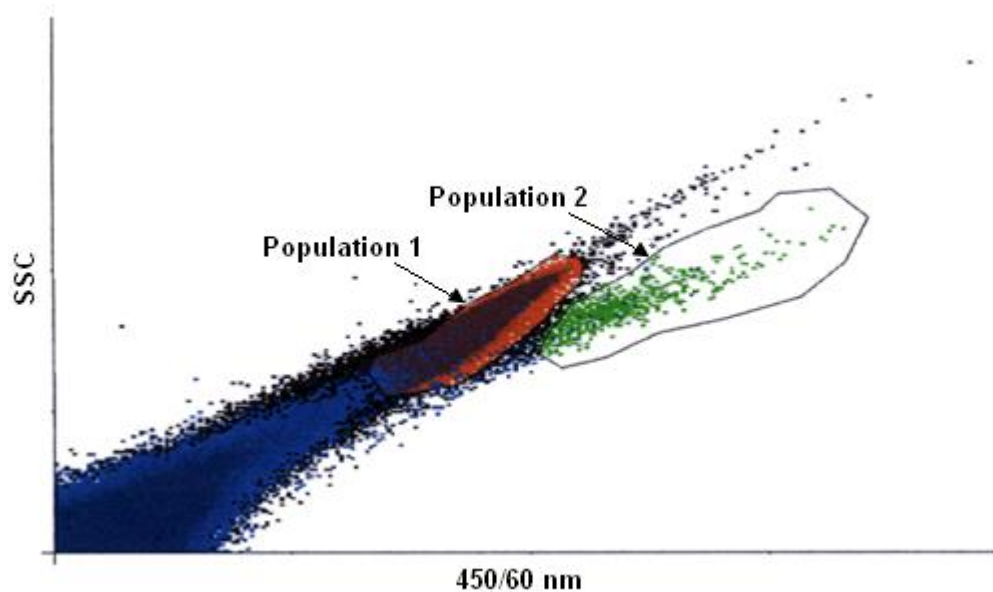


**Figure 1.31** Flow cytometry analysis of *atsfgh(C59S)*-expressing cells showing population 2 which exhibited increased fluorescence

Analysis of the cells collected from population 2 was undertaken with PCR using primers directed to the start and end of the *atsfgh* sequence. After 20 cycles of amplification an 800-bp product was present, which was absent from population 1 (See Figure 1.32). Sequencing confirmed the band at 800-bp to be that of the *atsfgh* mutant. However, no intact protoplasts were recovered from the sorting.

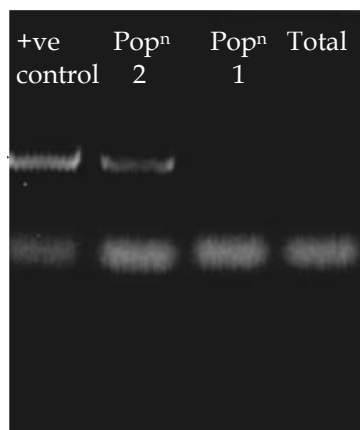


**Figure 1.32** PCR analysis showing the present of *atsfgh* only in population 2

This work by Cummins has shown that methylumbelliferyl esters can be utilised as probes for esterase activity with the subsequent activation of fluorescence being detected by FACS. However, a number of areas remained to be investigated:

1. The synthesis of profluorescent, methylumbelliferyl-based probes of *AtSFGH*, expanding the library of compounds to include amino acid derivatives, with the aim of synthesising a probe capable of selecting an optimised esterase.
2. The development of random mutagenesis techniques towards the directed evolution of *AtSFGH* and another esterase enzyme, *AtCXE12*.
3. The improvement of FACS screening protocols to enable the successful isolation and sorting of individual protoplasts.
4. The synthesis of reactivity probes based on phenylacetylene and BODIPY fluorophores to isolate biotransformation enzymes such as oxidative cytochrome p450.

This thesis now describes research involving the synthesis of novel profluorescent reactivity probes used for the isolation of specific enzymes, directed evolution experiments to enable the optimisation and/or alteration of the wild type activity and the subsequent screening using FACS techniques. Chapter 2 begins with approaches towards the synthesis of probes to be used for the directed evolution of the esterase enzyme *AtSFGH*.

## **2 STUDIES TOWARDS THE DIRECTED EVOLUTION OF ESTERASES**

This chapter details the work undertaken in the broad area of directed evolution and in particular the studies undertaken on two enzyme systems, *AtSFGH* and *AtCXE12*. The aim of this work was to utilise mutagenesis methods to produce and select a variant enzyme with desired properties. Work undertaken on *AtSFGH* will be discussed first, followed by the results obtained with *AtCXE12*.

### **2.1 S-Formylglutathione Hydrolase**

#### **2.1.1 Introduction**

This section will deal with S-formylglutathione hydrolase (SFGH), one of the enzyme systems of interest, to which the technique of directed evolution will be applied. It will cover aspects of its role in nature and recent developments in both its cloning and characterisation.

Formaldehyde is a toxic compound that plant cells encounter either as an atmospheric pollutant or as a product of endogenous demethylating reactions. In order to prevent its accumulation to phytotoxic concentrations, formaldehyde is rapidly chemically coupled to glutathione (GSH) to form S-hydroxymethylglutathione. This resulting compound is subsequently oxidised by the action of a glutathione-NAD-dependent formaldehyde dehydrogenase (FMDH) to form the thioester S-formylglutathione, **32**. The activity of S-formylglutathione hydrolase (SFGH) regenerates GSH and renders formate available to the  $C_1$  pathway.<sup>86</sup>  $C_1$  metabolism is essential in plants and supplies the  $C_1$  units needed for the synthesis of proteins, nucleic acids and many methylated compounds. The role of SFGH is therefore crucial in formaldehyde detoxification and recycles GSH, thereby preserving the pool of this detoxification compound (See Figure 2.1). This discussion focuses solely on plants, although it is worth noting that GSH is ubiquitous in all living cells.

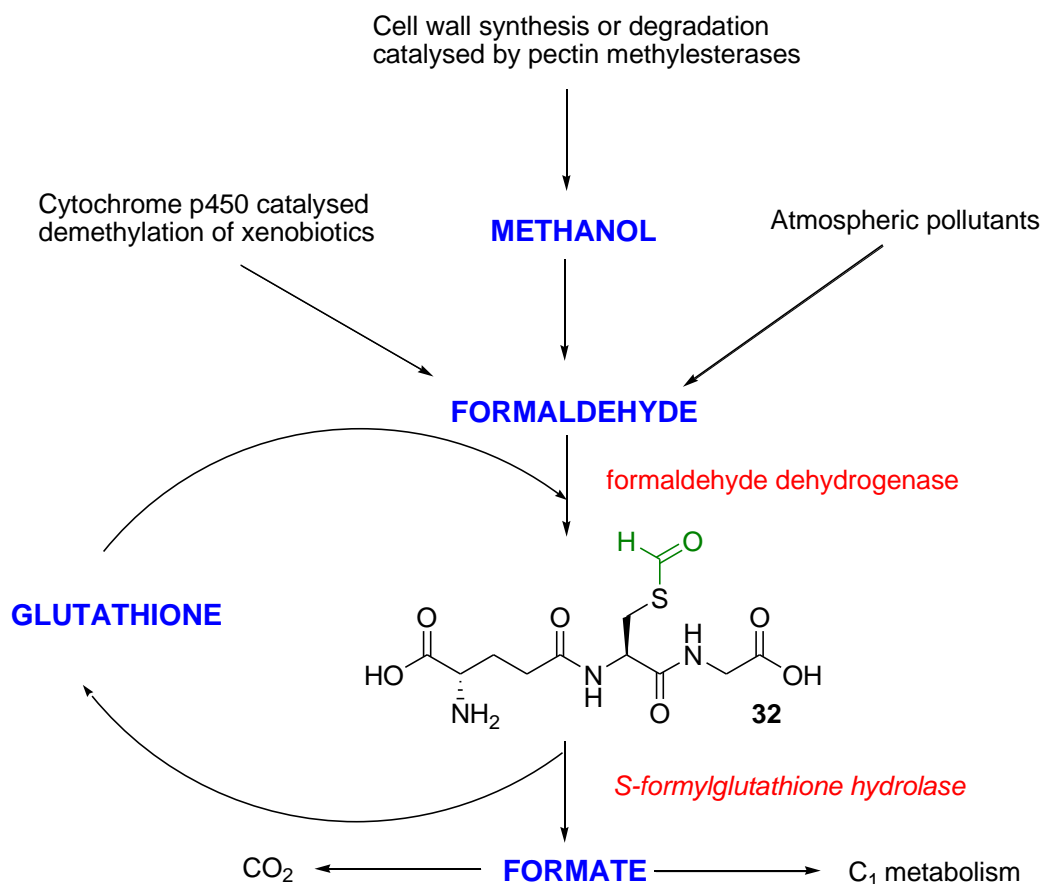
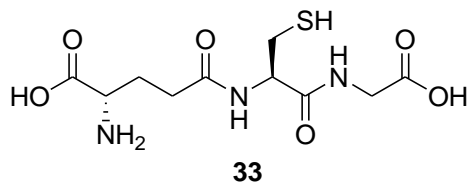


Figure 2.1 Detoxification pathway of formaldehyde using SFGH

Glutathione (GSH), **33**, is a tripeptide consisting of  $\gamma$ -glutamyl-cysteinylglycine and is the major source of non-protein thiol in most plant and mammalian cells. It is synthesised from standard amino acids in two steps.  $\gamma$ -Glutamyl-Cys synthetase combines Glu and Cys in an ATP-dependent reaction to form  $\gamma$ -glutamyl-Cys, with a second enzyme, glutathione synthetase, catalysing the ATP-dependent reaction between  $\gamma$ -glutamyl-Cys and Gly to generate GSH.<sup>87</sup>



The nucleophilic character of the thiol group is important in the formation of disulphide bonds with cytotoxic electrophilic species. This is particularly important in detoxification processes within the cell. A class of enzymes known as glutathione S-



transferases (GST) mediate the reaction between GSH and any xenobiotics present, exporting the GSH-conjugate product into the vacuole.<sup>88</sup> The thiol group has a redox potential of -0.24 V at pH 7, which allows it to act as an electron acceptor and donor for many biological reactions. Along with this reactivity, its relative stability and high water solubility make GSH an excellent molecule in the protection of plants against oxidative stress and certain endogenous and exogenous chemicals. Mutation studies by Xiang *et al* have shown that GSH is essential in protecting plants from heavy metal toxicity.<sup>89</sup>

## 2.1.2 Enzymology

### 2.1.2.1 Characterisation of SFGH

SFGH was first studied in humans and termed esterase D.<sup>90</sup> This enzyme hydrolyses glutathione esters, particularly s-formylglutathione, and was found to have high activity towards methylumbelliferone esters. The human form also has sialic acid O-acyl esterase activity. It has been shown that SFGH in both humans and *E. coli* is highly conserved, with the formaldehyde detoxification pathway also conserved in prokaryotes and eukaryotes.<sup>91</sup>

Edwards and co-workers have studied SFGH in the plant *Arabidopsis thaliana* and found a single SFGH-like sequence. *At*SFGH has previously been cloned and characterised from *Arabidopsis thaliana* and it has been shown that the purified recombinant enzyme was a dimer composed of 31-kDa subunits.<sup>92</sup> Inhibition studies using 1 mM *N*-ethylmaleimide, a compound which alkylates sulfhydryl groups, has shown that a thiol group is essential for hydrolytic activity. Supporting evidence for this finding was shown in further inhibition studies using metal ions which bind to SH groups, such as 0.01 mM CuCl<sub>2</sub> and 0.01 mM ZnSO<sub>4</sub>, which reduced catalytic activity by 90 and 50% respectively. Esterase activity towards *p*-nitrophenylacetate (*p*NPAc), the model substrate used in their experiments, was unaffected by 1 mM phenylmethylsulfonyl fluoride, (PMSF) an inhibitor of catalytic serine residues.

SFGH has previously been cloned from human tissues<sup>93</sup> and shown to be identical to a non-specific carboxylesterase, which exhibited high activity towards 4-methylumbelliferone acetate (4-MUA). Kordic assessed *At*SFGH esterase activity against various substrates and using  $k_{cat}/K_m$  calculations determined the order of

substrate preference to be 4-MUA, closely followed by S-formylglutathione and S-acetylglutathione (See Table 2.1).

Substrate	Specific activity (nkatmg <sup>-1</sup> )	K <sub>m</sub> (mM)	v <sub>max</sub> (nkatmg <sup>-1</sup> )	k <sub>cat</sub> /K <sub>m</sub> (mM <sup>-1</sup> s <sup>-1</sup> )
s-formylglutathione	174	0.13	219	46
s-acetylglutathione	242	0.15	311	133
<i>p</i> -nitrophenyl acetate	95	1.02	185	2.9
α-naphthyl acetate	254	0.57	350	14
β-naphthyl acetate	21	0.54	22	1.3
Fluorescein diacetate	2	0.03	3	2.3
4-methylumbelliferyl acetate	605	0.12	714	158

**Table 2.1** Hydrolysing activities of the purified recombinant *AtSFGH* cloned from *Arabidopsis thaliana*

Recent studies have resulted in the crystallisation of *AtSFGH* and enabled detailed active site data to be gained. These studies show *AtSFGH* to be a serine hydrolase containing a classical Ser-His-Asp triad. In addition, a non-catalytic cysteine (Cys59) is located a short distance from this triad which regulates enzyme activity *in vitro* through a gatekeeper role. Importantly mutation of this residue to Ser allows a wider range of substrates to be accepted by this enzyme (See Figure 2.2 and Figure 2.3).<sup>85</sup>

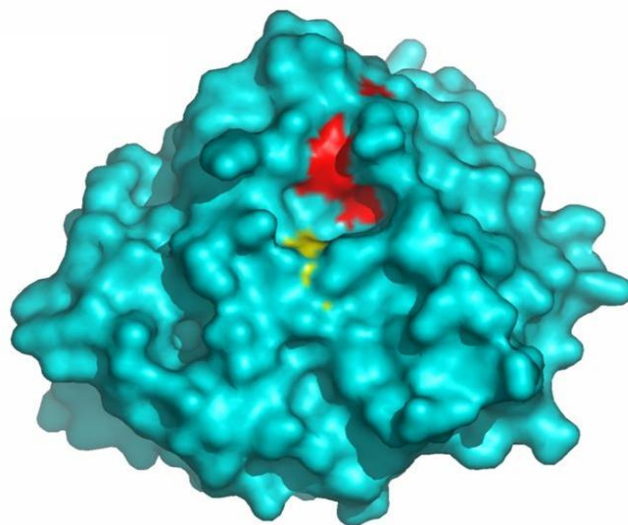


Figure 2.2 X-ray crystal structure of *AtSFGH*.<sup>94</sup> Ser-His-Asp are coloured red, Cys59 is coloured yellow.

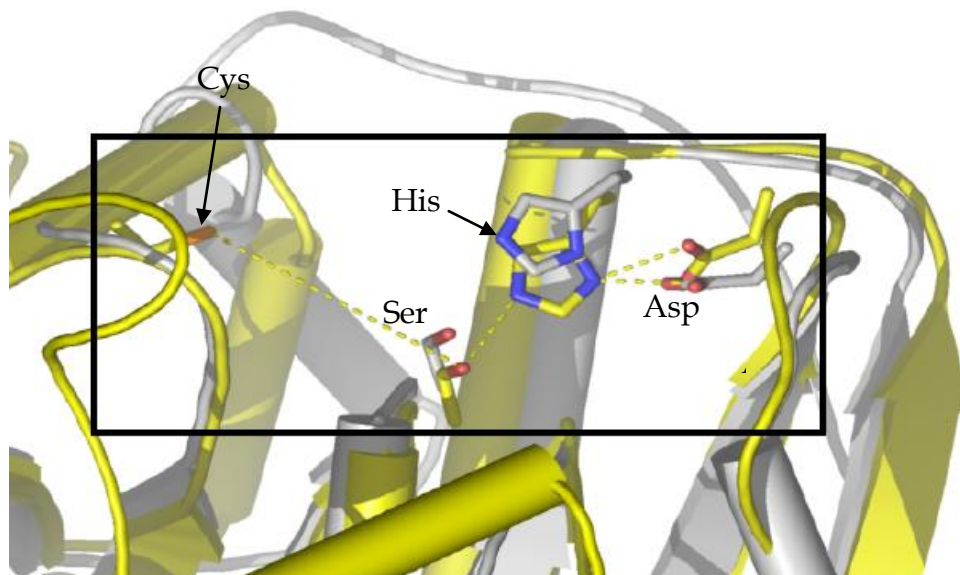
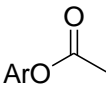
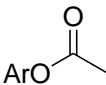
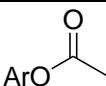
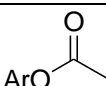
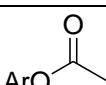
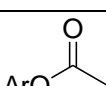
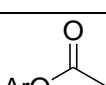
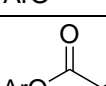
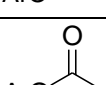
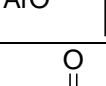
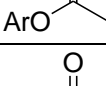
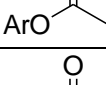


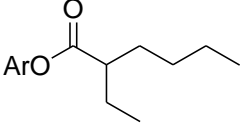
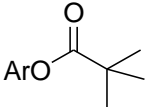
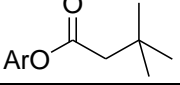
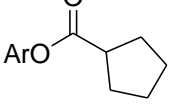
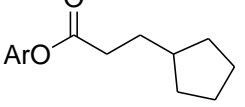
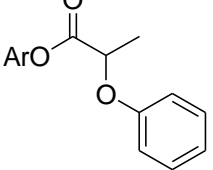
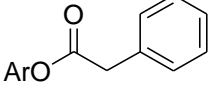
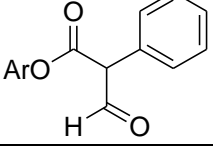
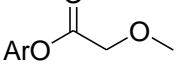
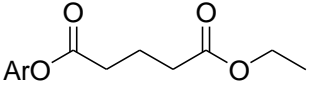
Figure 2.3 *AtSFGH* active site showing Cys, His, Ser and Asp residues

### 2.1.2.2 Substrate Mapping

Previous work within the group involved the production of a library of methylumbelliferyl probe substrates based on simple alkyl esters. These compounds were synthesised using standard chemistry techniques by the reaction of the appropriate acyl chloride with 4-MU.<sup>95</sup> Each substrate was screened against the *AtSFGH*-C59S mutant allowing a model of the active site conformation to be established. The assay was undertaken with  $\lambda_{\text{ex}}$  350 nm and  $\lambda_{\text{em}}$  450 nm. Substrate concentrations were in the range 500  $\mu\text{M}$  to 10  $\mu\text{M}$ . The assay was performed in Tris

buffer (0.1 M, pH 7.4) and a 1:1 ratio of substrate to enzyme. All measurements were recorded at 37 °C. Table 2.2 shows the results of these assays.

Methylumbelliferyl esters	Specific activity (nkatmg <sup>-1</sup> protein) 0.33 mM substrate at 37 °C				
	PLE	<i>AtCXE18</i>	<i>AtSFGH</i>	<i>AtSFGH</i> K <sub>m</sub> (mM)	<i>AtSFGH</i> k <sub>cat</sub> /K <sub>m</sub> (mM <sup>-1</sup> s <sup>-1</sup> )
 <b>34</b>	2120 ± 33	238 ± 4	588 ± 12	0.08	283
 <b>35</b>	1796 ± 78	218 ± 14	399 ± 9	0.08	202
 <b>36</b>	3566 ± 124	225 ± 13	437 ± 11	0.07	264
 <b>37</b>	4135 ± 228	388 ± 32	330 ± 8	0.05	291
 <b>38</b>	8645 ± 241	474 ± 9	604 ± 15	0.09	243
 <b>39</b>	1374 ± 62	105 ± 2	162 ± 2	0.04	217
 <b>40</b>	587 ± 35	0	49 ± 7	0.03	98
 <b>41</b>	0	0	0		
 <b>42</b>	1143 ± 41	8 ± 0.5	265 ± 8	0.09	132
 <b>43</b>	1989 ± 42	8 ± 0.2	230 ± 3	0.08	103
 <b>44</b>	794 ± 13	45 ± 4	34 ± 4	0.08	19
 <b>45</b>	220 ± 27	7 ± 0.5	11 ± 1	0.06	9

 <b>46</b>	$427 \pm 9$	$3 \pm 0.4$	$7 \pm 1$	0.1	3
 <b>47</b>	$1948 \pm 67$	$4 \pm 0.3$	$9 \pm 1$	0.1	4
 <b>48</b>	$12 \pm 2$	0	$12 \pm 3$	0.09	5
 <b>49</b>	$1971 \pm 54$	$344 \pm 28$	$226 \pm 1$	0.04	224
 <b>50</b>	$158 \pm 18$	$63 \pm 2$	$76 \pm 0$	0.05	68
 <b>51</b>	$988 \pm 112$	$272 \pm 34$	$186 \pm 6$	0.08	97
 <b>52</b>	$117 \pm 22$	0	$4 \pm 1$	0.05	3
 <b>53</b>	$281 \pm 14$	NA	$49 \pm 12$	0.06	33
 <b>54</b>	$2635 \pm 53$	NA	$226 \pm 3$	0.08	110
 <b>55</b>	$1267 \pm 133$	$114 \pm 4$	$258 \pm 27$	0.07	141

**Table 2.2** Hydrolysing activity of methylumbelliferyl esters against PLE, AtCXE18 and AtSFGH

The  $k_{cat}/K_m$  measurements of the array show the hexanoate ester, **38** has the greatest activity. Increases in the chain length or the presence of bulky substituents lead to diminished activity, whilst heteroatoms in the  $\alpha$ -position do not appear to be tolerated by AtSFGH. Interestingly, the binding affinity ( $K_m$ ) was little affected by changes in the substrates, whereas a profound effect was seen on turnover ( $k_{cat}$ ).

Enzymology studies have shown that 4-methylumbelliferone esters are suitable probes for *AtSFGH*. In addition, large differences in activity can be seen, with compound **38** shown to be the most active. In an effort to gain a greater understanding of the active site conformation of *AtSFGH*, a large library of 4-MU esters containing a wide variation in the substitution pattern were to be synthesised. Details of this are described in the following section. Previous work carried out on the synthesis of 4-MU esters involved the reaction of commercially available acyl chlorides with 4-MU. In an attempt to produce a large library of multiply substituted esters a larger selection of acyl chlorides were needed. Although a selection of these substituents was commercially available many were not and therefore efforts were directed towards the synthesis of multiply substituted 4-MU esters.

### **2.1.3 4-methylumbelliferone (4-MU) esters**

The following sections will detail the results achieved, which have built upon the previous results attained with 4-methylumbelliferone (4-MU) derivatives (See Section 2.1.2.2). The results obtained with amino acid derivatised 4-MU will also be discussed.

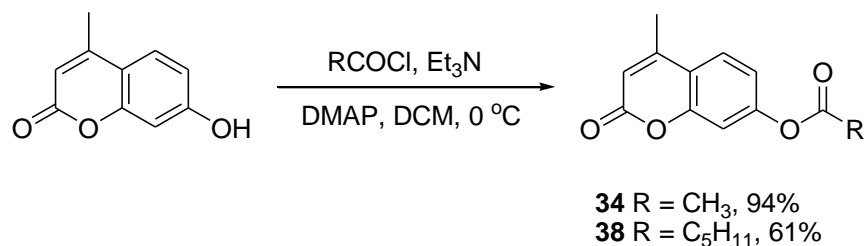
#### **2.1.3.1 Previous Results**

Previous results within the group have involved the parallel synthesis of a series of 4-methylumbelliferone (4-MU) esters. A selection of these, along with their relative activities was shown in Table 2.2.

Analysing the biological results showed that the highest activity was achieved with a *n*-hexyl chain, but it was not clear as to whether the enzyme active site would accommodate a methyl group at the C2 position of the alkyl chain. The following sections deal with the synthesis of a variety of novel 4-MU esters.

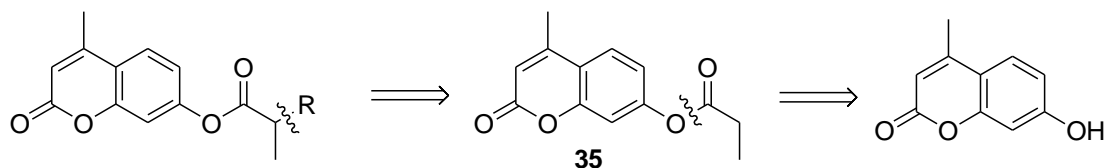
#### **2.1.3.2 Synthesis of 4-MU esters**

In order to compare the biochemical results achieved from screening any novel substrates with those previously attained it was necessary to synthesise compounds **34** and **38**.



Scheme 2.1

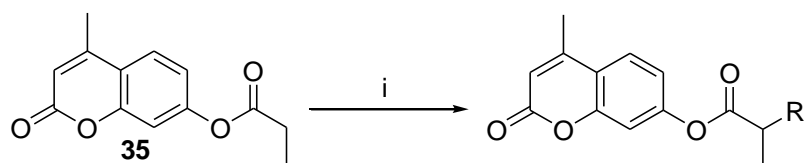
In order to synthesise a library with a large variety of 4-MU esters the retrosynthetic strategy shown in Scheme 2.2 was used. To achieve the target C2 substituted compound, 4-methylumbelliferyl propionate **35** was synthesised, using the conditions in Scheme 2.1. **35** was successfully isolated as a white solid in a 89% yield. Mass spectral data confirmed the product with a single mass peak at 233.1, [M+H<sup>+</sup>].



Scheme 2.2 Retrosynthetic analysis of 4-methylumbelliferyl esters bearing a C2 methyl substituent

### 2.1.3.2.1 Lithium Enolates

Enolate chemistry has been used in the synthesis of alkyl-substituted esters and was employed here as it opened up the ability for a wide array of C2 substituted methylumbelliferyl esters. The general scheme for the reaction can be seen in Scheme 2.3 below.

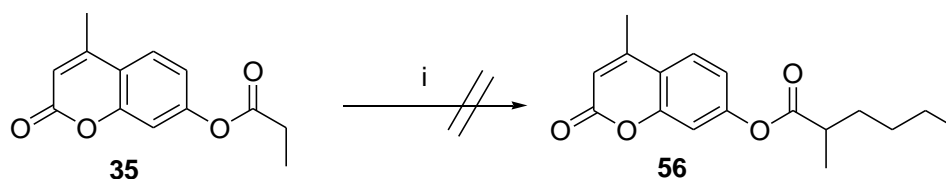


i) LDA, THF, -78 °C then RX

Scheme 2.3 General reaction scheme for the synthesis of alkyl-substituted esters using lithium enolate chemistry

Following generation of the enolate by treatment of ester **35** with LDA at -78 °C, 1-iodobutane was added and the reaction allowed to attain ambient temperature,

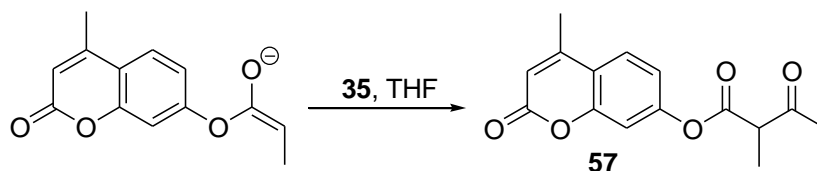
Scheme 2.4. However, upon work-up no product was detected. Both  $^1\text{H}$  NMR and LC-MS data indicated that the starting material **35** had been regenerated.



i) LDA, THF,  $-78\text{ }^\circ\text{C}$  then 1-iodobutane

Scheme 2.4

It was thought that the increase in temperature during the reaction may be responsible for the failure of the enolate alkylation. To test this, the reaction temperature was maintained at  $-78\text{ }^\circ\text{C}$  for the entire reaction, however, again only starting material was recovered. A common problem encountered with ester enolates is the formation of the Claisen condensation product,<sup>96</sup> which occurs when the enolate reacts with the unenolised starting material. This proposed formation of compound **57** is shown below in Scheme 2.5. However,  $^1\text{H}$  NMR data did not show any evidence for this product.



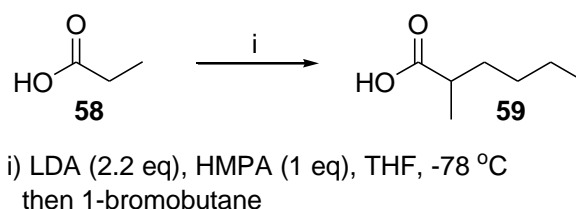
Scheme 2.5 Claisen condensation reaction

Lithium bases are known to form aggregates in solution which lowers their basicity. The addition of complexing or chelating reagents such as HMPA, DMPU or TMEDA break up these aggregates and serves to promote the basicity and hence reactivity towards enolate production.<sup>97</sup> Three separate reactions were carried out using HMPA (23% vol.), DMPU (19% vol.) and TMEDA (1.2 eq), however, these reagents were ineffective, with only starting material recovered. Due to the repeated attempts towards the synthesis of **56** being unsuccessful, this method was abandoned and an alternative approach was sought.



### 2.1.3.2.2 Carboxylic Acid Dianion Chemistry

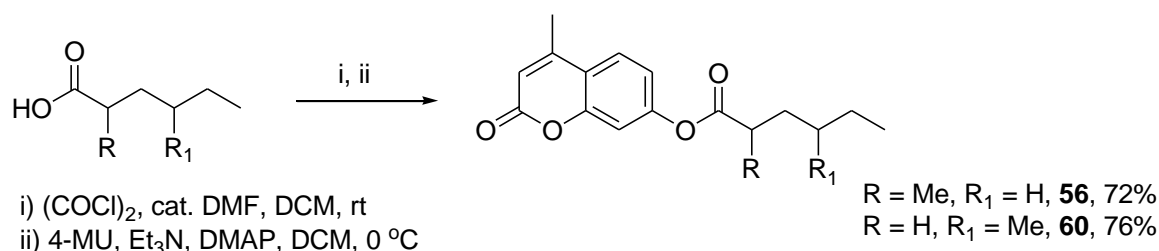
A second reason for the failure of the above reaction may be due to the bulky nature of the 4-MU group hindering the reaction. In an effort to circumvent this problem this was removed and the use of a carboxylic acid starting material was explored. This approach has considerable precedent in the works of Pfeffer who has shown that such species have increased nucleophilicity when compared to simple ester enolates.<sup>98</sup> One example is shown in Scheme 2.6. It was shown that treatment of acid **58** with two equivalents of LDA gave the dianion as determined by deuterium oxide and carbon dioxide quenching. Following this, alkylation with 1-bromobutane afforded **59** in a 78% yield.



Scheme 2.6 Functionalisation of carboxylic acids using dianion chemistry

Using the above conditions, synthesis of **59** was attempted. Unfortunately, following addition of 1-bromobutane no functionalised carboxylic acid product was formed and therefore could not be reacted with 4-MU. At this stage in order to advance the project a selected number of the required carboxylic acids were obtained from commercial sources.

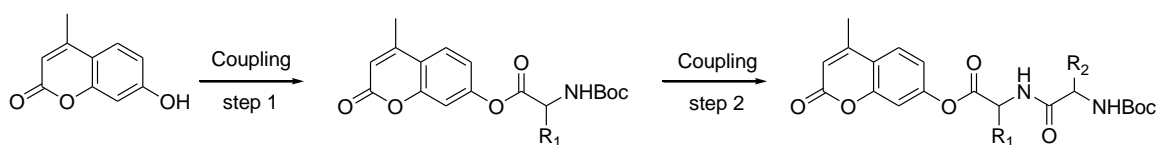
Each methylhexanoic acid derivative was then combined in a two step procedure involving initial conversion to the acyl chloride using (COCl)<sub>2</sub> and a catalytic amount of DMF. Following complete conversion to acid chloride as observed through the IR spectra addition of 4-MU proceeded smoothly (See Scheme 2.7). Product formation was confirmed by the splitting patterns observed in the <sup>1</sup>H NMR spectra.



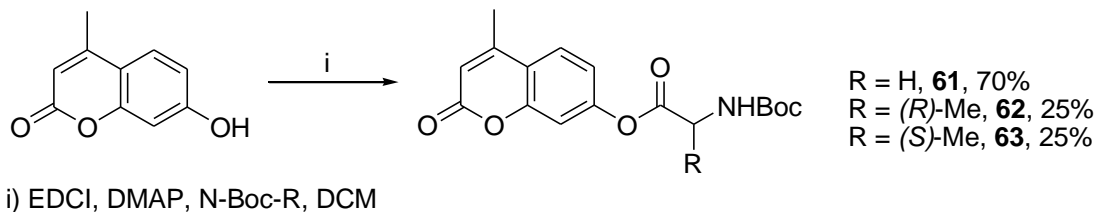
Scheme 2.7 Preparation of methylhexyl 4-MU derivatives, **56** and **60**

### 2.1.3.2.3 Amino Acid Derivatives

Given the difficulties in the preparation of the substituted alkyl esters an alternative approach was explored. It was proposed that a substrate based on an amino acid would allow a more accurate description of the key interactions within the active site. These interactions include covalent bonds, electrostatic,  $\pi$ -stacking, hydrophobic, H-bonding and dipole-dipole interactions. With this in mind a series of arrays were designed. The synthetic strategy involved the sequential coupling of Boc-protected amino acids and is outlined in Scheme 2.8. Three amino acid derivatives were synthesised and the general reaction scheme for the synthesis of these derivatives is shown in Scheme 2.9.



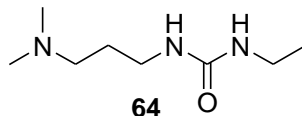
Scheme 2.8 Synthetic strategy for the production of amino acid derivative probes



Scheme 2.9 Preparation of amino acid derivatised 4-MU esters

The first step of this reaction scheme involves the conjugation of an amino acid to 4-MU. The synthesis of **61** involved the reaction of 4-MU with N-Boc-protected glycine, in the presence of a coupling agent and DMAP, and was achieved in a 70% yield, following purification by recrystallisation from hot EtOAc (Scheme 2.9). Using the same conditions compounds **62** and **63** were synthesised using N-Boc-L-alanine and N-Boc-D-alanine respectively. The yields for these two compounds were lower than that of **61** at 25 and 26%.

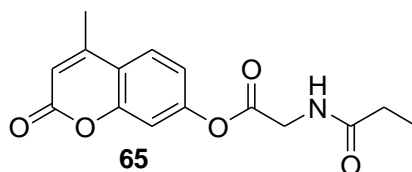
Although many coupling agents exist EDCI was chosen as it forms the water-soluble by-product 1-[3-(dimethylamino)propyl]-3-ethylcarbodiimide urea, **64**, which can be easily removed during an aqueous work-up. This was to be utilised during the library synthesis to enable much easier purification of the products.



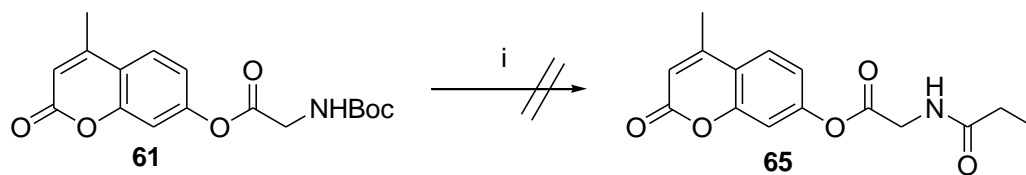
Compounds **61** - **63** were to be used as starting materials for the coupling of a second amino acid, using the coupling techniques outlined previously. A wide selection of amino acids, with differing electronic and steric side chains would hopefully give a greater indication of the active site environment.

As previous results with alkyl-derivatised 4-MU esters were unable to produce a substrate which was able to bind strongly enough to allow co-crystallisation with the enzyme *AtSFGH*, it was hoped that this could be gained with amino acid derivatives. If an x-ray crystal structure with the substrate bound in the active site could be achieved it would enable the identification of the key interactions and residues, allowing a better understanding of the enzymes modes of action and hence the design of further probes.

Before any peptide derivatives were synthesised, it was deemed necessary to have an indication as to the ability of the enzyme to hydrolyse 4-MU esters containing an amide bond within the chain. As the previous studies had shown that the *n*-hexyl chain had the greatest activity, compound **65** was identified as a suitable model bearing an amide bond in the middle.



Initial attempts used **61** as the starting material, which was treated with TFA to remove the Boc group, followed by reaction with DIPEA, EDCI and propionic acid to afford the product (See Scheme 2.10). Unfortunately no product was formed, with only 4-MU observed.

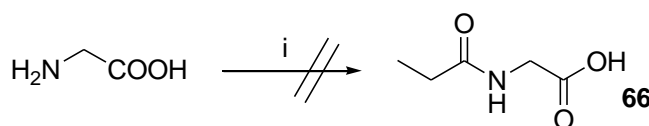


i) TFA, DCM then DIPEA, EDCI, propionic acid, DCM, rt

**Scheme 2.10 Attempted preparation of 65 from 61**

The TFA salt of **61** was stirred with DIPEA to yield the free amine, which was then reacted with propionyl chloride in the presence of Et<sub>3</sub>N at rt. However, this did not lead to the desired product, with only decomposition seen.

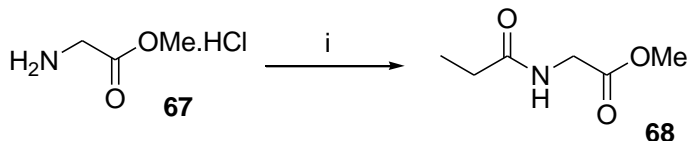
Due to the reactivity of the product as an activated ester, it was decided to synthesise the amide chain first with the final step being the ester formation with 4-MU. To this end, a solution of glycine in DCM was reacted with two equivalents of propionyl chloride in the presence of DIPEA. However, despite repeated efforts no product was formed. Repeating the reaction in DMF or a DMF/H<sub>2</sub>O (1:1) solution did not affect the reaction, with no product being formed. (See Scheme 2.11).



i) propionyl chloride (2 eq), DIPEA, DCM or DMF or DMF/H<sub>2</sub>O

**Scheme 2.11 Attempted synthesis of 66 from glycine**

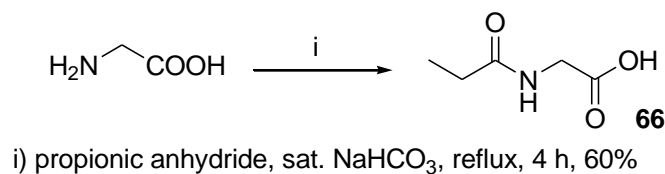
It was thought that the low solubility of glycine was responsible for the lack of reaction and therefore attention turned to the use of the methyl ester of glycine, **67**. Pleasingly, the reaction of **67** with propionyl chloride yielded the desired product, **68**. However, the yield for the reaction was disappointingly low and therefore the reaction was repeated in DMF, which yielded enough material for further manipulation.



i) propionyl chloride, Et<sub>3</sub>N, DMAP, DMF, rt, 13%

**Scheme 2.12 Synthesis of 68 from the methyl ester of glycine, 67**

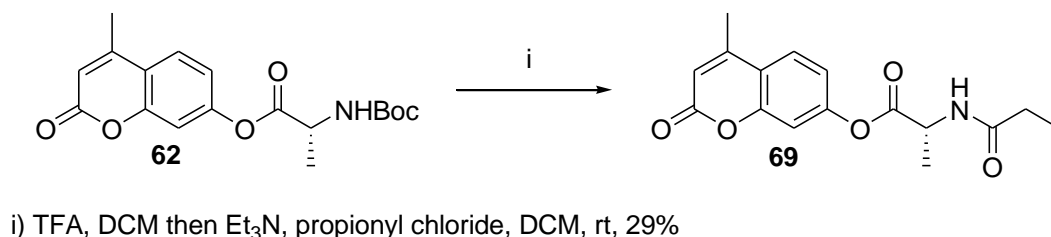
Before coupling to 4-MU could be carried out, hydrolysis of the methyl ester was undertaken to reveal the carboxylic acid. This was attempted several times using 1 M and 3 M NaOH and 1 M LiOH, however, no reaction was seen with any of these hydroxide ion sources. Changing the solvent from H<sub>2</sub>O to THF/H<sub>2</sub>O did not have any effect. Due to the failure of the reaction an alternative route was sought. There was literature precedent for the production of the desired compound **66** by the reaction of glycine with propionic anhydride in a sodium hydrogen carbonate solution as shown in Scheme 2.13.<sup>99</sup>



**Scheme 2.13** Synthesis of **66** from glycine

Repeating this reaction yielded the product in a 60% yield, with the melting point being in agreement with that of the paper (126 °C, Lit. value<sup>99</sup> 128 °C). LC-MS also confirmed the formation of the product by the appearance of the mass peak at 132.2 [M+H<sup>+</sup>]. Compound **66** was coupled with 4-MU using the standard coupling conditions of EDCI and DMAP in DCM to yield the desired product **65** in an 80% yield.

In order to see what effect a methyl substituent in the α-position would have on enzyme activity of these amide derivatives, the analogous compound **69** was synthesised. Initial attempts to couple the TFA salt of **62** with propionic acid using EDCI failed. Interestingly, whereas attempts to synthesise **65** from its mono-peptide derivative failed, the reaction of **62** with propionyl chloride successfully afforded **69**, albeit in a low yield of 29% (See Scheme 2.14).

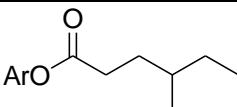
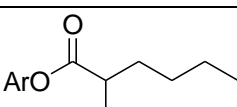
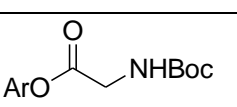
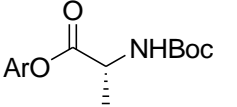
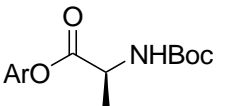


**Scheme 2.14** Synthesis of **69** from **62**

The small library of compounds **56**, **60**, **61** – **63**, **65** and **69** were assayed against *At*SFGH in order to gain an insight into their activity before any further compounds were synthesised.

### 2.1.3.3 *At*SFGH Enzyme assays

Compounds **56** and **60** were tested for activity against purified *At*SFGH, along with the amino acid and amide derivatives, **61** – **63**, and **65** and **69** to ascertain the ability of the enzyme to hydrolyse methylumbelliferyl esters containing an amide bond. The assay was undertaken on a fluorimeter equipped with a plate reader (FLASHScan®), with  $\lambda_{\text{ex}}$  350 nm and  $\lambda_{\text{em}}$  450 nm. Substrate concentrations were in the range 500  $\mu\text{M}$  to 10  $\mu\text{M}$ . The assay was performed in Tris buffer (0.1 M, pH 7.4) and a 1:1 ratio of substrate to enzyme. All measurements were recorded at 37 °C. Table 2.3 shows the results of these assays.

Methylumbelliferyl esters	Specific activity (nkatmg <sup>-1</sup> protein) 0.33 mM substrate at 37 °C			
	PLE	<i>At</i> SFGH	<i>At</i> SFGH K <sub>m</sub> (mM)	<i>At</i> SFGH k <sub>cat</sub> /K <sub>m</sub> (mM <sup>-1</sup> s <sup>-1</sup> )
 <b>60</b>	210 ± 47	9 ± 2	0.05	5
 <b>56</b>	476 ± 51	-----	-----	-----
 <b>61</b>	11 ± 1	3 ± 0.5	0.15	0.12
 <b>62</b>	3 ± 0.7	2 ± 0.2	0.62	0.03
 <b>63</b>	5 ± 1	2 ± 0.5	0.27	0.44

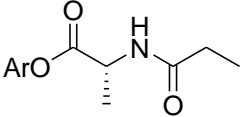
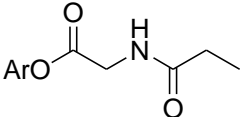
	<b>70</b>	NA	$0.2 \pm 0.1$	0.78	0.06
	<b>65</b>	NA	$0.4 \pm 0.2$	0.34	0.16

Table 2.3 Hydrolysing activity of amide derivatives against purified *At*SFGH and PLE. Ar = 4-methylumbelliferyl (NA = not assayed)

From the specific activity results, **60** can be seen to be a poor substrate for both PLE and *At*SFGH when compared to that of the *n*-hexyl derivative **38**. When **56** was screened against *At*SFGH the rate of hydrolysis was seen to decrease with increasing substrate concentration (See Figure 2.4). This type of pattern is typical for product inhibition, which is known to occur in enzymes such as galactase which is inhibited by galactose.<sup>100</sup>

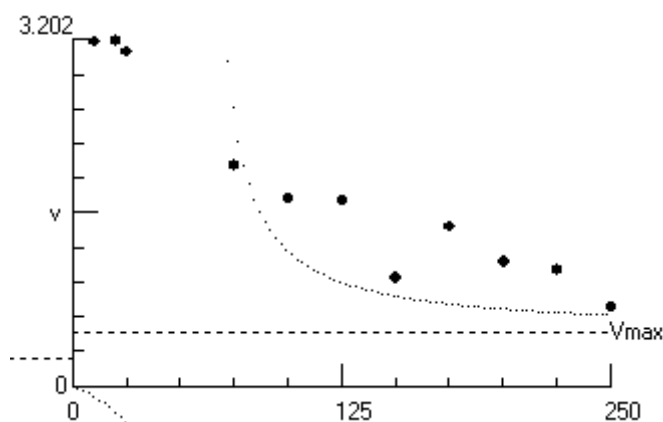


Figure 2.4 Rate of hydrolysis of **56** screened against *At*SFGH

In order to show that product inhibition was occurring with **56**, a variety of inhibition studies were performed, with the aim of attaining altered  $K_m$  or  $v_{max}$  figures. The product of the hydrolysis of **56** is 2-methylhexanoic acid and therefore this was used as the inhibitor. Compound **38** was chosen as the substrate as this showed the greatest activity with *At*SFGH, with varying concentrations of 2-methylhexanoic acid used (0 – 1 mM). Assays were undertaken using the same methodology as that used previously. No change in rate was observed with the reaction of **38** and inhibitor. This may be due to the high affinity of **38** for *At*SFGH which may prevent inhibition from occurring. For this reason two other ester derivatives were chosen as substrates, **34** and **46**. **34** is a good substrate for *At*SFGH, whereas **46** is relatively poor. Unfortunately, using 2-

methylhexanoic acid in the presence of these substrates no change in rate and hence inhibition was observed. From these results it would suggest that product inhibition between **56** and 2-methylhexanoic acid was not occurring.

Using **56** as the inhibitor with **34** as the substrate it was seen that at high concentrations (above 450  $\mu\text{M}$ ) a slight decrease in rate was observed. This result suggests that excess substrate inhibition may be the cause for this decrease in rate. This type of inhibition is seen in around 20% of all known enzymes, *e.g.* the enzyme invertase is inhibited at high concentrations of sucrose.<sup>101</sup> However, no conclusive evidence was obtained to identify the reason for the decrease in rate when using only **56**.

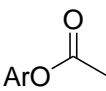
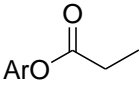
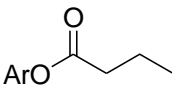
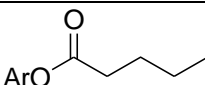
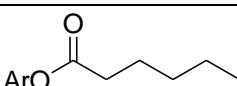
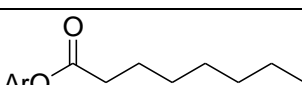
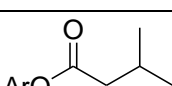
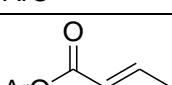
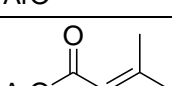
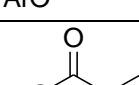
The results from the amide and amino acid derivatives screened also revealed a number of interesting features. Due to the presence of the large Boc group, low hydrolytic activity is seen with both *AtSFGH* and PLE for the 4-MU amino acid substrates. Therefore, the Boc group was removed using standard deprotection techniques, with the resulting TFA salt produced used without further purification. The white solid formed was analysed using  $^{19}\text{F}$  NMR spectroscopy which showed the presence of a single peak at -77.78 ppm, indicating that the TFA salt had been formed. Unfortunately, these TFA salts were unstable to the assay conditions and no meaningful data could be obtained. When **65** and **69** were assayed, very low activity was seen. This suggests that *AtSFGH* is unable to hydrolyse these esters due to the lack of conformational rotation which is brought about by the introduction of the rigid amide bond. This indicated that a library of dipeptides would have very low, if any, activity with *AtSFGH* and for this reason further work was not undertaken with a dipeptide series.

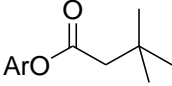
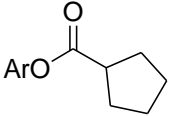
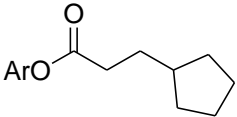
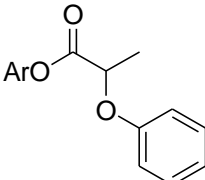
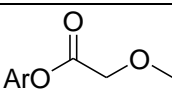
#### **2.1.3.4 Assays *In Planta***

Although a general representation of *AtSFGH* activity *in vitro* was established with the substrate mapping experiments, an idea of the corresponding activity within whole plant cells was needed. This would allow the activity of *AtSFGH* in whole cells to be established. It would also enable the comparison of *AtSFGH* and PLE activity with the activity of esterases *in planta*. Current techniques for predicting the rates of ester hydrolysis uses PLE,<sup>102</sup> a mammalian serine hydrolase which contains the classic  $\alpha/\beta$  structural fold and the catalytic motif GX SXG,<sup>103</sup> which is similar to that in *AtSFGH*.



A protein extract of *Arabidopsis* leaves was performed (See Experimental Section for details) and using Bradford's reagent the concentration was calculated to be 2.4 mg/ml. A selection of substrates bearing the alkyl substituents were selected and assayed against the protein extract. The amino acid derivatives were not assayed due to the poor specific activity seen with *AtSFGH*. The order of preference for the substrates roughly correlated with the results from the screen against the purified enzyme (See Table 2.4).

Methylumbelliferyl esters	Specific activity (nkatmg <sup>-1</sup> protein) 0.33 mM substrate at 37 °C			
	PLE	<i>AtCXE18</i>	<i>AtSFGH</i>	<i>At</i> protein extract
 <b>34</b>	2120 ± 33	238 ± 4	588 ± 12	15 ± 2
 <b>35</b>	1796 ± 78	218 ± 14	399 ± 9	1 ± 0.1
 <b>36</b>	3566 ± 124	225 ± 13	437 ± 11	7 ± 2
 <b>37</b>	4135 ± 228	388 ± 32	330 ± 8	1 ± 0.25
 <b>38</b>	8645 ± 241	474 ± 9	604 ± 15	21 ± 1
 <b>39</b>	1374 ± 62	105 ± 2	162 ± 2	0
 <b>43</b>	1989 ± 42	8 ± 0.2	230 ± 3	2 ± 0.5
 <b>44</b>	794 ± 13	45 ± 4	34 ± 4	1 ± 0.4
 <b>45</b>	220 ± 27	7 ± 0.5	11 ± 1	0.2 ± 0.1
 <b>47</b>	1948 ± 67	4 ± 0.3	9 ± 1	0

 <b>48</b>	$12 \pm 2$	0	$12 \pm 3$	0
 <b>49</b>	$1971 \pm 54$	$344 \pm 28$	$226 \pm 1$	$6 \pm 1$
 <b>50</b>	$158 \pm 18$	$63 \pm 2$	$76 \pm 0$	$6 \pm 3$
 <b>51</b>	$988 \pm 112$	$272 \pm 34$	$186 \pm 6$	$3 \pm 0.2$
 <b>54</b>	$2635 \pm 53$	NA	$226 \pm 3$	$9 \pm 6$

**Table 2.4 Methylumbelliferyl ester substrate activity against PLE, *At*SFGH, *At*CXE18 and *At* protein extract. Ar = 4-methylumbelliferyl (NA = not assayed)**

The results of this study, in addition to the larger range of esters assayed previously, suggest that the acyl binding pocket of *At*SFGH is more constrained than that of PLE ( $6.2 \times 4.7 \times 3.1 \text{ \AA}^3$ ).<sup>104</sup> This probably accounts for the ability of PLE to hydrolyse longer chain esters (compounds **39** - **41**). Therefore *At*SFGH probably has a smaller binding pocket due to the complete lack of activity with substrates bearing an alkyl chain longer than C6.

Figure 2.5 clearly shows that *At*SFGH activity more closely resembles the activity seen in whole cells, *i.e.* protein extract activity. These results indicate that *At*SFGH is a better determinant of hydrolysis of methylumbelliferyl esters *in planta* than PLE.<sup>95</sup>

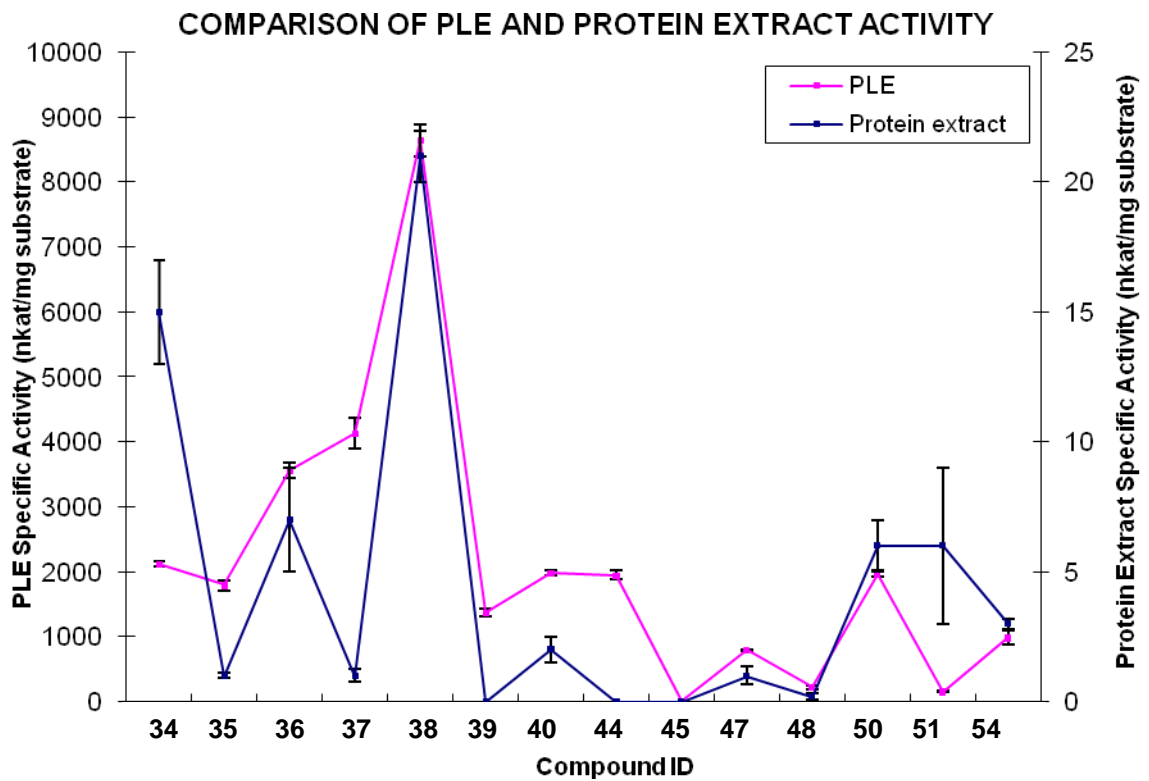
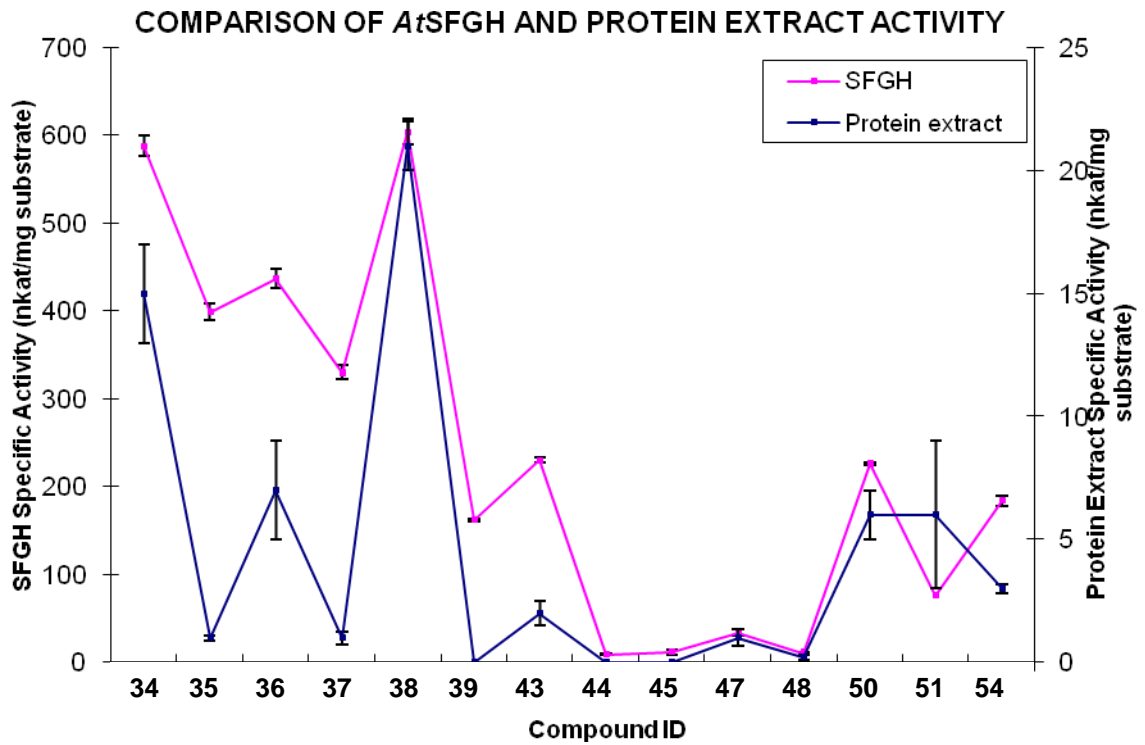


Figure 2.5 Comparison of *At*SFGH and PLE enzyme activity and protein extract activity against 4-MU substrates

### 2.1.3.5 Screening in protoplasts

With the substrates being screened against the purified enzyme and protein extract, *i.e. in vitro*, the next step was to show that this trend could be seen *in vivo*, *i.e.* in whole, living cells. Several challenges exist in the screening of whole cells with the main obstacles being uptake of substrates and autofluorescence.<sup>105</sup> In order to avoid uptake issues across plant cell walls protoplasts were used in this experiment. Protoplasts uptake compounds by passive diffusion and can therefore be used in the FLASHScan experiment, using the same protocol as for the purified enzyme screens.

The usual method used in the group for harvesting protoplasts from leaves was to use an enzyme solution containing 1.5% cellulase and 0.4% pectinase,<sup>84</sup> which causes degradation of the cell wall. However, this cellulase based solution produced a very low concentration of protoplasts and the complete degradation of many of the cells. A variety of conditions were tested, however, protoplast formation occurred with the greatest success when a Driselase enzyme solution was used. Employing this methodology with 200 mg of leaf material, concentrations in the region of  $3 \times 10^5$  protoplasts/ml were commonly achieved.

#### 2.1.3.5.1 Uptake of Substrates

Protoplasts were suspended in sucrose solution and assayed against MU-A, **33** and the *n*-hexyl methylumbelliferyl substituent, **37**. Unfortunately no fluorescence was detected using the FLASHScan equipment with a concentration of  $1 \times 10^5$  protoplasts/ml. Increasing this concentration had no affect. The substrates were also prepared in DMSO to determine if changing the carrier solvent had any affect. However, no fluorescence was detected.

**34** is broken down by esterase enzymes to form 4-MU, which emits in the blue region (maxima 452 nm). Using fluorescence microscopy no fluorescence was seen with a solution of **34** incubated with protoplasts. Initially it was thought that the autofluorescence seen in the cells was preventing any 4-MU fluorescence being detected. A major problem associated with the measurement of fluorescence, and hence substrate hydrolysis, within whole protoplasts is autofluorescence. Using a fluorescence microscope camera linked to a spectrophotometer the autofluorescence spectrum showed two distinct bands; one broad band from 430 - 540 nm and one sharp band at 700 nm. The latter band can be attributed to the chlorophyll present in the chloroplasts

within the cell. The band in the blue-green region of the spectrum may be due to a variety of compounds naturally occurring in plants cells, *e.g.* flavinoids. As the emission maximum for 4-MU falls within this region any fluorescence measurements may be inaccurate. However, upon placing a suspension of protoplasts into a solution of **34** (1:1 ratio) and measuring the fluorescence over time on a fluorimeter, no increase at 452 nm was seen. This lead to the possibility of uptake problems and experiments using fluorescein diacetate were undertaken to test this.

Fluorescein diacetate (FDA) is often used as a viability test within cell biology.<sup>106</sup> Cells that are alive and have an intact cellular membrane, readily uptake FDA whereupon esterases present within the cell hydrolyse it to form the highly fluorescent compound fluorescein, which is retained within the cell. This retention is achieved by the cell maintaining membrane integrity. Fluorescein has an excitation maximum at 490 nm and an emission maximum at 514 nm and can be visualised by fluorescence microscopy. Any protoplasts which do not fluoresce green in an FDA solution are assumed to be dead. Before testing uptake of **34**, the protoplasts were incubated with FDA and observed under the fluorescence microscope. Bright green fluorescence was seen in the vast majority of cells indicating they were viable. When incubating protoplasts with **34** first, followed by FDA green fluorescence was still observed, demonstrating that **34** does not inhibit the uptake and hydrolysis of FDA. Previous results have shown that the specific activity of *AtSFGH* towards FDA is very low<sup>92</sup> and therefore the fluorescence seen within the cells is due to other esterases hydrolysing FDA. This was proven by the addition of 1 mM PMSF to a suspension of protoplasts, followed by incubation with FDA and upon analysis, no fluorescence was detected.

Attention now turned to the technique of flow cytometry, which may enable the detection of 4-MU fluorescence within protoplasts, where other techniques have failed. This technique allows for the interrogation of particles (usually cells) in solution at rates of up 100,000 events per second. The cells in suspension are passed as a core stream, surrounded by another wider stream which contains phosphate-buffered sheath fluid. The principle of hydrodynamic focussing ensures that the cells stay in the centre of the stream. The cells are forced into a single line and pass through up to three lasers at which point they are interrogated. The equipment utilised in this project will be the DakoCytomation MoFlo®, which has an optics platform that allows the detection of up to 9 fluorescent channels, in addition to forward scatter (FSC) and side scatter (SSC). The latter two give an indication of the cell's size and granularity respectively.

The sorting feature of a flow cytometer is the ability to select any population defined by a logical combination of regions, known as gates, and to isolate this population from the sample. Achievable sorting rates on the MoFlo® are in the region of 30,000 events per second. This high-throughput screening can be undertaken with purity levels in excess of 99%. Populations of cells can be sorted both 2- and 4-ways, with the option of sorting into micro well plates.

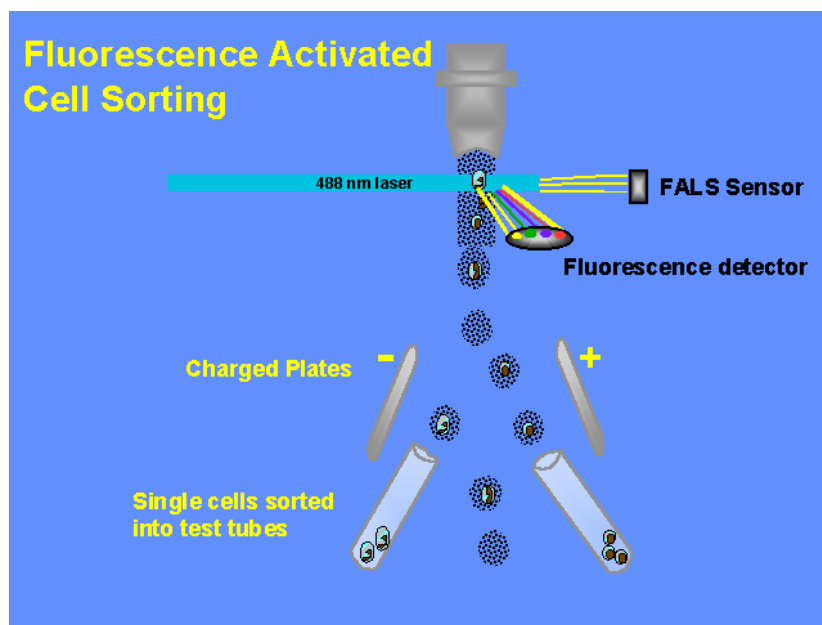


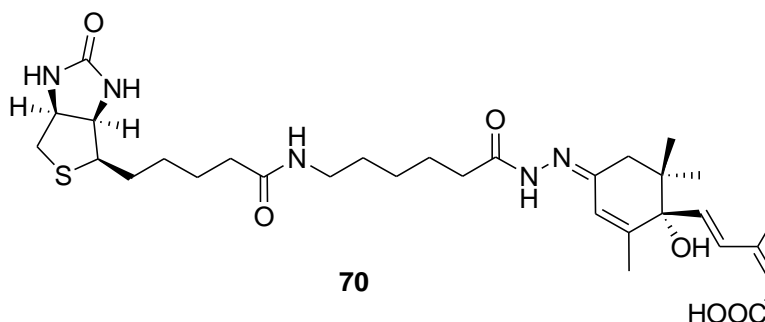
Figure 2.6 Fluorescent Activated Cell Sorting (FACS)

Cell separation can be achieved by breaking the sample stream into droplets, using a piezoelectric sensor at a set frequency and amplitude. The point at which droplets break off from the main stream is kept at a fixed distance downstream from the observation point. Between the time the cell passes through the laser until it reaches the droplet break off point, the measured parameter values (fluorescence, SSC or FSC) are recorded and used to generate a sort decision signal.

If the cell is to be sorted the decision signal is applied to drop charging circuitry, which applies a voltage to the stream at the time at which the cell should lie somewhere in the droplet breaking off from the stream. This leaves an electric charge on those droplets selected for sorting. The stream passes through the electrically charged plates, to which high voltages of opposite polarities have been applied. Charged droplets, which contain those cells to be sorted, are deflected out of the stream towards the plate bearing the opposite charge. Uncharged droplets are not deflected and pass into the waste collector

(See Figure 2.6). Flow cytometry has found application in a variety of areas, examples of which are highlighted in the following section.

Abscisic acid (ABA) receptors have been investigated using flow cytometry.<sup>107</sup> ABA is involved in developmental processes in plants, such as stomatal closure and the inducement of dormancy. A biotin-labeled abscisic acid derivative, **70** was synthesised and was incubated with barley aleurone protoplasts cells, which are often used as model systems for ABA studies.



Protoplasts were incubated with **70**, followed by addition of fluorescently labeled streptavidin. Analysis of the subsequent fluorescent population was achieved using flow cytometry, with an increase in fluorescence clearly seen in those cells treated with **70**, Figure 2.7.

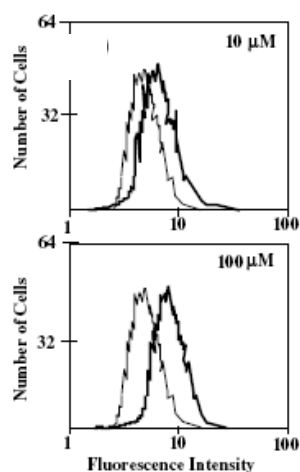


**Figure 2.7** Flow cytometric analysis of cells treated with **70** (black line) showing an increased level of fluorescence compared to the control cells (grey line). Reprinted from *Bioorganic & Medicinal Chemistry*, vol. 13, Kitahata N., Nakano T., Kuchitsu K., Yoshida S. and Asami T., *Biotin-labeled abscisic acid as a probe for investigating abscisic acid binding sites on plasma membranes of barley aleurone protoplasts*, 3351-3358, Copyright (2005), with permission from Elsevier.

Flow cytometry has been used to analyse the link between cell cycle control and programmed cell death of BY-2 tobacco cells following treatment with cryptogein.<sup>108</sup> Cryptogein is known to induce the production of reactive oxygen species (ROS), cause protein phosphorylation and cell death. BY-2 cells were incubated with aphidicolin, **71** and propyzamide, **72** which causes the cell cycle to stop at the M phase. Following removal of these compounds, the cells were monitored using flow cytometry and DAPI staining and treated after 0.5 h and 5.5 h with cryptogein (500 nM). Figure 2.8 shows the histograms which highlight the ability of cryptogein to induce cell cycle arrest during the G1 phase. Changes in the cell cycle occurred after 6 h, whereas cell death was detected after 10 h, which shows that cell cycle arrest occurs before cell death.

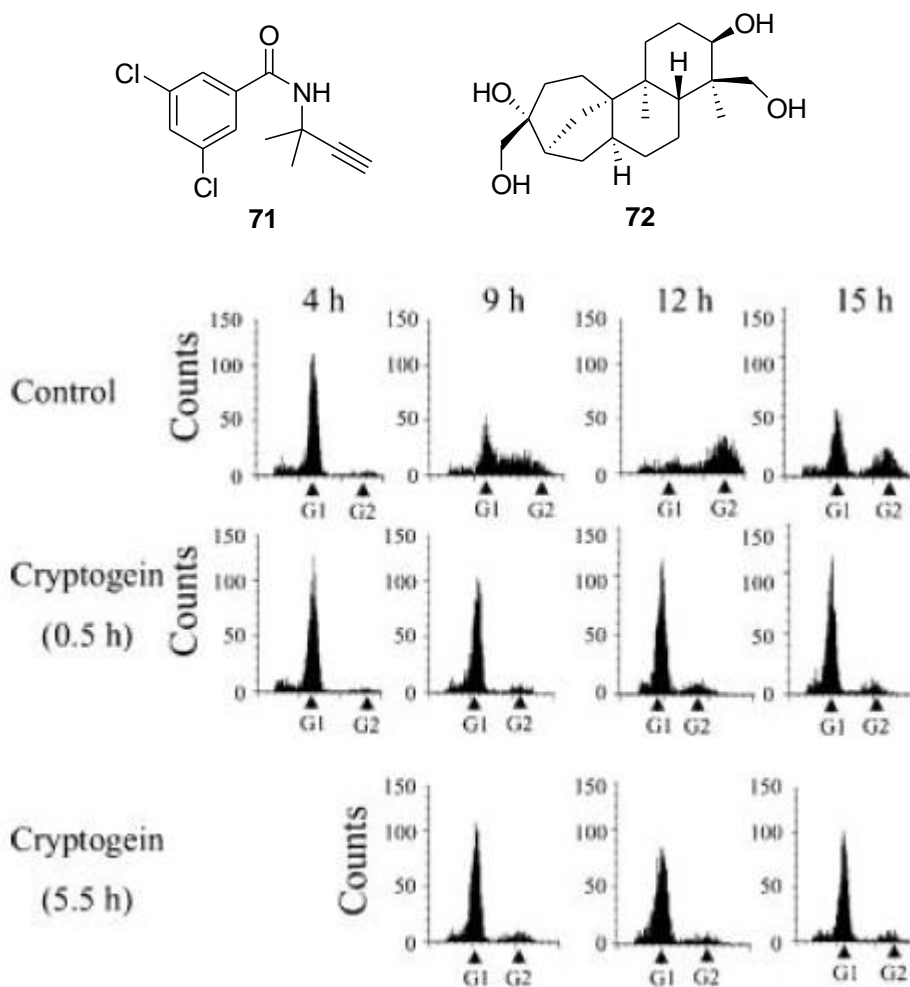


**Figure 2.8** Flow cytometric analysis of non-treated cells (control) and cells treated with cryptogein in the M (0.5 h) or G1 (5.5 h) phase. Kadota Y., Watanabe T., Fujii S., Higashi K., Sano T., Nagata T., Hasezawa S. and Kuchitsu K., Crosstalk between elicitor-induced cell death and cell cycle regulation in tobacco BY-2 cells, *Plant J.*, 2004, **40**, 131-142. Copyright Wiley-Blackwell. Reproduced with permission.



A major advantage of the MoFlo® is that autofluorescence can be removed by the process of compensation. Using statistical methods, compensation allows for the removal of unwanted fluorescence signals from any of the detection channels. By dedicating one channel to autofluorescence and compensating for it across the others, the problem can be overcome.<sup>109</sup> Hence, any increase in fluorescence can be attributed to the hydrolysis of **34**. Fluorescence detection can be amplified on the MoFlo® and it is therefore very sensitive to small changes in fluorescence.

In order to visualise the hydrolysis of **34** a plot of 450/60 nm against computed time was plotted. If uptake and hydrolysis occurred an increase in fluorescence intensity would be seen. However, no increase was detected (See Figure 2.9) and this would suggest uptake was not occurring.

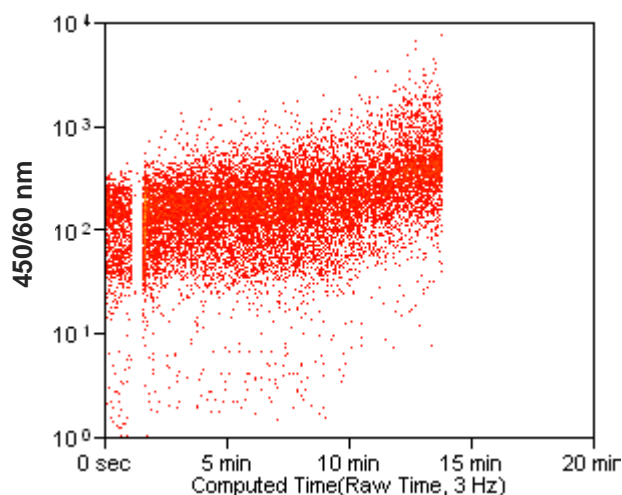


**Figure 2.9** 450/60 nm against computed time for the hydrolysis of **34**

In order to show uptake and hydrolysis could be detected on the MoFlo® the suspension of protoplasts was incubated with FDA and the increase in fluorescence intensity over time recorded. In the plot below (Figure 2.10) an increase in fluorescence over time can clearly be seen. The fluorescence intensity levels off after 12 minutes, showing that no further hydrolysis of the substrate is occurring.

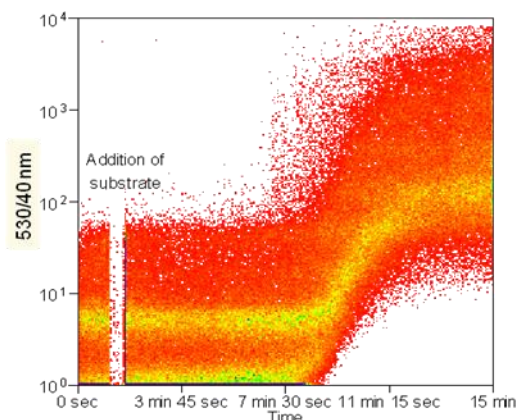
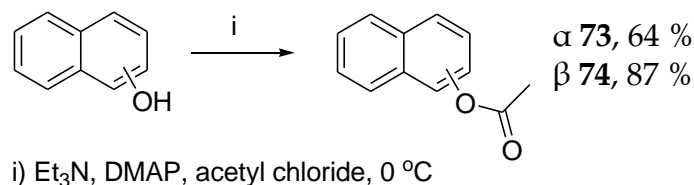


Figure 2.10 Addition of FDA with increase in fluorescence at 530/40 nm over time recorded

The above results indicate that methylumbelliferyl esters are not hydrolysed within protoplasts and therefore attention turned to synthesising alternative probes.

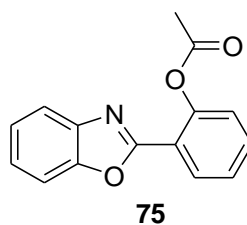
#### 2.1.4 Alternative Probes

Previous results have shown that *At*SFGH shows activity towards both  $\alpha$ - and  $\beta$ -naphthyl acetates **73** and **74** (See Table 2.1). These two compounds were synthesised in good yields from acetyl chloride (See Scheme 2.15). Mass spectra confirmed synthesis in both cases (187.1 and 186.9,  $[M+H]^+$ ).



Scheme 2.15 Acetylation of  $\alpha$ - and  $\beta$ -naphthol

2-(2-hydroxyphenyl)benzoxazol acetate **75** was also synthesised by the reaction of 2-(2-hydroxyphenyl)benzoxazole and acetyl chloride, using identical conditions to those in Scheme 2.15, in a 99% yield



In order to examine the uptake and subsequent hydrolysis within cells of **73** – **75**, these compounds were incubated with protoplasts and observed using fluorescence microscopy. With **73** and **74**, fluorescence was seen within the protoplasts, although it was much less intense than that seen with FDA. Moreover, photobleaching occurred with both compounds after 2 minutes. Unfortunately, when **75** was incubated with a suspension of protoplasts, no fluorescence could be seen.

### 2.1.5 Summary

- \* The synthesis of **56** could not be achieved *via* enolate or carboxylic dianion chemistry, with the addition of complexing or chelating agents proving ineffective.
  
- \* The reaction of the appropriate alkyl halide with 4-MU produced **56** in 72% yield, with the isomer **60** synthesised in 76% yield.
  
- \* Synthesis of **61** involving the reaction of 4-MU with the Boc-protected glycine was achieved in a 70% yield. A lower yield of 25 and 26% were obtained when synthesising **62** and **63** from Boc-protected L-alanine and D-alanine respectively.
  
- \* Those derivatives which contained an amide bond were poor substrates for both PLE and *At*SFGH when compared to that of the *n*-hexyl derivative, **38**. This suggests that some sort of conformational flexibility within the substrate is needed.
  
- \* *At*SFGH activity towards a variety of methylumbelliferyl esters more closely resembles the activity seen in whole cells than that seen with PLE. This indicates that *At*SFGH is a better determinant of hydrolysis of these compounds *in planta* than PLE.
  
- \* The methylumbelliferyl esters did not appear to be taken up by the protoplast cells and hence no fluorescence was seen. However, the protoplasts readily hydrolysed FDA with the resulting fluorescence being detected on a fluorescence microscope and the MoFlo®.

## 2.2 AtCXE12

### 2.2.1 Introduction

This section will introduce another esterase isolated from *A. thaliana*, AtCXE12. Some of the background research undertaken on the enzyme will be discussed and work undertaken to apply the technique of directed evolution will be presented.

### 2.2.2 Previous Research

Carboxylesterases (CXE), of which AtCXE12 is an example, are a large class of enzymes that hydrolyse short-chain esters to the corresponding carboxylic acid. They belong to the  $\alpha/\beta$  hydrolase fold superfamily of proteins<sup>110</sup> and contain a conserved structural core consisting of eight  $\beta$ -strands, with connecting  $\alpha$ -helices and loops interspersed within and around the eight  $\beta$ -strand core (See Figure 2.11).<sup>103</sup> This sheet of  $\beta$ -strands is highly twisted and bent so that it forms a half-barrel, with the first strand at almost 90° to the last.

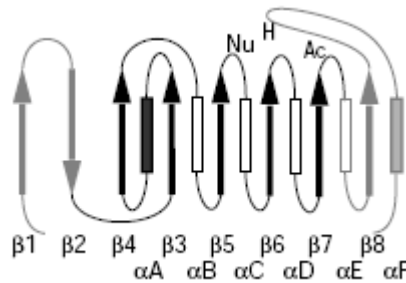


**Figure 2.11 Schematic representation of the structural core of the  $\alpha/\beta$  hydrolase fold proteins.** Reprinted from *Structure*, vol. 7, Heikinheimo P., Goldman A., Jeffries C. and Ollis D.L., *Of barn owls and bankers: a lush variety of  $\alpha/\beta$  hydrolases*, R141-R146, Copyright (1999), with permission from Elsevier.

They also contain the classic serine hydrolase catalytic triad of a nucleophilic residue (serine or cysteine), histidine and aspartic acid (although in some cases this can be glutamic acid) and an oxyanion hole which is able to stabilise the substrate-enzyme intermediate during hydrolysis. The nucleophilic residue is located after  $\beta 5$  in an area called the nucleophilic elbow, which is the best conserved feature across the  $\alpha/\beta$  hydrolases. The twist of the central  $\beta$ -sheet allows the catalytic triad residues to be brought close together to form the active site.

Marshall and co-workers used RT-PCR experiments to determine the expression of 20 CXEs present within *A. thaliana* in a variety of tissues within the plant.<sup>111</sup> *AtCXE12* was detected across all tissue types and this can be seen in Figure 2.12.

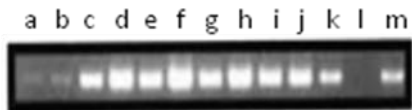
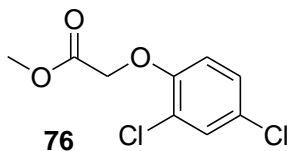


**Figure 2.12** Expression pattern of *AtCXE12* in a variety of tissues as determined by RT-PCR a) young root, b) mature root, c) 2 leaf seedling, d) 4 leaf seedling, e) 6 leaf seedling, f) leaf, g) stem, h) flower bud, i) flower, j) young silique, k) mature silique, l) negative control, m) positive control. With kind permission from Springer Science+Business Media: *Journal of Molecular Evolution*, The Carboxylesterase Gene Family from *Arabidopsis thaliana*, 57, 2003, 487, Marshall S.D.G., Fig 4.

Work within the Edwards group has shown *AtCXE12* to be sensitive to inhibition by the fluorophosphonate paraoxon, an inhibitor of serine hydrolases. They have also demonstrated that *AtCXE12* is the principal enzyme responsible for the hydrolysis of methyl-2,4-dichlorophenoxyacetate, **76**.



**76** is a pro-herbicide, which is hydrolysed to the phytotoxic compound 2,4-dichlorophenoxyacetic acid and is commonly used in the control of dicotyledonous weeds.<sup>112</sup> Gershater *et al* used the trifunctional probe **77** to detect and isolate four carboxylesterases which hydrolysed **76**.<sup>113</sup> The reactivity probe contained a fluorophosphonate group which was able to selectively modify the serine residue present in the catalytic triad, a biotin tag to aid isolation and a fluorescent moiety (rhodamine) for detection and quantification.

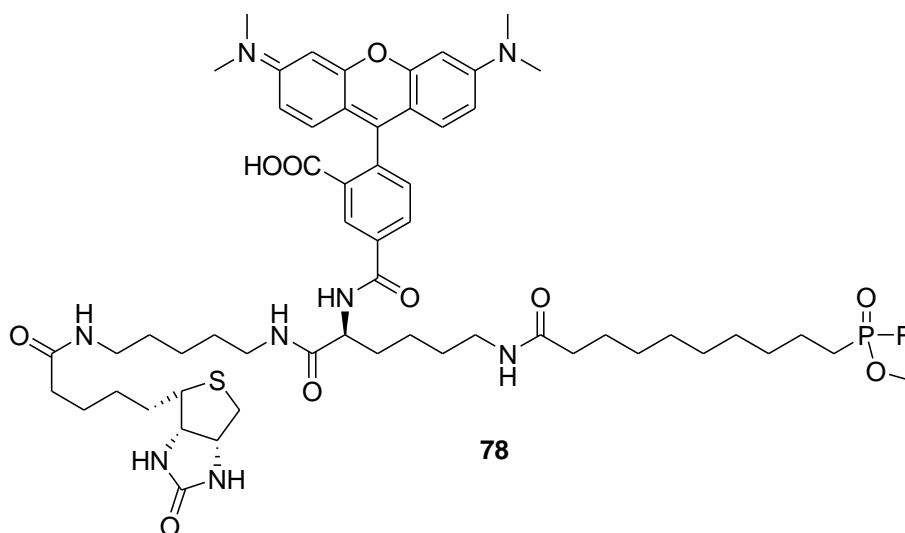


Figure 2.13 Trifunctional probe, **77** used to isolate *AtCXE12*

Three of the serine hydrolases identified (*AtCXE5*, *AtCXE12* and *AtCXE20*) were cloned and recombinantly expressed. Following purification each of these enzymes were assayed against **76** with hydrolysis only seen with *AtCXE12*.

### 2.2.3 Directed Evolution of *AtCXE12*

As previous work had shown that *AtCXE12* was a classic serine hydrolase which shows high activity within plants (both from the protein extract and *in planta*) this enzyme was used as the model enzyme system to test the directed evolution methodology outlined in Section 1.2. Due to the mechanistic similarities of esterase and lipase action, the aim was to evolve *AtCXE12* from an esterase to a lipase-like enzyme, *i.e.* show a greater activity towards long chain esters.

#### 2.2.3.1 Hormone Sensitive Lipase

Work undertaken by Wei *et al* on the carboxylesterase Brefeldin A Esterase (BFAE) revealed similarities to the human enzyme Hormone Sensitive Lipase (HSL).<sup>114</sup> BFAE and HSL have different substrate specificities, with the latter preferring longer chain esters. HSL is larger than most  $\alpha/\beta$  hydrolases with the C-terminal domain containing the catalytic machinery.<sup>115</sup> Wei performed sequence alignment with BFAE and HSL and found 45% alignment between the two sequences. Figure 2.14 shows the catalytic sites for both BFAE and HSL, with the high sequence identity clearly identifiable.

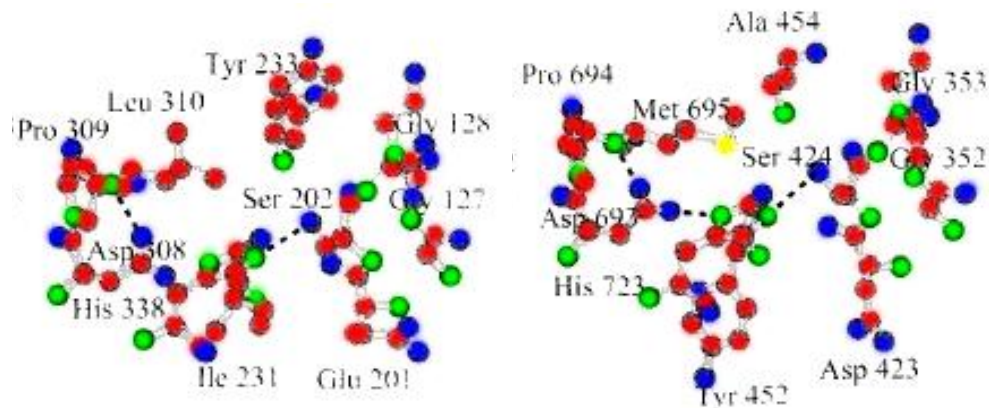


**Figure 2.14** Catalytic sites of BFAE and HSL, with the catalytic triad of Ser202, His 338 and Asp308 in BFAE and Ser424, His723 and Asp693 in HSL. Reprinted by permission from Macmillan Publishers Ltd: *Nature Structural Biology* (1999, 6, 340-345), copyright (1999)

Sequence alignment and the catalytic site diagrams suggest that Ala454 in human HSL is located at a site which is occupied by Try233 in BFAE. This tyrosine residue is thought to fold over the binding site of BFAE and prevent long chain esters from being hydrolysed. In order to gain evidence for this the residue Ala454 in HSL was mutated to phenylalanine, which is a more bulky residue. This was achieved using site-directed mutagenesis and using Western blotting the A454F mutant was shown to be expressed at similar levels to the wild type enzyme. When the A454F mutant was screened against a range of *p*-nitrophenyl esters it was shown to have similar levels of activity with *p*-nitrophenylbutyrate (C4), valerate (C5) and caproate (C6) as that seen with the wild type. However, the A454F mutant was completely inactive towards *p*-nitrophenyl caprylate (C8), trolein and a diolelylglycerol analogue. The authors postulate that this result indicates the role of Tyr233 in esterase activity within BFAE.

Looking at the sequence alignment of BFAE and *AtCXE12*, several overlaps can be seen to occur, Figure 2.15. Producing a homology diagram of the two enzymes to show the tertiary structure clearly identifies the Tyr233 in BFAE is occupied by Tyr198 in *AtCXE12* (See Figure 2.16).

	$\beta 2$	$\beta 3$	
BFAE	GNEITLHVFRPAGVEGVLP----GLVYTHGGGMTILT TDNRVHRRWCTDLAAAGS-		
AtCXE12	DNNSVRIYLPKAAAE TDSKLPLLVFYFHGGGFIIETAFSPTYHTEFLTTSVSA SNC		
	$\beta 4$		$\beta 5$
BFAE	VVVMVDFRNAWTAE GHH PFP SGVEDCLAAVLWF DEHRESI GLSG-----VVVQ		
AtCXE12	VAVSVD--YRRAPEHPI SVPFDDSWTALKWVFTHITGSGQEDWLNKHADEF SRVFLS		
		$\beta 6$	
BFAE	GESGGENLAIATTLAKRRGR LDAID----GVYASIPYISGGYAWDHERRLTELPS		
AtCXE12	GDSAGANIVHHAMRAAKEKLS PGLNDTGISGII LLHPYFW SKT PIDEKDTKDET LR		
			$\beta 7$
BFAE	LVENDGYFIENGGMALLVRA YDPTGEHAEDPIAWPYF ASEDELRLGLPPFVVAVNELD		
AtCXE12	MKIEAFWMMASENS KDGTGG PLLNVVQSESVDLSGLGCGK-----VLVMVAEKD		
		$\beta 8$	
BFAE	PLRDEGIAFARRLARAGVD--VAARVNIGLVHGS DVI FRHWLPAALESTVRDVAGFAAD		
AtCXE12	ALVRQGMGYAAKLEKSGWKGEVEVVESEGEDHVFHLLKPECDNAIEVMHKFSGFIKGGN		

**Figure 2.15** Structure-aided sequence alignment of amino acid sequences of BFAE and *AtCXE12*. The sequences were first aligned using Scratch Protein Predictor<sup>116</sup> and then manipulated manually to achieve maximum similarity within the secondary structure. Boxes represent  $\alpha$ -helices as determined from the BFAE structure.

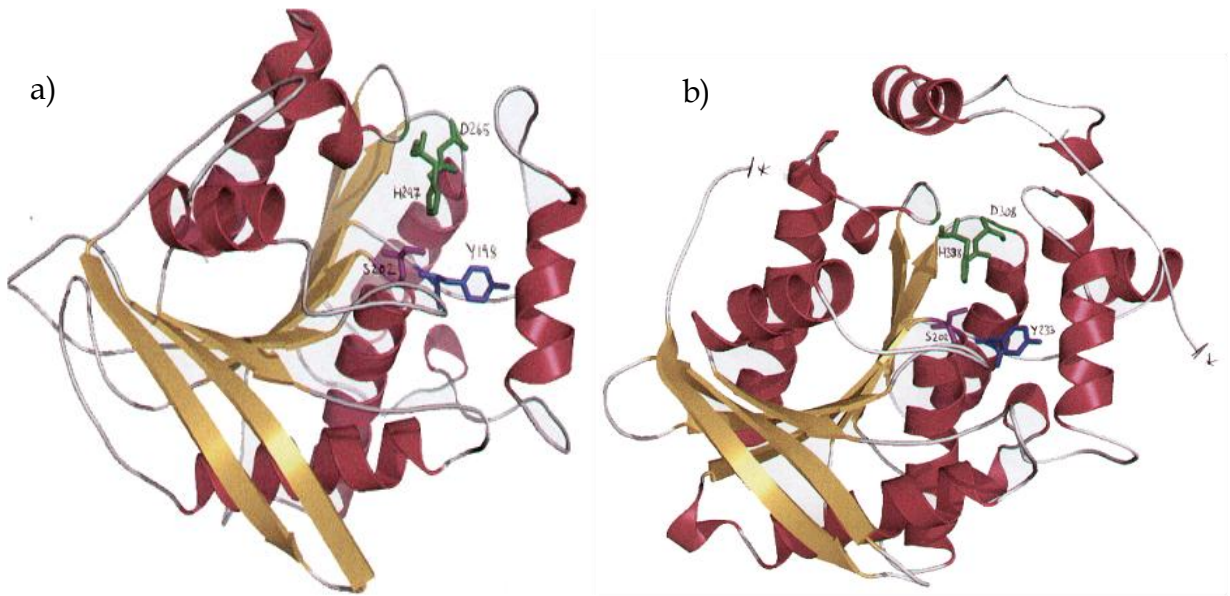


**Figure 2.16** Predicted tertiary structure of a) *AtCXE12* and b) BFAE using homology alignment. The catalytic triad can be seen in both cases, along with the tyrosine residues (Tyr233 in BFAE and Tyr198 in *AtCXE12*). \*  $\alpha$  helix which joins these two points has been removed for clarity

Using this information studies were undertaken to mutate Tyr198 in *AtCXE12* to a less bulky residue with the aim of producing a more lipase-like enzyme. However, before



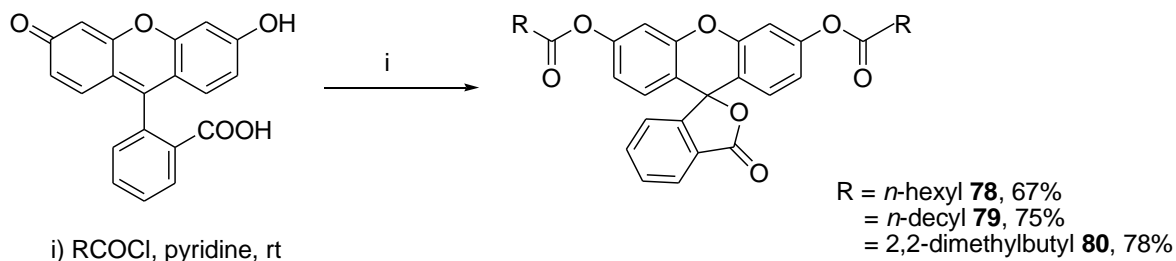
any mutagenesis and screening could be performed, probe molecules were designed and synthesised to enable the selection of an improved enzyme. The following section details the synthesis and preliminary assays which were undertaken.

### 2.2.3.2 AtCXE12 probe molecules

Previous work with *AtSFGH* had highlighted several issues with using methylumbelliferyl esters as probes for directed evolution studies. These included problems with emission profiles overlapping with cellular autofluorescence and limited uptake within protoplasts. As FDA is readily taken up by protoplasts and the hydrolysis product fluorescein is highly fluorescent at wavelengths beyond autofluorescence, probes were developed based on the fluorescein moiety.

#### 2.2.3.2.1 Fluorescein probes

Using the data gathered in the *AtSFGH* substrate mapping experiments, four fluorescein derivatives were chosen for synthesis. These were FDA, fluorescein dihexanoate, fluorescein didecanoate and fluorescein di-(2,2-dimethyl)butanoate. All derivatives, except FDA which was purchased from Aldrich, were synthesised under identical conditions by the treatment of fluorescein with the appropriate acyl chloride in the presence of pyridine (See Scheme 2.16).



Scheme 2.16

Synthesis was confirmed in each case by the appearance of signals with the correct integration corresponding to the alkyl protons in the  $^1\text{H}$  NMR spectrum and the presence of two carbonyl signals in the  $^{13}\text{C}$  NMR spectrum at 171.9 and 169.3 ppm. Compounds **78** - **80** and FDA were then assayed against purified *AtCXE12*, with the results outlined in the following section.

### 2.2.3.2.2 *AtCXE12 in vitro assays*

The synthesised fluorescein esters, **78** – **80** and FDA were screened against purified *AtCXE12*. This was undertaken on a FLASHScan®, with  $\lambda_{\text{ex}}$  490 nm and  $\lambda_{\text{em}}$  512 nm. Substrate concentrations were in the range 500  $\mu\text{M}$  to 10  $\mu\text{M}$ . The assay was performed in Tris buffer (0.1 M, pH 7.4) and a 1:1 ratio of substrate to enzyme. All measurements were recorded at 37 °C. However, no meaningful data could be identified from the screen and upon investigation it could be seen that a white precipitate had formed during the analysis. This was thought to be due to the relatively low solubility of the fluorescein esters within acetone. For this reason, the solvent was changed to DMSO and the assay repeated. Disappointingly, this change did not affect the outcome and again solubility issues were a concern.

Due to the solubility issues at high concentrations, it was decided to lower the concentration of the fluorescein derivatives to below 10  $\mu\text{M}$  and four different concentrations were produced in DMSO: 2.5  $\mu\text{M}$ , 5  $\mu\text{M}$ , 7.5  $\mu\text{M}$  and 10  $\mu\text{M}$ . When these compounds were assayed against *AtCXE12*, data relating to the catalytic activity of the enzyme was gathered. Table 2.5 shows this data.

Substrate	Specific Activity ( $\text{nkatmg}^{-1}$ )	$K_m$ (mM)
Fluorescein diacetate, FDA	$479 \pm 31$	0.003
Fluorescein dihexanoate, <b>78</b>	$54.3 \pm 2$	0.004
Fluorescein didecanoate, <b>79</b>	$23.8 \pm 6$	0.001
Fluorescein di(2,2-dimethyl)butanoate, <b>80</b>	$29.1 \pm 2$	0.001

Table 2.5 Fluorescein ester substrate activity against *AtSFGH*

### 2.2.3.2.3 *Flow cytometry screening*

With a difference in activity seen with **78** – **80**, efforts now concentrated on the ability to distinguish between this activity using the flow cytometer. In order to achieve this, a simple screening experiment was performed. Using protoplasts harvested from *Arabidopsis* leaves, each of the probes were incubated with the solution and analysed using the MoFlo®. Incubation time was 30 minutes, with probe concentration at 5  $\mu\text{M}$ . An example of a typical histogram obtained, before and after addition of the substrate can be seen in Figure 2.17.

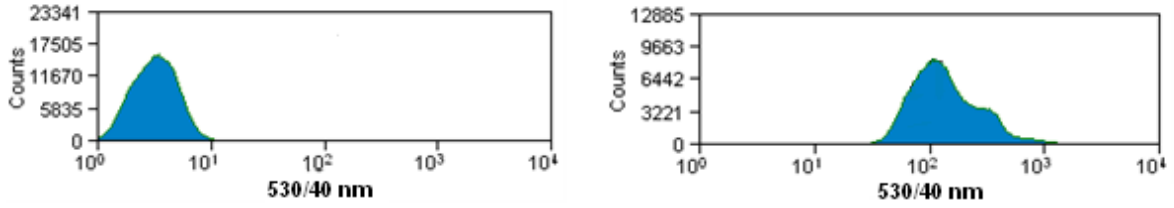


Figure 2.17 Increase in fluorescence at 530/30 nm upon incubation with FDA

A plot of 530/40 nm against 580/30 nm clearly shows a new population forming upon addition of the fluorescein probe, Figure 2.18. This population has an increased fluorescence and is the result of esterases present within the protoplasts hydrolysing the ester to form fluorescein.

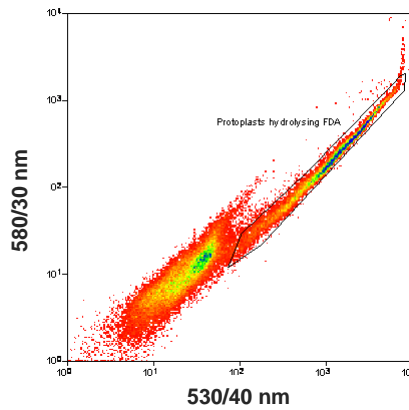


Figure 2.18 Plot of 530/40 nm against 580/30 nm showing the population which exhibits increased fluorescence

78 - 80 were incubated as for FDA and a relative rate of hydrolysis against *AtCXE12* was recorded. The dot plots below (Figure 2.19) show that the cells turn over the longer chain substrates at a slower rate as seen by the smaller side population which shows increased fluorescence.

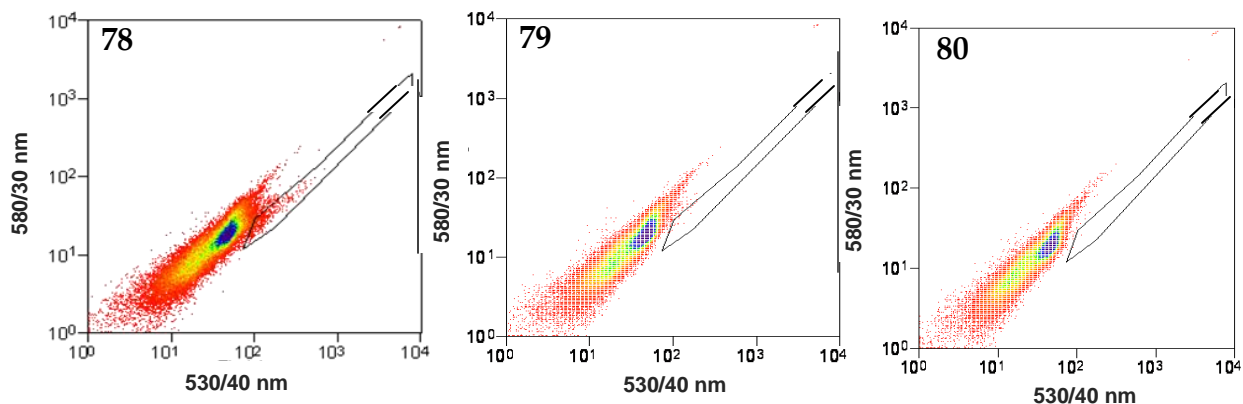


Figure 2.19 Dot plots showing the difference in hydrolysis of substrates 78 – 80

The order of hydrolysis was found to be FDA > 78 > 79 ≈ 80. When observing the rate of hydrolysis over time, an increase can clearly be seen for FDA, with much slower rates seen with increasing chain length (See Figure 2.20).

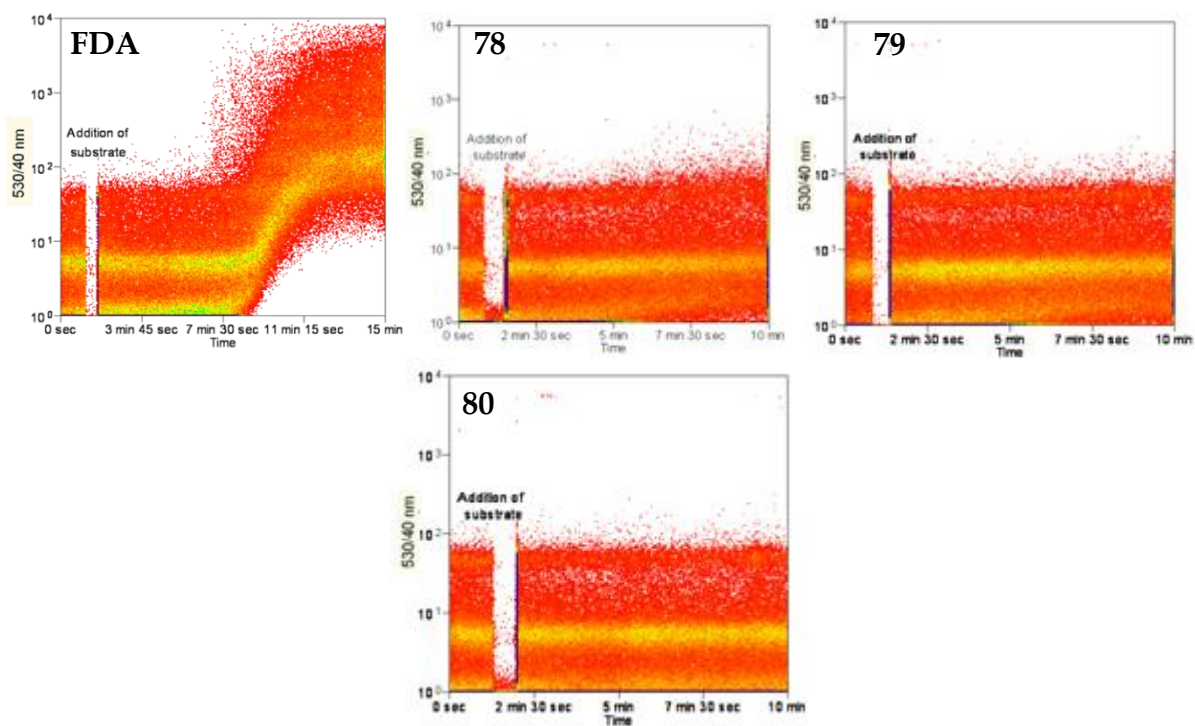


Figure 2.20 Addition of FDA and 78 – 80 with increase in fluorescence at 530/40 nm over time recorded

Importantly, the relative rates of hydrolysis within protoplasts were the same as that observed with purified *AtCXE12* and therefore compounds 78 and 79 could be used as probes for the directed evolution experiments. In addition to this, when viewed under the fluorescent microscope excellent uptake of all substrates was observed with no

interference seen from cellular autofluorescence. Attention now focussed on mutagenesis techniques with the aim of producing an improved lipase-like enzyme.

### 2.2.3.3 Site directed mutagenesis

As discussed in Section 2.2.3.1, both *AtCXE12* and BFAE contain a tyrosine residue in the analogous position within the respective protein. With HSL no longer exhibiting lipase activity with a smaller alanine residue in the analogous position, it was hypothesised that mutation of Tyr198 to alanine would result in the ability of *AtCXE12* to hydrolyse longer chain esters. Experiments were undertaken to affect this mutation using site directed mutagenesis.

Site directed mutagenesis is a technique which is able to introduce specific mutations at a desired point within a DNA sequence and is discussed in Section 1.2.3. The Quick Change II kit from Stratagene was used with the DNA polymerase *Pfu* turbo and oligonucleotides which contained two nucleotide base changes (T - G, A - C), which caused the amino acid change from tyrosine to alanine. Gel electrophoresis (Figure 2.21) showed a single band of the correct size. Following transformation in *E. coli* and subsequent plasmid purification using the Promega Wizard MiniPrep kit, DNA sequencing confirmed the successful mutation of tyrosine to alanine.

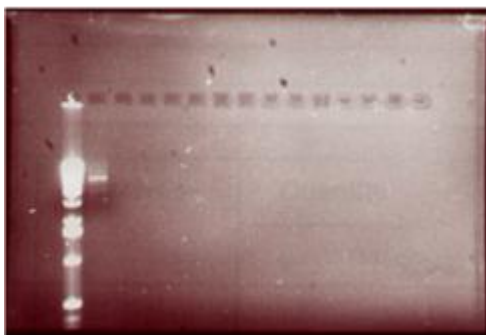
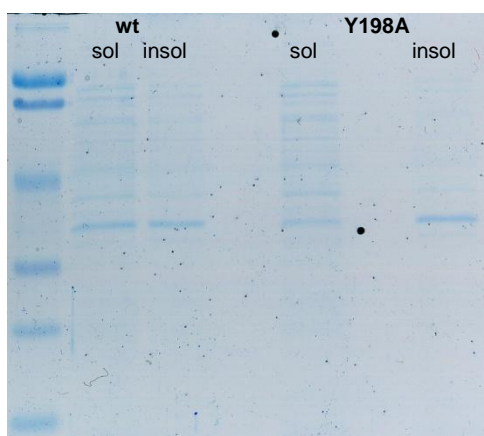


Figure 2.21 Gel electrophoresis of *AtCXE12* Y198A

The mutated Y198A protein was overexpressed using tuner(DE3)pRARE cells and purified using a nickel chelate column. The purified protein was then used in screening experiments with the fluorescein ester probes. The screening conditions employed were identical to those used for the previous *AtCXE12* wild-type enzyme. Unfortunately, no activity was seen with any of the substrates, even with FDA. In order to show that the lack of activity was not due to problems with protein expression, analysis was

undertaken to show this. Expression of the *AtCXE12* Y198A mutant was shown using SDS-PAGE and Western blot analysis. Following lysis of the bacteria by sonication both the soluble and insoluble fraction were heated to 90 °C in SDS loading buffer. These were loaded onto an SDS-PAGE gel alongside the soluble and insoluble fraction of the wild-type enzyme for comparison. Bands could be seen in all four lanes (Figure 2.22). Western Blot analysis using the monoclonal anti-His tag antibody conclusively proved that expression had occurred in both the soluble and insoluble fraction by the presence of a single band in all four lanes (Figure 2.23). The levels of expression were comparable in both the wild-type and the Y198A mutant.



**Figure 2.22 SDS-PAGE analysis showing bands corresponding to *AtCXE12* in all four lanes**

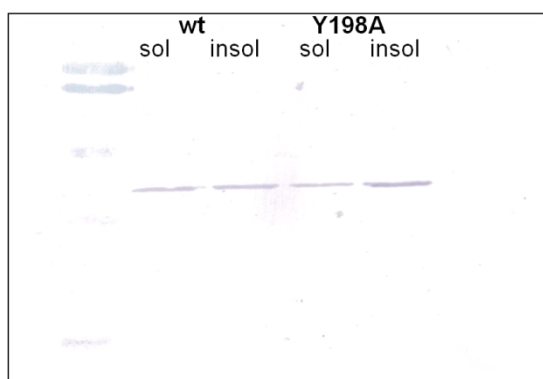


**Figure 2.23 Western blot showing expression of *AtCXE12* and *AtCXE12* Y198A mutant**

The lack of activity of the Y198A mutant was therefore not due to problems with expression but suggested that the Tyr198 residue is critical for catalytic activity.

Due to the disappointing result, efforts now concentrated on the use of random mutagenesis techniques in the directed evolution studies. Error-prone PCR was chosen as the preferred method and the work undertaken is described in the following section.

#### **2.2.3.4 Error-prone PCR**

Error-prone polymerase chain reaction (epPCR) is a random mutagenesis technique in which mutations are deliberately introduced during PCR through the use of error-prone DNA polymerases and reaction conditions (See Section 1.2.4). The error-prone polymerase which was used in these studies was developed by the Connolly group at Newcastle University.<sup>117</sup> A mutant of the high-fidelity DNA polymerase from *Pyrococcus furiosus* (Pfu-pol) was developed, which was able to introduce random errors using the same conditions as with the wild type enzyme. Pfu-pol contains 3'-5' proof reading activity in which any incorrectly placed nucleotides are removed and replaced with the correct base.<sup>118</sup>

DNA polymerases are multi functional proteins. They contain a pol domain, which consists of three sub-domains termed the palm, fingers and thumb. These sub-domains are responsible for DNA replication, with the fingers playing an important role in dNTP recognition. This finger sub-domain is highly conserved in archeal polymerases, of which Pfu-pol is an example. It contains two long anti-parallel  $\alpha$ -helices separated by a loop region (See Figure 2.24). A number of amino acids present on both of the  $\alpha$ -helices are brought in close proximity to each other as a result of the folding of the helix-loop-helix motif. Due to the highly conserved nature of these helix-loop-helix motifs a similar mechanism of dNTP recognition and accurate DNA replication can be inferred. The crystal structure of a viral polymerase enzyme/primer/template-dNTP complex has been solved and clearly showed a larger movement in the fingers sub-domain upon dNTP binding.<sup>119</sup> In addition to this, kinetic studies<sup>120</sup> have indicated that DNA polymerase fidelity is highly dependent on protein conformational changes. It shows that this involves the transient association of any dNTP with the enzyme-bound primer/template, with a conformational change triggered only when the incoming dNTP forms a Watson-Crick base pair. This change allows the assembly of the active site and subsequent polymerisation. In this way any incorrect dNTPs are rejected and fidelity is maintained.<sup>121</sup>

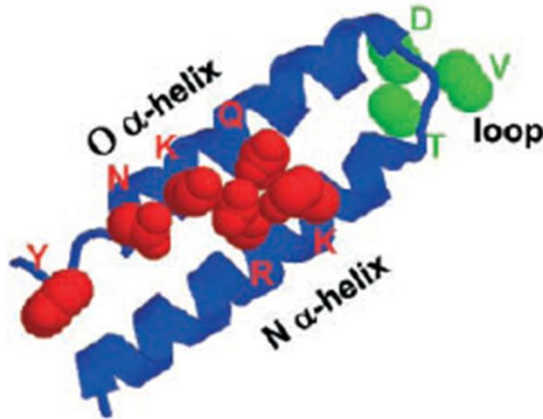


**Figure 2.24** Structure of the finger sub-domain of the DNA polymerase from *Thermococcus* species 9°N-7. The amino acid residues shown in green are those present in the loop region, with the highly conserved amino acid residues present in the  $\alpha$ -helices which are brought together on the same side of the motif shown in red. Biles B.D. and Connolly B.G., *Low-fidelity Pyrococcus furiosus DNA polymerase mutants useful in error-prone PCR*, *Nucleic Acids Research*, 2004, 32, e176, by permission of Oxford University Press.

In an attempt to produce a low-fidelity Pfu-pol, Connolly first removed the 3'-5' proof-reading activity with the mutation D215A. Three amino acid residues were then targeted for mutation: T471, Q472 and D473. These are all present within the loop region in Pfu-pol. Using site-directed mutagenesis all three targeted amino acids were changed to both alanine and glycine in the hope that these smaller residues would give increased flexibility within the loop region. In order to assess the accuracy of the mutant DNA polymerases, a *lacIOZ $\alpha$*  fidelity assay was performed. This assay makes use of the fact that DNA polymerases which make no mistakes copying the *lacI* gene result in an active lac repressor which prevents the transcription of the *lacZ $\alpha$*  gene. Therefore, those *E. coli* strains which are transformed with the amplified product cannot express an active  $\beta$ -galactosidase and plaques are unable to hydrolyse X-Gal and appear white. If the polymerase introduces errors into *lacI* this may give rise to a repressor unable to bind DNA and therefore subsequent transcription of *lacZ $\alpha$*  results in the production of  $\beta$ -galactosidase and blue plaques. The number of mutations which give rise to an inactive repressor in the *lacI* gene is known<sup>122</sup> and therefore the ratio of blue and white plaques can be converted to a mutation load and hence error rate of the polymerase. Screening the mutant Pfu-pol using this method showed that the mutants Q472A/G and D473A/G gave the highest error-rate.

D473G was then used to amplify the entire plasmid pET17b[Pfu-pol]. Following plating, 19 plasmids were isolated and sequenced over an identical stretch of 500



nucleotides, corresponding to the first 167 amino acids in the *Pfu-pol* gene. From the total 9500 bases sequenced, 68 mutations occurred across the whole stretch of DNA, with no hot spots observed. Table 2.6 shows the mutational bias of the D473G as compared to that of *Taq* in previous studies undertaken.<sup>117</sup>

Mutation	Pfu-pol(exo <sup>-</sup> ) D473G	Taq-pol (Mn <sup>2+</sup> / unbalanced dNTPs)	Taq-pol (unnatural mutagenic bases)
A→T/T→A	28	40.9	0.2
A→C/T→G	7.4	7.3	8.4
A→G/T→C	19.2	27.6	78.3
G→A/C→T	22	13.6	13.2
G→C/C→G	7.3	1.4	0.7
G→T/C→A	10.3	4.5	0.0
Insertion	2.9	0.3	~0
Deletion	2.9	4.2	~0

Table 2.6 Mutation spectra for D473G and Taq-pol in error-prone PCR<sup>117</sup>

An ideal, unbiased error-prone polymerase would exhibit all mutations with an equal frequency of 16.7%, preferably with no deletions or insertions. The mutational spectrum of D473G was shown not to be completely random, however, it did show much less bias than those of Taq-pol. Using this mutant polymerase, error-prone PCR methods were developed with the aim of mutating *AtCXE12*.

#### 2.2.3.4.1 epPCR methodology development

In order to ascertain the optimal reaction conditions for epPCR, several reactions were carried out using a variety of D473G and *AtCXE12* template dilutions, with the subsequent PCR products being analysed by gel electrophoresis. Dilutions were carried out using dH<sub>2</sub>O (See Experimental Section for full details of PCR cycling parameters). Table 2.7 below shows the different dilutions used in the test reactions. Another DNA polymerase, V93Q(exo<sup>-</sup>), which simply lacks the 3'-5' proof-reading activity was also used as a comparison.

TUBE	D473G(exo <sup>-</sup> )	V93Q(exo <sup>-</sup> )	<i>AtCXE12</i> template
A1	1/10	-----	1/10
A2	1/100	-----	1/10
A3	1/1000	-----	1/10
A4	1/10	-----	1/100
A5	1/100	-----	1/100
A6	1/1000	-----	1/100
B1	-----	1/10	1/10
B2	-----	1/100	1/10
B3	-----	1/1000	1/10
B4	-----	1/10	1/100
B5	-----	1/100	1/100
B6	-----	1/1000	1/100

**Table 2.7** Conditions employed for the test reaction to optimise the error-prone PCR reaction

Following analysis, it can clearly be seen from the gel (Figure 2.25) that the reaction containing 1/10 dilution of D473G(exo<sup>-</sup>) and 1/100 of *AtCXE12* template gave the best result.

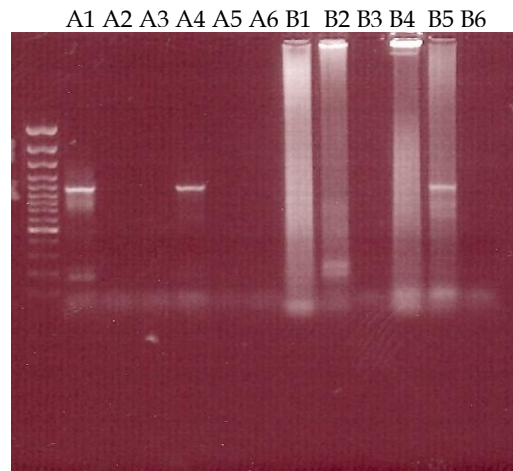


**Figure 2.25** Fluorescent image of conditions tested for the epPCR reaction showing 1/10 dilution of D473G and of 1/100 *AtCXE12* template (Lane A4) gave the best result.

The reaction was repeated on a larger scale to produce a large quantity of the *AtCXE12* megaprimer. The PCR products were purified using a Perfectprep Gel Cleanup Kit (Eppendorf). The concentration of the megaprimer was 134 ng/ $\mu$ L, as determined by a NanoDrop 1000 (Thermo Scientific).

The next step was the clone reaction, and again test reactions were performed to determine the optimal reaction conditions. A variety of megaprimer:*AtCXE12* template

ratios were prepared and the full set of reaction conditions can be seen in the table below (Table 2.8).

	Megaprimer	<i>AtCXE12</i> template	dNTPs	10x buffer	dH <sub>2</sub> O	Phusion Pol
<b>Control 1</b>	250 ng (2 µL)	100 ng (1 µL)	1 µL	5 µL	41 µL	-----
<b>Reaction 1</b>	250 ng (2 µL)	100 ng (1 µL)	1 µL	5 µL	41 µL	1 µL
<b>Control 2</b>	250 ng (2 µL)	300 ng (2.5 µL)	1 µL	5 µL	39.5 µL	-----
<b>Reaction 2</b>	250 ng (2 µL)	300 ng (2.5 µL)	1 µL	5 µL	39.5 µL	1 µL
<b>Control 3</b>	250 ng (2 µL)	500 ng (4 µL)	1 µL	5 µL	38 µL	-----
<b>Reaction 3</b>	250 ng (2 µL)	500 ng (4 µL)	1 µL	5 µL	38 µL	1 µL
<b>Reaction 4</b>	500 ng (4 µL)	100 ng (1 µL)	1 µL	5 µL	39 µL	1 µL
<b>Reaction 5</b>	500 ng (4 µL)	300 ng (2.5 µL)	1 µL	5 µL	37.5 µL	1 µL
<b>Reaction 6</b>	500 ng (4 µL)	500 ng (4 µL)	1 µL	5 µL	36 µL	1 µL

**Table 2.8 Reaction conditions for clone reaction tested. *AtCXE12* template concentration was 123 ng/µL**

Control reactions in which no DNA polymerase was added were performed as a negative control. Following PCR, the products were purified using a Qiagen PCR kit and the original DNA template was removed by *DpnI* digestion. The *DpnI* digestion product was transformed into *E. coli* and the number of colonies on each plate was recorded. There were no colonies present on any of the control plates, nor from reaction 1. Reaction 3 was deemed to give the optimal results and therefore these ratios were used in all subsequent reactions (See Figure 2.26).

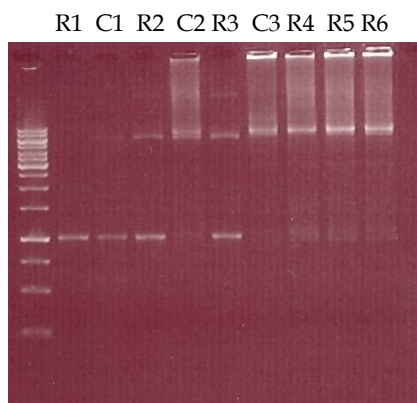


**Figure 2.26** Fluorescent image of gel showing reaction conditions for clone reaction, with R3 giving optimal results.

A selection of individual colonies was taken and the resulting purified plasmid was sequenced. Pleasingly, mutations had occurred in all the sequences and importantly were spread across the whole of the *AtCXE12* gene. The mutational frequency was an average of 7.5 mutations per reaction. Table 2.9 below shows the mutations that were achieved.

Mutation	Pfu-pol(exo) D473G
A→T/T→A	22.5
A→C/T→G	6.3
A→G/T→C	13.8
G→A/C→T	40.0
G→C/C→G	6.3
G→T/C→A	8.8
Insertion	1.3
Deletion	1.3

**Table 2.9** Mutational bias of D473G polymerase in the error-prone PCR of *AtCXE12*

Another criteria in the assessment of mutational bias is the transition:transversion (Ts/Tv) ratio. Transition mutations are purine to purine changes (A and G) and pyrimidine to pyrimidine changes (T and C), while transversions are purine to pyrimidine and pyrimidine to purine changes. There are eight possible transversions and four possible transitions and an enzyme completely lacking any bias would have a Ts/Tv ratio of 0.5. Mutational bias can also be assessed by calculating the ratio of transition mutations, which for an unbiased enzyme should equal 1.0 and by comparing the frequency of mutating A and T *vs.* the frequency of mutating G and C, which should ideally be equal. Table 2.10 below shows these additional criteria and compares them to those of *Taq* polymerase, obtained from a study by Shafikhau *et al.*<sup>8</sup>

<b>Bias indicators</b>	<b>Pfu-pol(exo-) D473G</b>	<b>Taq polymerase</b>
Ts/Tv	1.2	0.8
AT→GC/GC→AT	0.4	1.9
AT changes	47.2%	75.9%
GC changes	49.1%	19.6%
Mutational frequency	7.5	4.9

**Table 2.10 Bias indicators for D473G and Taq polymerase**

As the D473G mutant has a lowered ability to correctly recognise the incoming dNTPs it was decided to test whether the concentration of dNTPs in the initial PCR would have an effect on the mutational bias of the enzyme. To this end, the concentration of the dNTPs were reduced to 25% of the original amount, with all other factors kept constant. The clone reaction was carried out under identical conditions as described previously and 10 of the resulting colonies were picked and plasmid purification performed. The purified plasmids were sequenced and the mutational frequency and bias was determined and can be seen in the table below.

<b>Mutation</b>	<b>Pfu-pol(exo-) D473G with 25% dNTPs</b>
A→T/T→A	22.4
A→C/T→G	10.3
A→G/T→C	8.6
G→A/C→T	37.9
G→C/C→G	3.4
G→T/C→A	15.9
Insertion	1.7
Deletion	0.0
Ts/Tv	0.9
AT→GC/GC→AT	0.23
AT changes	41.4
GC changes	56.9
Mutational frequency	5.6

**Table 2.11 Mutagenesis bias and frequency exhibited with lower dNTP concentration**

It can be seen that decreasing the concentration of dNTPs causes a decrease in the mutational frequency during epPCR, but does not have a profound effect on the mutational bias. In this way, the mutational frequency of the D473G mutant can be controlled simply by altering the dNTP concentration.

### 2.2.3.4.2 On-plate screening

Before studies regarding protoplast transformation were carried out, screening in bacteria was performed in the hope of isolating an improved biocatalyst directly from bacterial cells. Two techniques were tested, both of which utilised on-plate screening. The first technique was based on previous work by Kunkel<sup>123,124</sup> in which the screening for specific activity was carried out directly on the agar plate. This method was repeated using colonies containing *AtCXE12* mutants, *AtCXE12* wild-type and pET28a (the latter two as positive and negative controls). Colonies were picked and streaked across a specific area, using the grid in Figure 2.27 as a template.

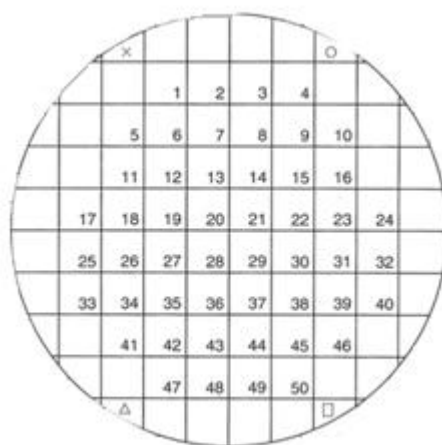
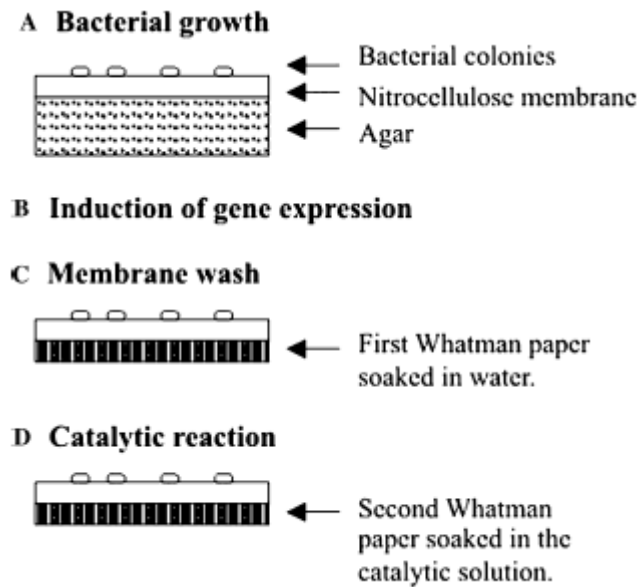


Figure 2.27 Grid template used for on-plate screening of recombinant esterases

Two duplicate plates were prepared and were incubated overnight at 37 °C. A nitrocellulose (NC) membrane was cut to size and 1 ml of a 1 mM solution of **79** in acetone was poured onto the membrane. Unfortunately this caused the NC membrane to dissolve. EtOH, MeOH and *i*PrOH were found to be suitable for the NC membrane, however, **79** showed poor solubility in these solvents. Chloroform was found to be the most suitable solvent and this was used in all subsequent on-plate screening experiments. **79** in chloroform (1 mM) was poured onto the NC membrane and blotted onto one of the plates. Disappointingly, when viewed under a UV lamp all the colonies exhibited fluorescence. This indicated that the background activity within the *E. coli* was too high to allow any meaningful results to be gained.

The second method, based on work done by Senn and Wolosiuk<sup>125</sup> screening for phosphatase activity in bacteria, was then investigated. In this method bacteria were

plated out directly on a NC membrane which had been placed on top of an agar plate (See Figure 2.28).



**Figure 2.28** Outline of the procedure for screening catalytic activity. A) Bacteria are plated directly onto a NC membrane. B) Appropriate inducer is added to the agar plate. C) NC membrane is placed, colonies side up, on a Whatman filter paper soaked in water. D) Whatman filter paper, pre-soaked in the catalytic solution, replaces the paper used in the previous step. Reprinted from *Analytical Biochemistry*, Senn A.M. and Wolosiuk R.A., *A high-throughput screening for phosphatases using specific substrates*, 150-156, Copyright (2005), with permission from Elsevier

This was repeated using the mutant *AtCXE12* library and the *AtCXE12* wild-type on separate plates. Again, when the colonies were viewed under a UV lamp they all fluoresced. Due to these poor results, all future efforts were concentrated on direct transformation and screening in protoplasts.

### 2.2.3.5 *Agrobacterium*-mediated transformation

Previous work within the group had focussed on the use of electroporation and PEG-mediated transformation of protoplasts. However, transformation yields were often as low as 5% and for this reason attention turned to the technique of *Agrobacterium*-mediated transformation of plants, with subsequent protoplast isolation being carried out on transformed plants. For a more detailed description of *Agrobacterium*-mediated transformation see Section 1.4.2.4. Before this transformation technique could be utilised molecular biology experiments were undertaken to clone *AtCXE12* into the

appropriate vectors necessary for this form of transformation. The work undertaken is described in the next section.

### 2.2.3.5.1 Cloning of *AtCXE12* into binary vectors

All previous experiments were undertaken with *AtCXE12* present in the pET24(d) bacterial vector. However, in order to transform plants *AtCXE12* needed to be cloned into a binary vector. Binary vectors are able to transform both *E. coli* and *Agrobacterium* and therefore *AtCXE12* was cloned into the correct binary vector.

The vector chosen for *Agrobacterium*-mediated transformation was the BIN-STRP3 vector. This contains a streptavidin tag which is used for purification of the resulting plasmid/protein by making use of the biotin-streptavidin affinity system.<sup>75</sup> However, direct cloning into this vector was not possible due to the absence of the appropriate restriction sites in the *AtCXE12*-pET24(d) construct. Therefore, initial experiments involved the introduction of the necessary cloning sites. The flowchart in Figure 2.29 highlights the required steps necessary for cloning into BIN-STRP3.

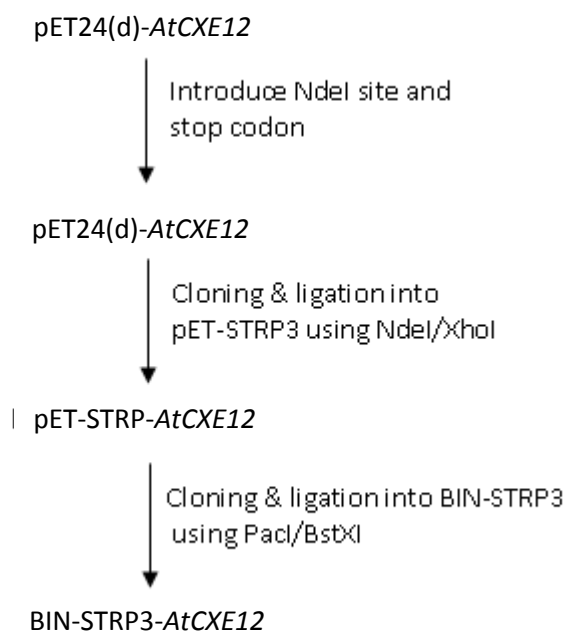


**Figure 2.29** Flowchart of cloning experiments necessary to produce the *AtCXE12* binary vector construct

The first step was to introduce a NdeI site at the beginning of the *AtCXE12* sequence and a stop codon at the end. The expression of *AtCXE12* from pET24(d) places a His tag



at the end of the sequence, which is used for purification of the protein. However, the BIN-STRP3 vector places a streptavidin tag onto the protein and therefore the His tag is no longer required. The stop codon placed at the end of the sequence prevents the His tag from being translated during protein overexpression. Two primers were designed with the appropriate nucleotide base changes and following PCR with KOD DNA polymerase, gel electrophoresis confirmed the successful reaction. The sequence changes were conclusively proven following DNA sequence analysis.

The modified pET24(d)-*AtCXE12* construct was then cloned and ligated into the pET-STRP3 vector. Digestion was achieved by incubating the *AtCXE12* construct with NdeI (1 µL) and XhoI (1 µL) restriction enzymes at 37 °C for 2.5 hours. In addition to this the pET-STRP3 vector was incubated with NdeI (1 µL) and SalI (1 µL). The digestion products were analysed by gel electrophoresis (See Figure 2.30) and the bands corresponding to the purified *AtCXE12* insert and pET-STRP3 vector were excised and purified using a QIAquick Gel Extraction kit (QIAGEN).

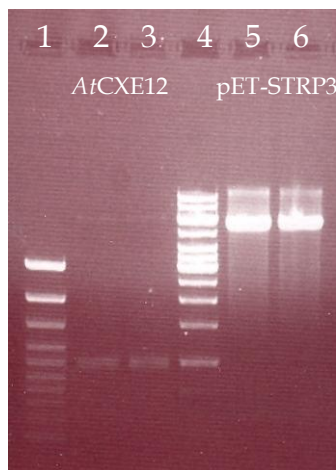


**Figure 2.30** Gel electrophoresis of *AtCXE12* insert and pET-STRP3 vector following digestion with NdeI/XhoI and NdeI/SalI respectively. Lanes 1 and 4 correspond to 100 bp and 1 kb ladder markers respectively.

Ligation was achieved using T4 DNA ligase (1 µL) and a 1:1 ratio of insert:vector, with incubation at 16 °C for 2.5 hours. As a control, the ligation was performed without an insert present. Following transformation into Top10 competent cells and overnight incubation, colonies were achieved for the ligation mixture, with no colonies present on the control plate. In order to check the presence of the *AtCXE12* insert, a NdeI/XhoI digest was undertaken. The purified pET-STRP3-*AtCXE12* was incubated with NdeI and XhoI as done previously and analysed by gel electrophoresis. Figure 2.31 clearly

shows two products in Lane 1, which correspond to the insert and vector indicating successful digestion and hence presence of *AtCXE12* insert. Again DNA sequencing showed that *AtCXE12* was present and, importantly, without errors.

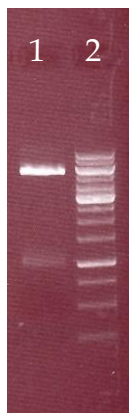


**Figure 2.31** The *AtCXE12* insert and vector can clearly be seen as two products in Lane 1. Lane 2 contains 1 kb ladder markers

In order to check that *AtCXE12* retained activity in the pET-STRP3 vector, the protein was overexpressed from tuner(DE3)pRARE cells and grown to kanamycin and chloramphenicol resistance. Several of the resulting colonies were incubated in LB media at 37 °C, with shaking, for 5 hours. IPTG was added to induce expression and following pelleting and lysis by sonication, the supernatant was tested for esterase activity against *pNPAc*. The colourless solution became a yellow colour rapidly, indicating that *AtCXE12* was still active in the pET-STRP3 vector.

The final step involved the cloning and ligation of *AtCXE12* into the binary vector, BIN-STRP3. However, several problems were encountered during this step. Initially, both *PacI* and *BstXI* were incubated together with pET-STRP3-*AtCXE12* in NE Buffer 2. However, gel electrophoresis indicated that the digestion enzyme *PacI* had not cut the construct. The digestion was repeated using only *PacI*, again in NE Buffer 2. This time, analysis showed that *PacI* did cut, as can be seen by the presence of two bands in Figure 2.32. Lane 2 contains the control reaction in which no *PacI* was added. However, this did show that *PacI* digestion was not 100% successful. This was probably due to NE Buffer 2 not being the optimal buffer for *PacI* digestion. The *PacI*/*BstXI* digestion was repeated; however, again analysis indicated that *PacI* was not cutting. Due to the disappointing results when both restriction enzymes were used together and the fact that using *PacI* only seemed to result in a successful reaction, it was decided to perform

this reaction in two separate steps. In this way optimal buffers for each individual restriction enzyme could be used.

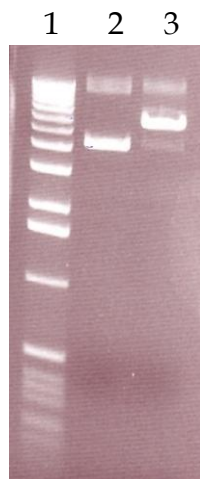


**Figure 2.32 Lane 3 shows two products from successful PacI digestion.**

To this end, digestion of pET-STRP3-*AtCXE12* using PacI in NE Buffer 1 was successfully achieved, following incubation at 37 °C for 3 hours. The digestion product was then purified before BstXI digestion was attempted. 2.5 volumes of 100% EtOH was added to the PacI digestion mixture and the solution was incubated on ice for 10 mins. This was then centrifuged at 14,000 rpm for 10 mins and the resulting supernatant removed. 100 µL 70% EtOH was added to the pellet to remove any traces of salts. Following centrifugation, the supernatant was removed and the DNA pellet was left to dry and then resuspended in dH<sub>2</sub>O. BstXI was added to an aliquot of the purified DNA in NE Buffer 3 and incubated at 55 °C for 3 hours. After analysis by gel electrophoresis, excision of the bands and subsequent purification was performed and the solution was dried on the freeze-drier and resuspended in dH<sub>2</sub>O. Ligation using T4 DNA ligase was performed and following transformation three colonies grew. Plasmid mini-preps were performed on each of these colonies and the resulting plasmids were analysed by gel electrophoresis following digestion with PacI/BstXI (See Figure 2.33). Lanes 2 and 3 show successful ligation and these plasmids were taken forward in the next steps.

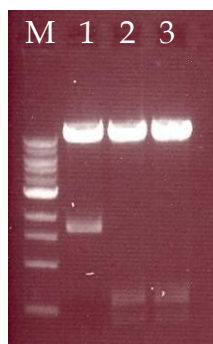


Figure 2.33 Fluorescent image of gel electrophoresis following digestion with PacI/BstXI. Lanes 2 and 3 show successful digestion. M = 1 kb markers

#### 2.2.3.5.2 Transformation and infiltration

BIN-STRP3-*AtCXE12* plasmid was transformed into XL-10 competent cells and the plasmid was recovered and purified using a Wizard Mini-Prep kit (Promega). This was then used to transform *Agrobacterium* by electroporation methods and following plating, they were incubated for 48 hours. One colony was picked and grown up in 10 ml LB media with overnight incubation. At this time, a plasmid containing p19 was also transformed into *Agrobacterium*. In plants, post-transcriptional gene silencing (PTGS) acts as a defence system against virus infection.<sup>126</sup> It does this by recognising foreign RNAs and causes their degradation in the cytoplasm. Some plant viruses have suppressors to counteract PTGS and one such example is p19. p19, a 19K protein from *Tomato bushy stunt virus* (TBSV), is a viral protein that has been identified as a PTGS suppressor.<sup>127</sup> In order to prevent the plant's defence system degrading the infiltrated *Agrobacterium*, a 1:1 mixture of *Agrobacterium*-transformed *AtCXE12* and *Agrobacterium*-transformed p19 were mixed together. After centrifugation, the resulting pellet was resuspended in 20 ml dH<sub>2</sub>O and this suspension was used for infiltrating *N. benthamiana* leaves. This was achieved using a 1 ml syringe placed against the underside of the leaf. Through the use of slight pressure, the suspension is forced into the leaf, whereupon transfer into the leaf cells can take place. A control plant, in which a suspension of only *Agrobacterium* transformed with p19 was present, was also prepared. All infiltrated plants were left for 4 days in the greenhouse.

After this time, several leaves were removed and the transformation and activity was checked. This was achieved by incubating a protein extract from the leaves with pNPac. The protein concentration was determined by Bradford assay and found to be 3.36 mg/ml for *AtCXE12* infiltrated leaves and 2.42 mg/ml for the p19 control leaves. 5 µL of pNPac was added to 1 ml of protein and the absorbance was recorded in

duplicate at 400 nm. *AtCXE12* protein extract was found to have a rate of  $0.6322 \pm 0.008 \text{ min}^{-1}$  with the p19 control being  $0.0320 \pm 0.003 \text{ min}^{-1}$ . This result showed that those leaves that had been infiltrated with *AtCXE12* had been successfully transformed and pleasingly, that the rate of hydrolysis of *pNP*Ac was 20-fold higher than the background activity. This meant that during the screening process, background activity would have a negligible effect and the chance of false positives would be greatly reduced.

With *AtCXE12* now successfully cloned into the binary vector and *Agrobacterium*-mediated transformation proving to be a viable method, efforts now concentrated on using epPCR techniques on the BIN-STRP3-*AtCXE12* construct to produce a recombinant library.

#### **2.2.3.5.3 *BIN-STRP3-AtCXE12* recombinant library**

Using the optimised epPCR conditions described previously, efforts to introduce random errors into the *AtCXE12* gene in the BIN-STRP3 construct were undertaken. Unfortunately, despite numerous attempts, the first step of the methodology was unsuccessful, with no megaprimers ever isolated from the PCR mixture. Due to time constraints this work was not completed.

### **2.2.4 Summary**

\* Fluorescein esters **78** – **80** were shown to be hydrolysed by *AtCXE12* in the order FDA > **78** > **79**  $\approx$  **80**, with **78** and **79** identified as potential probes in directed evolution experiments.

\* Tyrosine198 was targeted as a possible residue for mutation. This was successfully mutated into alanine by site-directed mutagenesis.

\* When **78** – **80** were screened against the *AtCXE12* Y198A mutant no activity was seen, even with FDA. Western blotting analysis revealed that the lack of activity was not due to expression problems and therefore Tyr198 is critical for enzyme activity.

\* Error-prone PCR techniques were employed in an effort to create a recombinant library. Protocol development revealed a 1/10 dilution of D437G(exo-) and 1/100 of

*AtCXE12* template gave the best mutation results, with the clone reaction employing a 1:2 ratio of megaprimer:*AtCXE12* template.

\* The mutational frequency of the D473G polymerase could be controlled by altering the dNTP concentration.

\* On-plate screening in *E. coli* indicated that the background activity was too high to allow any meaningful results to be gained.

\* *AtCXE12* was successfully cloned into the *Agrobacterium* vector BIN-STRP3.

\* *Nicotiana benthamiana* leaves infiltrated with *Agrobacterium* containing the BIN-STRP3-*AtCXE12* vector have been successfully transformed and the rate of hydrolysis of *p*NPAc was 20-fold higher than the background activity.

\* Efforts to introduce random errors into the *atcx12* gene contained within the BIN-STRP3 construct were unsuccessful.

## **2.3 Conclusions**

To enable an improved mutant of an enzyme to be identified, relatively poor substrates selected from the enzyme kinetic studies are used as probes. Using directed evolution techniques to generate recombinant biocatalysts, a much improved enzyme can be identified as one which hydrolyses the probe molecule at a faster rate than the wild type. The model system first chosen to develop this process was *AtSFGH*.

Enzyme kinetic experiments with *AtSFGH* have shown that an increase in the chain length beyond C6 or the presence of bulky substituents led to diminished activity, whilst heteroatoms in the  $\alpha$ -position do not appear to be tolerated by the enzyme. In addition to this, compounds containing a peptide bond were also poorly hydrolysed which may have been due to a lack of conformational rotation.

Efforts to evolve *AtSFGH* were unsuccessful as the methylumbelliferyl ester derivatives were not uptaken by the protoplasts and therefore these were not deemed to be viable probes for the directed evolution and screening experiments. Although the naphthyl esters were uptaken by the cells the low intensity of fluorescence seen indicated that

longer chain esters would have no activity and would therefore be difficult to use in screening experiments. Based on the excellent ability of the protoplasts to uptake FDA, four fluorescein-based probes were targeted for synthesis, with their structure chosen using the data from the *AtSFGH* assays. As *AtSFGH* has a low activity towards FDA, another esterase enzyme, *AtCXE12* was used in the directed evolution experiments.

*AtCXE12* has shown to be a classic serine hydrolase responsible for the hydrolysis of a variety of esters, including **76**, within plant cells. The aim was to evolve this enzyme, which shows no activity towards long chain esters, to a more lipase-like enzyme, which will readily hydrolyse these compounds. A difference in activity was seen between *AtCXE12* and the different probes when screened *in vitro* and *in vivo* and therefore the fluorescein esters were shown to be applicable as probes in the directed evolution experiments.

Mutagenesis techniques included site directed mutagenesis, in which Tyr198 was successfully mutated to Ala198. Unfortunately, this change abolished all enzyme activity and was therefore postulated to be critical in the activity of the enzyme. Efforts turned towards the use of random mutagenesis techniques, in particular error prone PCR (epPCR). Using an error prone DNA polymerase, D473G(exo<sup>-</sup>), epPCR techniques were optimised and shown to randomly introduce errors throughout the *AtCXE12* sequence, at an average rate of 7.5 errors *per* PCR round. Attempts to screen in bacteria proved unsuccessful due to the high background enzyme activity rate.

Transformation of *Nicotiana benthamiana* plants using *Agrobacterium tumefaciens* was shown to be successful and following cloning into the appropriate binary vector, *AtCXE12* was transformed into *Nicotiana* plants. Subsequent activity assays of the transformed leaves showed them to have a 20-fold increase in activity towards *pNPAC* over the background activity. Unfortunately, efforts to introduce random errors in the binary construct were unsuccessful and due to time constraints no recombinant *AtCXE12* library was produced.

## 3 REACTIVITY PROBES

### 3.1 Introduction

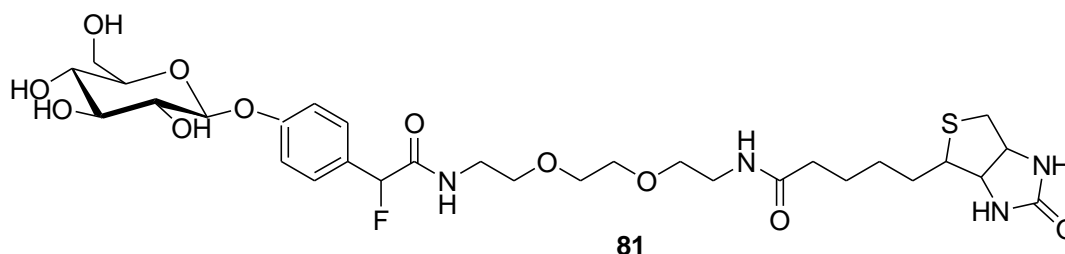
This chapter will consider the work undertaken on the isolation of proteins from cells by the use of reactivity probes. It will detail the rationale of the probe design, along with the synthesis, analysis and biological experiments undertaken with the aim of isolating specific enzymes from within a plant cell.

#### 3.1.1 Previous research

The reactivity probes discussed in the following sections can be described as mechanism-based probes, which make use of an electrophilic part of the molecule which is able to specifically react with catalytic residues within the vicinity of the active site. In these cases probes only bind to active forms of the target enzyme and subsequent measurement of probe modification can be used as an indication of the enzyme activity.

##### 3.1.1.1 *p*-Quinone methide systems

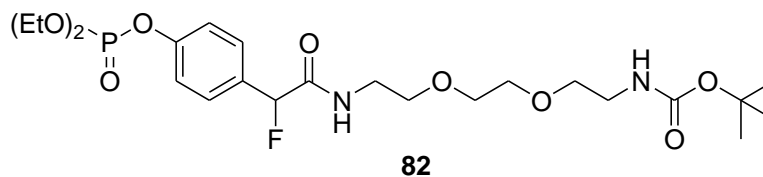
Several groups have made use of the quinone methide moiety as a trapping reagent. Tsai *et al*<sup>128</sup> reported on the use of **81** as a probe towards  $\beta$ -glucosidase activity.



This probe does not contain a fluorophore but instead has a biotin group which allows the isolation of covalently modified proteins using the biotin-streptavidin affinity system. Using  $^{19}\text{F}$  NMR spectroscopy it was shown that fluoride was released due to the appearance of a peak at -122 ppm, which supported the 1,6-elimination reaction. Following SDS-PAGE and Western Blotting analysis, a biotinylated  $\beta$ -glucosidase was isolated, although it was unable to be shown that this enzyme still retained its activity, which suggests either active site labelling or multiple labelling of the protein had occurred.



In an attempt to isolate phosphatase enzymes, Janda<sup>129</sup> designed the reactivity probe **82**, which was able to react with phosphatase enzymes by active site modification, resulting in an inactive enzyme.



**82** was synthesised in four steps in an overall yield of 30%. Upon addition of **82** to a phosphotriesterase enzyme, a precipitate began to form after three minutes. Using LC-MS it was observed that multiple modifications were occurring. The number of enzyme site modifications ranged from one to four and this can be seen in the MS profile in Figure 3.1.

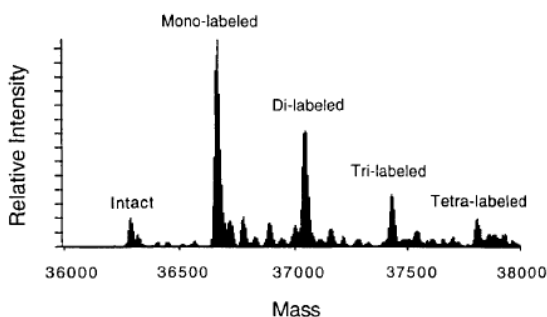


**Figure 3.1** MS profile of **82**-labelled phosphotriesterase proteins. Reprinted from *Bioorganic & Medicinal Chemistry Letters*, Lo L-C., Lo C-H.L., Janda K.D., Kassel D.B. and Raushel F.M., *A versatile mechanism based reaction probe for the direct selection of biocatalysts*, 2117-2120, Copyright (1996), with permission from Elsevier

In an extension to this work Zhu and co-workers utilised a *p*-quinone methide trapping reagent to selectively bind phosphatase enzymes<sup>130</sup> with a fluorescent molecule **83**. As with **82**, the leaving group employed was a fluoride ion and **83** was successfully shown to covalently link to a variety of phosphatases from different sources. In addition to this no labelling was seen when **83** was incubated with different classes of proteases or lipases, which highlights the selectivity of **83** (Figure 3.2). By making use of the fluorescent moiety Cy3, the fluorescent bands within the gel can easily be visualised and excised from the gel for further manipulation. However, due to the permanent state of fluorescence of **83**, sensitivity issues or false positives may be encountered.

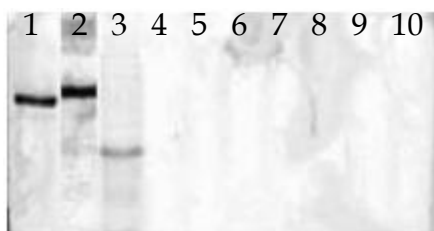
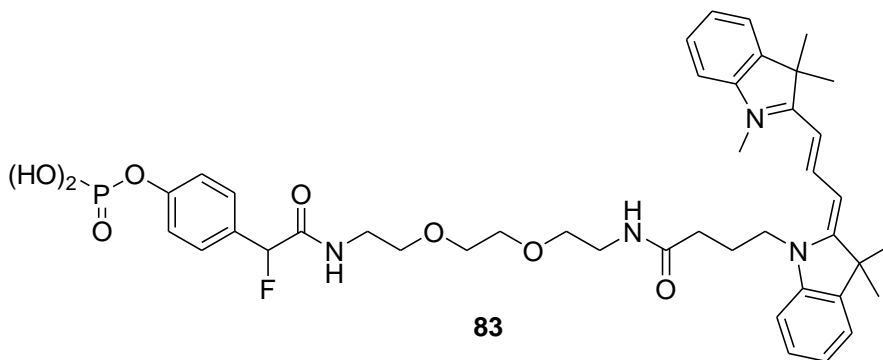
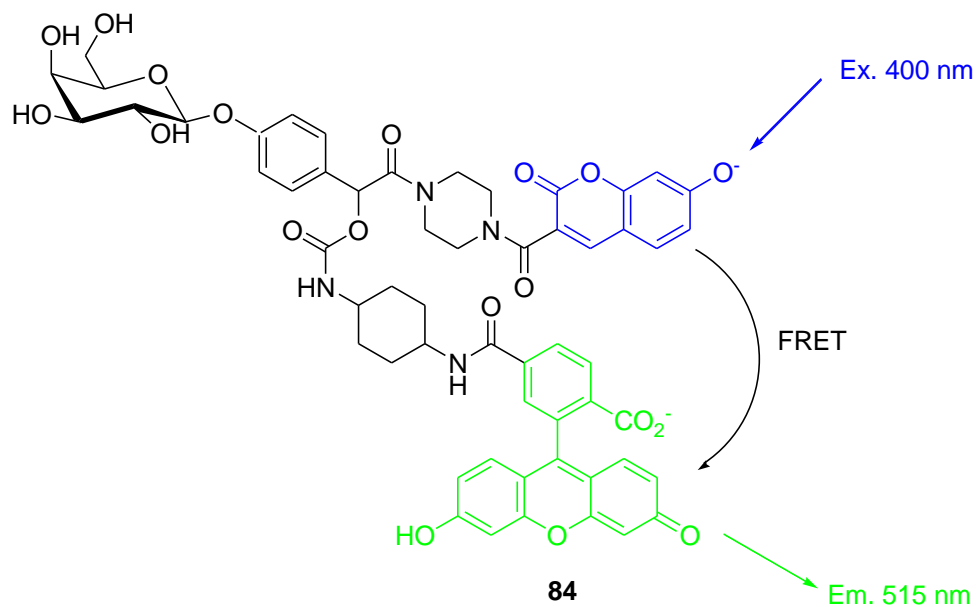


**Figure 3.2** Fluorescent image of SDS gel following incubation with **83**. Lanes **1 - 3** contain phosphatases with lanes **4 - 8** contain proteases and lanes **9 - 10** lipases. Reprinted from *Tetrahedron Letters*, vol 44, Zhu Q., Huang X., Chen G.Y.J. and Yao S.Q., *Activity-based fluorescent probes that target phosphatases*, 2669-2672, Copyright (2003), with permission from Elsevier

In an adaption to the techniques described above Komatsu *et al* developed a reactivity probe which upon binding to the enzyme resulted in a spectral change.<sup>131</sup> This allows for the easy visualisation of enzyme activity upon the probe and overcomes the issues which may be associated with probes such as **83**. The probe **84** was synthesised in 10 steps from the commercially available 4-hydroxymandelic acid. By utilising Förster resonance energy transfer (FRET), **84** can undergo a spectral change when a structural change has occurred. **84** has two fluorophores, 7-hydroxycoumarin and fluorescein which are able to undergo FRET. 7-hydroxycoumarin acts as the energy donor, with fluorescein acting as the energy acceptor. In the intact probe, the two fluorophores are spatially close together and FRET occurs efficiently, with emission seen only from the fluorescein moiety. Following enzymatic action, the  $\beta$ -galactopyranosyl group is removed, which results in loss of the carbamate linked fluorescein group in an analogous way to the loss of the fluoride ion seen in previous probes. This now results in the loss of FRET and emission from the 7-hydroxycoumarin is now observed.



It was calculated that the efficiency of FRET was greater than 93%. Upon addition of a  $\beta$ -galactosidase a rapid increase in the emission of 7-hydroxycoumarin and a corresponding rapid decrease in the emission of fluorescein was observed (See Figure 3.3). Using SDS-PAGE it was shown that **84** selectively bound  $\beta$ -galactosidase in the presence of  $\beta$ -glucosidase. When the gel was illuminated with 365 nm light, blue fluorescence was observed.

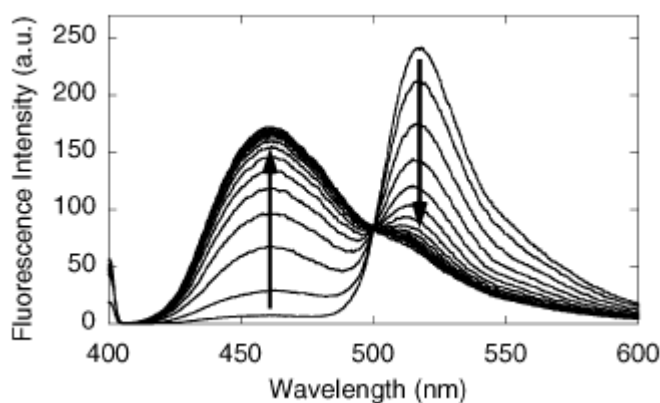
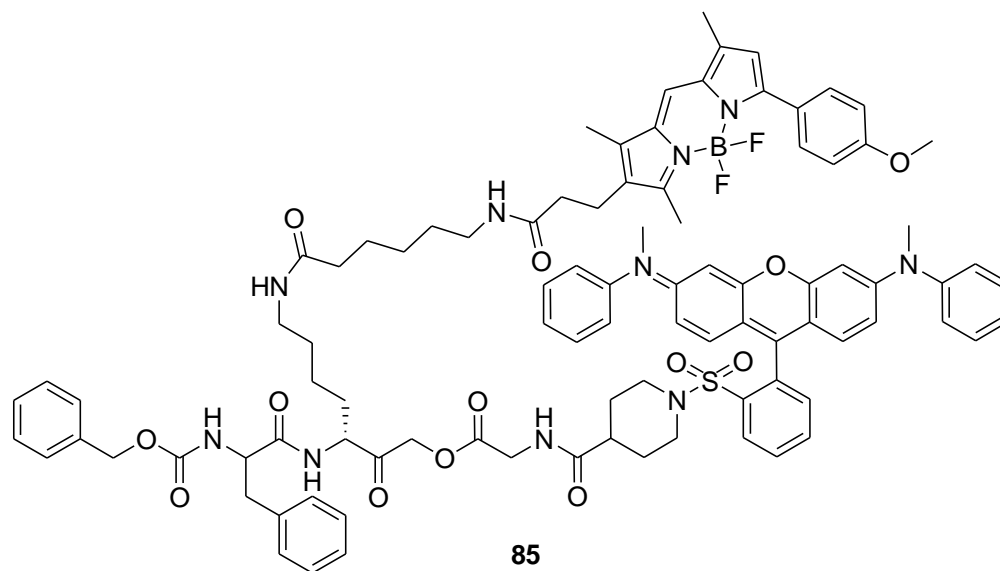


**Figure 3.3** Fluorescent spectrum of  $\beta$ -galactosidase incubated with **84**, with the change in fluorescence that can clearly be observed. Reprinted with permission from *Journal of the American Chemical Society*, 2006, 128, 15946-15947. Copyright 2006 American Chemical Society.

### 3.1.1.2 Fluorescently quenched reactivity probes

Although the use of FRET allows for a spectral change to be observed with **84** the ability to switch from a non-fluorescent probe to a fluorescent one upon enzyme activation would allow potentially overcome the disadvantages seen with the above mentioned probes. In this way it combines the advantages of **83** and **84** in that a change in emission gives increased sensitivity, with the ease of visualisation that comes from the use of a fluorescent tag.

The first example of a fluorescently quenched reactivity probe was published in 2005.<sup>132</sup> Due to the limitations of intrinsically fluorescent reactivity probes which include general fluorescence both when bound to an enzyme target and when free in solution, Blum *et al* designed a fluorescently quenched probe, **85**. This probe offers the advantage that it only becomes fluorescent after covalent modification by a protease enzyme. Using **85**, the authors claim that the experimental investigation of tumour pathophysiology can be achieved.



The acyloxymethyl ketone (AOMK) group was utilised as the recognition head for a class of proteases known as the cysteine cathepsins. Upon removal of this recognition head by the enzyme, the fluorescent quencher group, in this case QSY7, is eliminated and the fluorescence from the BODIPY analogue can be observed. Upon treatment in NIH-3T3 cells, **85** shows strong fluorescence in specific areas, which were later shown to be lysosomes. In contrast a control probe, which did not contain QSY7, shows diffuse fluorescence, which was removed by washing to show the specific fluorescence seen



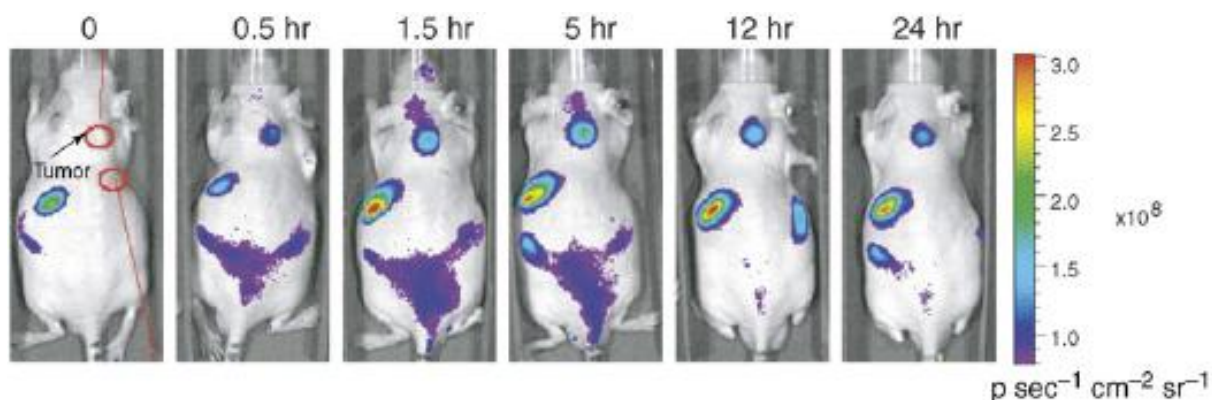


Figure 3.5 Optical imaging of tumours in live mice. Tumour cells were injected subcutaneously into the back of BALB/c nude mice 2 wks before imaging. 86 ( $2 \text{ mg g}^{-1}$ ) dissolved in DMSO/PBS was injected intravenously *via* the tail vein and fluorescent images of the dorsal side of living mice were taken at various time points after injection. Images are presented using a colorimetric scale based on photons per second per square centimetre per steradian ( $\text{p s}^{-1} \text{ cm}^{-2} \text{ sr}^{-1}$ ) overlaid on bright-light images. Reprinted by permission from Macmillan Publishers Ltd: *Nature Chemical Biology* (2007, 3, 668-677), copyright (2007).

### 3.2 Probe Design

The design of the reactivity probes discussed in this chapter is based on previous work carried out within the group which utilises the reactivity of a *p*-quinone methide. The probe contains a recognition head which is able to selectively react with specific enzymes and a fluorescent moiety to allow for easy visualisation. It also contains a fluorescent quencher group which prevents any emission from the fluorophore. Upon removal of the recognition head by enzymatic activity, the molecule undergoes a 1,6-elimination with loss of the fluorescent quencher group and generates the reactive quinone methide. This intermediate serves as the trapping device and due to its highly electrophilic nature is able to react with nearby nucleophilic residues present within the protein (See Figure 3.6).

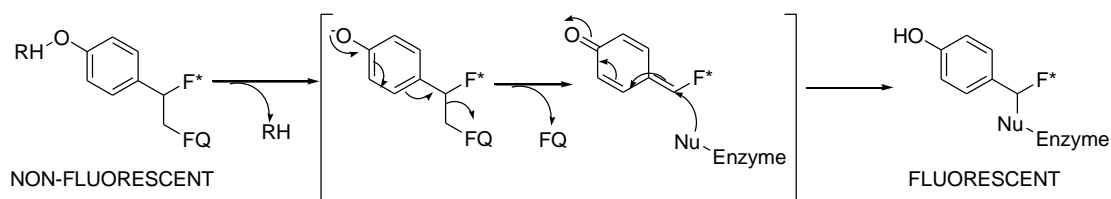
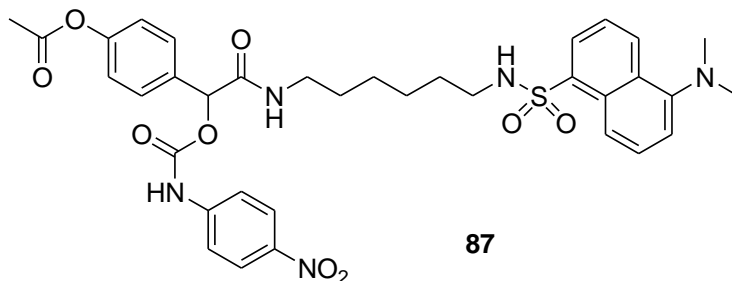


Figure 3.6 Mechanism of action of the reactivity probes. RH recognition head, F\* fluorophore, FQ fluorescent quencher, Nu nucleophilic residue present within the protein

The fluorophore was based on phenylacetylene, with *p*-nitrophenylisocyanate utilised as the fluorescent quencher. This was based on work done within the group, which

made use of this fluorescent quencher, albeit with the different fluorophore, dansyl chloride (unpublished results), **87**.

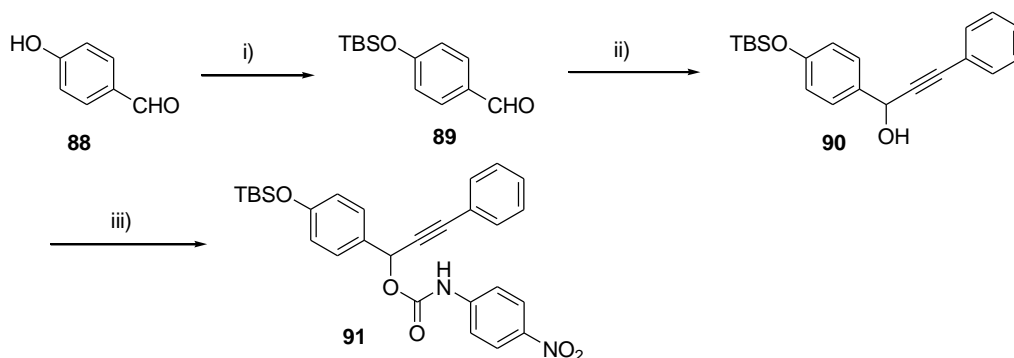


### 3.3 TBS probe

In order to test the design and action of the proposed reactivity probe, the current work synthesised a proof-of-concept probe based on a TBS protected phenol. This group was chosen as removal of the TBS group could easily be affected by treatment with TBAF. This would therefore allow the breakdown of the molecule by a 1,6-elimination to be confirmed.

#### 3.3.1 Synthesis

The TBS probe was synthesised as shown in Scheme 3.1



i) TBS-Cl, Et<sub>3</sub>N, DMAP, DCM, 0 °C, 2 h, 65%; ii) n-BuLi, phenylacetylene, THF, -78 °C, 1 h, 16%; iii) p-nitrophenylisocyanate, Et<sub>3</sub>N, rt, 1 h, 35%

Scheme 3.1 Synthesis of 91

4-hydroxybenzaldehyde, **88**, was treated with TBS-Cl in the presence of Et<sub>3</sub>N and DMAP to afford **89** as a pale yellow oil in almost quantitative yield. The presence of the TBS group was confirmed in the <sup>1</sup>H NMR spectrum by the appearance of peaks

corresponding to the *t*-butyl group (0.97 ppm, 9H) and the two methyl groups (0.22 ppm, 6H). **89** was subsequently reacted with *n*BuLi followed by phenylacetylene to furnish the propargylic alcohol **90** in a moderate yield of 16%. Two distinctive doublets that coupled to each other in the  $^1\text{H}$  NMR spectrum corresponding to the OH (2.24 ppm,  $d$   $^3J$  7) and the propargylic proton (5.62 ppm,  $d$   $^3J$  7) confirmed the structure. Finally reaction with *p*-nitrophenylisocyanate in the presence of a catalytic amount of  $\text{Et}_3\text{N}$  afforded the probe molecule **91**. Confirmation of the structure was obtained from the shift of the propargylic proton from 5.62 ppm to 5.52 ppm and a peak in the HRMS of 502.1918 ( $\text{M}^+$ ,  $\text{C}_{28}\text{H}_{30}\text{N}_2\text{O}_5\text{Si}$  requires 502.1924). UV/Vis analysis revealed **91** to have an absorption maximum at 371 nm (See Figure 3.7).

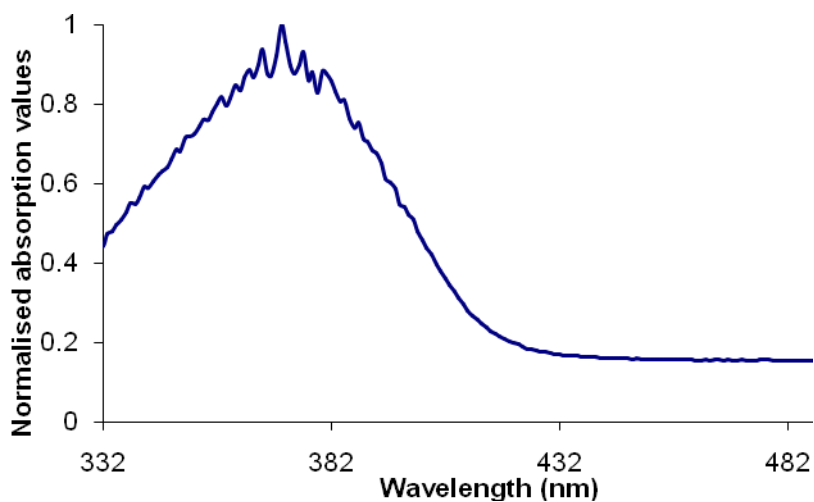


Figure 3.7 Absorption profile of **91**

### 3.3.2 1,6-elimination analysis

Having successfully prepared the probe the next stage was to test the hypothesis for the activation of the probe. Consequently, TBAF (100  $\mu\text{L}$ ) was added to a solution of **91** (1 mg/ml in acetone) in water and the resulting increase in fluorescence was recorded, Figure 3.8.



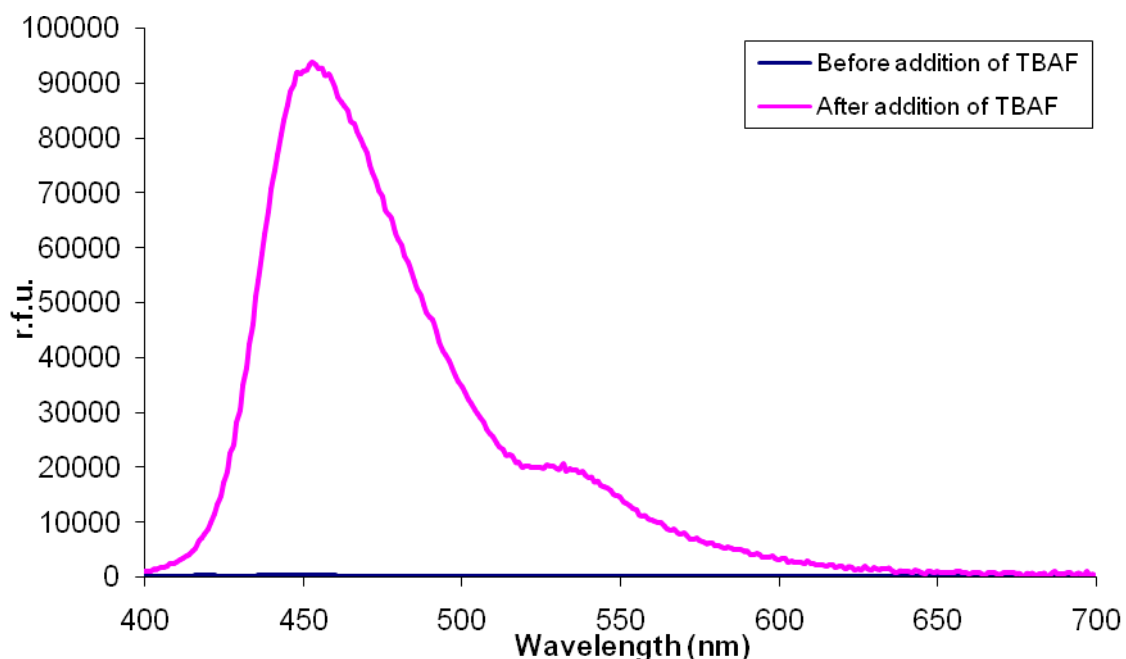
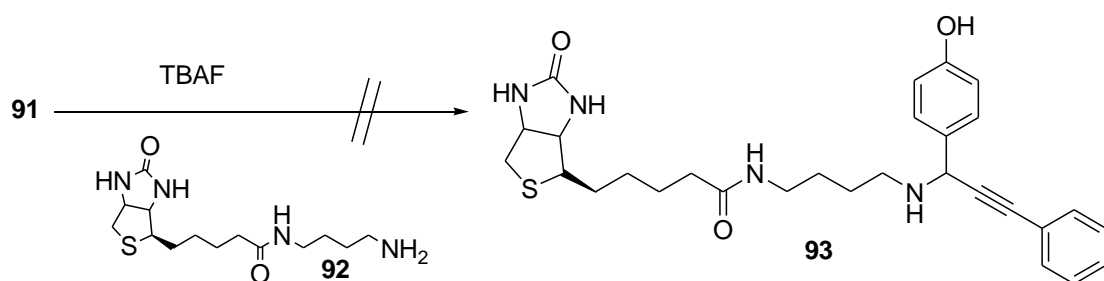


Figure 3.8 Fluorescence change of 91 after treatment with TBAF

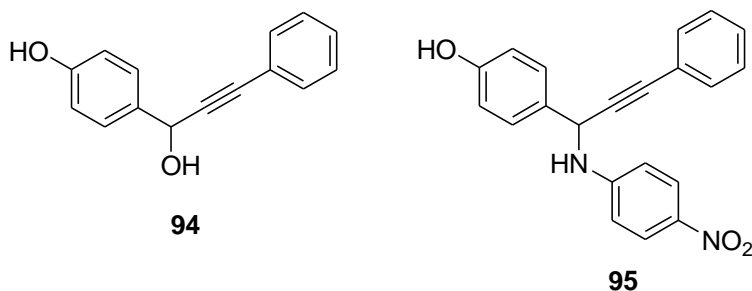
This shows that the probe is broken down as hypothesised and that an increase in fluorescence can be detected. In order to show that the probe was able to react with nucleophiles as predicted **91** was treated with TBAF followed by a biotin derivative **92** Scheme 3.2. Subsequent purification using streptavidin labelled beads would allow for the isolation of any fluorescently labelled biotin, **93**.



Scheme 3.2

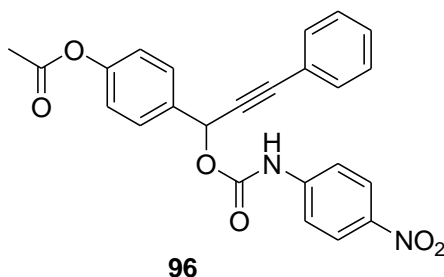
Unfortunately **93** was not isolated from the reaction mixture. Changing the order of addition of TBAF and **91** had no effect. However, analysis of the LC-MS spectra revealed two peaks at 225.1 and 345.2 which was attributed to the H<sub>2</sub>O quenched product, **94** and the 4-nitro-aniline quenched product, **95**. This products may form due to the close proximity of both water and the fluorescent quencher group to the reactive

quinone methide. Despite this, efforts now turned to the synthesis and use of a probe capable of isolating specific enzymes.



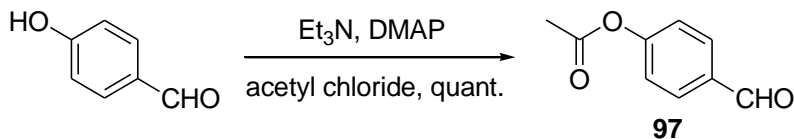
### 3.4 Esterase Probe

As previous work had focused on esterases, as discussed in Chapter 2, a probe, **96**, was designed and synthesised which would be able to react and isolate these from a protein mixture or cell. Work undertaken towards this is described in the following sections.



#### 3.4.1 Synthesis

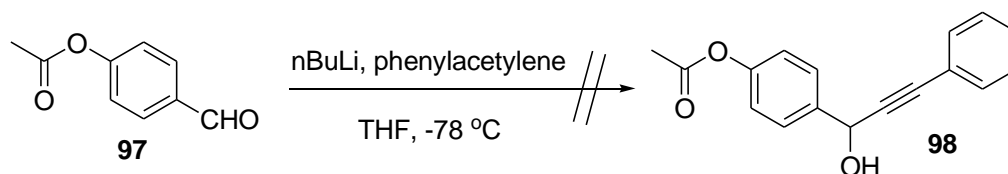
Initial attempts to synthesise **96** began by the acylation of 4-hydroxybenzaldehyde, which was successfully achieved using acetyl chloride in the presence of  $\text{Et}_3\text{N}$  and DMAP, in a near quantitative yield, Scheme 3.3.



Scheme 3.3

**97** was then subjected to treatment with  $n\text{BuLi}$  and phenylacetylene, however, despite repeated attempts no product, **98** was detected by either  $^1\text{H}$  NMR or LC-MS, Scheme

3.4. Table 3.1 below shows the various conditions and reagents employed in the attempted synthesis of **98**.

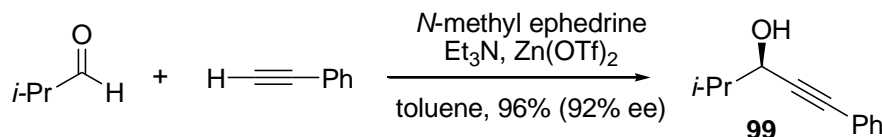


Scheme 3.4

REACTION	REAGENTS	SOLVENT	RESULT
A	<i>n</i> BuLi, phenylacetylene	THF	No product
B	<i>n</i> BuLi, phenylacetylene, ZnBr <sub>2</sub>	THF	No product
C	<i>i</i> PrMgBr, phenylacetylene	THF	No product
D	<i>i</i> PrMgBr, phenylacetylene, ZnBr <sub>2</sub>	THF	No product

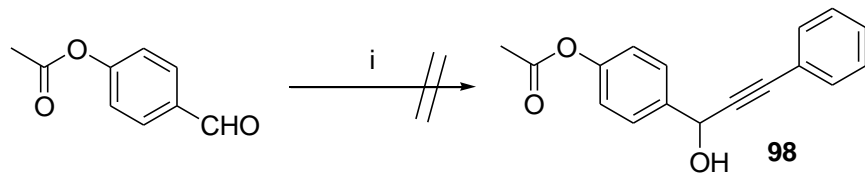
Table 3.1 Reagent conditions for the attempted synthesis of **98**

Carriera has shown that phenylacetylene can undergo direct nucleophilic addition to substituted benzaldehydes in the presence of Zn(OTf)<sub>2</sub> to give the corresponding secondary alcohols.<sup>135</sup> In one example, the product **99** was prepared from the starting material *iso*-propranal in the presence of a chiral agent, (+)-*N*-methyl ephedrine, with a 92% ee, Scheme 3.5.



Scheme 3.5

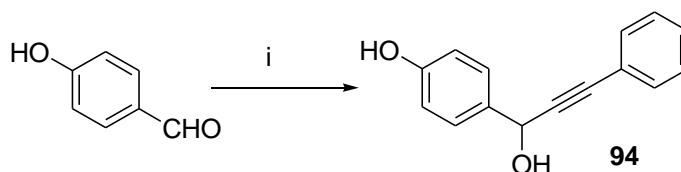
Using the conditions described the synthesis of **98** was attempted, Scheme 3.6. However, this failed to give the desired product. From the above reactions only decomposition products were seen, which included 4-hydroxybenzaldehyde. It was thought that due to the reactivity of the phenolate ion, preferential attack at the ester was occurring. Due to the instability of the molecule under the reaction conditions an alternative route was investigated.



i)  $\text{Zn}(\text{OTf})_2$ ,  $\text{Et}_3\text{N}$ , phenylacetylene, THF,  $-78\text{ }^\circ\text{C}$

Scheme 3.6

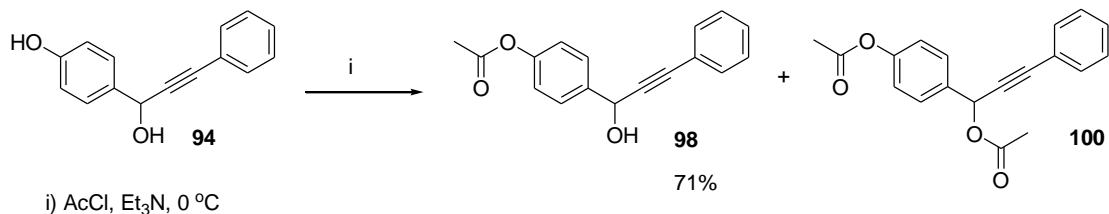
As the ester moiety was unstable, it was therefore decided that the initial step would involve the formation of the propargylic alcohol **94** before acetylation was attempted. **94** was obtained using 2 eq of  $n\text{BuLi}$  with a slight excess of phenylacetylene and successfully isolated in a moderate 45% yield as a pale yellow solid (See Scheme 3.7). A doublet in the  $^1\text{H}$  NMR at 5.53 ppm corresponding to the propargylic proton confirmed synthesis of **94**.



i)  $n\text{-BuLi}$ , phenylacetylene,  $-78\text{ }^\circ\text{C}$ , 15 mins, then warmed to rt, 2 h, 35%

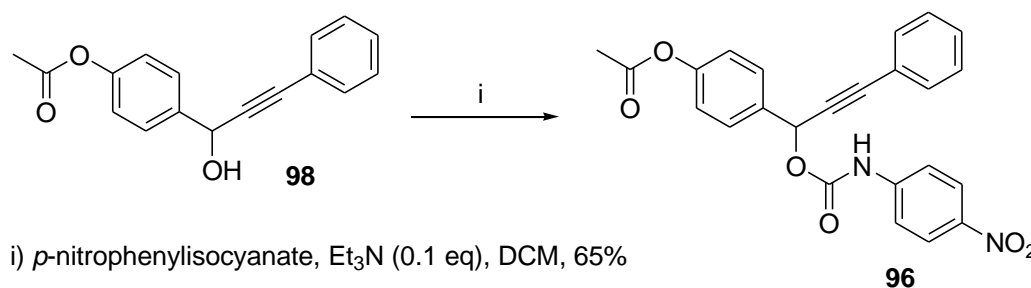
Scheme 3.7 Synthesis of **94**

The challenge now faced was to selectively acylate the phenolic hydroxyl group in the presence of the secondary alcohol. This was attempted using the weak base  $\text{K}_2\text{CO}_3$ , which makes use of the  $\text{pK}_a$  differences between the two hydroxyl groups (phenolic  $\text{OH} \sim 11$ ,  $2^\circ \text{OH} \sim 16$ ). The reaction was undertaken with 1 eq of acetyl chloride; however no product was detected within the  $^1\text{H}$  NMR spectrum. The reaction was repeated, replacing  $\text{K}_2\text{CO}_3$  with  $\text{Et}_3\text{N}$ . The reaction gave a mixture of two products, **98** and **100** (See Scheme 3.8).



Scheme 3.8

Attempts to stop the reaction at the mono-acylated product, **98** were unsuccessful, despite the use of 1 eq and using a much shorter reaction time (15 minutes compared to 1 hour). Isolation of the desired compound, **98** was achieved using flash column chromatography. Evidence of formation was seen by the presence of a carbonyl signal in the  $^{13}\text{C}$  NMR spectrum (169.9 ppm) and a peak at 2.30 ppm (3H, s, Me) in the  $^1\text{H}$  NMR spectrum. Subsequent reaction with *p*-nitrophenylisocyanate and  $\text{Et}_3\text{N}$  afforded the final probe molecule, **96** (See Scheme 3.9). Photophysical analysis revealed **96** to be non-fluorescent, with an absorption maxima at 331 nm.



Scheme 3.9

### 3.4.2 1,6-elimination analysis

The ester functionality of probe **96** allows it to be used as an esterase probe. **96** can therefore undergo a 1,6-elimination to release the fluorescent quencher either biologically by esterase enzymes or chemically using a hydroxide source. The following sections describe the experiments which were undertaken to show whether this was indeed the case.

#### 3.4.2.1 Chemical-mediated 1,6-elimination

Using  $\text{NaOH}$  and  $\text{KOH}$  solutions (both at 1 M), an increase in fluorescence was seen indicating the proposed 1,6-elimination of **96** was occurring (See Figure 3.9 and Figure 3.10). A 1 M solution of the appropriate hydroxide source in water was added to a solution of **96** in Tris buffer (1% in acetone). This was excited at 331 nm and the subsequent emission was recorded at regular intervals until a plateau in fluorescence was observed.

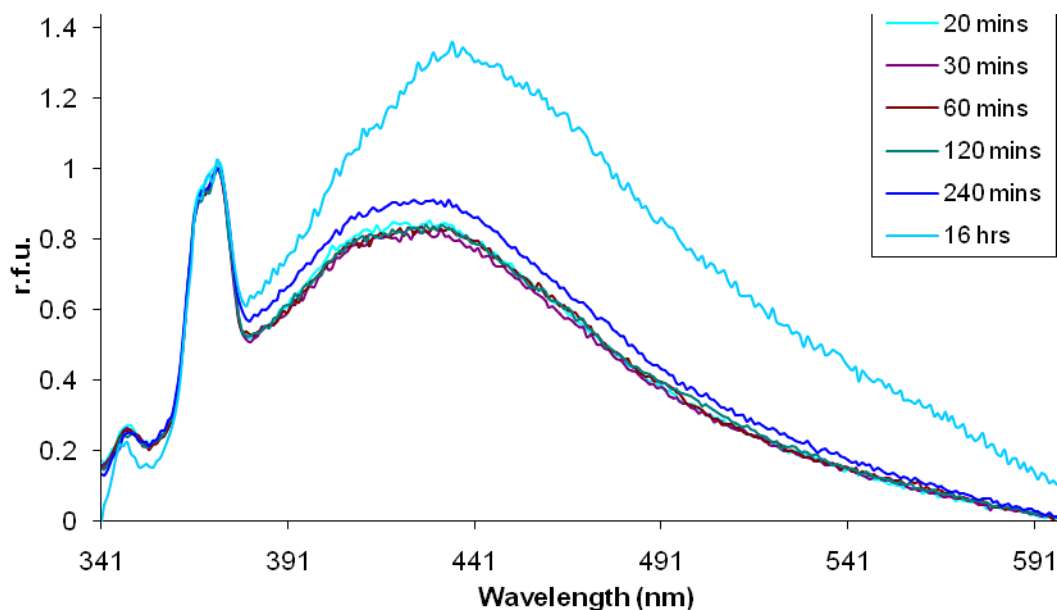


Figure 3.9 Increase in fluorescence seen when 96 is treated with KOH (1 M) over time

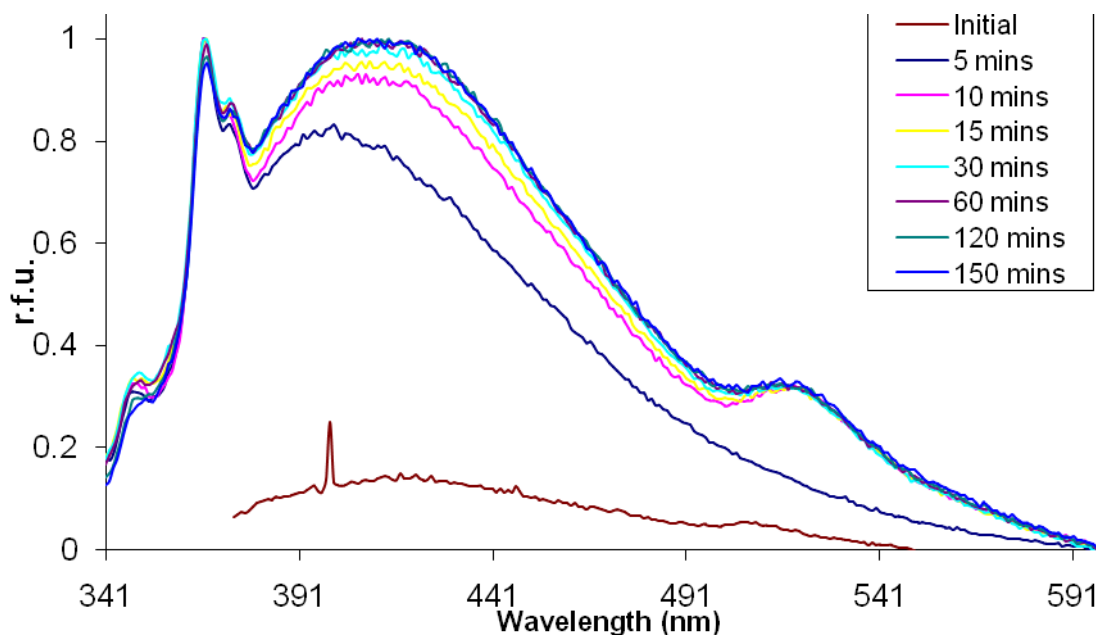


Figure 3.10 Increase in fluorescence observed when 96 is treated with NaOH (1 M) over time

### 3.4.2.2 Enzymatic-mediated 1,6-elimination

Having shown that treatment with a hydroxide source afforded the activated fluorescent probe, attention now turned to the enzymatic-mediated activation of **96**.

### 3.4.2.2.1 Porcine Liver Esterase (PLE)

A 1 mg/ml solution of PLE in Tris buffer was added to a solution of **96** in Tris buffer (1% in acetone). This was excited at 331 nm and the subsequent emission was recorded every 5 minutes for one hour, followed by a reading at 90 minutes and 120 minutes. An increase in fluorescence at 508 nm was observed (Figure 3.11). Initial hydrolysis occurred rapidly with a plateau reached after around 1 hour (Figure 3.12).

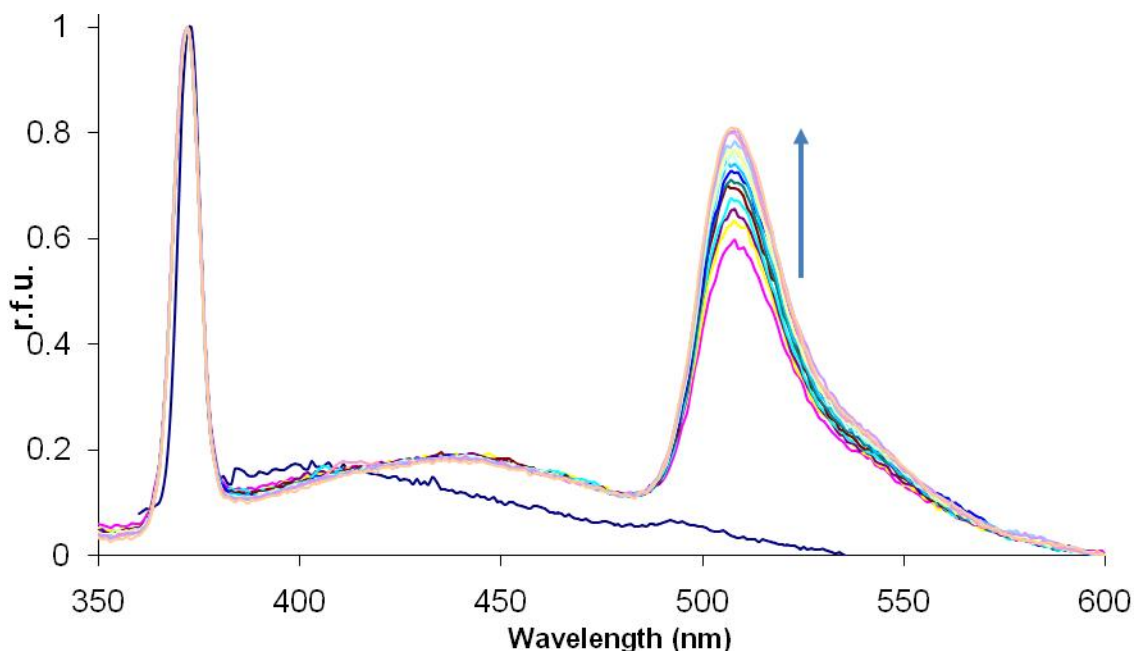


Figure 3.11 Increase in fluorescence over time when **96** is treated with PLE

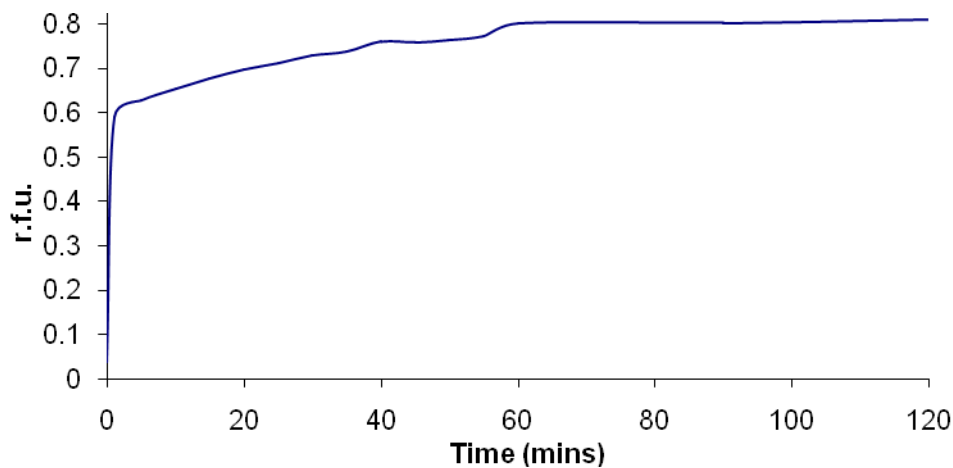


Figure 3.12 Change in fluorescence at 508 nm over time

### 3.4.2.2.2 Binding studies

As an increase in fluorescence occurred upon treatment of **96** with PLE it was a clear indication that the probe was undergoing a 1,6-elimination, with concomitant loss of the fluorescent quencher group. Attention now turned to gaining evidence for the enzyme binding to **96** and hence isolation of a fluorescently tagged protein.

In order to prove that enzymatic action on **96** resulted in a fluorescently tagged protein, mass spectrometry studies were carried out. To this end, 3  $\mu\text{L}$  of **96** (in acetone) was added to 1 ml of PLE (1 mg/ml in 0.1 M Tris buffer, pH 7.4) and incubated for one hour at rt. 300  $\mu\text{L}$  was transferred to a clean eppendorf and four volumes of acetone was added. This was incubated for one hour at 4  $^{\circ}\text{C}$ . The tube was spun down and the supernatant removed. The resulting white pellet was resuspended in MeCN/ $\text{H}_2\text{O}$  and subjected to MS (positive electrospray) analysis. Unfortunately, MS showed that PLE is highly impure and contains many isoenzymes. This made analysis extremely difficult and the isolation of a peak corresponding to a **96**-labelled protein was not possible.

Due to the impure nature of PLE SDS-PAGE techniques were employed with the aim of isolating a pure PLE enzyme. The method undertaken was the same as for the mass spec experiment described above and following incubation at 80  $^{\circ}\text{C}$  with SDS loading buffer, the sample was ran out on the gel. Unfortunately, following imaging no fluorescent bands could be seen. Repeating this without the incubation period at 80  $^{\circ}\text{C}$  still did not result in any fluorescent bands being detected. Staining with Coomassie Blue revealed a multitude of bands within all lanes (See Figure 3.13).

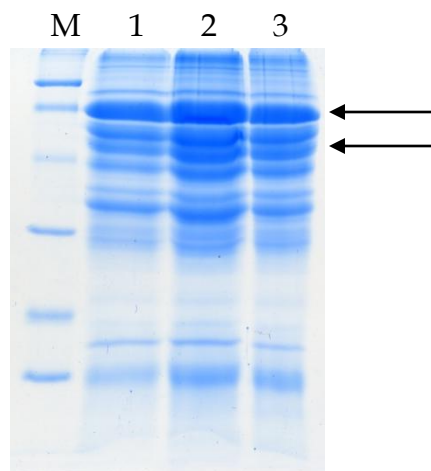


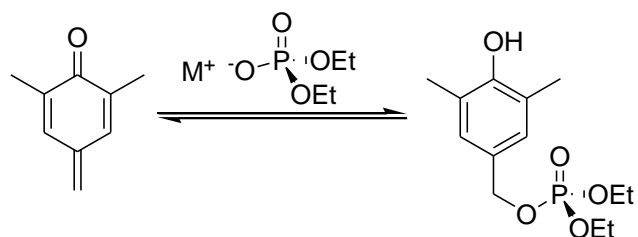
Figure 3.13 SDS-PAGE analysis of **96** treated with PLE. Lane 1 and 2 are PLE + **96**, Lane 3 is a negative control (PLE only), M markers.



Two bands were chosen, as indicated by the arrows in Figure 3.13, for further experimentation. Following washing of the gel with dH<sub>2</sub>O, both bands were excised and destained. Several treatments with MeCN resulted in a small white ball of gel. After cooling on ice for 30 seconds, 25 μL of working trypsin was added and incubated overnight at 34 °C. The supernatant was removed and the peptide material extracted. The resulting dried peptide material was then dissolved in acetone and MALDI MS experiments were performed.

Pleasingly, analysis of the peptides showed that the trypsin digest had been successful due to the detection of the peaks at 1117.5, 1434 and 2193 which were attributed to autosomal trypsin digestion.<sup>136</sup> Disappointingly no evidence was gained for the probe binding to the enzyme. Despite repeated attempts, no real differences between the negative control samples and the **96** treated samples could be seen. This indicated that treatment with **96** was not resulting in a covalently modified protein.

In support of this recent work by Wang *et al* towards the isolation of DNA through forming crosslinks with quinone methide electrophiles has highlighted the reversible nature of the resulting covalent bond<sup>137</sup>. Using an *ortho*-quinone methide they were able to show the reversible nature of the DNA alkylation and the subsequent irreversible quenching by H<sub>2</sub>O. The reversibility of quinone methide alkylation is sensitive to the electronics of the π-system of the quinone methide and the strength of the departing leaving group and incoming nucleophile<sup>138</sup>. In addition to this, Zhou and Turnbull<sup>139</sup> were able to show that *p*-quinone methides also exhibit reversibility upon alkylation by phosphodiester (Scheme 3.10). The reversible nature of this reaction may account for the lack of any fluorescently labelled PLE due to the apparent transient nature of the covalent bond.



Scheme 3.10

### 3.5 p450 O-demethylation probe

Concurrent to the previously described work, efforts were also directed towards the synthesis of a probe capable of isolating cytochrome p450 O-demethylation enzymes. The following sections introduce this class of enzymes and describe both the synthesis and photophysical analysis of the probe molecule.

#### 3.5.1 p450 O-demethylation enzymes

p450 O-demethylating enzymes detoxify xenobiotics by demethylation reactions, which renders the substrate more polar and therefore easier to extrude from cell. This class of enzymes is used to affect the O-demethylation of a wide variety of compounds including the NSAID Naproxen, **101**,<sup>140</sup> the pesticide methoxychlor, **102**,<sup>141</sup> the topoisomerase II inhibitor etoposide, **103**<sup>142,143</sup> and the reporter molecule 7-methoxyresorufin, **104**<sup>144</sup> (See Figure 3.14). The p450 O-demethylation enzyme p450 1A2 isolated from humans has been subjected to random mutagenesis techniques and the triple mutant E163K/V193M/K170Q has a 5-fold higher  $k_{cat}$  than the wild type towards the O-demethylation of 7-methoxyresorufin.<sup>144</sup>

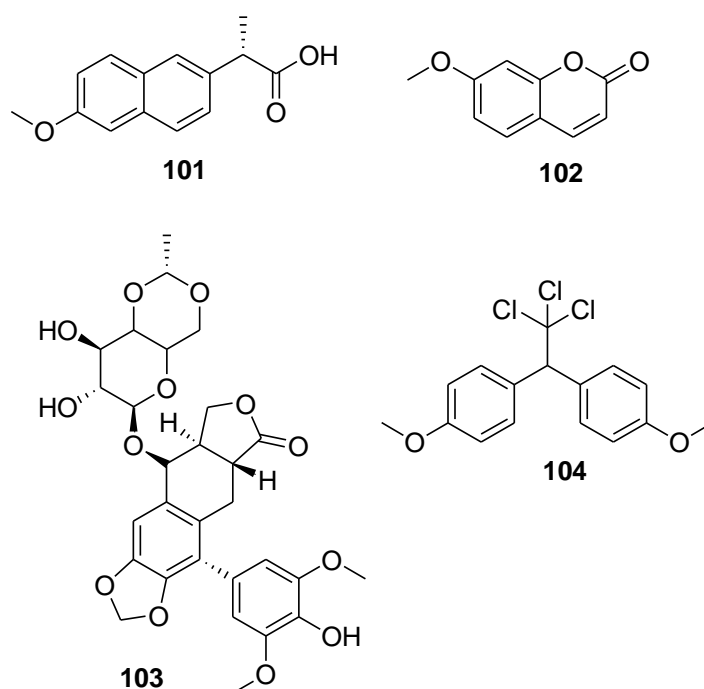
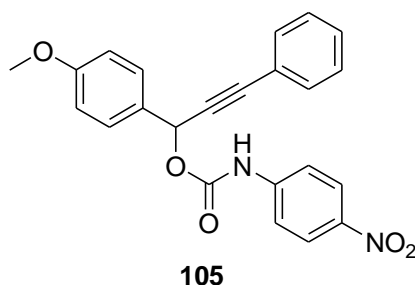


Figure 3.14 The variety of compounds which are acted upon by p450 O-demethylation enzymes

The mechanism of action of this class of p450 enzymes is similar to that of oxidative p450s (See Chapter 4). O-demethylation proceeds *via* direct oxidation of the carbon

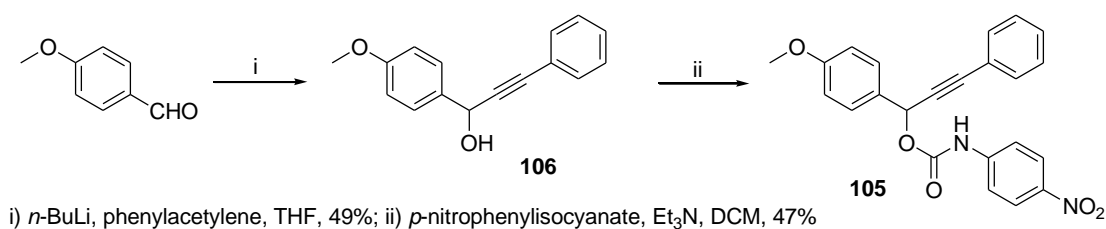
adjacent to the oxygen as the oxygen oxidation potential is too high for electron abstraction. In addition to this, oxygen transfer to the oxygen does not occur.<sup>145</sup>

The reactivity probe **105** designed to isolate this class of enzymes from plant cells has the same structure as the esterase probe **96** with the exception of the recognition head, which is a methoxy substituent. The following sections detail the work undertaken in the synthesis and photophysical evaluation of this probe.



### 3.5.2 Synthesis

The synthesis of **105** was achieved in two steps, starting from the commercially available *p*-anisaldehyde in an overall 13% yield, Scheme 3.11.



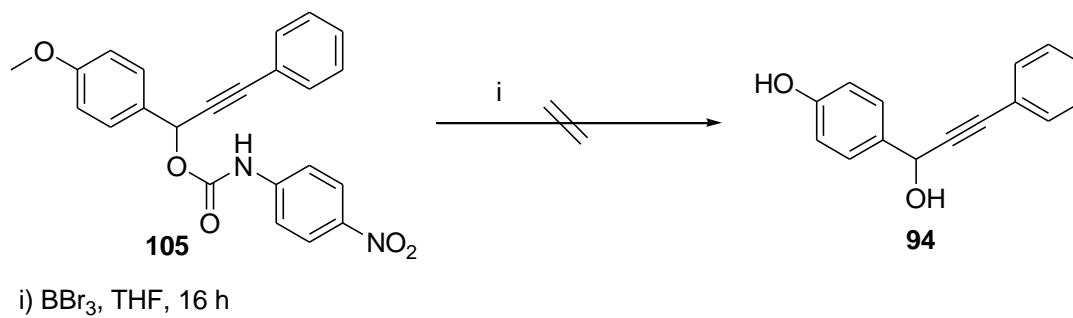
Scheme 3.11

Characterisation techniques used to confirm synthesis included <sup>1</sup>H and <sup>13</sup>C NMR spectroscopy, along with mass spectrometry. Reagents and conditions were employed as for the previous two probes **91** and **96** and photochemical analysis showed the probe to be non-fluorescent.

### 3.5.3 Chemical-mediated 1,6-elimination Analysis

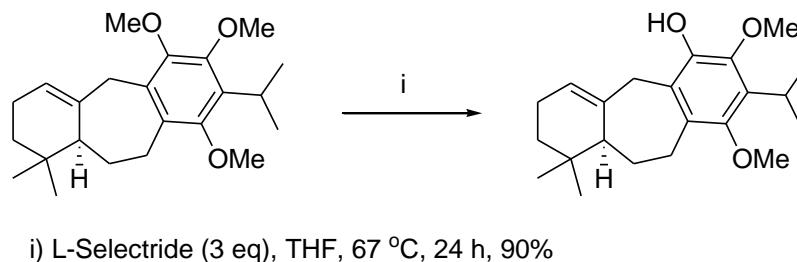
In order to show that this probe also undergoes the 1,6-elimination mechanism, several chemical reactions were undertaken to remove the methyl group and result in loss of the fluorescent quencher group. The first attempted utilised BBr<sub>3</sub> based on a method by

McOmie *et al.*<sup>146</sup> **105** was treated with one equivalent of  $\text{BBr}_3$  and the reaction allowed to stir for 16 hours (See Scheme 3.12). Unfortunately, the product **94** was not detected from the reaction. A product was isolated which retained the methoxy signal within the  $^1\text{H}$  NMR spectrum (3.79 ppm, 3H, s), however, the exact structure could not be elucidated at the time.



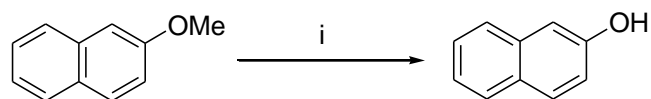
**Scheme 3.12** Attempted demethylation of **105** using  $\text{BBr}_3$

Due to failed use of  $\text{BBr}_3$  to afford **94**, an alternative reaction was sought. A search of the literature revealed the use of L-Selectride as a demethylating agent, see Scheme 3.13.<sup>147</sup> This was attempted under identical conditions with **105**, however, only a complex mixture of products was formed, which could not be separated by FCC.



**Scheme 3.13**

A final attempt used thiophenol in the presence of a catalytic amount of KF, which has been shown to remove the methyl group from a wide range of substrates, Scheme 3.14.<sup>148</sup>



i) PhSH (1 eq), KF (10 mol%), NMP, reflux, 1 h, 80%

Scheme 3.14

This reaction was attempted with **105** and a product was isolated from the reaction. However, upon investigation of the data it could be seen from the  $^{13}\text{C}$  NMR spectrum that there were no alkyne carbons present. Furthermore, the methoxy signal remained in both the  $^{13}\text{C}$  and  $^1\text{H}$  NMR spectra. IR spectroscopy showed a carbonyl stretching band at  $1668\text{ cm}^{-1}$ , and a signal due to a carbonyl carbon could be seen in the  $^{13}\text{C}$  NMR spectrum. HRMS analysis suggested a molecular mass of 349.1257, with a distinctive splitting of a peak two mass units higher, indicative of a sulfur atom, Figure 3.15.

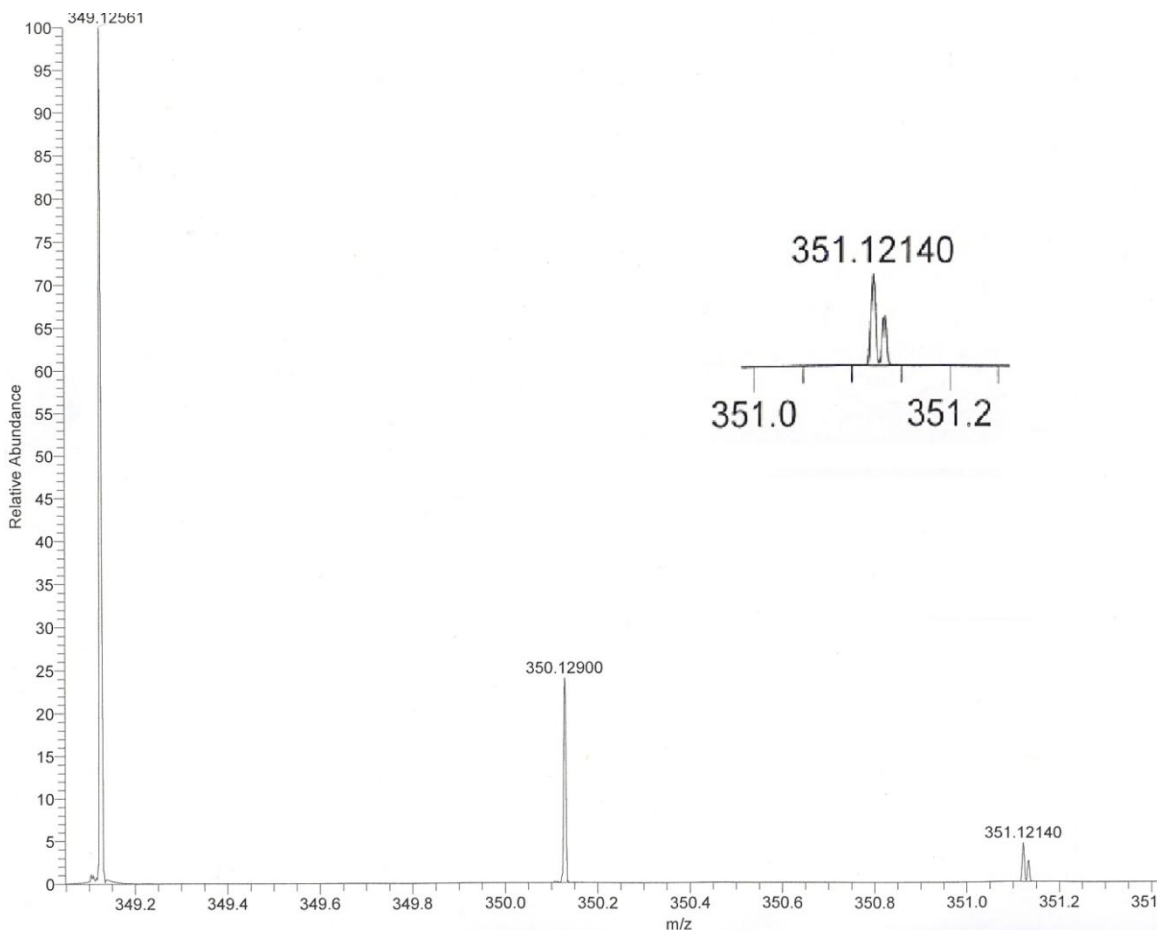
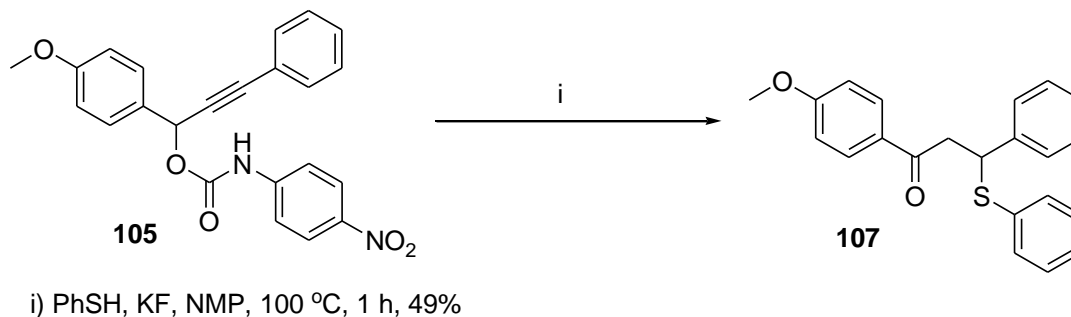


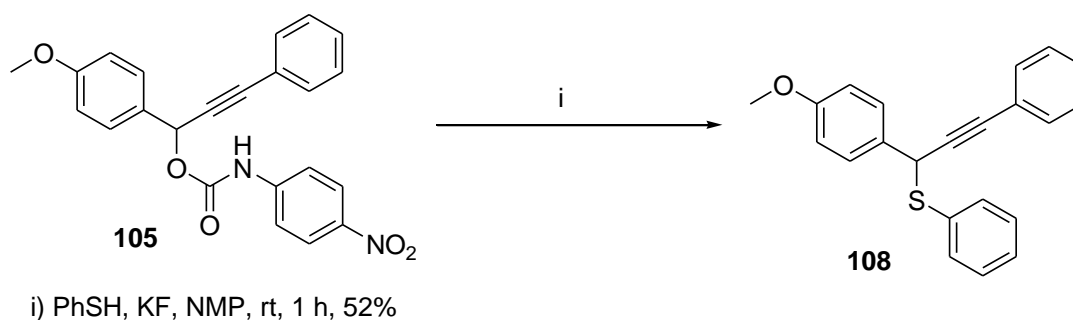
Figure 3.15 HRMS spectrum of **105** showing the splitting of the peak at 351.1214

The molecular formula to give this mass is  $C_{22}H_{21}O_2S$ , which requires 349.1257. This data, coupled with the splitting patterns in the  $^1H$  NMR and correlations in both HSQC and HMBC spectra are consistent with the possible structure **107** (See Scheme 3.15).



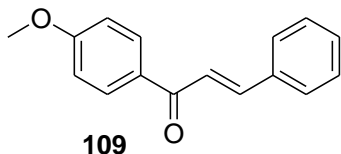
Scheme 3.15

A possible reason for this reaction may be the high temperatures employed. Therefore the reaction was repeated at room temperature, Scheme 3.16.  $^1H$  and  $^{13}C$  NMR spectra showed the presence of the methoxy group and the  $^{13}C$  NMR spectrum indicated that the two alkyne carbons had remained. However, the mass (331.11533) did not correlate to the expected product **94**, but to the molecular formula  $C_{22}H_{19}OS$ . Analysing the correlations within the 2D NMR showed that **108** is the likely structure for the isolated compound.

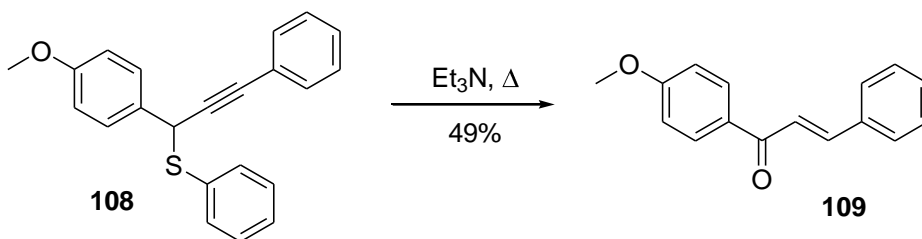


Scheme 3.16

This gave some insight to the  $BBr_3$  reaction (Scheme 3.12). Referring back to this reaction and the resulting product isolated, data analysis now indicated that a similar reaction had occurred, giving rise to the suggested product **109**.



This was evidenced by the presence of two doublets which couple to each other at 7.72 and 7.35 ppm in the  $^1\text{H}$  NMR spectrum. The latter of these shows HMBC correlations to the carbonyl signal at 201.6 ppm in the  $^{13}\text{C}$  NMR spectrum. It was thought that **109** formed by the elimination of a bromo alcohol initially formed in the reaction. In order to test this **108** was subjected to reaction with  $\text{Et}_3\text{N}$  and the reaction heated to encourage elimination, Scheme 3.17. Product **109** was isolated from the reaction mixture and this therefore gives evidence for the initial formation of the proposed bromo alcohol.



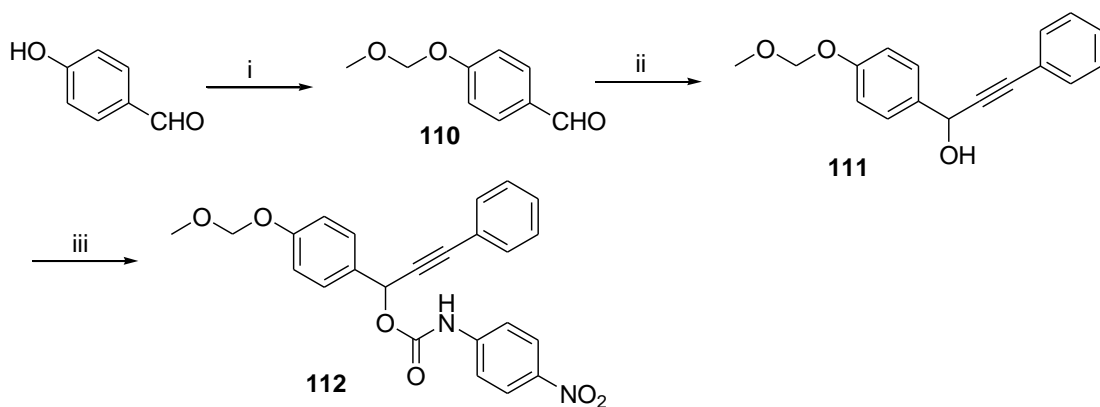
Scheme 3.17

As none of the attempted demethylation reactions were successful, a further probe was synthesised. This probe was to be used to show that removal of the methoxy group could still affect the 1,6-elimination and subsequent loss of the quencher group. The reactive group within this probe was based on the MOM protecting group, which is easily removed using acidic conditions.<sup>149</sup>

## 3.6 MOM Probe

### 3.6.1 Synthesis

Scheme 3.18 shows the route used for the synthesis of **112** which was synthesised in an overall 16% yield. Protection of the hydroxyl functionality with MOM<sup>150</sup> was achieved in a quantitative yield as shown by LC-MS and the product, **110**, was used without further purification. The following two steps were carried out in an identical fashion to those for the previous probes **91**, **96** and **105**. Characterisation of each compound was undertaken using NMR and LC-MS. Photochemical analysis showed **112** to be non-fluorescent.



i) DIPEA, MOMCl, DCM, rt, 2 h, 99%; ii) nBuLi, phenylacetylene, THF, -78 °C, 2 h, 96%; iii) p-Nitrophenylisocyanate, Et<sub>3</sub>N, DCM, rt, 1 h, 35%

Scheme 3.18

### 3.6.2 1,6-elimination analysis

**112** was treated with HCl (1 M) and the change in fluorescence was recorded over time. The increase in fluorescence can clearly be seen in Figure 3.16.

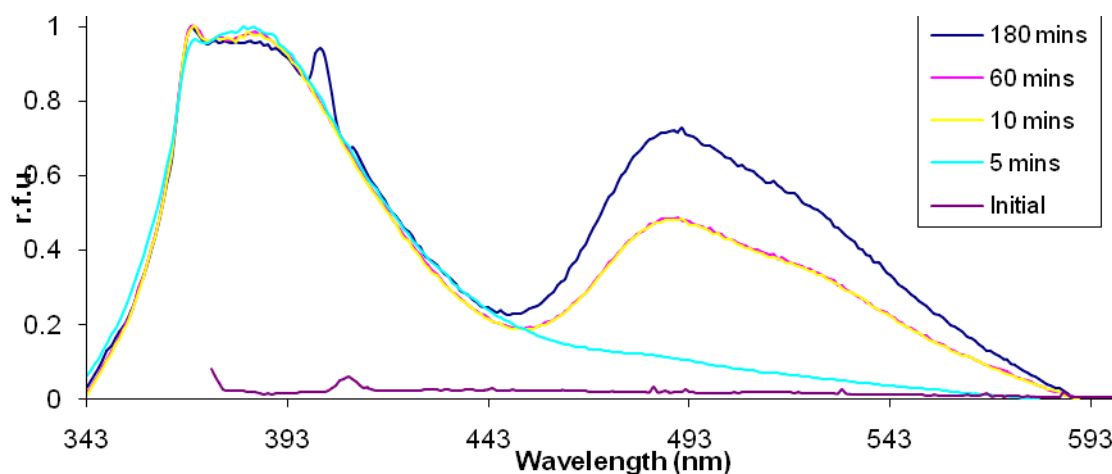


Figure 3.16 Increase in fluorescence at 490 nm upon addition of 1 M HCl to **112**

This result shows that the MOM probe **112** and hence the methoxy probe **105** undergo a 1,6-elimination in the expected way, releasing the fluorescent quencher group and allowing the fluorescence emission from the phenylacetylene group. Due to time constraints its use in biological systems was not explored.



### **3.7 Summary**

- \* Probe **91** was successfully synthesised and adding TBAF to a solution of this resulted in an increase in fluorescence.
- \* The esterase probe **96** was successfully synthesised in a 16% yield. Photophysical analysis revealed it to be non-fluorescent, with an absorption maximum of 331 nm.
- \* Treatment of **96** with NaOH or KOH resulted in an increase in fluorescence indicating that the proposed 1,6-elimination was occurring.
- \* Adding a solution of PLE (1 mg/ml) in Tris buffer to a solution of **96** resulted in an increase in fluorescence at 510 nm. Isolation of a fluorescently-labelled PLE protein was unsuccessful. No evidence was gained for the binding of **96** to PLE.
- \* **105** was synthesised in an overall 13% yield, however attempts to chemically remove the methoxy group were unsuccessful.
- \* The MOM probe **112** was synthesised and shown to breakdown upon treatment with 1 M HCl, resulting in the release of the fluorescent quencher group and a concomitant fluorescence increase.

### **3.8 Conclusions**

The design, synthesis and biological use of reactivity probes to react with, and isolate, proteins from plant cells has had mixed success. Fluorescently quenched reactivity probes based on *p*-quinone methide chemistry were successfully synthesised with a variety of different recognition heads. They were all shown to be non-fluorescent until the appropriate reaction, either chemically or biologically, removed the recognition head and restored fluorescence.

Unfortunately, attempts to covalently modify a protein, in particular using **96** with PLE did not succeed. Despite repeated attempts, including modified reaction conditions, a fluorescently tagged PLE was never observed, either by SDS-PAGE or MALDI MS. This may be due to the covalent bond being relatively weak and unstable to SDS-PAGE analysis, or that there is not sufficient space between the bulky fluorescent quencher group and the nucleophilic residue to allow attack to occur.

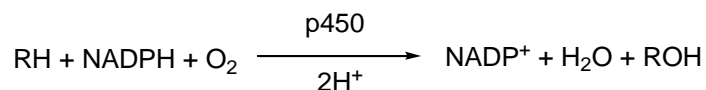
## 4 Oxidative Cytochrome p450

### 4.1 Introduction

A probe which can isolate oxidative p450 enzymes would be invaluable as this class of enzymes is able to detoxify a huge variety of compounds, by catalysing a large diversity of reactions such as hydroxylations, epoxidations, and peroxygenations<sup>151</sup>. This chapter describes efforts directed towards the synthesis of a molecule able to isolate oxidative cytochrome p450 enzymes. The following section describes the enzymology and mechanism of action of this class of enzymes.

#### 4.1.1 Mechanism of action

Cytochrome p450 is a haemoprotein containing iron protoporphyrin, which uses NADPH as a co-factor. The transfer of electrons from NADPH to p450-reductase and then to p450 leads to the reductive activation of molecular oxygen followed by the insertion of one oxygen atom into the substrate. The second oxygen atom is converted to H<sub>2</sub>O. This is summarised below in Scheme 4.1.



Scheme 4.1

The haem unit of p450 is bound to the rest of the protein through an axially-ligated cysteinal sulphur. The resting state contains Fe<sup>3+</sup>, although it exists as an equilibrium mixture of low spin (6 co-ordinate) and high spin (5 co-ordinate). This perturbation takes place upon substrate binding. Figure 4.1 below shows the catalytic cycle of p450, with oxygenation of a substrate, RH into a product, ROH.<sup>152</sup>

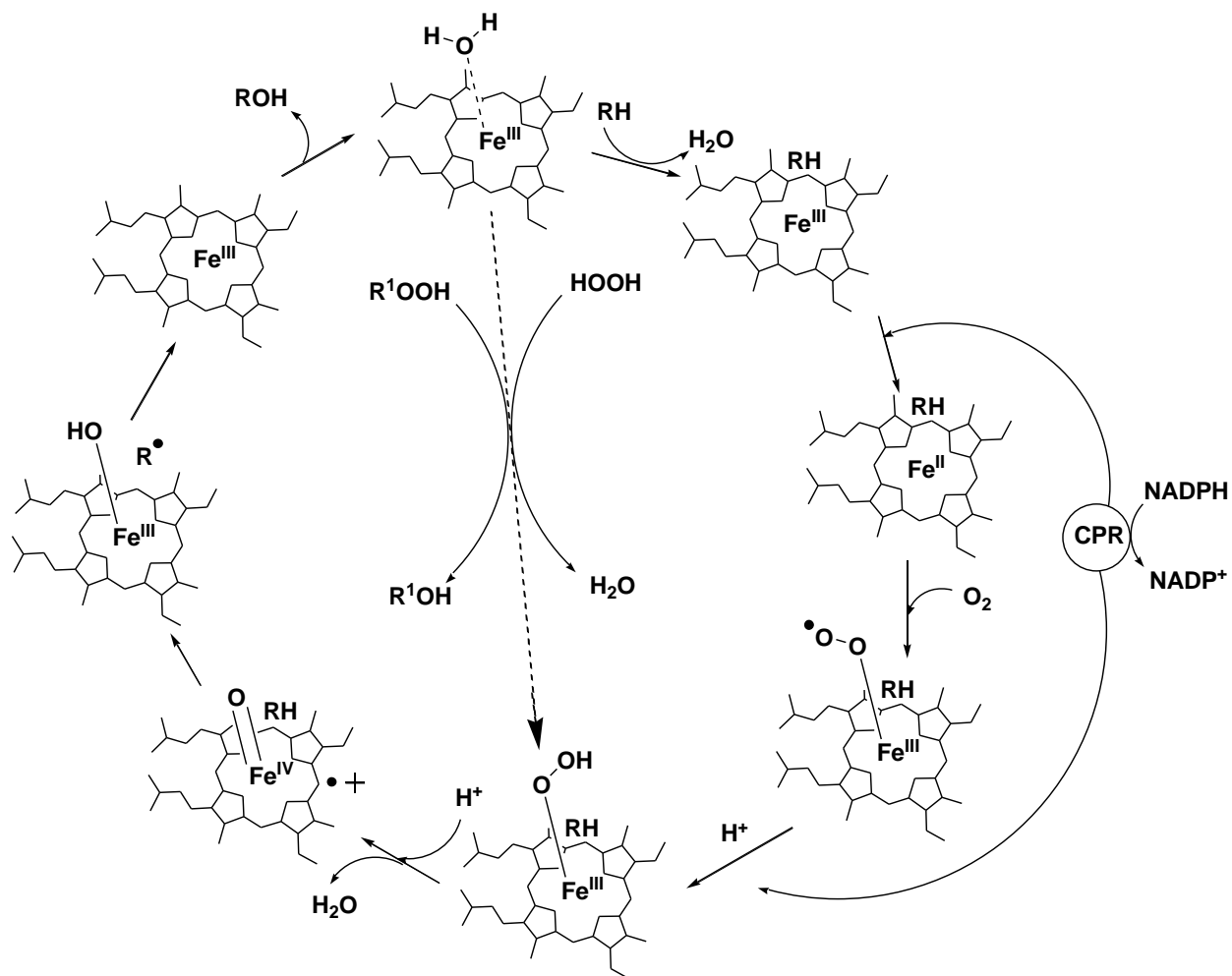


Figure 4.1 Mechanism of action of cytochrome p450. *RH* substrate, *CPR* cytochrome p450 reductase, *ROH* product. *Mol. Biosyst.*, 2006, 2, 462 – Reproduced by permission of The Royal Society of Chemistry

#### 4.1.2 Evolution of the Enzyme

The use of p450s in biotransformation techniques has been limited due their low activity, poor stability, high substrate specificity and the need for cofactors. In order to overcome this several groups have applied molecular biology techniques with the aim of producing p450 variants with modified enzymatic properties.

Much of the work carried out on p450 has focussed on p450 BAM from *Bacillus megaterium* due to their high expression levels in *E. coli*.<sup>153</sup> Wild-type p450 BAM catalyses the hydroxylation of long chain (C12 – C22) saturated fatty acids, with virtually no activity seen towards those bearing a shorter chain. Hydroxylation usually takes place at the  $\omega$ -1,  $\omega$ -2 or  $\omega$ -3 position. Oliver *et al* mutated Phe87 to Ala87 which

resulted in the enzyme being able to hydroxylate various fatty acids exclusively at the  $\omega$ -position.<sup>154</sup> In addition to this work it has also been shown that using site-specific random mutagenesis at residue 87 of the F87A mutant led to an improved activity towards shorter chain fatty acids.<sup>155</sup>

Another p450 commonly studied is p450 CAM from *Pseudomonas putida*, again due to the high expression in *E. coli*. p450 CAM catalyses the hydroxylation of camphor to 5-*exo*-hydroxycamphor. Bell *et al* have used site-directed mutagenesis to create several mutants which showed improved activity towards the metabolism of (S)-limonene<sup>156</sup> and (+)- $\alpha$ -pinene<sup>157</sup>, both of which are unnatural substrates for the enzyme.

Due to the large number of reactions p450 is involved in and the much greater number of p450 genes present within plants (2401 compared to 55 in humans and 874 in *E. coli*)<sup>158</sup>, these enzymes represent an untapped resource for use in biotransformation applications. In order to apply directed evolution techniques to p450 they must first be isolated from the cell. The following section details the work undertaken to isolate p450 enzymes using reactivity probes based on the BODIPY structure.

## **4.2 Probe Design Rationale**

Initial studies directed towards a p450 probe was based on previous work carried out in which the metabolic activation of lead drug candidates was analysed using LC-MS.<sup>159</sup> Molecules containing a fluorinated phenyl derivative were incubated with both rat and human liver microsomes, with the metabolites identified *via* ion trap LC-MS. The proposed metabolites were conjugates of GSH, which appeared to be the product of the reaction between GSH and the *ortho*-quinone of the parent compound at the phenyl ring. The proposed metabolic activation pathway is shown below in Figure 4.2. As the electrophilic *ortho*-quinone intermediate formed by the action of p450 within liver microsomes is able to react with nucleophiles such as GSH, it could be expected that nucleophilic residues within the enzyme could also react with these intermediates. Evidence for this could be seen by a high degree of irreversible binding of radioactivity to microsomal proteins when a tritiated analogue of the lead drug candidate was used.

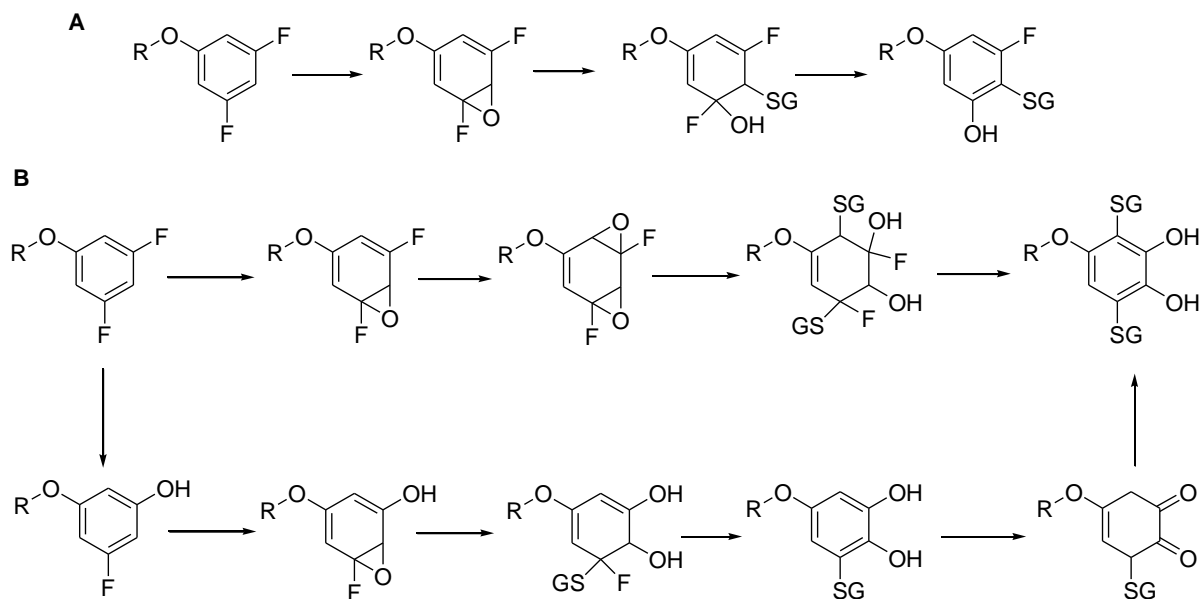


**Figure 4.2 Proposed metabolic activation mechanisms of halogenated phenyl derivatives**

By making use of the *ortho*-quinone intermediate mechanism as described above the proposed structure of the probe, **113**, is shown in Figure 4.3. **113** involved the use of a nitrobenzofurazan (NBD) fluorophore derivative. As with the reactivity probes described in Chapter 3, the proposed p450 probe also made use of a fluorescent quencher group. However, in this case a bromo-substituent was used, which makes use of the heavy atom effect. Heavy atoms such as bromine can lead to a decrease in fluorescence intensity due to the increase in intersystem crossing induced by the interaction between the fluorophore and the heavy atom.<sup>160</sup> Following the loss of the heavy atom quencher the resulting product would be a covalently bound, fluorescently tagged p450. The proposed mechanism of action is shown in Figure 4.4.

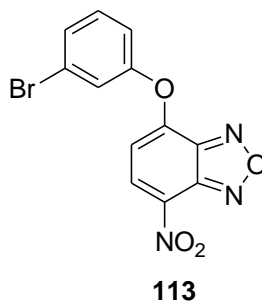


**Figure 4.3 Structure of p450 probe containing the NBD fluorophore**

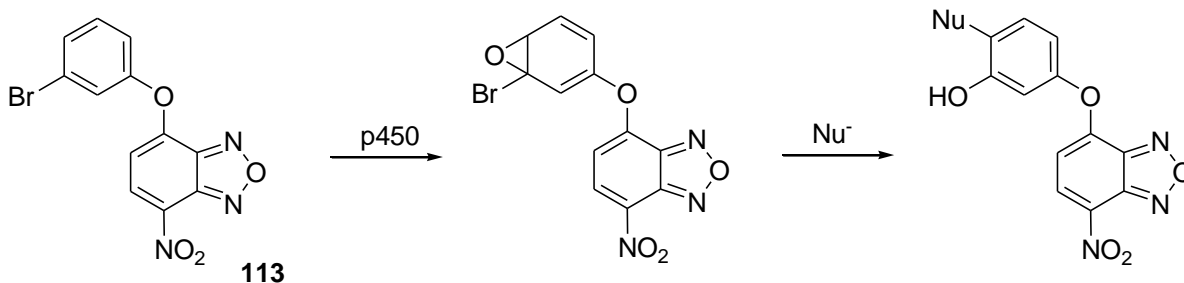
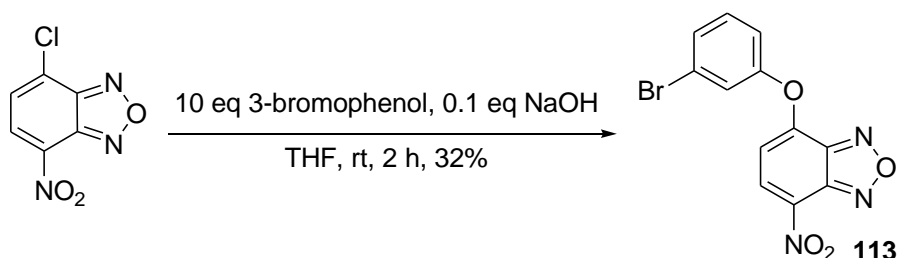


Figure 4.4 Proposed mechanism of action of **113** treated with cytochrome p450

#### 4.2.1 Synthesis

Work by Crampton *et al*<sup>161</sup> had shown the synthesis of molecules based on **113** could be achieved by the reaction of NBD-chloride with an excess of an appropriate phenol. To this end the synthesis of **113** was undertaken by treatment of NBD-chloride with 10 eq of 3-bromophenol, which afforded the probe molecule **113**. Evidence for this was seen in the correct integration of signals within the <sup>1</sup>H NMR spectroscopy.



Scheme 4.2

In order to establish that the loss of the bromo substituent would result in the switching on of fluorescence a control, the unsubstituted phenol derivative, **114** was also analysed in the current study. This compound was donated by Michael Crampton. Both of these compounds were analysed and the resulting fluorescent spectra are shown below (Figure 4.5). Disappointingly, **113** was found to exhibit a higher level of fluorescence than the control, **114**, and therefore this approach was abandoned.

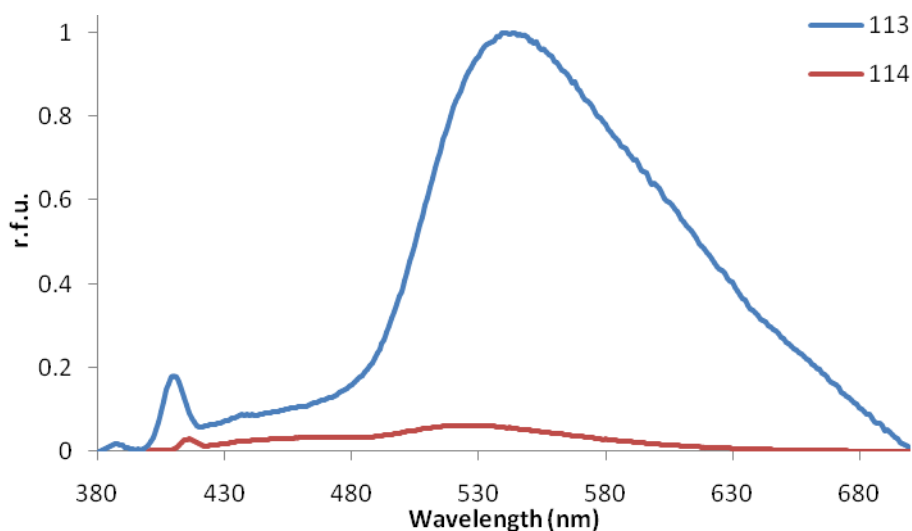
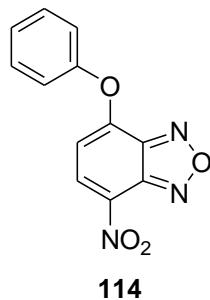
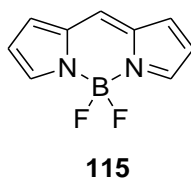


Figure 4.5 Comparison of emission of 114 and 115

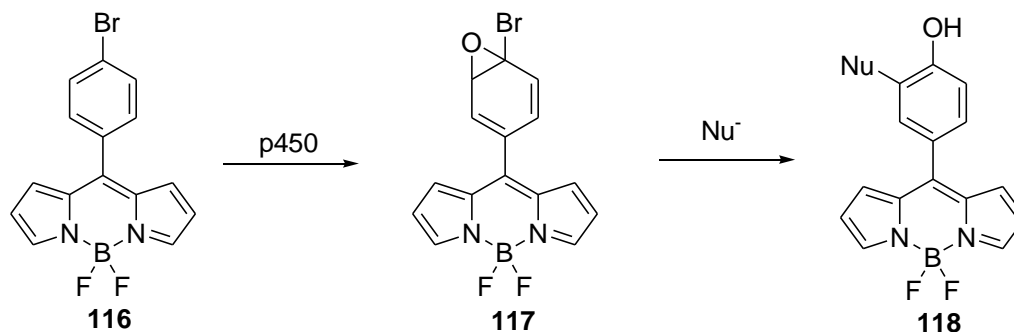
### 4.3 BODIPY-based Probe

As an alternative, a different p450 probe was designed which was based on the BODIPY structure **115**. This molecule can be highly substituted without seriously affecting its fluorescent profile.



The rationale design of this p450 probe was similar to the NDB probe in that it involved a *para*-bromo substituted phenyl ring at the 4-position, **116**. This would allow the isolation of p450 enzymes through the oxidation of the ring and subsequent attack of the epoxide intermediate, **117**, by a nucleophilic residue within the protein resulting in

loss of the bromine atom. The loss of the bromine would result in the switching on of the fluorescence due to the loss of the heavy atom. As explained previously (Section 4.2), following the loss of the heavy atom quencher the resulting product would be a covalently bound, fluorescently tagged p450, **118** (Scheme 4.3).



Scheme 4.3

There have been a number of publications involving BODIPY derivatives in use as reactivity probes including the targeting of  $\beta$ -amyloid plaques<sup>162</sup>, the detection of hypochlorous acid,<sup>163</sup> nitric acid,<sup>164</sup> BSA,<sup>165</sup> potassium<sup>166</sup> and cyanide ions<sup>167</sup> and as pH sensors.<sup>168</sup> In addition to this, BODIPY derivatives have seen use in other areas such as light harvesting systems,<sup>169</sup> triplet sensitisers<sup>170</sup> and laser dyes.<sup>171</sup>

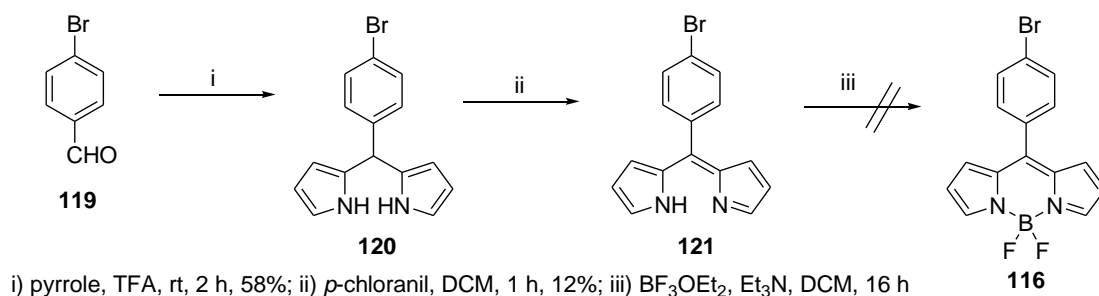
### 4.3.1 Synthesis of probes

Using literature based methods, efforts were undertaken to synthesise the proposed BODIPY probe, **116**. This work is detailed in the following section.

#### 4.3.1.1 From benzaldehyde derivatives

Initial methods to synthesise the bromo BODIPY derivative was undertaken in three steps starting from the commercially available *p*-bromobenzaldehyde (See Scheme 4.4).<sup>172</sup>

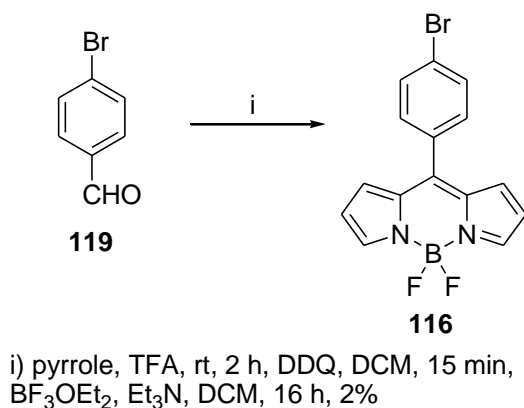




Scheme 4.4

The starting material, **119**, was dissolved in pyrrole (25 eq), to which was added a drop of TFA and this was stirred for 3 h, during which time a deep red colour developed. FCC gave the title compound, **120** in a 43% yield. This was evidenced by the signal in the  $^1\text{H}$  NMR spectrum at 5.43 ppm for the proton at the bridging C4 position. **120** was treated with the oxidising agent *p*-chloranil to yield the dipyrromethene derivative **121**. This could be seen by the loss of the above mentioned signal at 5.43 ppm and the molecular ion at  $m/z = 299.2$  seen in the mass spectra ( $\text{ES}^+$ ). The final step in producing the BODIPY derivative **116** involved complexation with  $\text{BF}_3\cdot\text{OEt}_2$  in the presence of  $\text{Et}_3\text{N}$ . Unfortunately, no product was detected and therefore efforts were made towards an alternative method which would enable the isolation of **116**.

Kollmannsberger *et al* have shown that a one-pot reaction can yield BODIPY analogues.<sup>173</sup> This again involved the condensation of **119** with pyrrole, however, DDQ was used as the oxidant in this synthesis.  $\text{BF}_3\cdot\text{OEt}_2$  and  $\text{Et}_3\text{N}$  were used to introduce the  $\text{BF}_2$  bridge (See Scheme 4.5).



Scheme 4.5

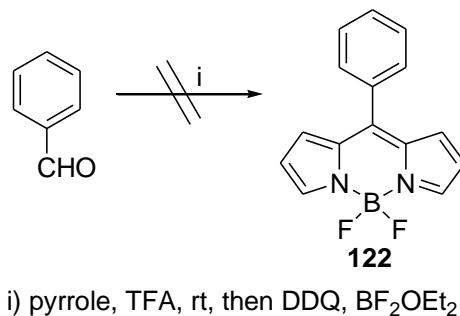
**116** was successfully synthesised, albeit in the very poor yield of 2%. Analysis of the  $^1\text{H}$  NMR spectrum revealed the presence of the correct signals and the  $^{19}\text{F}$  NMR spectrum exhibited the quartet signal for both fluorine atoms (q, -122.2 - 122.4 ppm). The photoluminescence properties are shown in Table 4.1 below.

Excitation (nm)	Emission (nm)	Quantum yield ( $\phi_F$ )	Lifetime ( $\tau$ )
504	520	30%	6 ns

**Table 4.1 Photoluminescent properties of 116**

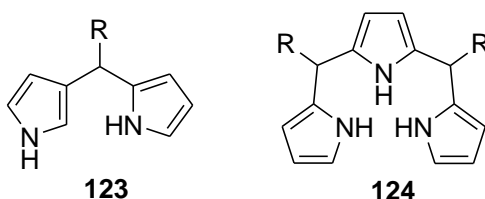
Disappointingly, **116** was shown to be fluorescent, albeit with a slightly longer lifetime than the 3 ns exhibited by the corresponding fluorescent molecule, phenyl BODIPY **122**.<sup>173</sup>

Unfortunately, when attempting to synthesise compound **122**, which was to be used as a control probe in future biological experiments, no product could be detected (See Scheme 4.6). A complex mixture of products was formed, which were very difficult to separate by FCC.



**Scheme 4.6 Attempted synthesis of 122**

A possible reason for this failed reaction and the low yield of **116** has been highlighted by Lindsey and co-workers.<sup>174</sup> They have shown that several other dipyrromethane products, including the so-called N-confused **123** and N-frustrated **124** forms can arise during the initial dipyrromethane formation step.

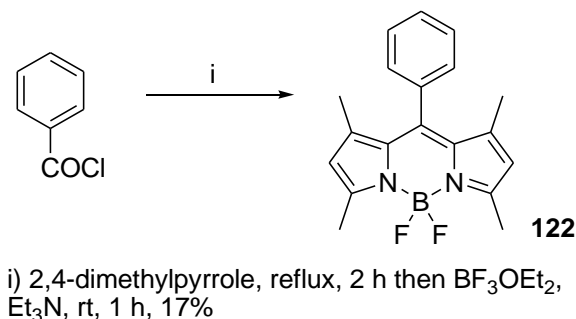


By altering the ratio of pyrrole to aldehyde they were able to suppress formation of **123** and **124**, however, pure dipyrromethanes were only ever isolated following several rounds of purification including distillation and recrystallisation.

In order to prevent formation of **123** and **124** and in an attempt to improve the yield of BODIPY formation, 2,4-dimethylpyrrole was used in all further reactions. The 2,4-dimethylpyrrole derivative of **122** was synthesised in a one-pot procedure, identical to that shown in Scheme 4.6. A small amount of product was detected by  $^1\text{H}$  NMR spectroscopy, however, it could not be isolated pure from the reaction mixture. Given the difficulties in the oxidation step, an alternative synthetic strategy was investigated.

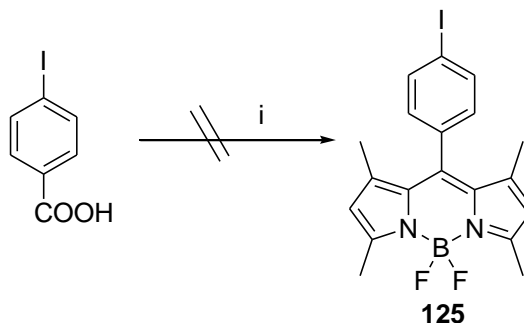
#### 4.3.1.2 From benzoylchloride derivatives

A search of the literature revealed an alternative starting material, in which an acyl chloride was utilised which removed the necessity of DDQ oxidation.<sup>175</sup> It was hoped that this would increase the yield of the reaction by the removal of this step. The synthesis of **122** was successfully achieved in a 17% yield using this method (See Scheme 4.7).



Scheme 4.7 Synthesis of control probe, **122**

As the bromo derivative was shown to be fluorescent, attention now turned to the use of other substituents which could affect the quantum yield, and hence fluorescence, of BODIPY. It was thought that perhaps iodine could induce the heavy atom effect and its synthesis was attempted (See Scheme 4.8).

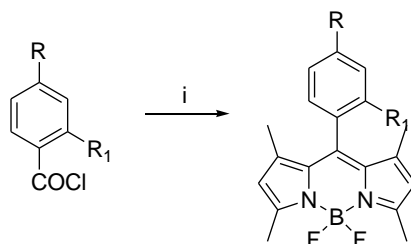


i)  $(\text{COCl})_2$ , DMF (cat.), DCM; 2,4-dimethylpyrrole, reflux, 2 h then  $\text{BF}_3\text{OEt}_2$ ,  $\text{Et}_3\text{N}$ , rt, 1 h

**Scheme 4.8 Attempted synthesis of 125**

Unfortunately, no product could be isolated after FCC and this led to the use of the classic fluorescent quencher, the nitro group. Synthesis was achieved using identical conditions to those employed in Scheme 4.7 and gave **126** in a modest 30% yield. This increase in yield can probably be attributed to the electron withdrawing effect of the nitro group, increasing the yield of the dipyrromethene synthesis step. However, the ability of the probe to function as hypothesised relies on the leaving group potential of the *para* substituents. The nitro group is a poor leaving group and in addition to this the electron density of the phenyl ring will be diminished and may prevent the initial oxidation step of the p450 enzyme. In order to overcome this potential downfall, a second BODIPY derivative was synthesised. This time the starting material was 2-methoxy-4-nitrobenzoic acid with the initial step being the conversion of the starting carboxylic acid to an acyl chloride by the treatment with oxalyl chloride in the presence of a catalytic amount of DMF. IR spectroscopy confirmed the successful conversion by the disappearance of the band at  $1710\text{ cm}^{-1}$  and the appearance of a band at  $1791\text{ cm}^{-1}$ . This intermediate was then redissolved in DCM and used further without additional purification. The product **127** was isolated in a 22% yield. These results are summarised below in Table 4.2.

Table 4.2 Synthesis of BODIPY derivatives starting from benzoyl chlorides



Compound ID	R	R <sub>1</sub>	Yield
122	H	H	17%
126	NO <sub>2</sub>	H	30%
127	NO <sub>2</sub>	OMe	22%
125	I	H	-

i) 2,4-dimethylpyrrole, reflux, 2 h then BF<sub>3</sub>·OEt<sub>2</sub>, Et<sub>3</sub>N, rt, 1 h

### 4.3.2 Photophysical analysis

Having successfully identified a viable synthetic route, the photoluminescent properties of the probes synthesised were then analysed. All were shown to exhibit a very similar excitation and emission profile, which is typical of that of BODIPY. In all cases a small Stokes shift was seen, typically less than 20 nm, which can be seen in Figure 4.6. Table 4.3 below summarises the photoluminescent data achieved for the probes synthesised.

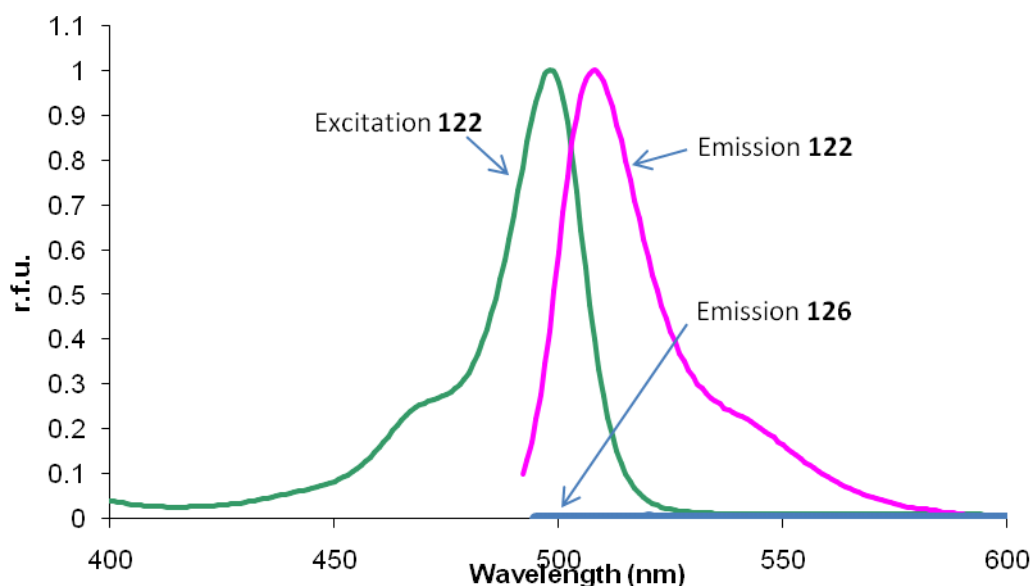
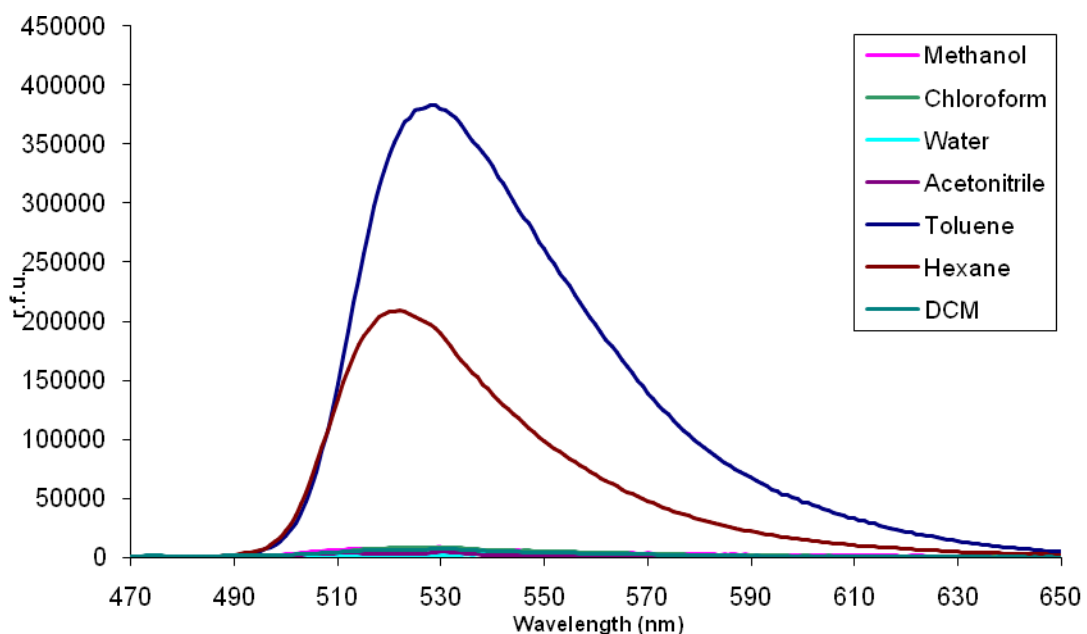


Figure 4.6 Comparison of emission of 122 and 126 (CHCl<sub>3</sub>, 24 °C)

Compound	Solvent	$\lambda_{\text{ex}}$ (max/nm)	$\lambda_{\text{em}}$ (max/nm)	$\phi_f$	$\tau$ (ns)
<b>122</b>	acetone	498	508	59	4
<b>126</b>	acetone	502	n/a	0.3	n/a
	chloroform	509	n/a	n/a	n/a
	MeOH	503	n/a	n/a	n/a
	H <sub>2</sub> O	510	n/a	n/a	n/a
	MeCN	502	n/a	n/a	n/a
	hexane	507	522	n/a	n/a
	toluene	509	528	n/a	n/a
<b>127</b>	acetone	502	n/a	n/a	n/a

**Table 4.3** Photoluminescent properties of **122**, **126** and **127**

Importantly, **126** exhibits no fluorescence in polar solvents, including H<sub>2</sub>O, acetone, methanol, acetonitrile, chloroform, and dichloromethane. However, when **126** was dissolved in either toluene or hexane a strong fluorescence signal was observed. The overall results can be seen in Figure 4.7 with an expanded section showing the polar solvents in Figure 4.8.



**Figure 4.7** Fluorescence spectra of **126** when dissolved in a range of solvents

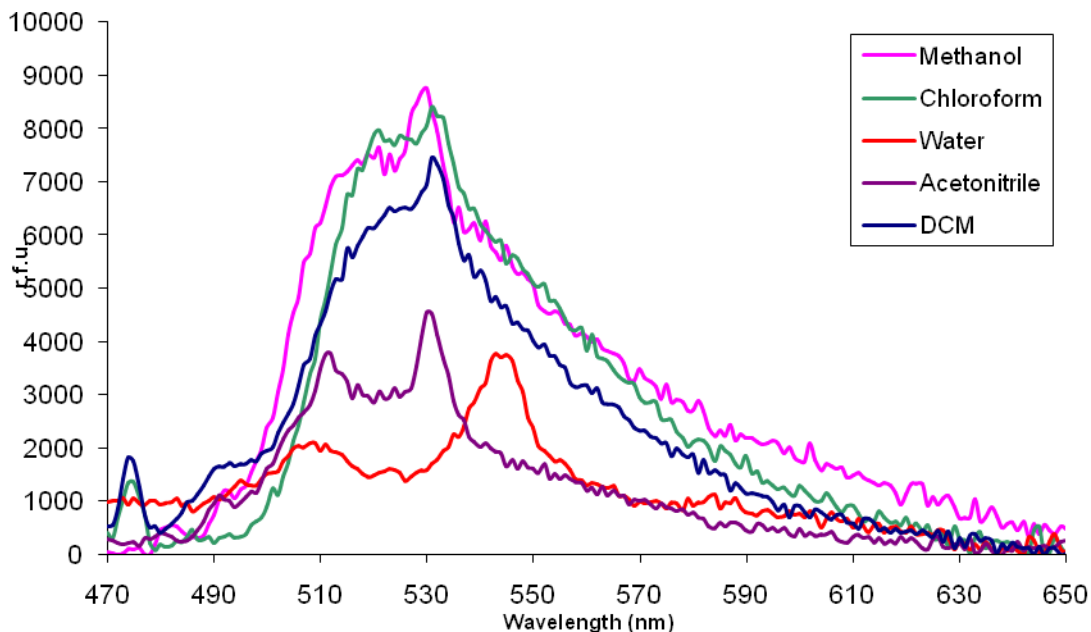


Figure 4.8 Enlarged section of fluorescence spectra of 126 showing polar solvents

This result suggests that the cause of fluorescent quenching is photoinduced electron transfer (PeT). PeT is commonly accepted as a mechanism of fluorescent quenching in polar environments at ambient temperatures.<sup>176</sup> Electron transfer from a donor system to the excited fluorophore causes the quenching of the fluorescence. It is normally the case that the two systems are separated by a linker that holds the fluorophore close to, but separately from, the electron donor.<sup>177</sup> However, recent work by Nagano *et al* has shown that fluorescein derivatives can be thought to exhibit PeT.<sup>178</sup> They believe this is the case as the fluorescein molecule can be thought of as two separate parts. This is due to the orthogonality of the benzoic moiety to the xanthene fluorophore, Figure 4.9. By altering the R substituent, changes in the HOMO energy can be brought about resulting in an altered quantum yield. They have shown that increasing the HOMO energy results in a diminished quantum yield.

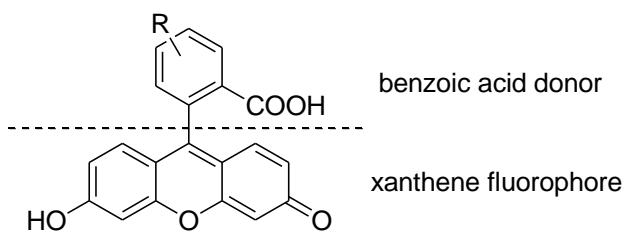
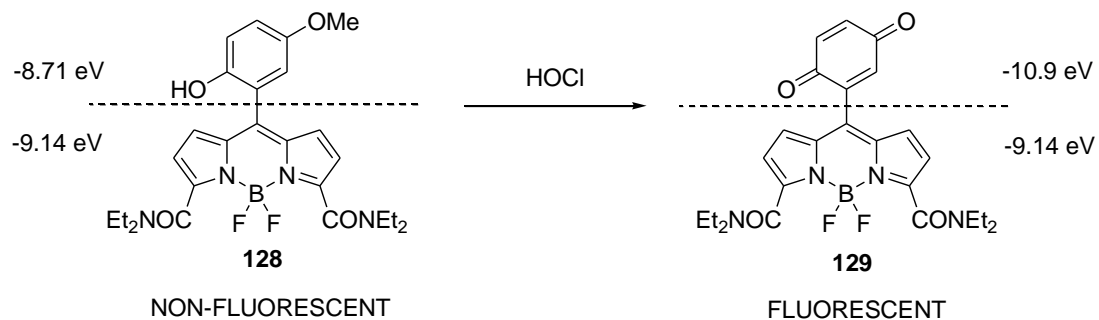


Figure 4.9 Fluorescein structure divided into two orthogonal parts.

In a similar fashion, the structure of phenyl-substituted BODIPY derivatives, such as **122**, **126** and **127**, can also be thought of as exhibiting PeT due to the orthogonality between the phenyl ring and BODIPY fluorophore. Reported evidence for this is seen in various X-ray crystal structures which have shown a variety of BODIPY derivatives which adopt this conformation.<sup>179</sup> In addition, work published recently by Sun and co-workers where a non-fluorescent BODIPY derivative, **128** was designed, which upon addition of hypochlorous acid (HOCl) became fluorescent, Figure 4.10.<sup>163</sup>



**Figure 4.10** Switching on of fluorescence of **128** upon treatment with HOCl

It is rationalised that due to the decrease in the energy of the phenyl substituent (-8.71 eV to -10.9 eV), the PeT quenching process is prohibited due to the lower energy of the phenyl substituent as compared to the BODIPY fluorophore and hence the molecule, **129**, fluoresces.

### 4.3.3 Computational Studies

Due to the proposed mechanism of quenching being PeT, theoretical calculations could be carried out to determine the fluorescent properties of any other BODIPY analogues. This is due to the fact that following excitation of an electron from the BODIPY chromophore to an excited state, relaxation of that electron falls into the LUMO of the nitrophenyl substituent, resulting in a non-fluorescent molecule. This is summarised in Figure 4.11.<sup>180</sup>



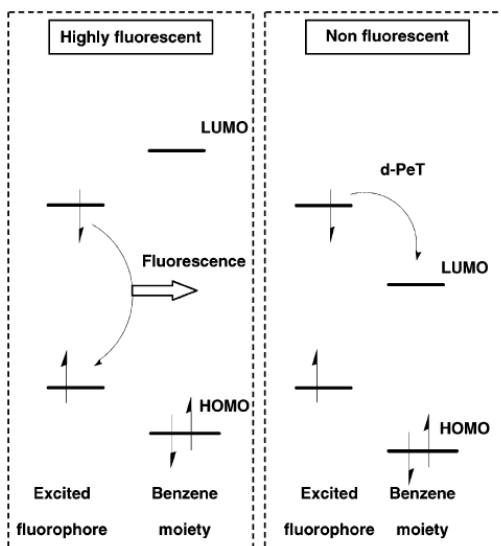


**Figure 4.11** Cartoon representation of proposed PeT mechanism. Reprinted with permission from *Journal of the American Chemical Society*, 2004, 126, 14079-14085. Copyright 2004 American Chemical Society

Density functional theory (DFT) gives information on electron density within both the filled and unfilled molecular orbitals within a molecule. By analysing the electron density of both the HOMO and the LUMO of BODIPY derivatives, an indication of the PeT quenching mechanism and hence fluorescence of the molecule can be predicted.

Using Gaussian several DFT calculations were performed to the B3LYP level of theory, using the basis sets 6-31G\*(d).<sup>181</sup> Figure 4.12 shows both the predicted electron density within HOMO and LUMO orbitals.

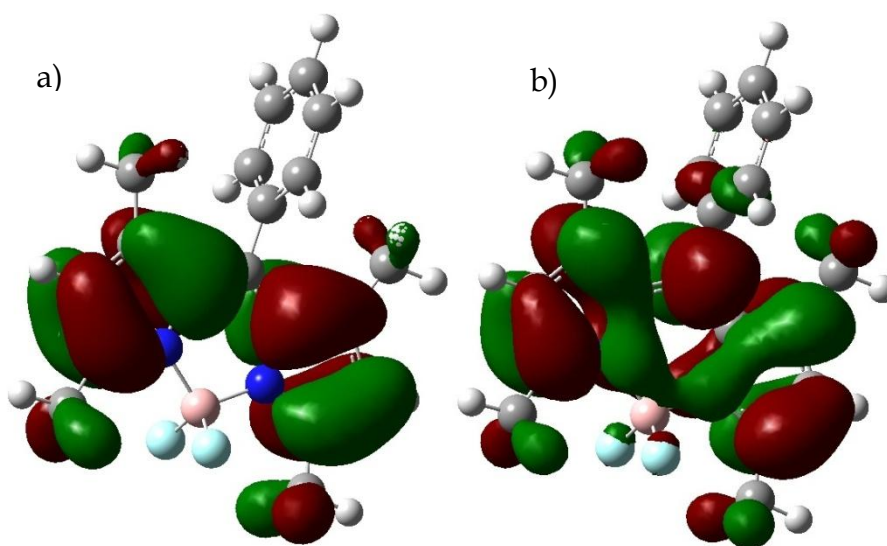


**Figure 4.12** DFT analysis of 122 showing the electron density in both a) the HOMO and b) the LUMO

It can be seen that the electron density is over the bora-s-indacene part of **122** in both the HOMO and the LUMO and therefore this molecule is predicted to be fluorescent, which photoluminescent analysis has shown. Performing the same calculation with **126** and **127**, it can be seen that the electron density is now completely different, Figure 4.13.

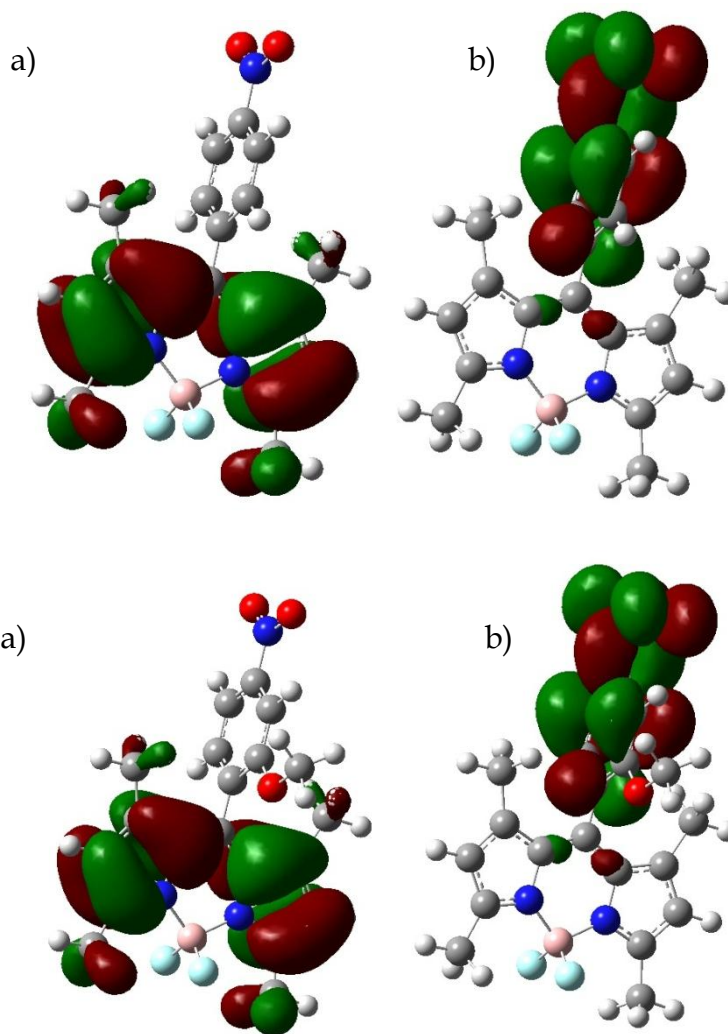
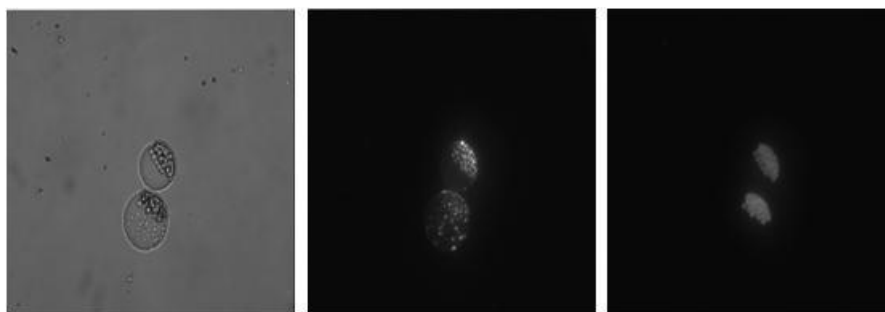


Figure 4.13 DFT analysis of 126 and 127 showing the electron density in both a) the HOMO and b) the LUMO

In both these cases, the electron density in the LUMO is predicted to be in the nitrophenyl substituent, which is as predicted by PeT quenching. In this way, DFT calculations can now be used to assess the likelihood of a BODIPY derivative displaying fluorescence.

### 4.3.4 Cellular/biological Studies

In order to test the biological viability of compounds **122**, **126** and **127**, they were tested in protoplasts harvested from *Arabidopsis thaliana* leaves. The probes were tested at a final concentration of 5  $\mu\text{M}$ , using acetone as the carrier solvent (less than 1%). The incubation time was typically 15 mins, after which time the cells were loaded onto a microscope slide and viewed using a fluorescence microscope. Fluorescence was observed in all cells as green, punctuate spots. For some examples see Figure 4.14.



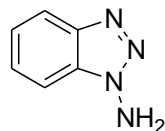
**Figure 4.14** Two *A. thaliana* protoplasts incubated with **126**. From L-R: White image, Punctuate fluorescence can clearly be seen, Red emission from the chloroplasts. Images are at 40x magnification

It is known that when hydrophobic BODIPY derivatives bind to biomolecules within cells, aggregation effects can cause the formation of micellular-like environments<sup>182</sup> and it was thought that this was the reason for the punctuate fluorescence pattern.

In order to determine protein binding, SDS-PAGE analysis was carried out. To this end, **127** was incubated with freshly harvested protoplasts and following cell lysis by heating to 90 °C in SDS loading buffer, SDS-PAGE analysis was performed. Unfortunately, the only fluorescent bands present on the gel were at a very low molecular weight, and this was attributed to free probe. Despite repeated attempts, including microsome isolation, no fluorescent bands corresponding to protein conjugates were seen.

#### 4.3.4.1 Inhibition Studies

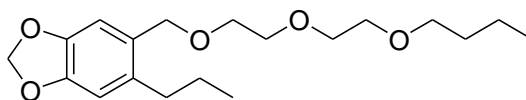
In order to show that the observed fluorescence was due to the interaction of the probe and p450 oxidative enzymes a variety of inhibition studies were carried out. The aim was to show that by inhibiting p450, the green fluorescence would not be seen. The first inhibitor tested was 1-aminobenzotriazole (ABT), which causes inhibition of cytochrome p450.<sup>183</sup>



**130**

ABT is a mechanism-based inhibitor which inactivates p450 by the alkylation of the haem group.<sup>184</sup> ABT undergoes p450-catalysed oxidation which produces benzyne. It is this benzyne that causes the alkylation of the haem group, resulting in the production of an abnormal porphyrin and the irreversible loss of activity.<sup>185</sup> Protoplasts were first incubated with 250  $\mu\text{M}$  ABT for 30 mins, followed by a 5 min incubation with **126**. When viewed under the fluorescence microscope, green punctuate fluorescence could still be seen. Repeating the reaction with 1 mM ABT did not result in prevention of the fluorescence. This indicated that the cause of the fluorescence was not due to the action of cytochrome p450. As a control reaction, ABT (250  $\mu\text{M}$ ) and **126** were mixed and incubated at rt for 30 mins and the emission spectrum recorded. No fluorescence was seen.

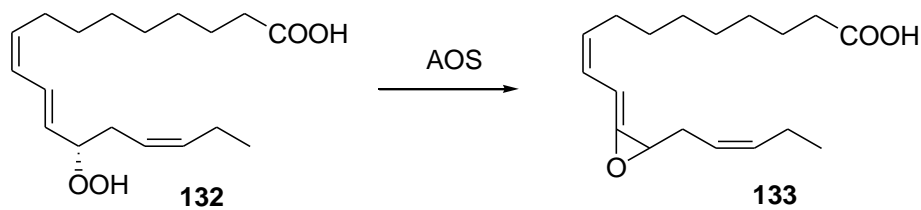
To confirm this, another p450 inhibitor, piperonyl butoxide (PBO, **131**) was tested.



**131**

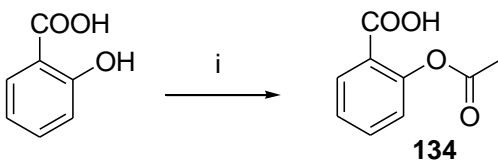
PBO is able to bind in the active site of p450 therefore preventing enzyme activity from occurring.<sup>186</sup> Protoplasts were incubated with 250  $\mu\text{M}$  PBO for 30 mins, followed by treatment with **126** and incubation for 5 mins. Again, fluorescence was seen in all cells. This results confirms that the fluorescence seen is not due to cytochrome p450 action.

As there are such a large number of cytochrome p450 enzymes, a search through the protein crystal databank revealed that allene oxide synthase (AOS) has characteristics similar to those of p450s.<sup>187</sup> AOS catalyses the conversion of 13-hydroperoxy-linoleic acid **132** to allene oxide **133**, Scheme 4.9.



Scheme 4.9

**132** is a very important lipid intermediate in plants as it is converted to the plant signalling molecule jasmonic acid.<sup>188</sup> A known inhibitor of AOS is 2-acetoxybenzoic acid, **134**<sup>189</sup>. This was synthesised in a 83% yield by the acylation of 2-hydroxybenzoic acid followed by recrystallisation from water (See Scheme 4.10).



i) Acetic anhydride, phosphoric acid, 60 °C,  
10 min, 83%

Scheme 4.10

The product was confirmed by the appearance of a peak at 2.35 ppm in the <sup>1</sup>H NMR spectrum due to the methyl ester and a *m/z* peak of 179.0350 by ES<sup>-</sup>. Inhibition studies were carried out in the same way as with ABT and PBO using 1 mM **126**. When the protoplasts were viewed under the microscope, green fluorescence could clearly be seen.

It was postulated that the reason for the increase in fluorescence may be the action of nitroreductase enzymes, which reduce the nitro group to an amino group. In order to show that the amino derivative is fluorescent, DFT calculations were carried out. The HOMO and LUMO can be seen in Figure 4.15. It can clearly be seen that the electron density in the LUMO is almost completely over the bora-indacene core, which suggests that **135** will be fluorescent.

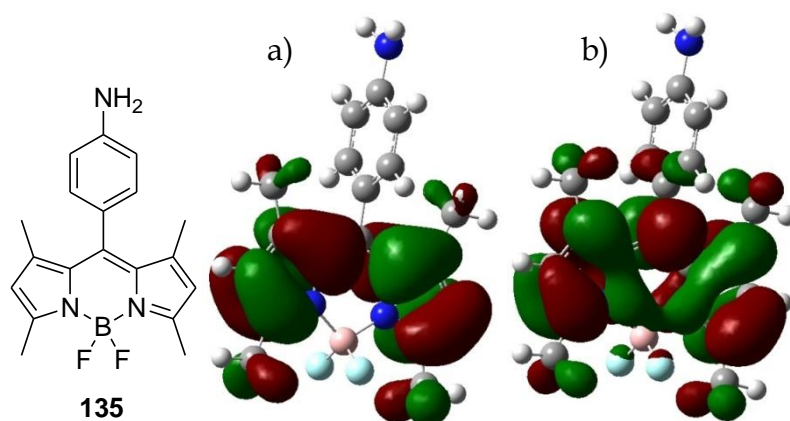
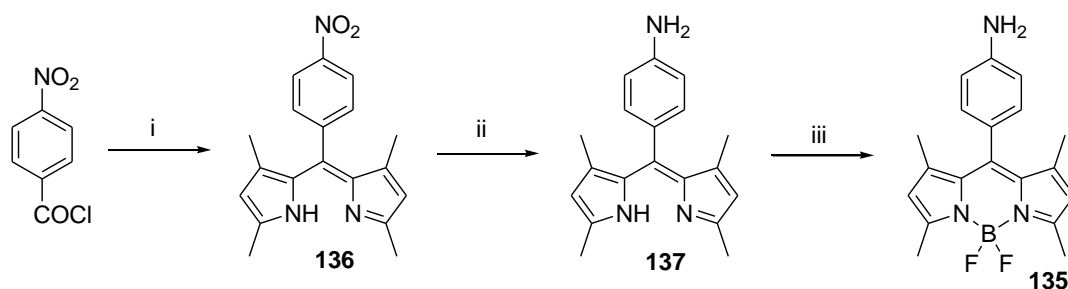


Figure 4.15 DFT analysis of **135** showing the electron density within both a) the HOMO and b) the LUMO

In order to verify this theoretical result **135** was synthesised. Li *et al* have shown that amino BODIPY derivatives can be formed from the reduction of the appropriate nitro derivative.<sup>190</sup> **126** was subjected to hydrogenation using a Thales H-Cube®. Unfortunately no product was formed, with only starting material being recovered. This may have been due to the low solubility of **126** in both MeOH and EtOH, however, chlorinated solvents are not useable on the H-Cube®. It was then attempted to synthesise **135** starting from 4-aminobenzoic acid in a one-pot procedure, using TFA as a catalyst in the dipyrromethene step. Disappointingly no product was formed, with only a complex mixture of unknown products observed.

Due to the failure of the one-pot reaction it was decided to firstly synthesise and isolate the 4-aminophenyl substituted dipyrromethene before complexation with  $\text{BF}_3 \cdot \text{OEt}_2$  (See Scheme 4.11).



i) 2,4-dimethylpyrrole, DCM, reflux, 1 h, 15%; ii)  $\text{SnCl}_2 \cdot 2\text{H}_2\text{O}$ , 35%; iii)  $\text{BF}_3 \cdot \text{OEt}_2$ ,  $\text{Et}_3\text{N}$ , DCM, rt, 2 h, 32%

Scheme 4.11

To this end, the first step was the formation of the nitro-dipyrromethene **136** by reaction of 4-nitrobenzoyl chloride with 2,4-dimethylpyrrole. This successfully gave the product in a 15% yield, with formation being confirmed by the  $m/z$  peak 322.2 ( $ES^+$ ). **136** was reduced using  $SnCl_2 \cdot 2H_2O$  to give the amino derivative **137**. The successful conversion could clearly be seen in the  $^1H$  NMR spectrum by the large shift in the aromatic protons, which shifted upfield from 8.33 – 8.35 ppm to 6.72 – 6.74 ppm and 7.51 – 7.53 ppm to 7.03 – 7.04 ppm respectively. The final step was the complexation with  $BF_3 \cdot OEt_2$  in the presence of  $Et_3N$  to give **135** in a 32% yield (overall yield 2%). The photophysical properties of **135** was examined and it was found to be fluorescent, as was predicted by DFT calculations. The excitation and emission maxima were 500 and 515 nm, in the same range as the other BODIPY derivatives synthesised.

When incubated with protoplasts **135** shows the same pattern of fluorescence as the previously tested probes. In *A. thaliana* NADPH:thioredoxin reductase (TR) is the enzyme responsible for the reduction of nitroaromatic compounds.<sup>191</sup> TR and the disulfide reducing enzyme thioredoxin (TRX) form a redox system which is able to pass electrons from NADPH to FAD, then onto the catalytic disulfide of TR and finally to the disulfide of TRX. In this way the nitro group can be reduced to an amino group, Figure 4.16

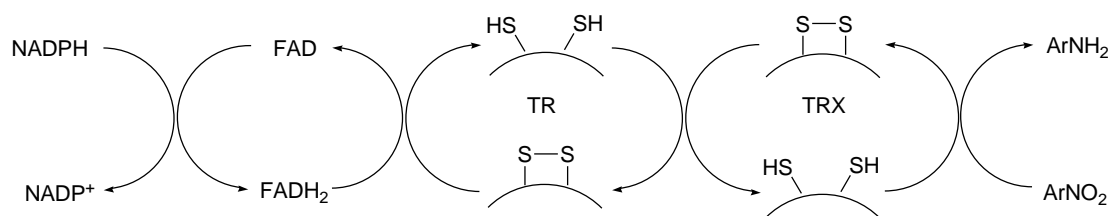
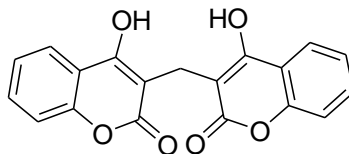


**Figure 4.16** NADPH dependent pathway for the reduction of aromatic nitro compounds to aromatic amino compounds

In order to test whether TR activity was responsible for the biological results seen two inhibitors were tested: dicumarol, **138** and 1-chloro-2,4-dinitrobenzene (CDNB). Dicumarol has been found to be a competitive inhibitor towards the binding of NADPH, thereby preventing the redox system from occurring.<sup>192</sup> CDNB is able to inhibit reduced TR by the modification of the active site reduced thiol.<sup>193</sup>



**138**

20  $\mu\text{M}$  dicumarol was incubated with protoplasts for 30 mins at rt. 2  $\mu\text{L}$  of **126** was added and the cells were incubated for a further 10 mins. Green punctuate fluorescence was seen in all cells. Dicumarol was tested again at an increased concentration of 200  $\mu\text{M}$ , but again fluorescence was observed in all cells. CDNB (200  $\mu\text{M}$ ) was tested in an identical way to that of dicumarol. When viewed under the microscope fluorescence was still seen. These results indicated that TR/nitroreductase activity was not the system of interest.

Looking at the protoplast images, it was observed that the fluorescence was often in association with the chloroplasts and therefore it was thought that the increase may be due to a system associated with photosynthesis. One such system is photosystem II (PSII). PSII is one part of a two part system used in photosynthesis, with the other being photosystem I (PSI). PSII absorbs light and this is used to promote the electrons from chlorophyll into a higher energy state. These electrons are then passed through the cytochrome b6f complex to PSI *via* an electron transport chain to enable the transport of a proton through the membrane to generate ATP. Atrazine is a known inhibitor of PSII<sup>194</sup> and this was tested with protoplasts in an attempt to ascertain the nature of the fluorescence. 200  $\mu\text{M}$  atrazine was incubated with protoplasts for 30 mins, followed by a 10 min incubation time with **126**. When the cells were viewed under the microscope, fluorescence could clearly be seen.



The following table (Table 4.4) illustrates the inhibitors that were tested, the system that they inhibit and the results obtained.

Inhibitor	Concentration	System probing	Result
ABT	250 $\mu$ M	Cytochrome p450	Green, punctuate fluorescence
ABT	1 mM	Cytochrome p450	Green, punctuate fluorescence
PBO	250 $\mu$ M	Cytochrome p450	Green, punctuate fluorescence
2-acetoxybenzoic acid	1 mM	Allene Oxide Synthase	Green, punctuate fluorescence
Dicumarol	20 $\mu$ M	TR/Nitroreductase	Green, punctuate fluorescence
Dicumarol	200 $\mu$ M	TR/Nitroreductase	Green, punctuate fluorescence
CDNB	200 $\mu$ M	TR/Nitroreductase	Green, punctuate fluorescence
Atrazine	250 $\mu$ M	Photosystem II	Green, punctuate fluorescence

**Table 4.4 Summary of inhibitors tested on *A. thaliana* protoplasts followed by incubation with 126**

#### 4.3.4.2 Flow cytometry analysis

A suspension of protoplasts were analysed by flow cytometry both before and after treatment with **126**. The resulting histograms can be seen in the figure below (Figure 4.17).

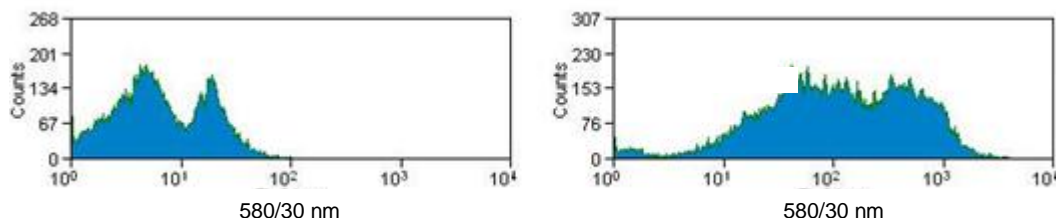


**Figure 4.17 Histograms showing the increase in fluorescence exhibited by protoplasts after incubation with 126**

It can be seen that an increase in fluorescence is detected by the flow cytometer. A time dependent plot was then taken, from which it was hoped the reaction kinetics could be calculated. Blank protoplasts were analysed by the flow cytometer and after 90 secs, the

analysis was halted, 2  $\mu\text{L}$  of **126** was added and the analysis was restarted. Data was collected for 15 mins. The dot plot can be seen in Figure 4.18.

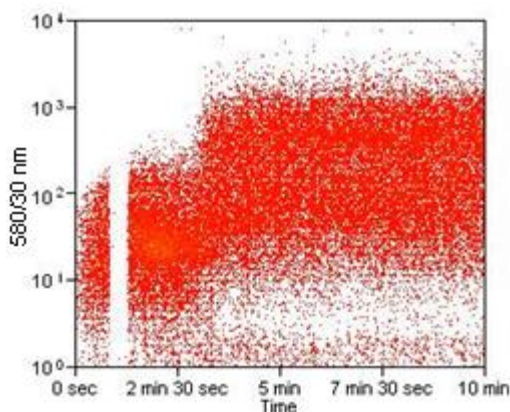


**Figure 4.18** Increase in fluorescence seen upon addition of **126** to *Arabidopsis thaliana* protoplasts. The break in the dot plot occurring at around 90 secs is due to the addition of the substrate, during which time no data is collected.

It can clearly be seen that a 10-fold increase in fluorescence occurs at around 2 minutes after the addition of **126**. This large jump is not typical of enzyme kinetics but of some sort of switch, *e.g.* a change in pH. In order to test this theory, a variety of buffers were made up with varying pH and upon addition of **126** the fluorescence was recorded. The results can be seen in Figure 4.19.

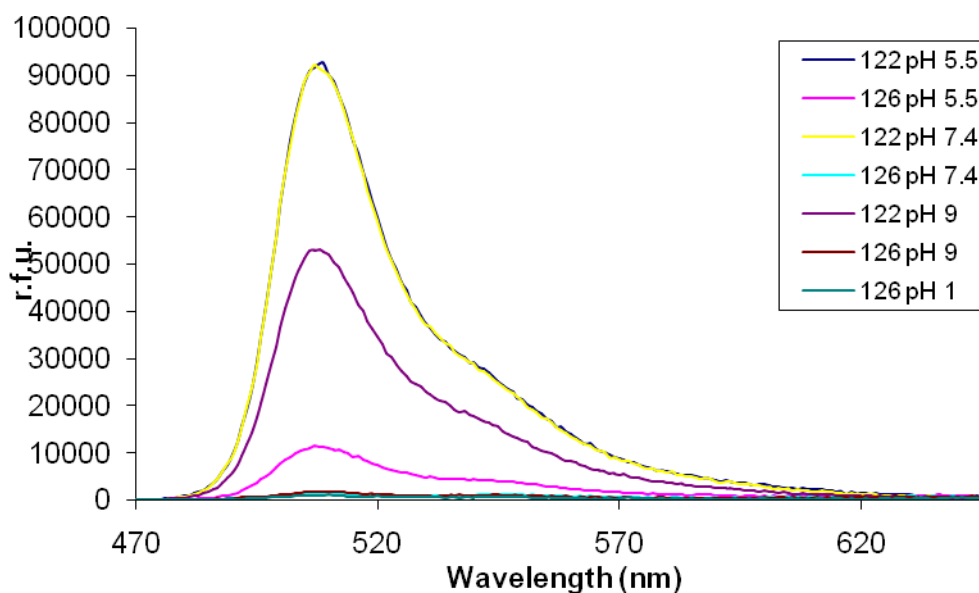


**Figure 4.19** Fluorescence spectra of **123** and **127** at differing pH

It can be seen from the graph above that changing the pH has no effect on the fluorescence of the probes. This is in agreement with Carriera who has also shown that BODIPY derivatives are insensitive to changes in pH.<sup>195</sup>

#### 4.3.4.3 Metabolite studies

As the inhibition studies had failed to determine the cause of fluorescence intensity increase attempts to isolate the metabolite of **126** were undertaken. It was hoped that this would allow the identification of the system **126** was reacting with.

Protoplasts were freshly harvested from *A. thaliana* and incubated with **126**. Following centrifugation the resulting pellet was resuspended in MeOH:H<sub>2</sub>O (1:1). This was again centrifuged and the resulting supernatant was used in MS studies. Disappointingly, both MS and MS/MS analysis did not show any evidence for metabolite formation, with only free probe observed. This was repeated using *A. thaliana* cell cultures, however again no metabolite(s) could be detected.

#### 4.3.4.4 Different cellular types

A variety of *A. thaliana* cell types were treated with **126** in order to determine whether different cell types gave the same fluorescent result. Protoplasts were isolated from both *A. thaliana* mesophyll cell cultures and root cultures (See Figure 4.20), with green, punctuate fluorescence seen in all cases.

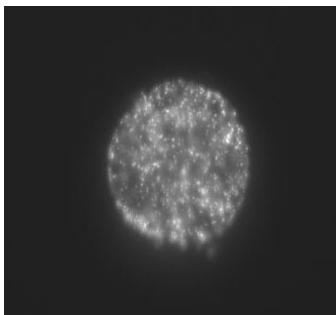


Figure 4.20 Protoplast isolated from *A. thaliana* root culture treated with **126**

Interestingly, when mesophyll cell culture protoplasts were incubated with **126** a much higher level of fluorescence was seen, both in terms of intensity and cellular amount. Upon further investigation it was discovered that these cell cultures had cooled to 15 °C for a period of two days and were therefore stressed cells. It is known in stressed cells

that the number of peroxisomes increases and therefore further studies were undertaken to show this. This work is detailed in Chapter 5.

#### **4.4 Summary**

\* **113** was successfully synthesised, however, attempts to utilise this a p450 probe were abandoned as it had a higher level of fluorescence than the control probe, **114**.

\* The synthesis of several BODIPY probes was successfully achieved and the introduction of a nitro group resulted in complete quenching of fluorescence.

\* When **126** was dissolved in either toluene or hexane a strong fluorescent signal was observed, suggesting that photoinduced electron transfer (PeT) is the quenching mechanism.

\* DFT calculations can now be used to assess the likelihood of a BODIPY derivative displaying fluorescence.

\* Upon incubation of **126** with *A. thaliana* protoplasts, fluorescence could be seen. However, attempts to isolate a fluorescently labelled protein were unsuccessful.

\* Inhibition studies undertaken with ABT and PBO confirmed that the fluorescence seen was not due to cytochrome p450 action.

\* Changing the pH of the solution had no effect on the fluorescent profile of the BODIPY probes.

\* A variety of enzyme inhibitors were tested in an attempt to ascertain the cause of fluorescence. However, none of the inhibitors tested affected the fluorescence of **126**.

#### **4.5 Conclusions**

Several BODIPY derivatives were synthesised, with **126** and **127** shown to be non-fluorescent in polar solvents. Theoretical calculations using DFT allowed the fluorescent properties of the probes to be predicted accurately, further demonstrating the likely mechanism of quenching to be PeT. These calculations can also allow for the design of any future profluorescent probes.

Cellular studies have shown that these probes are able to cross the cell membrane and results in the restored fluorescence of **126** and **127**. This was totally reproducible and was also seen across a variety of cell types. Identical fluorescence patterns were seen with all probes, with incubation times as low as 5 mins. Disappointingly no fluorescently tagged proteins could be isolated and inhibition studies and flow cytometric analysis showed that the cause of the fluorescence was unlikely to be enzymatic in nature. A variety of enzyme inhibitors were tested, with no affect seen on the fluorescent profile of the probes. In addition, changes in pH has shown to have no affect on the fluorescence intensity of any of the probes tested. Further studies have shown that these BODIPY probes localise exclusively within the peroxisome organelle within cells and this work and further studies are discussed in Chapter 5.

## 5 BODIPY

### 5.1 Introduction

This chapter describes work undertaken which shows that small fluorescent probes based on the BODIPY structure localise exclusively within the peroxisome in both plant and mammalian cells. The original aim of these probes were to react with, and isolate, oxidative cytochrome p450 enzymes (for a detailed description see Chapter 4).

### 5.2 Peroxisomes

Peroxisomes are small, membrane-bound organelles ubiquitous in eukaryotic cells.<sup>196</sup> These organelles are normally spherical in shape with diameters in the range 0.1 – 1  $\mu\text{m}$ , however, their shape can alter depending on the cell type. They are highly dynamic organelles which are able to move rapidly throughout the cell along microtubule and actin filaments.<sup>197</sup> Peroxisomes contain coarsely granular or fibrillar matrix, dotted with crystalline inclusions containing enzymes, *e.g.* catalase.

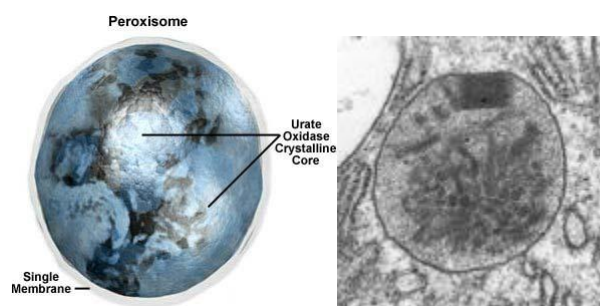


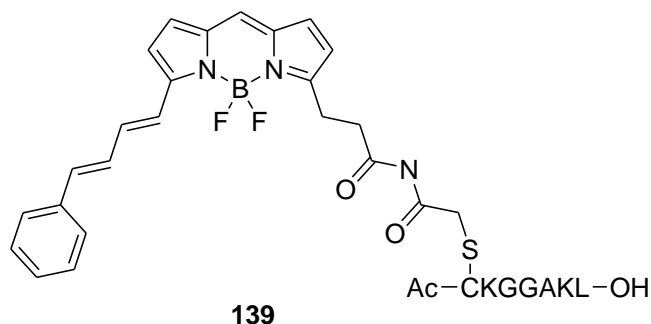
**Figure 5.1** Cartoon representation of a peroxisome alongside a scanning electron micrograph of a mammalian peroxisome

They are responsible for fatty acid  $\beta$ -oxidation and the defence against oxidative stress through the breakdown of hydrogen peroxide. The proliferation of peroxisomes occurs in response to a variety of factors<sup>198</sup> including xenobiotics, herbicides, biotic and abiotic stress<sup>199</sup> and nutrient deprivation. Deficiencies in peroxisome function or biogenesis can lead to several disorders including Zellweger syndrome and Infantile Refsum disease.<sup>200</sup> The ability to visualise the peroxisome directly in living cells would be a distinct advantage as this would allow scientists to monitor a variety of processes within cells including stress responses.

### 5.2.1 Peroxisome Markers

In order to study peroxisomes *in vivo* several techniques have been developed. These include the expression analysis of genes which encode for peroxisomal proteins,<sup>201</sup> and the direct measurement of enzymatic activity, such as catalase.<sup>202</sup> However, these techniques do not give any direct information on the peroxisome numbers within cells, but rather report on the changes in peroxisomal activity. In order to allow the visualisation of these organelles, immunolabelling experiments are often performed on fixed cells. These experiments involve the treatment of cells with antibodies specific for peroxisomal membrane proteins conjugated to a fluorophore, followed by visualisation. The most common method for this is electron microscopy coupled with either 3,3'-diaminobenzidine or cerium staining.<sup>203</sup> Recently Colton and co-workers have synthesised an antibody-Qdot conjugate.<sup>204</sup> Qdots are fluorescent nanocrystals and the authors claim that the use of these molecules offer several advantages over immunolabelling techniques. These include the large Stokes shift which removes autofluorescence problems, increase photostability and increased reliability. Whilst these methods allow for accurate peroxisomal imaging, they are very time consuming, expensive and labour-intensive.

In an effort to overcome these problems, new techniques are emerging which involve the use of fluorescent molecules which are able to localise within the peroxisome and allow the direct visualisation of these organelles. Following the discovery that a conserved tripeptide (S/A/C)-(K/R/H)-(L) located at the carboxy terminus of proteins targets those proteins to the peroxisome,<sup>205</sup> fluorescent compounds utilising this peroxisome targeting signal (PTS1) have been synthesised. Nebenführ and co-workers have developed a multicolour set of peroxisome markers for *A. thaliana* by the conjugation of PTS1 with four different fluorescent proteins (green, yellow, cyan and red). The fluorescent proteins were cloned these into expression vectors and following particle bombardment it has been shown that localisation within the peroxisome can be seen.<sup>206</sup> Dansen *et al* developed a BODIPY labelled heptapeptide, which contained the AKL tripeptide at the carboxy terminus, **139**. Following treatment with human fibroblasts, punctuate fluorescence was seen in all cells after as little as 10 minutes.<sup>207</sup>

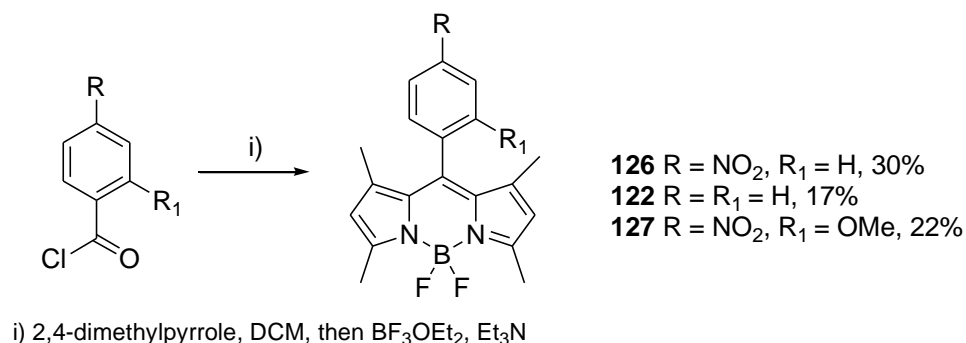


However, to date no fluorescent molecules for peroxisomal targeting exist without a peptide recognition unit, specifically PTS1. The results from the present study discussed in this chapter will show how small molecules without PTS1 can localise exclusively within the peroxisome of plant and mammalian cells.

### 5.3 Cell Studies

#### 5.3.1 Probe synthesis

A variety of BODIPY-based probes were synthesised and details of this, along with the photochemical analysis can be found in Section 4.3.1. The typical method of formation involved the acyl chloride condensation with 2,4-dimethylpyrrole, followed by complexation with  $\text{BF}_3 \cdot \text{OEt}_2$  in the presence of  $\text{Et}_3\text{N}$ , Scheme 5.1.



**Scheme 5.1**

**126** exhibits no fluorescence in polar solvents, including  $\text{H}_2\text{O}$ , acetone, methanol, acetonitrile, chloroform, and dichloromethane. However, when **126** was dissolved in either toluene or hexane a strong fluorescence signal was observed. This result reinforces the DFT calculations and therefore suggests that photoinduced electron transfer (PeT) is the quenching mechanism in operation (See Section 4.3.2).



Initial work was carried out in protoplasts isolated from *Arabidopsis thaliana* leaves. Upon incubation with **126**, green punctuate fluorescence could be seen in virtually all cells, Figure 5.2. Protoplasts were harvested from a variety of sources including root and mesophyll *Arabidopsis* cultures and upon incubation with **126**, identical localisation was seen. Attention now turned to the possibility of **126** being able to cross the plant cell wall.

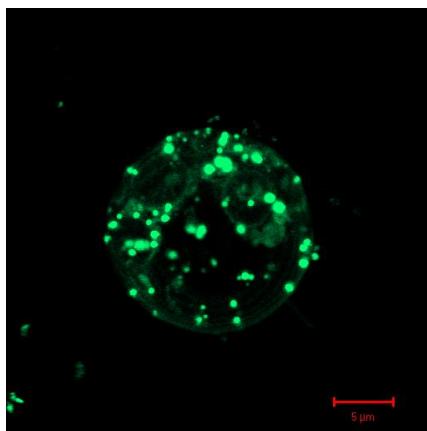


Figure 5.2 *A. thaliana* protoplast incubated with 126

### 5.3.2 Species/cell types

In order to test the possibility of **126** crossing the plant cell wall, Bright Yellow (BY-2) tobacco cells were incubated with **126**. BY-2 cells are tobacco culture cells that are commonly used by plant physiologists due to their stability in culture and rapid growth. Cells were incubated with the corresponding probe (5  $\mu$ M final concentration) at rt for 5 – 30 minutes prior to being mounted on a glass slide and viewed using confocal microscopy. Identical localisation was seen in all cases, with punctuate green fluorescence observed (for a typical example see Figure 5.3).

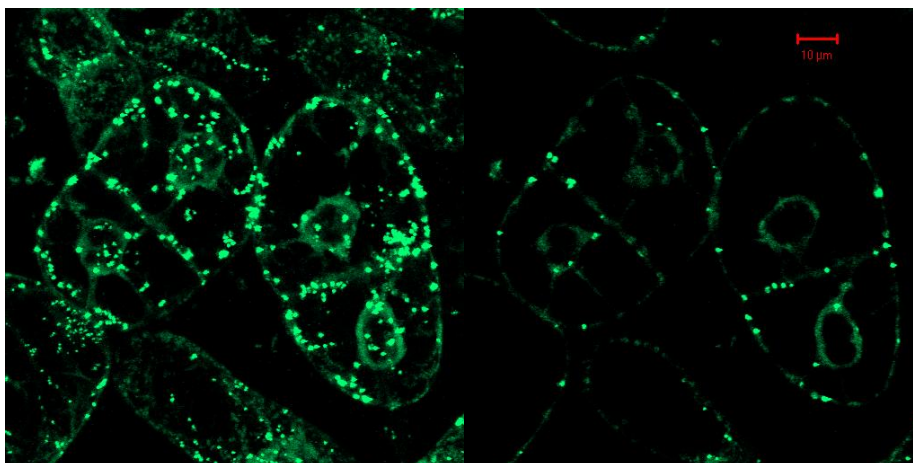


Figure 5.3 BY-2 cells incubated with 126

Localisation was also seen in the root tips of *Arabidopsis* plants which had been grown in media, Figure 5.4 These results clearly illustrate that **126** is able to cross the plant cell wall.

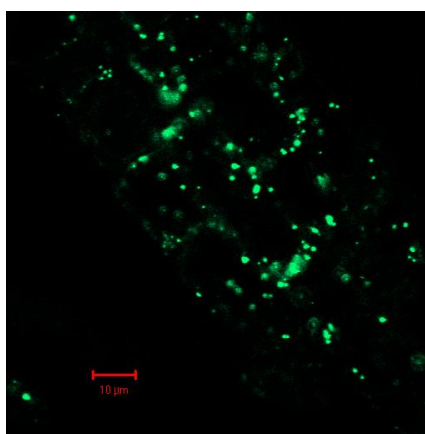


Figure 5.4 *Arabidopsis thaliana* root tips incubated with 126

After the failed attempts to isolate p450 enzymes using this class of probes, investigations were carried out to elucidate the cause of localisation. At this point, other work being carried out within the Edwards group on GSH conjugation involved the staining of peroxisomes within *A. thaliana* leaf epidermis cells. Comparing these images with those obtained on the confocal microscope (Figure 5.2 - Figure 5.4), led to the hypothesis that the cause of the fluorescence was localisation within the peroxisome organelle. In addition to this, the GSH conjugation images highlighted the rapid movements exhibited by peroxisomes, which could also be seen with cells treated with

BODIPY probes. Efforts were now directed towards gaining evidence to show that these probes localised within the peroxisome organelle.

### 5.3.3 Viability and uptake studies

To be useful as a marker for stress, the probes should not exhibit cytotoxic effects within the cells. To test this BY-2 cells were incubated with **126** (375 nM) for 1 week. After this time an aliquot was removed and visualised. Identical fluorescence and localisation could be seen when compared to previous images indicating that cells remain viable for up to one week with no toxicity observed, Figure 5.5. Pleasingly it appeared that the peroxisomes are not affected by treatment with **126** as evidenced by their continued rapid movement, which could be visualised in real time. The peroxisomes exhibited rapid translational movement, as well as oscillations and movement was up to  $10 \mu\text{ms}^{-1}$ .

Photobleaching was a minor effect, however a slight increase in laser power still enabled the peroxisomes to be easily visualised. It is interesting to note that no significant leaching from the peroxisome was seen with **126**. This suggests that the import rate is greater than the export rate. This has also been seen in the work of Pap when mammalian cells were incubated with **139**.<sup>208</sup> It was shown that the concentration gradient across the peroxisomal membrane is steep, with active import resulting in a 30-fold concentration increase of **139**. Due to the observed internalisation and retention of **126** it was also of interest to determine the mechanism of uptake. One such mechanism of uptake is endocytosis, which can be tested by both temperature and molecular inhibition experiments.

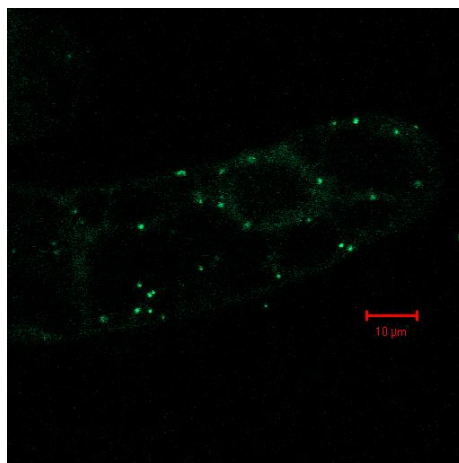
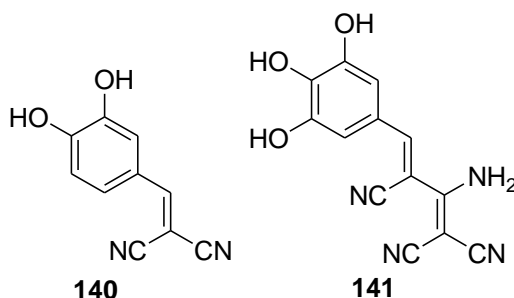


**Figure 5.5** Confocal microscope image of BY-2 cells after 1 week incubation with **126**

Cells were routinely incubated at room temperature, therefore to test the possibility of endocytosis, cells were incubated at 4 °C for 30 minutes prior to treatment with **126**. After incubation with 5 μM **126** at 4 °C for 20 minutes, fluorescence and therefore uptake was still observed. This suggests that endocytosis is not the mechanism of uptake. This is in agreement with the work of Pap who also observed this.<sup>207,209</sup> Tyrphostin A23 and A51 are known to inhibit endocytosis and therefore in addition to the temperature dependent results, these compounds were also tested.

The internalisation of many proteins depends upon motifs found within their cytosolic domains. One such motif contains a tyrosine residue, which can interact with complexes ( $\mu 2$ ) involved in the intracellular trafficking pathways through endocytosis by clathrin-coated vesicles. A class of compounds known as tyrphostins are able to inhibit the interaction between the tyrosine residue of the cytosolic motif and the  $\mu 2$  complex, of which tyrphostin A23, **140** is an example.<sup>210</sup> Tyrphostin A51, **141** is used as a control as it is unable to inhibit the above interaction but is able to inhibit tyrosine kinases. Although the majority of work carried out with **140** and **141** has been in mammalian cells, **140** has been shown to inhibit the endocytotic pathway in *A. thaliana* protoplasts<sup>211</sup> and therefore these compounds were tested.



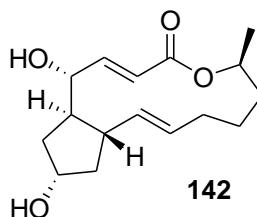
**140** was incubated with *A. thaliana* protoplasts (100  $\mu$ M) for 30 minutes, followed by **141** (100  $\mu$ M) for 10 mins. When the cells were viewed under the confocal microscope, green punctuate fluorescence could still be seen, indicating that clathrin-dependent endocytosis is not the mechanism of uptake. However, at this time it is not possible to ascertain the exact mechanism of uptake of the probes within cells.

### 5.3.4 Inhibition Studies

In order to provide further evidence for the localisation of **126**, inhibition studies were undertaken with a variety of cellular process inhibitors, which are described in the following sections.

#### 5.3.4.1 Brefeldin A

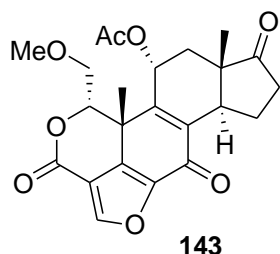
Brefeldin A, **142** is a macrocyclic lactone that is synthesised from palmitate by a variety of fungi.<sup>212</sup> In cells treated with **142** protein secretion is inhibited at an early stage in the secretory pathway and it has been shown that the block occurs in a pre-Golgi compartment.<sup>213</sup> Proteins become retained in the ER and cannot be processed further or transported around the cell.<sup>214</sup>



*A. thaliana* protoplasts were incubated with 100  $\mu$ M **142** for 30 mins. Following treatment with **126**, confocal imaging showed that fluorescence was the same as the control with movement of peroxisomes still seen. This implies that the protein secretory pathway, including the ER and Golgi apparatus are not involved in the localisation of **126**.

### 5.3.4.2 Wortmannin

Wortmannin, **143** was originally isolated from *Penicillium wortmanni* and has been shown to be a potent inhibitor of important regulatory kinases, such as phosphoinositide 3- kinase (PI 3-kinase). **143** binds to the ATP site of PI 3-kinase by covalently modifying the Lys802 residue. PI 3-kinase is the final part of a signalling cascade that produces D-3-phosphorylated phosphoinositides which are essential for cell growth and differentiation.<sup>215</sup>



*A. thaliana* protoplasts were incubated with 15  $\mu\text{M}$  **143** for 30 mins. Following treatment with **126**, confocal imaging showed that fluorescence was the same as the control with movement of peroxisomes still seen. This implies that kinase enzyme activity is not involved in the localisation of **126**.

**143** is also known to inhibit endocytosis within plants,<sup>216</sup> therefore these results support those demonstrated earlier with **140** and **141** and reinforce the fact that endocytosis is not the mechanism of uptake for the BODIPY probes.

### 5.3.5 Co-localisation Studies

In order to conclusively prove that **126** localised exclusively in peroxisomes co-localisation studies were performed. These studies utilised the peroxisomal targeting signal (PTS1) pmP90 linked to the fluorescent protein mCherry. The PTS1-mCherry construct was transformed into GV3101 *Agrobacterium tumefaciens* and infiltrated into *Nicotiana benthamiana*. A section of leaf was removed after 3 days and confocal microscopy confirmed successful transformation. A small section of leaf was soaked in **126** (in  $\text{H}_2\text{O}$ , 5  $\mu\text{M}$  final concentration) for 30 minutes. Co-localisation could only be seen in stomata cells (See Figure 5.6). In order to observe localisation within leaf epidermal cells, a solution of **126** in  $\text{dH}_2\text{O}$  was infiltrated into a transformed leaf and after 90 minutes a section of the leaf was imaged. Pleasingly, green fluorescence could

be seen within leaf epidermal cells and co-localisation was also confirmed (See Figure 5.7).

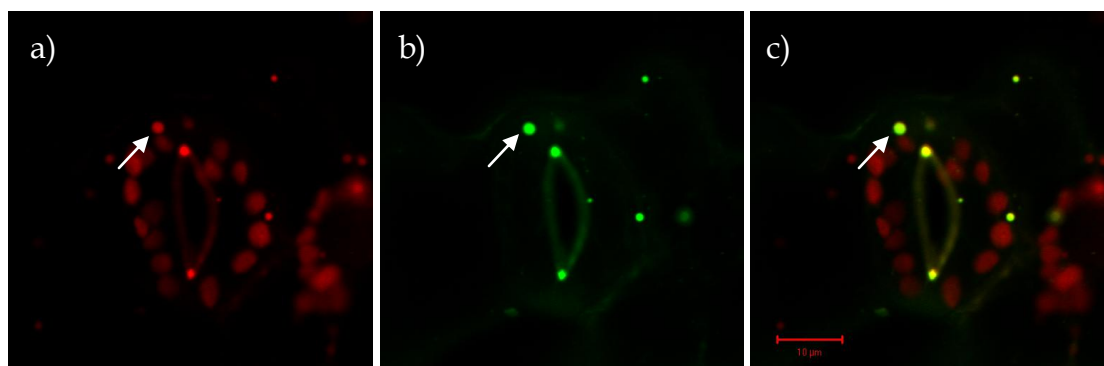


Figure 5.6 Co-localisation studies confirm BODIPY is targeted to the peroxisome. *Nicotiana benthamiana* stomata cells were infiltrated with the peroxisome marker GV3101 (pmP90) mCherry and subsequently incubated with 126. a) mCherry marker; b) 126; c) images superimposed. White arrows indicate peroxisomes.

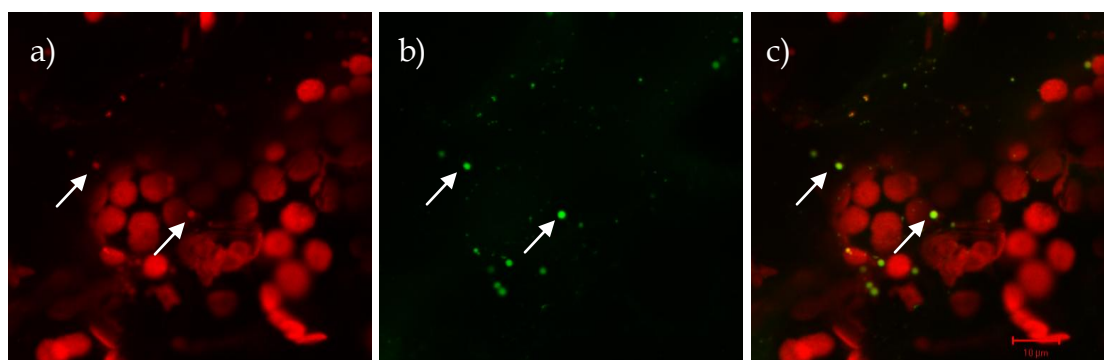


Figure 5.7 Co-localisation studies confirm BODIPY is targeted to the peroxisome. *Nicotiana benthamiana* epidermal cells were infiltrated with the peroxisome marker GV3101 (pmP90) mCherry and subsequently incubated with 126. a) mCherry marker; b) 126; c) images superimposed. White arrows indicate peroxisomes.

Small red dots are mCherry labelled peroxisomes, with green dots being peroxisomes labelled with 126. Superimposed dots appear yellow and it can be seen that there are no structures that show only 126, which confirms its unique peroxisomal localisation. It can also be seen that the peroxisomes are often in close proximity with chloroplasts with the preliminary observation being discussed in Section 4.3.4.1. It has been shown that in photosynthetically active cells peroxisomes are often associate with chloroplasts where they participate in photorespiration.<sup>217</sup> This can be seen as further evidence for the localisation of the BODIPY probes within the peroxisome.

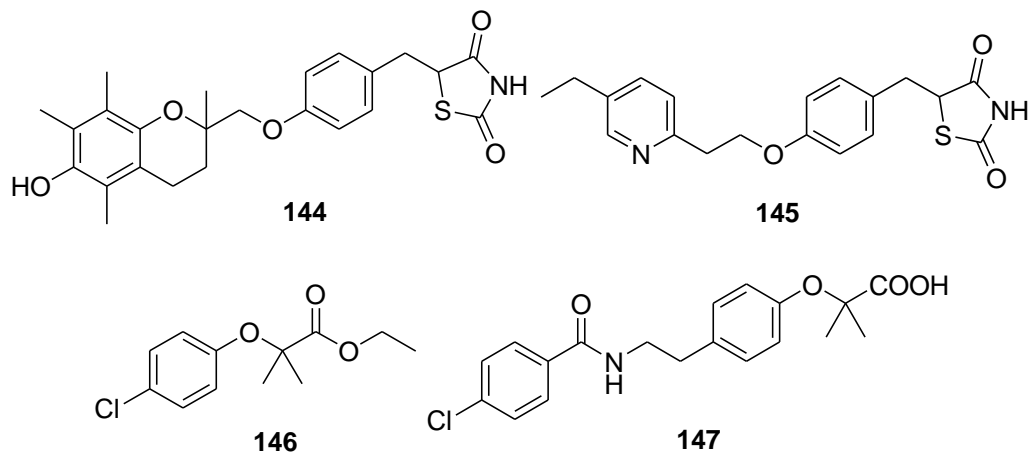
The studies undertaken so far had shown that the BODIPY probes were able to localise exclusively within plant peroxisomes at low concentrations and with a very short incubation period. In addition to this, no perceived cytotoxicity was observed and indeed cells remain viable for up to one week.

#### 5.4 Peroxisome Proliferator-activated Receptor (PPAR) Studies

In order to test the ability of the BODIPY probes to respond to changes in peroxisome numbers, peroxisome proliferator-activated receptor (PPAR) studies were undertaken.

Peroxisome numbers are known to increase to a wide variety of stimuli such as increased fatty acids, reactive oxygen species, xenobiotics<sup>218</sup> and herbicides.<sup>219</sup> The mechanism by which proliferation occurs is a result of the induction and transcription of a number of biogenesis genes. These genes are in turn induced by the presence of receptors known as PPARs. There are three main types of PPARs known as PPAR $\alpha$ , PPAR $\beta$  and PPAR $\gamma$  and each of these is distinguishable by the function that they undertake.<sup>220</sup> Once activated by the above mentioned stimuli, PPARs bind to DNA and regulate gene transcription, ultimately resulting in the proliferation of peroxisomes.

Both natural and synthetic ligands exist for all isoforms of PPARs. PPAR $\alpha$  tends to bind polyunsaturated fatty acids such as Leukotriene B, whereas PPAR $\gamma$  interacts with prostaglandins and oxidised metabolites of linoleic acid. Synthetic ligands often belong to one of two classes: thiazolidinediones or fibrates.<sup>221</sup> The thiazolidinedione class contains compounds such as troglitazone, **144** and pioglitazone, **145** and these activate PPAR $\gamma$ . The fibrate class has compounds which include clofibrate, **146** and bezafibrate, **147** and these bind mainly to PPAR $\alpha$ .<sup>222</sup>





It has been shown that clofibrate can induce peroxisome proliferation in plant cells.<sup>223</sup> Palma *et al* showed that treatment of *Pisum sativum* L (pea leaves) with 1 mM clofibrate causes a 5-fold increase in the number of peroxisomes.<sup>224</sup> In order to show that **126** could allow an increase in peroxisome numbers to be observed, BY-2 cells were treated with clofibrate.

#### 5.4.1 Clofibrate

Treatment with the PPAR $\alpha$  agonist clofibrate, **146**, which is known to increase peroxisome numbers, indicated that **126** was able to selectively stain peroxisomes in treated cells, with no interference seen. BY-2 cells were treated with 50  $\mu$ M **146** and incubated for 1 hour. Following this, treatment with **126** (final concentration 5  $\mu$ M) was performed and the cells were viewed under the microscope. The peroxisome population had increased dramatically in the **146** treated cells (Figure 5.8b) when compared to the control (Figure 5.8a) and this could clearly be visualised following treatment with **126**.

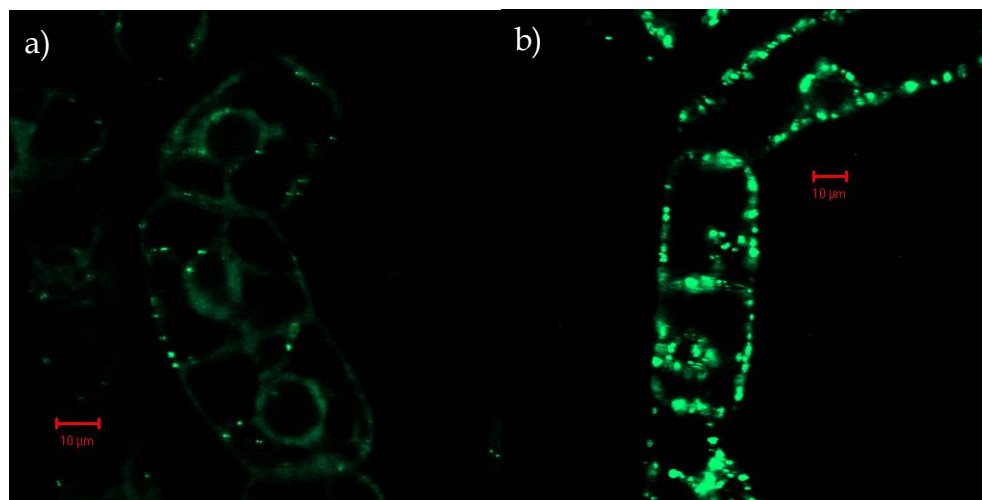


Figure 5.8 BY-2 cells treated with clofibrate, **146**, followed by incubation with **126**. a) control; b) clofibrate treated cells

This highlights that **126** is able to respond to changes in peroxisome numbers and therefore shows that it has an application towards being a marker for stress within cells.

#### 5.5 Localisation Causes

Co-localisation studies have conclusively shown that **126** localises exclusively within the peroxisome (See Section 5.3.5). It has also been shown that these probes are able to

localise within the peroxisome of a variety of species and cell types, with only a very short incubation time needed. However, the reason for this localisation was unknown. Efforts now concentrated on studies to elucidate the cause of this localisation.

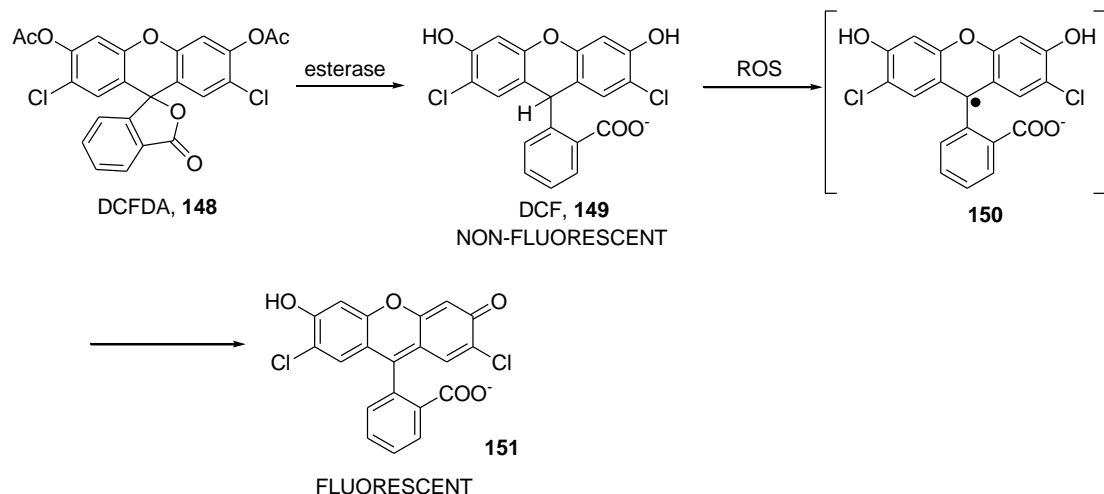
### 5.5.1 Reactive Oxygen Species

Peroxisomes are known to be involved in the production and metabolism of reactive oxygen species. It was thought that the reason for the localisation of **126** within peroxisomes may be due to its reaction with these species and experiments were undertaken to prove this.

Reactive oxygen species (ROS) is a collective term which includes oxygen radicals such as  $\cdot\text{OH}$ ,  $\cdot\text{OOR}$  and  $\text{O}_2\cdot^-$  and certain non radicals that are oxidising agents or easily converted into radicals, *e.g.*  $^1\text{O}_2$ ,  $\text{H}_2\text{O}_2$  and  $\text{O}_3$ . ROS are widely believed to contribute to the development of several age related diseases by causing oxidative damage to cells.<sup>225</sup> The ability to measure ROS is crucial for the diagnosis and treatment of these age related diseases, and this can be achieved by several methods. One such example is the use of molecules to trap the ROS and the subsequent measurement of the trapped species. 5,5-dimethyl-1-pyrroline *N*-oxide (DMPO) is used in this manner, with ESR used to measure the decrease in DMPO levels.<sup>226</sup>

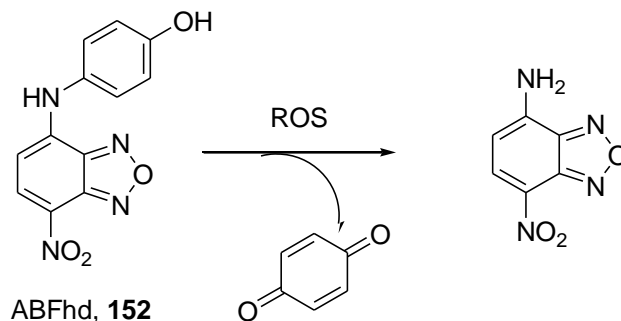
Another method involves the measurement of levels of oxidative damage to cellular components. Examples include the detection of DNA damaged products such as base and sugar modifications<sup>227</sup> and protein modifications such as methionine sulfoxide<sup>228</sup> which can be achieved using HPLC and GC/LC-MS.

Finally, fluorescent probes are also used to detect cellular ROS. Dichlorofluorescein diacetate (DCFDA), **148** is a non-fluorescent molecule which is taken up by cells and through the action of endogenous esterases is converted to dichlorofluorescein (DCF), **149**. **148** is also non-fluorescent and reacts with ROS present within the cell to form the radical species **150**, which rearranges to give the fluorescent molecule, **151** (See Scheme 5.2).<sup>229</sup>



**Scheme 5.2** Reaction of DCFDA with esterases to form DCF and its subsequent reaction with ROS to give the fluorescent molecule 151.

Another example of a fluorescent ROS probe was recently developed by Scaiano.<sup>230</sup> The simple reaction of NBD-Cl with 4-aminophenol gives ABFhd, **152**. This is a non-fluorescent molecule which upon reaction with ROS, releases the fluorescent NBD group, Scheme 5.3.



**Scheme 5.3**

It was proposed that the increase in fluorescence seen with **126** in cells may be due to a reaction with ROS and experiments were undertaken to investigate this.

### 5.5.1.1 ROS Studies

Several reactive oxygen species were tested with **126** in an attempt to show that one of them caused an increase in fluorescence and were therefore responsible for the green fluorescence seen within the peroxisome of cells. All spectra were recorded with the same slit width and over the same emission wavelength.

### 5.5.1.1.1 Hydrogen peroxide

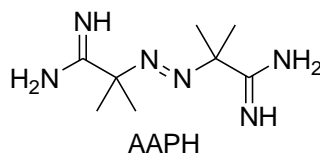
H<sub>2</sub>O<sub>2</sub> is able to cross cell and organelle membranes easily and can lead to displacement of the inhibitory subunit from the cytoplasmic transcription factor nuclear factor κB, allowing the activated factor to migrate to the nucleus.<sup>231</sup> H<sub>2</sub>O<sub>2</sub> can also stimulate transcription of *c-jun* and can activate mitogen-activated protein kinases.<sup>232</sup> Although many ROS can attack DNA, H<sub>2</sub>O<sub>2</sub> does not react with DNA bases at all.<sup>233</sup>

1 mM H<sub>2</sub>O<sub>2</sub> was added neat to a solution of **126** in dH<sub>2</sub>O. The fluorescence measurement showed no increase in emission. No change was seen after leaving the solution for 1 hr. The reaction was repeated but following H<sub>2</sub>O<sub>2</sub> addition the solution was incubated at 40 °C for 30 mins. However, no change in fluorescence was seen. It would appear that H<sub>2</sub>O<sub>2</sub> has no effect on the fluorescent intensity of **126** and is therefore not responsible for the fluorescence seen *in vivo*.

### 5.5.1.1.2 Hydroperoxyl and peroxy radical

Both hydroperoxyl (<sup>•</sup>OOH) and peroxy (<sup>•</sup>OOR) radicals are responsible for the peroxidation of lipids within cells. They are also able to oxidise proteins by the attack of hydroperoxyl radicals generating amino acid radicals, which may crosslink or react with O<sub>2</sub> to generate peroxy radicals. These peroxy radicals may abstract H<sup>•</sup>, triggering more radical generation and form protein peroxides which can decompose in a variety of ways.<sup>234</sup>

Two different sources of <sup>•</sup>OOH were used: *t*BuOOH and cumenehydroperoxide. Both were added to a solution of **126** in dH<sub>2</sub>O, however no change in fluorescence was seen. In order to generate <sup>•</sup>OOR, 2,2-azobis(2-amidinopropane) (AAPH) was used.



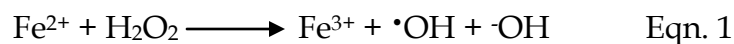
AAPH is a water-soluble azo compound which is used extensively as a free radical generator, often in the study of lipid peroxidation and the characterization of antioxidants. Decomposition of AAPH produces molecular nitrogen and two carbon radicals. The carbon radicals may combine to produce stable products or react with molecular oxygen to give peroxy radicals. The half-life of AAPH is about 175 hours

(37 °C at neutral pH), making the rate of free radical generation essentially constant during the first several hours in solution.<sup>235</sup> AAPH was added to a solution of **126** in dH<sub>2</sub>O, however despite several attempts and incubation at 40 °C no changes in fluorescence were observed. This would indicate that neither •OOH or •OOR are responsible for the changes in fluorescence seen with **126**.

#### 5.5.1.1.3 Hydroxyl radical, •OH

Hydroxyl radicals (•OH) plays many important cellular roles including, messenger roles in T-cell activation<sup>236</sup> and the mediation of redox alteration of cell-membrane Ca<sup>2+</sup>.<sup>237</sup> In addition to this •OH can also damage DNA bases, inducing cells to undergo apoptosis.<sup>238</sup>

Two reactions were employed in the generation of the hydroxyl radical. The first of these was the Fenton reaction. This involves the reaction of FeSO<sub>4</sub>·7H<sub>2</sub>O with H<sub>2</sub>O<sub>2</sub> to generate •OH, Equation 1. However, when this was attempted no change in fluorescence was observed, even with a second addition of FeSO<sub>4</sub>·7H<sub>2</sub>O.



The second reaction utilised KNO<sub>3</sub>, Equation 2.<sup>239</sup> A sample of KNO<sub>3</sub> was ground using a pestle and mortar to a fine powder. This was irradiated with UV light until the powder changed from white to yellow. After this time, 5 mg was added to the solution containing **126** and the emission spectra was recorded. No change in fluorescence was seen. These two results suggest that •OH are not responsible for the change in fluorescence seen.

#### 5.5.1.1.4 Superoxide, O<sub>2</sub><sup>•-</sup>

The superoxide anion (O<sub>2</sub><sup>•-</sup>), which is characterised by a small lifetime in aqueous media, has a prolonged lifetime within cellular membranes and is capable of hydrolysing certain lipids, such as phospholipids.<sup>240</sup> In this experiment KO<sub>2</sub> was used as the superoxide source. All fluorescence measurements were carried out at a final concentration of 100 μM. After an addition of 5 mg of KO<sub>2</sub>, measurements were recorded at 0 mins, 40 mins and 120 mins. However, no increase in fluorescence was

observed despite repeated attempts. This indicates that  $O_2^{\bullet-}$  is not the cause of the fluorescence within cells.

#### 5.5.1.1.5 Singlet oxygen, $^1O_2$

In photosynthesis, singlet oxygen ( $^1O_2$ ) can be produced and is scavenged by the carotenoids by direct quenching to prevent any damaging effects. In mammalian systems,  $^1O_2$  can cause the oxidation of lipids and result in cardiovascular effects. As with  $H_2O_2$ ,  $^1O_2$  does not react with DNA bases.<sup>233</sup>

In order to generate singlet oxygen zinc tetraphenylporphyrin (ZnTPP) was used. Irradiation of ZnTPP forms an excited state, ZnTPP\*, which is able to react with molecular oxygen to generate  $^1O_2$  and regenerate ZnTPP. ZnTPP has a  $\lambda_{ex}$  at 420 nm (Figure 5.9) and therefore irradiation at this wavelength provides the greatest opportunity for  $^1O_2$  generation.

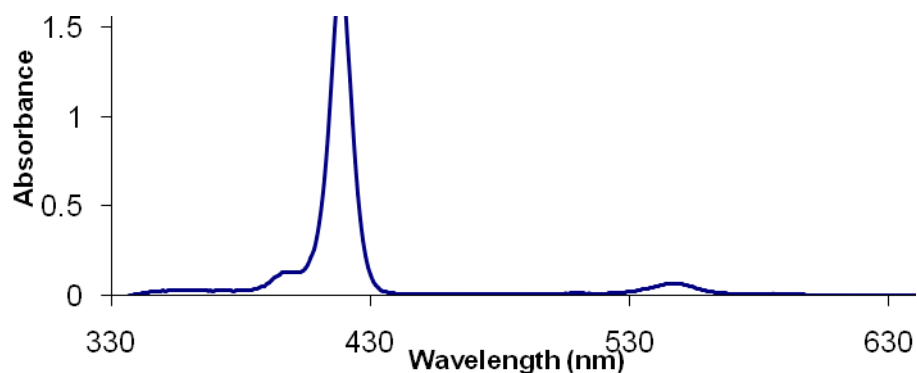


Figure 5.9 Absorbance spectrum of ZnTPP

Probe **126** was added to a solution of ZnTPP in  $dH_2O$  and the solution was illuminated at 420 nm for 30 mins. After this time the fluorescence spectrum was recorded, however no change was seen. The solution was illuminated for a further 30 mins but again no change in fluorescence was observed. This result indicates that  $^1O_2$  is not the species responsible for the increase in fluorescence.

The following table summarises the ROS tested with **126** and the results obtained.

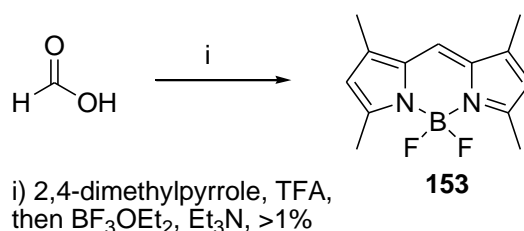
ROS	SOURCE	FLUORESCENCE
H <sub>2</sub> O <sub>2</sub>	H <sub>2</sub> O <sub>2</sub>	NO
•OOH	<i>t</i> BuOOH	NO
•OOH	Cumenehydroperoxide	NO
•OOR	AAPH	NO
•OH	Fenton Reaction	NO
•OH	KNO <sub>3</sub>	NO
O <sub>2</sub> •-	KO <sub>2</sub>	NO
<sup>1</sup> O <sub>2</sub>	ZnTPP	NO

Table 5.1 Summary of ROS tested with **126** and the results observed

As the ROS tested had no effect on the fluorescent properties of **126**, it was decided to systematically alter the structure in the hope of elucidating the part of the molecule which was responsible for the localisation within peroxisomes.

### 5.5.2 Phenyl substituent substitution

Initial attempts focused on the phenyl substituent. Compound **153** was synthesised to show whether a phenyl substitution was essential for peroxisomal localisation. **153** was synthesised according to Scheme 5.4 in less than a 1% yield. Due to the poor yield there was not enough product for NMR studies, however, LC-MS indicated successful production by the presence of the molecular ion, 249.2 [M+H<sup>+</sup>]. In addition to this, the photoluminescence of **153** exhibited a classic BODIPY excitation and emission profile, which again indicated successful synthesis of **153**, Figure 5.10.



Scheme 5.4 Synthesis of **153**

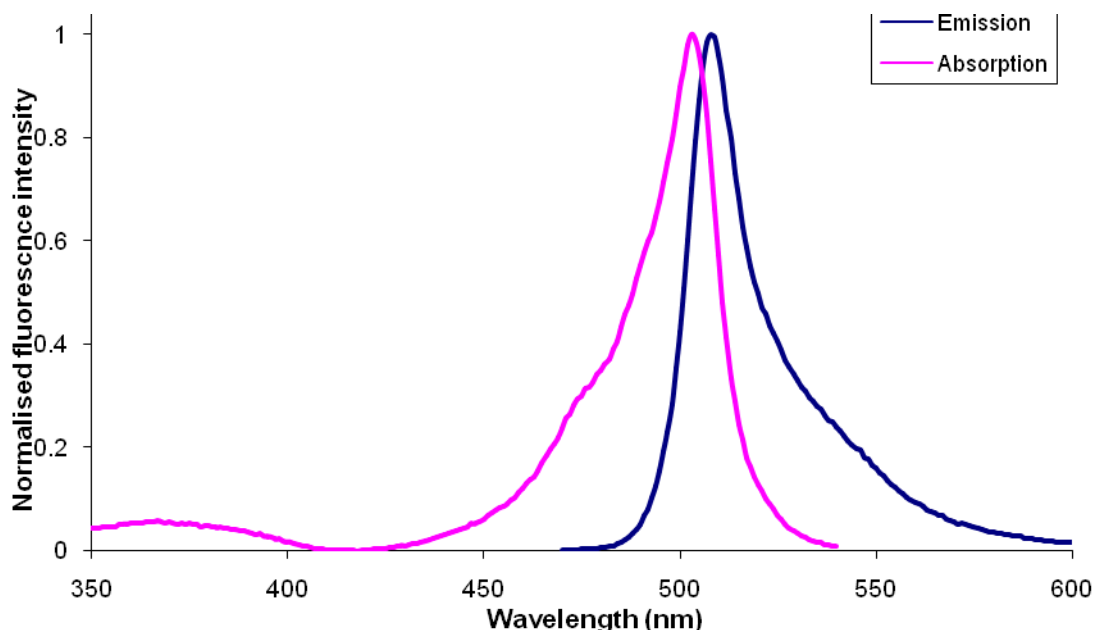


Figure 5.10 Excitation and emission profile of **153**

BY-2 cells were treated with **153** and localisation was seen within peroxisomes. This result suggests that it is the bora-indacene core which is essential for localisation. Furthermore, the original bromo-BODIPY derivative **116** which contained no methyl groups on the pyrrole was also tested. This also showed identical localisation and fluorescence within cells, indicating that the methyl groups are not needed for peroxisomal localisation.

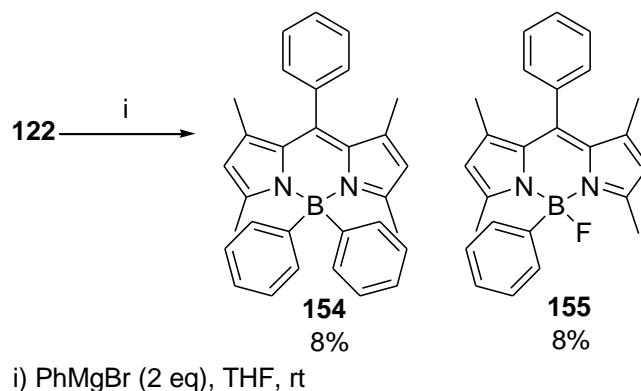
**153** was also purchased from Molecular Probes and when treated with BY-2 cells, identical localisation was seen. However, due to the high quantum yield a small amount of background fluorescence was seen and therefore it would appear that **126** is a better marker for peroxisomes due to the very low background fluorescence, allowing for a greater contrast. As the phenyl substituent had no effect on the localisation attention now turned to the B-F bonds.

### 5.5.3 Fluorine substitution

In order to ascertain what importance the fluorine groups had and whether the B-F bond was the cause of the localisation, each fluorine was substituted starting from compound **122** (See Scheme 5.5). This was achieved following recent reports by Ziessel, in which the fluorine can be substituted by the reaction with an appropriate Grignard



reagent.<sup>241</sup> Following FCC both the mono- and disubstituted compounds could be isolated. A molecular ion peak at 440.3 in the MADLI MS showed the presence of **154**, whilst in the spectrum of **155**, peaks at 382.2 and 363.2 was seen, with the latter being attributed to the loss of HF. In both cases the isotope pattern for boron could clearly be seen. In addition to this, both <sup>19</sup>F and <sup>11</sup>B NMR confirmed the correct number of boron and fluorine atoms in the respective compounds. Photoluminescence showed that both **154** and **155** were fluorescent, with virtually identical excitation and emission maxima (**154** 502 and 523 nm; **155** 503 and 523 nm).



Scheme 5.5

Both **154** and **155** were incubated with BY-2 cells (5  $\mu$ M final concentration), with both exhibiting identical subcellular localisation as with all of the previous probes. This would suggest that neither the fluorine groups nor the B-F bond are responsible, nor required, for the localisation within peroxisomes (See Figure 5.11).

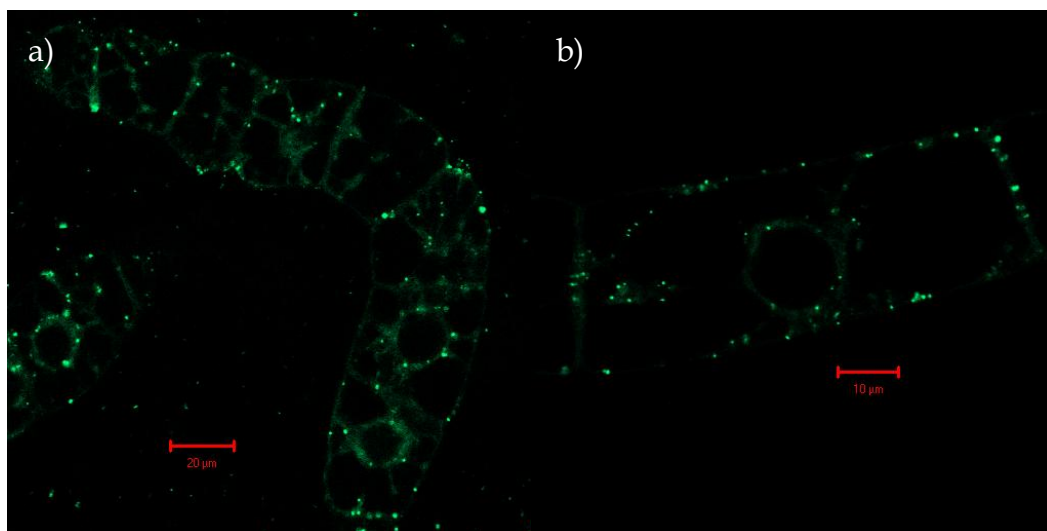
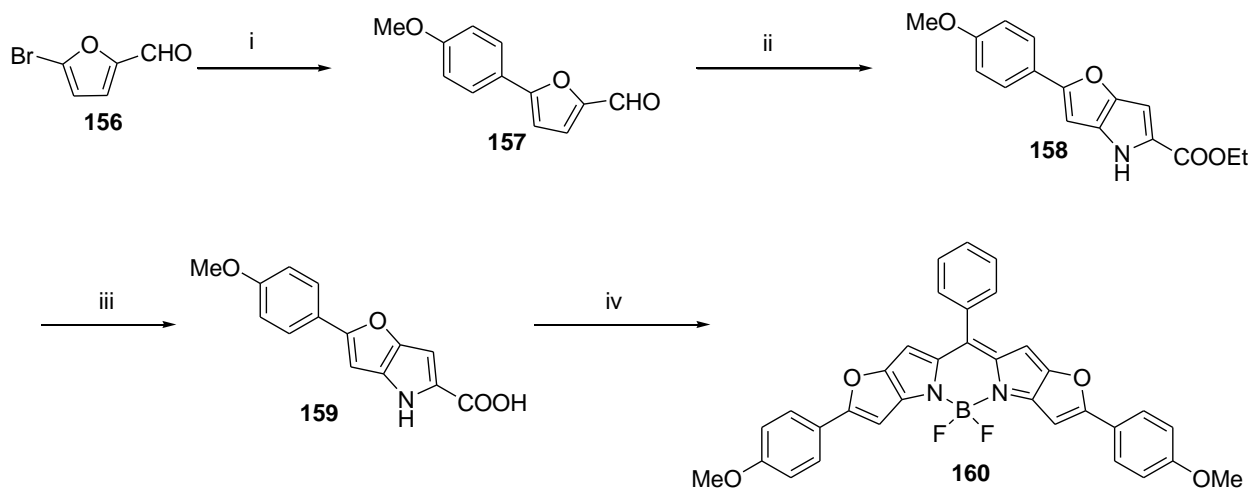


Figure 5.11 Treatment of BY-2 cells with a) 154 and b) 155

### 5.5.4 Pyrrole conjugation

In order to test the possibility of localisation being dependent on the pyrrole group, efforts towards modifying this group were undertaken. In addition to this it has also been shown that a different fluorescence emission wavelength, and hence colour, can be achieved with BODIPY molecules containing an extended conjugated pyrrole system.<sup>242</sup> This probe was based on recent literature by Suzuki, where far-red emitting probes were synthesised.<sup>243</sup> A slightly modified probe was synthesised based on the synthetic route below, Scheme 5.6.



i) 4-methoxyphenylboronic acid, Pd(dppf)<sub>2</sub>Cl<sub>2</sub>·DCM, toluene, EtOH, Na<sub>2</sub>CO<sub>3</sub>, 110 °C, 13 h, 80%; ii) ethylazidoacetate, NaOEt, EtOH, rt, 2 h then reflux, 1 h, 26%; iii) NaOH, EtOH, reflux 1 h, 99%; iv) TFA, reflux, 15 min, benzoyl chloride, DCM, then BF<sub>3</sub>OEt<sub>2</sub>, Et<sub>3</sub>N, 30%

Scheme 5.6 Multi-step synthesis of 160

**156** was coupled under standard Suzuki conditions with 4-methoxyphenylboronic acid to yield **157** in an 81% yield. This was confirmed by the presence of two multiplets in the  $^1\text{H}$  NMR spectrum corresponding to the protons of the phenyl ring (7.75 – 7.76 and 6.95 – 6.96 ppm). In addition, a molecular ion in the  $m/z$  spectrum was observed which is fully consistent with the molecular formula  $\text{C}_{12}\text{H}_{10}\text{O}_3$ . The next step involved the synthesis of the fused furan-pyrrole ring system. The initial stage involves the formation of the azide derivative, which undergoes spontaneous cyclisation upon heating in toluene. The fused furan-pyrrole molecule **158** was formed in a 26% yield, as ascertained by the appearance of peaks corresponding to the pyrrole proton and furan proton (6.67 ppm,  $d^4J$  0.5 and 6.49 ppm,  $d^4J$  0.5 respectively) in the  $^1\text{H}$  NMR spectrum. The ethyl ester was hydrolysed by treatment with NaOH in EtOH in a 99% yield to afford **159** as a purple solid. IR analysis showed successful hydrolysis by the disappearance of the band at  $1645\text{ cm}^{-1}$  and the appearance of  $1715\text{ cm}^{-1}$ . The final step of the synthesis involved the BODIPY formation, which was achieved in a one-pot procedure through the condensation with benzoyl chloride, followed by complexation with  $\text{BF}_3\cdot\text{OEt}_2$  in the presence of  $\text{Et}_3\text{N}$ . MALDI MS showed a peak corresponding to the molecular ion at 561.2, with the characteristic boron isotope pattern and a second peak corresponding to loss of HF. The overall yield for the synthesis of **160** was 6%. Fluorescence analysis showed **160** to emit in the red region, with the maximum at 687 nm (See Figure 5.12).

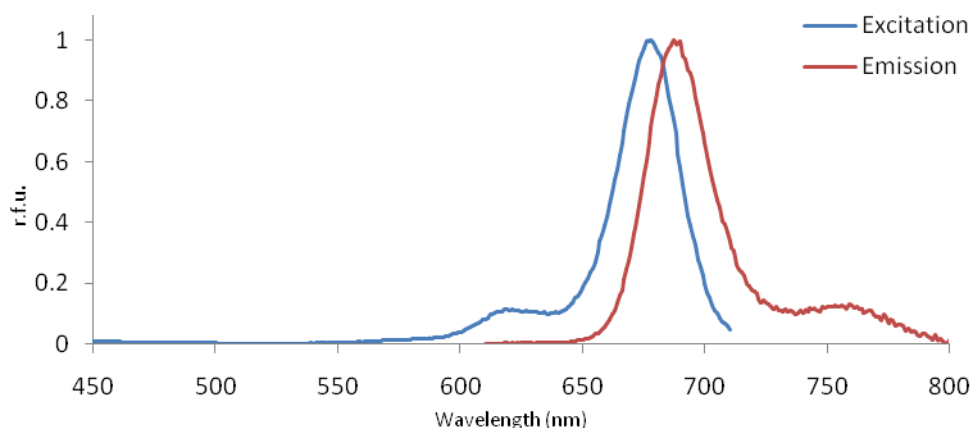


Figure 5.12 Fluorescence spectrum of **160**

**160** was tested on BY-2 cells (laser emission at 633 nm, 650 nm LP filter), using the same methodology as for the other BODIPY probes. Pleasingly, red punctuate fluorescence was observed in all cells (See Figure 5.13). Again movement was seen, hence no

perceived toxicity could be detected with this probe. This suggests that the pyrrole functionality can be adapted to tune the fluorescence without any effect on peroxisome localisation. This result leads the way for a multi colour set of peroxisome markers.<sup>244</sup>

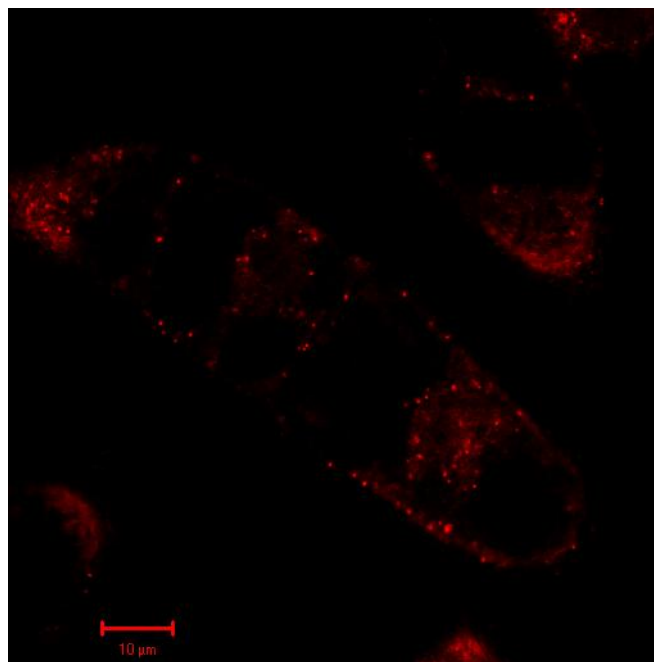
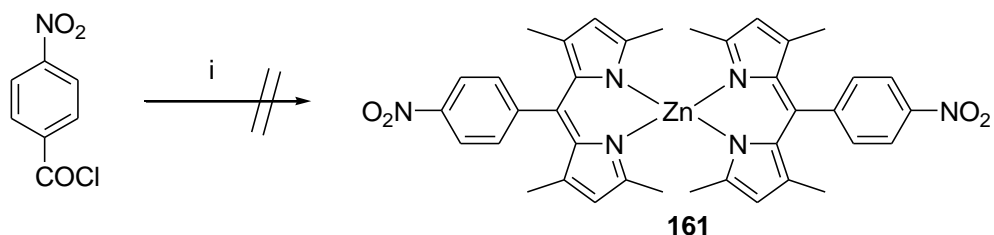


Figure 5.13 BY-2 cells incubated with **160**, with red, punctate fluorescence clearly seen

### 5.5.5 Boron substitution

The final part of the molecule which was highlighted for modification was the boron centre. It has been shown that dipyrromethene compounds can be complexed with a wide variety of metal salts to form bis(dipyrinnato)-metal(II) or tris(dipyrinnato)-metal(III) complexes. Examples of metals used include Zn(II),<sup>245</sup> Co(II),<sup>246</sup> Ni(II), Cu(II),<sup>247</sup> Fe(III) and Co(III)<sup>248</sup> amongst others. Of those synthesised the only one to exhibit fluorescence was the Zn complexes and for this reason the synthesis of this complex were attempted.

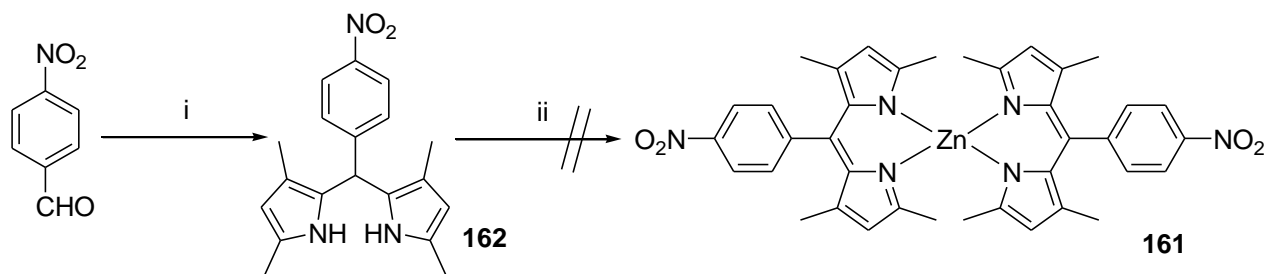
Attempts were made to synthesise **161** in a one pot procedure in a similar manner to **126**, with replacement of  $\text{BF}_3 \cdot \text{OEt}_2$  with  $\text{Zn}(\text{OAc})_2$ , Scheme 5.7. However, no product was isolated following FCC, with only 4-nitrodipyrromethene **136** isolated.



i) 2,4-dimethylpyrrole, DCM, then Zn(OAc)<sub>2</sub>, Et<sub>3</sub>N, DCM

**Scheme 5.7**

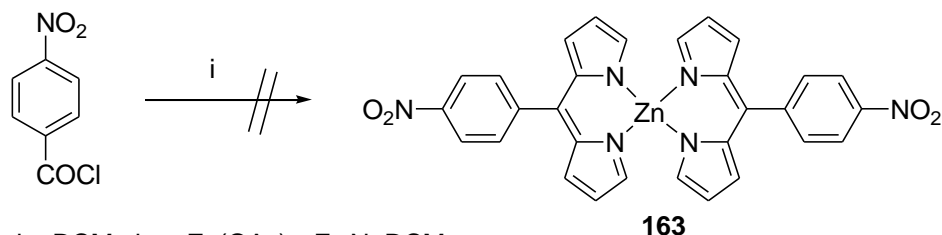
Due to the failure of the one pot procedure, synthesis of **161** was attempted by treatment of the purified 4-nitrodipyrromethane **162** with Zn(OAc)<sub>2</sub>, Scheme 5.8. Disappointingly, no reaction was seen. Despite repeated attempts, using both Zn(OAc)<sub>2</sub> and Zn(OAc)<sub>2</sub>·2H<sub>2</sub>O compound **161** could never be isolated.



i) 2,4-dimethylpyrrole, TFA, DCM, 4 h, 64%; ii) Zn(OAc)<sub>2</sub>·2H<sub>2</sub>O, Et<sub>3</sub>N, DCM

**Scheme 5.8**

It was thought that the reason for the failure may be due to the methyl groups on the pyrrole ring causing steric hindrance to the complexation step. For this reason the reaction was repeated using pyrrole, Scheme 5.9. Unfortunately no product could be detected, even when performing the two step reaction.



i) pyrrole, DCM, then Zn(OAc)<sub>2</sub>, Et<sub>3</sub>N, DCM

**Scheme 5.9**

A final attempt involved the synthesis of **163** using the one-pot procedure, however, no product was obtained. Due to time constraints this was not pursued any further.

## **5.6 Mammalian Studies**

As the biological studies undertaken so far involved the use of plant systems it was therefore of interest to see if the localisation of the BODIPY probes was exclusive to plant peroxisomes. To this end, probes **122** and **126** were tested within mammalian cells, in particular the mouse fibroblasts NIH 3T3 and human stem cells, MG63 osteoblasts. NIH 3T3 cells were kindly donated by Elizabeth New and MG63 osteoblasts were kindly donated by Stefan Przyborski. Details of the methodology and results obtained are outlined in the following section.

### **5.6.1 NIH 3T3**

NIH3T3 are mouse fibroblast cells that have become a well established cell line. Probe **126** was tested in NIH3T3 to ascertain the probes use within mammalian cells. Cells were grown to confluence on glass slides and treated with **126** (5  $\mu$ M final concentration) with a 1 hour incubation period at 37 °C. Punctuate green fluorescence could be seen within all cells showing that these probes also localise with the peroxisomes of mammalian cells. Figure 5.14 shows both a white light and fluorescent image of an fibroblast cell, where the peroxisomes can clearly be seen.

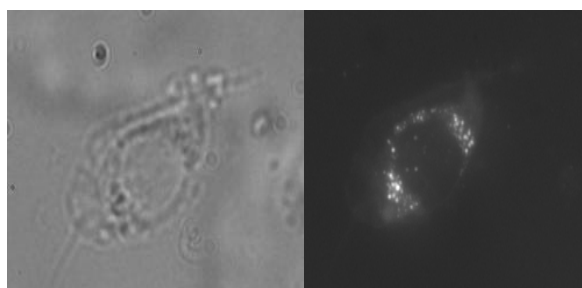


**Figure 5.14 NIH3T3 fibroblasts incubated with 126**

### **5.6.2 MG63 osteoblasts**

Osteoblasts are bone stem cells that have not undergone complete differentiation. Due to the several disorders which can affect humans it was of interest to see if the BODIPY probes are also able to localise in the peroxisomes of cells grown from a human cell line. To this end, **126** was incubated with MG63 osteoblasts, which had been grown to confluence at 37 °C. **126** (~5  $\mu$ M) was added at rt and incubated for less than 10

minutes. When viewed under the confocal microscope, green punctuate fluorescence could clearly be seen in all cells, Figure 5.15. As with the NIH3T3 cells, this would indicate that **126** is able to localise within the peroxisomes of mammalian cells. Conclusive proof of this would only be ascertained following co-localisation studies, which due to time constraints were not undertaken.

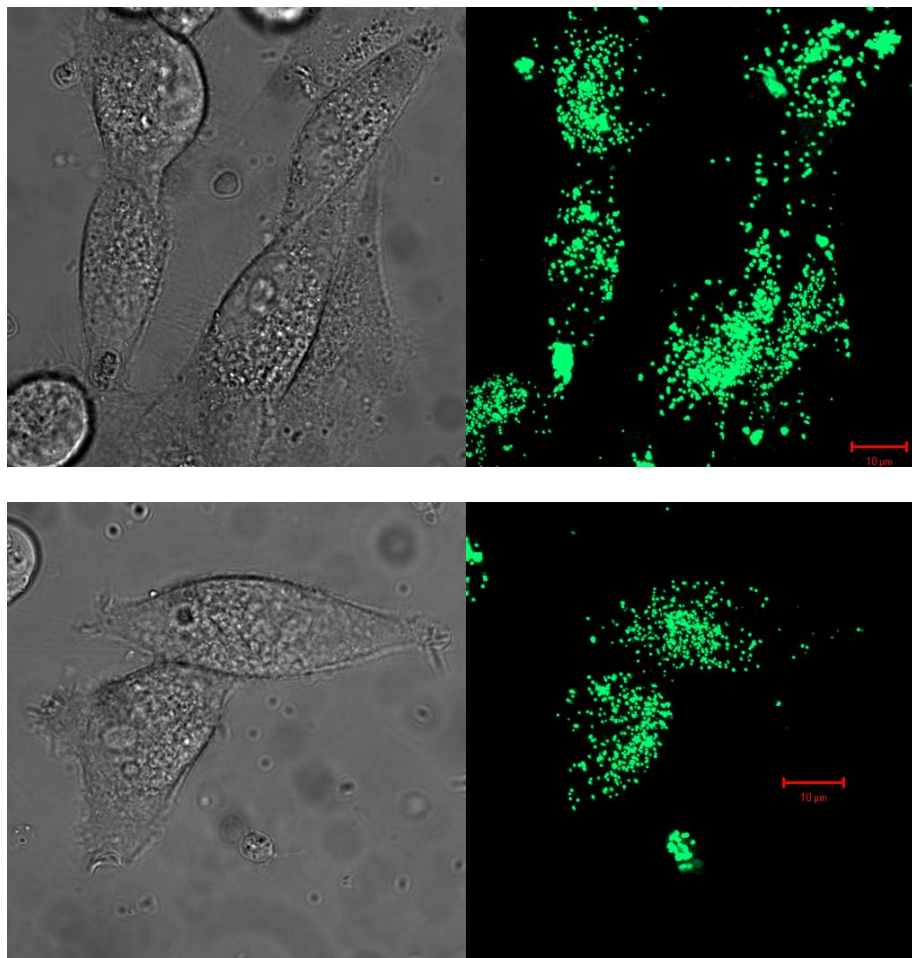


Figure 5.15 MG-63 osteoblasts incubated with **126**

## 5.7 Summary

\* Treatment of **126** with BY-2 cells indicate it is able to cross the plant cell wall.

\* After incubating cells with **143**, followed by **126**, fluorescence was still observed, suggesting that endocytosis is not the mechanism of uptake.

- \* The infiltration of **126** into *Nicotiana benthamiana* leaves transformed with the peroxisome marker PTS1-mCherry showed co-localisation thus confirming the uptake of **126** into the peroxisome.
- \* All probes tested were shown to have no perceived toxicity towards BY-2 cells.
- \* **126** is able to respond to changes in peroxisome numbers shown by prior treatment of cells with the PPAR $\alpha$ , clofibrate.
- \* When **126** was treated with H<sub>2</sub>O<sub>2</sub>,  $\cdot$ OH,  $\cdot$ OOH,  $\cdot$ OOR, <sup>1</sup>O<sub>2</sub> and O<sub>2</sub> $\cdot^-$  an increase in fluorescence was not seen.
- \* Results suggest that **126** is a better marker for peroxisomes than **153** due to the very low background fluorescence.
- \* Neither the fluorine groups, nor the B-F bond are responsible for the localisation within the peroxisomes.
- \* Pyrrole functionality can be adapted to tune the fluorescence without any effect on peroxisome localisation, leading the way for a multi colour set of peroxisome markers.
- \* Attempts to substitute the boron for zinc were unsuccessful, despite repeated attempts.
- \* It appears that **126** is able to localise with the peroxisomes of mammalian cells, but further co-localisation studies are required to prove this.

## **5.8 Conclusions**

It has been shown that the BODIPY probes **122**, **126** and **127** are able to localise exclusively within the peroxisomes of plants as established by co-localisation studies undertaken with a known peroxisomal marker. Incubation times were typically less than 10 minutes, after which time complete uptake and localisation was observed. In addition to this no perceived cytotoxic effects could be seen when BY-2 cells were incubated with **126**, even after one week. Uptake studies have indicated that



endocytosis is not the mechanism of uptake, although the exact mechanism is not known.

In an effort to ascertain the cause of localisation, several studies were performed. **126** was reacted with a wide variety of ROS including  $\text{H}_2\text{O}_2$ ,  $\cdot\text{OH}$ ,  $^1\text{O}_2$  and  $\text{O}_2^{\cdot-}$ , but no change in fluorescence was seen. Several structural modifications were done in an attempt to elucidate the part of the molecule which was responsible for the localisation. However, removal of the phenyl substituent, substitution of the fluorine atoms, extension of the pyrrole conjugation and removal of the pyrrole methyl groups did not affect the localisation in any way. Attempts to change the boron centre for zinc were unsuccessful.

Incubation of **126** was performed with the mouse fibroblast cells NIH3T3 and the human osteoblast stem cells MG63, with punctuate green fluorescence seen in these cells as well. Whilst it would seem that **126** is also localising with the peroxisome of mammalian cells, conclusive proof of this can only be given once co-localisation studies have been performed.

Due to the relative ease of synthesis of **126**, its photostability within aqueous environments, high fluorescence within cells, ease and speed of uptake in both plant and mammalian cells and the ability to produce multicoloured derivatives, it easily lends itself towards its application as a marker for peroxisomes.

## 6 CONCLUSIONS AND FUTURE WORK

### 6.1 Conclusions

Several conclusions can be drawn from this work. They include:

\* Several ester substrates based on methylumbelliferone were synthesised and screened against AtSFGH. Those derivatives which contained an amide bond were poor substrates for both AtSFGH and PLE when compared to that of the *n*-hexyl derivative, **38**. This suggests that some sort of conformational flexibility within the substrate is needed. AtSFGH activity towards a selection of these esters more closely resembled the activity seen in whole cells than that seen with PLE, which indicated that AtSFGH is a better determinant of hydrolysis of these compounds *in planta* than PLE. However, these esters did not appear to be taken up by protoplast cells. In contrast, the protoplasts readily hydrolysed FDA with the resulting fluorescence being detected on a fluorescence microscope and the MoFlo®.

\* Fluorescein esters **78 – 80** were shown to be hydrolysed by AtCXE12, both *in vitro* and *in vivo* in the order FDA > **78** > **79** ≈ **80**, with **78** and **79** identified as potential probes in directed evolution experiments. Tyrosine198 was targeted as a possible residue for mutation. This was successfully mutated into alanine by site-directed mutagenesis. When **78 – 80** were screened against the AtCXE12 Y198A mutant no activity was seen, even with FDA. Western blotting analysis revealed that the lack of activity was not due to expression problems and therefore tyrosine198 is critical for enzyme activity.

\* Error-prone PCR techniques were employed in an effort to create a recombinant library. Protocol development using the D473G polymerase revealed optimum conditions, with the mutational frequency controlled by alteration of the dNTP concentration. Efforts toward on-plate screening in *E. coli* indicated that the background activity was too high to allow any meaningful results to be gained. In order to screen directly in protoplasts, AtCXE12 was successfully cloned into the *Agrobacterium* vector BIN-STRP3. *Nicotiana benthamiana* leaves infiltrated with *Agrobacterium* containing the BIN-STRP3-AtCXE12 vector were successfully transformed. The rate of hydrolysis of pNPAc by AtCXE12-transformed leaves was 20-fold higher than the background activity. However, efforts to introduce random errors into the *atcxe12* gene contained within the BIN-STRP3 construct were unsuccessful.

\* The esterase probe **96** was successfully synthesised in a 16% yield. An increase in fluorescence was observed following chemical or enzymatic treatment, indicating that the proposed 1,6-elimination was occurring. Disappointingly, no evidence was gained for binding of **95** to PLE. **105** was synthesised in an overall 13% yield, however attempts to chemically remove the methoxy group were unsuccessful. The MOM probe **112** was synthesised and shown to breakdown upon treatment with 1 M HCl, resulting in the release of the fluorescent quencher group and a concomitant fluorescence increase.

\* The synthesis of several BODIPY probes was successfully achieved and the introduction of a nitro group resulted in complete quenching of fluorescence. When **126** was dissolved in either toluene or hexane a strong fluorescent signal was observed, suggesting that PeT is the quenching mechanism. DFT calculations were used to assess the likelihood of a BODIPY derivative displaying fluorescence. Upon incubation of **126** with *A. thaliana* protoplasts, fluorescence could be seen. However, attempts to isolate a fluorescently labelled protein were unsuccessful. A variety of enzyme inhibitors were tested in an attempt to ascertain the cause of fluorescence. However, known of the inhibitors tested affected the fluorescence of **126**. Treatment of **126** with BY-2 cells indicate that **126** is able to cross the plant cell wall. However, after incubating cells with several compounds including **143**, fluorescence was still observed, suggesting that endocytosis is not the mechanism of uptake.

\* The infiltration of **126** into *Nicotiana benthamiana* leaves transformed with the peroxisome marker PTS1-mCherry showed co-localisation thus confirming the uptake of **126** into the peroxisome. All probes tested were shown to have no perceived toxicity towards BY-2 cells. In addition, **126** is able to respond to changes in peroxisome numbers shown by prior treatment of cells with the PPAR $\alpha$ , clofibrate. Neither the fluorine groups, nor the B-F bond are responsible for the localisation within the peroxisomes. Pyrrole functionality can be adapted to tune the fluorescence without any effect on peroxisome localisation, leading the way for a multi colour set of peroxisome markers.

## **6.2 Future Work**

Future work on this project should concentrate on developing the directed evolution methodology to optimise conditions for introducing mutations. This should involve altering the primer to insert ratio, as well as the dNTP concentrations, in an effort to

produce a recombinant library within the BIN-STRP3 vector. Following this, the method should be transferred to other enzyme systems, such as cytochrome p450.

Work on the BODIPY peroxisome markers should focus on discovering the mechanism of uptake and localisation within both plant and mammalian cells. This should begin by investigating the reaction of substituting the boron centre with zinc, which should give an indication of the necessity of the BF<sub>2</sub> bridge. Further work could concentrate on developing a multicoloured set of peroxisome markers.

## **7 EXPERIMENTAL**

### **7.1 Chemistry**

#### **7.1.1 General Procedures**

All reactions were carried out under an argon atmosphere in glassware dried in an oven at 80 °C, unless otherwise stated.

#### **Solvents**

Petrol refers to the fraction of petroleum ether boiling between 40-60 °C and was redistilled before use. All solvents were distilled under a nitrogen atmosphere according to departmental procedures. In cases where mixtures of solvents were used, the ratios refer to the component volumes.

#### **Reagents**

Reagents were used as supplied unless otherwise stated.

#### **Chromatography**

Flash column chromatography was carried out using silica gel 40-63u 60A. Analytical thin layer chromatography (TLC) was performed using Merck aluminium backed silica gel 60 F<sub>254</sub> plates and visualised by UV radiation at 254 and/or 333 nm.

#### **IR Spectroscopy**

Infra-red spectra was recorded via use of a Diamond ATR (attenuated total reflection) accessory (Golden Gate) on a Perkin Elmer Paragon 1000 FT-IR spectrometer, or recorded as a solution in chloroform via transmission IR cells on a Perkin Elmer Series 1600 FT-IR spectrometer.

#### **NMR Spectroscopy**

<sup>1</sup>H NMR spectra were recorded in CDCl<sub>3</sub> on a Varian Mercury 200, Varian Unity-300, Bruker Advance 400, Varian Inova-500 or a Varian VNMRS 700 and reported as

follows; chemical shift  $\delta$  (ppm) (number of protons, multiplicity, coupling constant  $J$  (Hz), assignment). Residual protic solvent  $\text{CHCl}_3$  ( $\delta_{\text{H}} = 7.26$  ppm) was used as the internal reference.  $^{13}\text{C}$  NMR spectra were recorded at 176 MHz on a Varian VNMRS 700, 126 MHz on a Varian Inova-500 or at 101 MHz on Bruker Advance 400, using the central resonance of  $\text{CDCl}_3$  ( $\delta_{\text{C}} = 77.0$  ppm) as the internal reference.  $^{19}\text{F}$  NMR spectra were recorded at 376 MHz on Varian VXR-400 or 188 MHz on Varian Mercury 200 respectively.  $^{11}\text{B}$  NMR spectra were recorded at 128 MHz on a Bruker Advance 400. All chemical shifts are quoted in parts per million relative to the internal reference and coupling constants given in Hertz (Hz). Assignment of spectra was carried out using COSY, HSQC, HMBC and NOESY experiments.

### **Mass Spectrometry**

Electrospray mass spectra (ES) were obtained on a Micromass LCT mass spectrometer. MALDI mass spectra were obtained on an Applied Biosystems Voyager-DE STR. High resolution mass spectra were obtained using a Thermo LTQ mass spectrometer (ES) at the University of Durham.

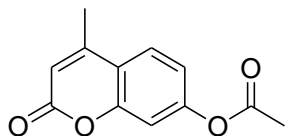
### **Photophysical Measurements**

UV-visible absorption spectra were recorded using a Biotech Instruments XS spectrometer operating with LabPower software. All samples were recorded in quartz cuvettes of 1 cm pathlength, against a reference of pure solvent contained within a matched cuvette.

Steady-state luminescence spectra were recorded using a Jobin Yvon-Spex Instrument SA Photomax II spectrometer, equipped with a Hamamatsu R928 photomultiplier tube. All samples were studied in quartz fluorescence cuvettes of 1 cm pathlength. Solutions were prepared so that the absorbance was  $\sim 0.1$  to minimise inner filter effects. Emission was detected at right angles to the excitation source, with appropriate filters used where required to remove second order peaks. All emission spectra were corrected after data acquisition for dark count and for the spectral response of the detector. Excitation spectra were automatically corrected for lamp output, through the use of a beam splitter which directed 8% of the excitation light to a reference photodiode.

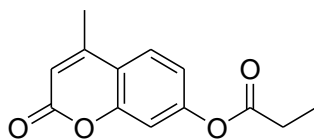
## 7.1.2 Experimental detail

### 4-methylumbelliferyl acetate, **34**



4-MU (3.79 g, 21.5 mmol), Et<sub>3</sub>N (6.01 ml, 2.0 eq) and DMAP (0.21 g, 0.1 eq) were dissolved in anhydrous DCM (55 ml), stirred and cooled to 0 °C. This was left to stir for 30 minutes. Acetyl chloride (0.45 ml, 1.8 eq) was added dropwise, upon which a cream precipitate formed with the evolution of a white gas. The resulting solution was warmed to rt and left to stir overnight. After this time the precipitate became an orange colour. The solution was taken up into water (50 ml), organic layer collected. This was repeated twice. Combined organic layers were added to aqueous saturated sodium hydrogen carbonate (50 ml) and the resulting organic layer collected. This was added to brine (50 ml), organic layer collected, dried using MgSO<sub>4</sub> and the solvent removed under reduced pressure to afford an off-white solid. Compound triturated using ether to yield **34** (0.87 g, 94%) as a white crystalline solid. **m.p.** 146 – 148 °C (Lit. 149 – 150 °C<sup>249</sup>); Found: C, 66.24 H, 4.65; Calc. for C<sub>12</sub>H<sub>10</sub>O<sub>4</sub>: C, 66.05 H, 4.62;  $\lambda_{\max}$  (DCM)/nm: 352;  $\nu_{\max}$  (ATR)/cm<sup>-1</sup>: 1742s (C=O), 1698m (lactone), 1140s, 875s;  $\delta_{\text{H}}$  (500 MHz, CDCl<sub>3</sub>): 7.61 (1H, d, <sup>3</sup>J 9, H5), 7.10 (1H, d, <sup>4</sup>J 2, H8), 7.07 (1H, dd, <sup>3</sup>J 9 and <sup>4</sup>J 2, H6), 6.27 (1H, d, <sup>4</sup>J 1, H3), 2.43 (3H, d, <sup>4</sup>J 1, C4-Me), 2.34 (3H, s, H2');  $\delta_{\text{C}}$  (100 MHz, CDCl<sub>3</sub>): 168.7 (C=O), 160.5 (C=O), 154.2 (QC), 153.1 (C7), 151.8 (QC), 125.4 (C5), 118.1 (C6), 117.9 (C4), 114.6 (C3), 110.5 (C8), 21.1 (C4-Me), 18.7 (C2'); *m/z* (ES<sup>+</sup>): 219.0 [M+H<sup>+</sup>]<sup>+</sup>

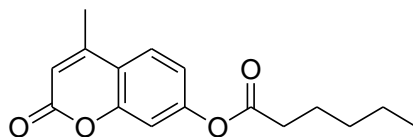
### 4-methylumbelliferyl propionate, **35**



4-MU (3.79 g, 21.5 mmol), Et<sub>3</sub>N (6.01 ml, 2.0 eq) and DMAP (0.21 g, 0.1 eq) were dissolved in anhydrous DCM (55 ml), stirred and cooled to 0 °C. This was left to stir for 30 minutes. Propionyl chloride (2.81 ml, 1.8 eq) was added dropwise, upon which a cream precipitate formed with the evolution of a white gas. The resulting solution was warmed to rt and left to stir overnight. After this time the precipitate became an orange

colour. The solution was taken up into water (50 ml), organic layer collected. This was repeated twice. Combined organic layers were added to aqueous saturated sodium hydrogen carbonate (50 ml) and the resulting organic layer collected. This was added to brine (50 ml), organic layer collected, dried using  $\text{MgSO}_4$  and the solvent removed under reduced pressure to afford an off-white solid. Compound triturated using ether to yield **35** (4.05 g, 81%) as a white crystalline solid. **m.p.** 145 - 146 °C; Found: C, 67.13 H, 5.20; Calc. for  $\text{C}_{13}\text{H}_{12}\text{O}_4$ : C, 67.23 H, 5.21;  $\nu_{\text{max}}$  (ATR)/ $\text{cm}^{-1}$ : 1744s (C=O), 1698m (lactone), 1140s;  $\delta_{\text{H}}$  (500 MHz,  $\text{CDCl}_3$ ): 7.60 (1H, d  $^3J$  8, H5), 7.11 (1H, d  $^4J$  2, H8), 7.08 (1H, dd  $^3J$  8 and  $^4J$  2, H6), 6.27 (1H, d  $^4J$  1, H3), 2.62 (2H, q  $^3J$  8, H2'), 2.43 (3H, d  $^4J$  1, C4-Me), 1.23 (3H, t  $^3J$  8, H3');  $\delta_{\text{C}}$  (125 MHz,  $\text{CDCl}_3$ ): 172.5 (C=O), 161.0 (C=O), 154.6 (QC), 153.7 (C7), 152.2 (QC), 125.6 (C5), 118.2 (C6), 118.0 (C4), 114.9 (C3), 110.8 (C8), 27.9 (C2'), 19.0 (C4-Me), 9.1 (C3');  $m/z$  (ES<sup>+</sup>): 233.1 [M+H<sup>+</sup>]<sup>+</sup>, 255.1 [M+Na<sup>+</sup>]<sup>+</sup>

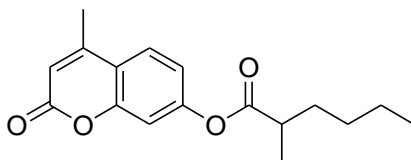
#### 4-methylumbelliferyl hexanoate, **38**



4-MU (750 mg, 4.23 mmol),  $\text{Et}_3\text{N}$  (1.19 ml, 2.0 eq) and DMAP (41.8 mg, 0.1 eq) were dissolved in anhydrous DCM (10 ml), stirred and cooled to 0 °C. This was left to stir for 30 minutes. Hexanoyl chloride (1.19 ml, 1.8 eq) was added dropwise, upon which a cream precipitate formed with the evolution of a white gas. The resulting solution was warmed to rt and left to stir for 150 minutes. The solution was taken up into water (20 ml), organic layer collected and repeated. Combined organic layers were added to aqueous saturated sodium hydrogen carbonate (20 ml) and the resulting organic layer collected. This was added to brine (20 ml), organic layer collected, dried using  $\text{MgSO}_4$  and the solvent removed under reduced pressure to afford a yellow solid. Compound triturated using ethyl acetate to yield **38** (0.71 g, 61%) as colourless crystals. **m.p.** 66 - 68 °C; Found: C, 69.80 H, 6.67; Calc. for  $\text{C}_{16}\text{H}_{18}\text{O}_4$ : C, 70.06 H, 6.61;  $\nu_{\text{max}}$  (ATR)/ $\text{cm}^{-1}$ : 3020s, 1760s (lactone), 1733 (C=O);  $\delta_{\text{H}}$  (400 MHz,  $\text{CDCl}_3$ ): 7.60 (1H, d,  $^3J$  9, H5), 7.10 (1H, d,  $^4J$  2, H8), 7.07 (1H, dd,  $^3J$  9,  $^4J$  2, H6), 6.27 (1H, d,  $^4J$  1, H3), 2.59 (2H, t,  $^3J$  7, H2'), 2.43 (3H, d,  $^4J$  1, C4-Me), 1.70 (2H, q,  $^3J$  7, H3'), 1.40 (4H, m, H4' and H5'), 0.94 (3H, t,  $^3J$  7, H6');  $\delta_{\text{C}}$  (100 MHz,  $\text{CDCl}_3$ ): 171.6 (C=O), 160.5 (C=O), 154.2 (QC), 153.2 (C7), 151.9 (QC), 125.3 (C5), 118.1 (C6), 117.7 (C4), 114.4 (C3), 110.4 (C8), 34.3 (C2'), 31.2 (C3'), 24.5 (C4'), 22.3 (C4-Me), 18.7 (C5'), 13.9 (C6');  $m/z$  (ES<sup>+</sup>): 274.9 [M+H<sup>+</sup>]<sup>+</sup>

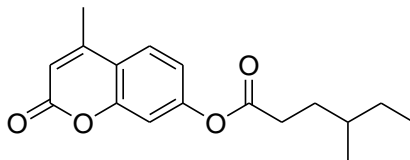


#### 4-methylumbelliferyl-(2'-methyl)hexanoate, 56



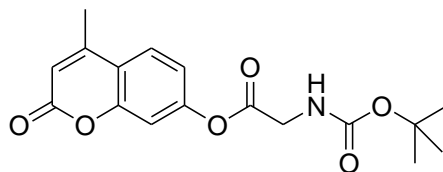
To a stirring solution of 2-methylhexanoic acid (0.13 ml, 0.92 mmol) and DMF (1 drop) in DCM (20 ml) was added oxalyl chloride (0.1 ml, 1.2 eq) dropwise, upon which a colourless gas evolved. The reaction was left stirring at rt until no further effervescence was observed. Oxalyl chloride and the solvent were removed under reduced pressure to afford a pale yellow solid. 4-MU (90.2 mg, 0.51 mmol), Et<sub>3</sub>N (0.26 ml, 2.0 eq) and DMAP (3.41 mg, 0.1 eq) were dissolved in DCM (20 ml), cooled to 0 °C and left to stir for 30 minutes. 2-methylhexanoyl chloride (1.8 eq) was re-dissolved in DCM (10 ml) and the resulting solution was added dropwise to the reaction mixture, upon which the solution changed from colourless to red, with the evolution of a white gas. The resulting solution was left to stir overnight at rt. The solution was taken up into water (20 ml), organic layer collected and repeated. Combined organic layers were added to aqueous saturated sodium hydrogen carbonate (20 ml) and the resulting organic layer collected. This was added to brine (20 ml), organic layer collected, dried using MgSO<sub>4</sub> and the solvent removed under reduced pressure to afford a yellow solid. Purified by flash column chromatography (5:95 MeOH:DCM) to yield **56** (0.23 g, 87%) as a colourless oil.  $\nu_{\max}$  (ATR)/cm<sup>-1</sup>: 3019s, 1757s (lactone), 1729m (C=O);  $\delta_{\text{H}}$  (400 MHz, CDCl<sub>3</sub>): 7.59 (1H, d <sup>3</sup>J 9, H5), 7.09 (1H, d <sup>4</sup>J 2, H8), 7.06 (1H, dd <sup>3</sup>J 9, <sup>4</sup>J 2, H6), 6.25 (1H, d <sup>4</sup>J 1, H3), 2.71 (2H, m, H2'), 2.43 (3H, d, <sup>4</sup>J 1, C4-Me), 1.82 (2H, m, H3'), 1.58 (2H, m, H4'), 1.39 (2H, m, H5'), 1.30 (3H, d <sup>3</sup>J 8, C2'-Me), 0.94 (3H, t <sup>3</sup>J 8, H6');  $\delta_{\text{C}}$  (100 MHz, CDCl<sub>3</sub>): 174.8 (C=O), 160.5 (C=O), 154.4 (QC), 153.5 (C7), 152.0 (QC), 125.4 (C5), 118.2 (C6), 117.8 (C4), 114.6 (C3), 110.5 (C8), 39.8 (C2'), 33.5 (C3'), 29.5 (C4'), 22.7 (C2'-Me), 18.8 (C4-Me), 17.0 (C5'), 14.0 (C6');  $m/z$  (ES<sup>+</sup>): 288.8 [M+H]<sup>+</sup>

#### 4-methylumbelliferyl-(4'-methyl)hexanoate, **60**



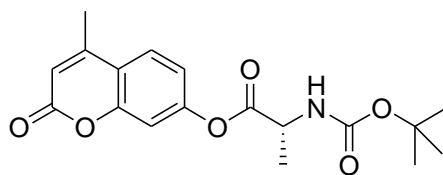
To a stirring solution of 4-methylhexanoic acid (0.13 ml, 0.92 mmol) and DMF (1 drop) in DCM (20 ml) was added oxalyl chloride (0.1 ml, 1.2 eq) dropwise, upon which a colourless gas evolved. The reaction was left stirring at rt until no further effervescence was observed. Oxalyl chloride and the solvent were removed under reduced pressure to afford a pale yellow solid. 4-MU (90.2 mg, 0.51 mmol), Et<sub>3</sub>N (0.26 ml, 2.0 eq) and DMAP (3.41 mg, 0.1 eq) were dissolved in DCM (20 ml), cooled to 0 °C and left to stir for 30 minutes. 4-methylhexanoyl chloride (1.8 eq) was re-dissolved in DCM (10 ml) and the resulting solution was added dropwise to the reaction mixture, upon which the solution changed from colourless to red, with the evolution of a white gas. The resulting solution was left to stir overnight at rt. The solution was taken up into water (20 ml), organic layer collected and repeated. Combined organic layers were added to aqueous saturated sodium hydrogen carbonate (20 ml) and the resulting organic layer collected. This was added to brine (20 ml), organic layer collected, dried using MgSO<sub>4</sub> and the solvent removed under reduced pressure to afford a yellow solid. Purified by flash column chromatography (5:95 MeOH:DCM) to afford **60** (0.19 g, 72%) as a white solid. **m.p.** 38 – 40 °C; **v**<sub>max</sub> (ATR)/cm<sup>-1</sup>: 3019s, 1759s (lactone), 1730m (C=O); **δ**<sub>H</sub> (400 MHz, CDCl<sub>3</sub>): 7.56 (1H, d <sup>3</sup>J 8, H5), 7.05 (1H, d <sup>4</sup>J 2, H8), 7.03 (1H, dd <sup>3</sup>J 8, <sup>4</sup>J 2, H6), 6.20 (1H, d <sup>4</sup>J 1, H3), 2.52 (2H, t <sup>3</sup>J 7, H2'), 2.49 – 2.63 (2H, m, H2'), 2.38 (3H, d, <sup>4</sup>J 1, C4-Me), 1.73 – 1.82 (1H, m, diastereotopic H3'), 1.50 – 1.59 (1H, m, diastereotopic H3'), 1.32 – 1.45 (2H, m, H5'), 1.15 – 1.23 (1H, m, H4'), 0.85 – 0.91 (6H, m, H6' and C4'-Me); **δ**<sub>C</sub> (100 MHz, CDCl<sub>3</sub>): 171.8 (C=O), 160.4 (C=O), 154.1 (QC), 153.2 (C7), 151.9 (QC), 125.4 (C5), 118.1 (C6), 117.7 (C4), 114.4 (C3), 110.3 (C8), 34.0 (C2'), 32.2 (C3'), 31.3 (C4'), 29.1 (C5'), 18.8 (C4-Me), 18.6 (C4'-Me), 11.3 (C6'); **m/z** (ES<sup>+</sup>): 289.2 [M+H]<sup>+</sup>

#### 4-methylumbelliferyl -N-Boc glycine, **61**



4-MU (2.61 g, 14.8 mmol) and Boc-Gly-OH (3.38 g, 1.3 eq) were dissolved in anhydrous DCM (60 ml). DMAP (1.12 g, 1.0 eq) and EDCI (2.84 g, 1.3 eq) were added to the reaction mixture and left to stir overnight. The solution was diluted with DCM (50 ml) and added to aqueous saturated sodium hydrogen carbonate (50 ml) and the organic layer collected. This was repeated twice and the organic layers were combined. These were added to brine (50 ml), dried with MgSO<sub>4</sub> and the solvent removed under reduced pressure to afford a yellow-white solid. Recrystallised from hot EtOAc to afford **61** (2.55 g, 70%) as a white crystalline solid. **m.p.** 120 - 124 °C;  $\delta_{\text{H}}$  (400 MHz, CDCl<sub>3</sub>): 7.61 (1H, d <sup>3</sup>J 9, H5), 7.13 (1H, d <sup>4</sup>J 2, H8), 7.10 (1H, dd <sup>3</sup>J 9 and <sup>4</sup>J 2, H6), 6.28 (1H, d <sup>4</sup>J 1, H3), 5.08 (1H, br s, NH), 4.20 (2H, d <sup>3</sup>J 6, H2'), 2.43 (3H, d <sup>3</sup>J 1, C4-Me), 1.48 (9H, s, BocH);  $\delta_{\text{C}}$  (125 MHz, CDCl<sub>3</sub>): 168.7 (C=O), 160.5 (C=O), 155.8 (C=O), 154.3 (QC), 152.7 (C7), 151.9 (QC), 125.6 (C5), 118.2 (C6), 117.9 (C4), 114.8 (C3), 110.4 (C8), 42.7 (QC), 31.1 (C2'), 28.4 (tBu), 18.9 (C4-Me); *m/z* (ES<sup>+</sup>): 334.2 [M+H<sup>+</sup>]<sup>+</sup>

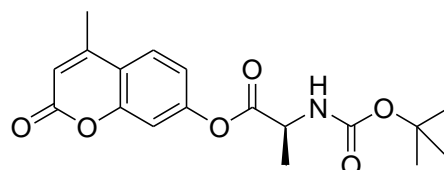
#### 4-methylumbelliferyl -N-Boc-L-Alanine, **62**



4-MU (2.61 g, 14.8 mmol) and Boc-Ala-OH (3.64 g, 1.3 eq) were dissolved in anhydrous DCM (60 ml). DMAP (1.12 g, 1.0 eq) and EDCI (2.84 g, 1.3 eq) were added to the reaction mixture and left to stir overnight. The solution was diluted with DCM (50 ml) and added to aqueous saturated sodium hydrogen carbonate (50 ml) and the organic layer collected. This was repeated twice and the organic layers were combined. These were added to brine (50 ml), dried with MgSO<sub>4</sub> and the solvent removed under reduced pressure to afford a yellow-white solid. Recrystallised from hot EtOAc to afford **62** (1.29 g, 25%) a white crystalline solid. **m.p.** 106 - 109 °C;  $\delta_{\text{H}}$  (400 MHz, CDCl<sub>3</sub>): 7.34 (1H, d <sup>3</sup>J 8, H5), 6.74 (1H, dd <sup>3</sup>J 8 and <sup>4</sup>J 2, H6), 6.70 (1H, d <sup>4</sup>J 2, H8), 6.20 (1H, d <sup>4</sup>J 1, H3), 5.08

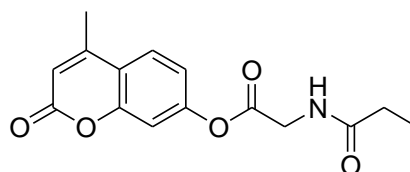
(1H, br s, NH), 4.51 (1H, br s, H2'), 2.36 (3H, d  $^3J$  1, C4-Me), 1.50 (3H, d  $^3J$  7, C2'-Me), 1.40 (9H, s, BocH);  $\delta_c$  (100 MHz, CDCl<sub>3</sub>): 160.5 (C=O), 157.1 (C=O), 154.1 (QC), 153.2 (C7), 152.0 (QC), 125.6 (C5), 118.2 (C6), 118.0 (C4), 114.8 (C3), 110.4 (C8), 42.4 (QC), 28.5 (<sup>t</sup>Bu), 23.6 (C2'), 18.8 (C4-Me), 18.3 (C2'-Me);  $m/z$  (ES<sup>+</sup>): 348.6 [M+H<sup>+</sup>]<sup>+</sup>

#### 4-methylumbelliferyl -N-Boc-D-Alanine, 63



4-MU (2.61 g, 14.8 mmol) and Boc-D-Ala-OH (3.64 g, 1.3 eq) were dissolved in anhydrous DCM (60 ml). DMAP (1.12 g, 1.0 eq) and EDCI (2.84 g, 1.3 eq) were added to the reaction mixture and left to stir overnight. The solution was diluted with DCM (50 ml) and added to aqueous saturated sodium hydrogen carbonate (50 ml) and the organic layer collected. This was repeated twice and the organic layers were combined. These were added to brine (50 ml), dried with MgSO<sub>4</sub> and the solvent removed under reduced pressure to afford a yellow-white solid. Purified by flash column chromatography (5% MeOH:DCM) to afford **63** (1.31 g, 25%) as a white crystalline solid. **m.p.** 105 - 107 °C;  $\delta_H$  (400 MHz, CDCl<sub>3</sub>): 7.34 (1H, d  $^3J$  8, H5), 6.74 (1H, dd  $^3J$  8 and  $^4J$  2, H6), 6.70 (1H, d  $^4J$  2, H8), 6.20 (1H, d  $^4J$  1, H3), 5.08 (1H, br s, NH), 4.51 (1H, br s, H2'), 2.36 (3H, d  $^3J$  1, C4-Me), 1.50 (3H, d  $^3J$  7, C2'-Me), 1.40 (9H, s, BocH);  $\delta_c$  (100 MHz, CDCl<sub>3</sub>): 160.5 (C=O), 157.1 (C=O), 154.1 (QC), 153.2 (C7), 152.0 (QC), 125.6 (C5), 118.2 (C6), 118.0 (C4), 114.8 (C3), 110.4 (C8), 42.4 (QC), 28.5 (<sup>t</sup>Bu), 18.8 (C4-Me), 18.3 (C2'-Me);  $m/z$  (ES<sup>+</sup>): 348.5 [M+H<sup>+</sup>]<sup>+</sup>

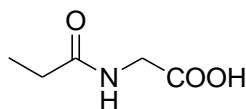
#### 4-methylumbelliferyl-N-propionyl glycine, 65



4-MU (168 mg, 0.95 mmol), EDCI (201 mg, 1.1 eq) and DMAP (9 mg, 0.1 eq) were dissolved in dry DCM (20 ml). This was left to stir for 10 minutes. To this a solution of **69** in dry DCM (5 ml) was added and the resulting solution left to stir overnight. The

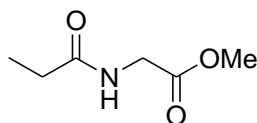
solution was taken up into saturated sodium hydrogen carbonate (2 x 30 ml) and the organic layer collected. Brine (20 ml) was added and the organic layer collected, dried with MgSO<sub>4</sub> and the solvent removed under reduced pressure to yield an off-white solid. This was washed with EtOAc which gave **65** (231 mg, 84%) as a white solid. **m.p.** 164 - 166 °C;  $\delta_{\text{H}}$  (400 MHz, CDCl<sub>3</sub>): 7.62 (1H, d <sup>3</sup>J 9, H5), 7.15 (1H, d <sup>4</sup>J 2, H8), 7.10 (1H, dd <sup>3</sup>J 9 and <sup>4</sup>J 2, H6), 6.28 (1H, d <sup>4</sup>J 1, H3), 6.01 (1H, br s, NH), 4.34 (2H, d <sup>3</sup>J 6, H2'), 2.44 (3H, d <sup>4</sup>J 1, C4-Me), 2.33 (2H, q <sup>3</sup>J 8, H5'), 1.21 (3H, t <sup>3</sup>J 8, H6');  $\delta_{\text{C}}$  (100 MHz, CDCl<sub>3</sub>): 174.6 (C=O), 168.5 (C=O), 160.6 (C=O), 154.3 (QC), 152.8 (C7), 152.2 (QC), 125.8 (C5), 118.3 (C6), 118.0 (C4), 114.9 (C3), 110.4 (C8), 41.7 (C2'), 29.5 (C4-Me), 18.9 (C5'), 9.8 (C6');  $m/z$  (ES<sup>+</sup>): 312.08416 ([M+Na]<sup>+</sup>, C<sub>15</sub>H<sub>15</sub>NO<sub>5</sub>Na requires 312.08424); 601.1790 ([2M+Na]<sup>+</sup>, C<sub>30</sub>H<sub>30</sub>N<sub>2</sub>O<sub>15</sub>Na requires 601.1792)

### N-propionyl glycine, **66**<sup>99</sup>



Glycine (320 mg, 4.26 mmol) was dissolved in saturated sodium hydrogen carbonate (10 ml). Propionic anhydride was added and the resulting solution stirred at reflux for 6 hours. Solution was acidified to pH 1 with HCl (5 M). The aqueous layer was washed 3 times with EtOAc (20 ml) and the organic layers collected. The combined organic layers were dried with MgSO<sub>4</sub> and the solvent removed under reduced pressure to yield **66** (334 mg, 60%) as a white solid, which was used without further purification. **m.p.** 126 °C (lit. 128 °C);  $\nu_{\text{max}}$  (ATR)/cm<sup>-1</sup>: 1715 (s);  $\delta_{\text{H}}$  (500 MHz, CDCl<sub>3</sub>): 6.43 (1H, br s, NH), 3.92 (2H, d <sup>3</sup>J 5, H $\alpha$ ), 2.20 (2H, q <sup>3</sup>J 8, H2'), 1.09 (3H, t <sup>3</sup>J 8, H3');  $\delta_{\text{C}}$  (125 MHz, CDCl<sub>3</sub>): 174.0 (C=O), 171.8 (C=O), 41.2 (C $\alpha$ ), 29.2 (C2'), 9.6 (C3');  $m/z$  (ES<sup>-</sup>): 130.0509 ([M-H]<sup>-</sup>, C<sub>5</sub>H<sub>8</sub>O<sub>3</sub> requires 130.0510)

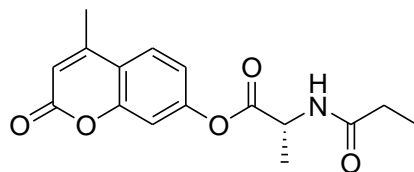
### N-propionyl-O-methoxy glycine, **68**



Glycine methyl ester (200 mg, 1.59 mmol), was dissolved in dry DMF (15 ml). Et<sub>3</sub>N (0.23 ml, 2.0 eq) and DMAP (16 mg, 0.1 eq) were added and the reaction allowed to stir for 20

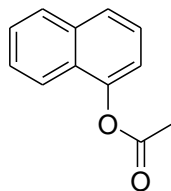
minutes. The reaction was cooled to 0 °C and propionyl chloride (0.21 ml, 1.5 eq) was added dropwise. The resulting solution was warmed to rt and left stirring overnight. The solution was diluted with EtOAc (30 ml) and added to aqueous saturated sodium hydrogen carbonate (30 ml) and the organic layer collected. This was repeated twice and the organic layers were combined. These were added to brine (30 ml), dried with MgSO<sub>4</sub> and the solvent removed under reduced pressure to afford **68** (55 mg, 13%) as a white solid, which was used without further purification. **m.p.** 37 - 38 °C;  **$\nu_{\max}$**  (ATR)/cm<sup>-1</sup>: 1736 (s);  **$\delta_{\text{H}}$**  (400 MHz, CDCl<sub>3</sub>): 6.19 (1H, br s, NH), 4.05 (2H, d <sup>3</sup>J 5, H<sub>α</sub>), 3.76 (3H, s, OMe), 2.29 (2H, q <sup>3</sup>J 8, H<sub>2</sub>'), 1.18 (3H, t <sup>3</sup>J 8, H<sub>3</sub>');  **$\delta_{\text{C}}$**  (125 MHz, CDCl<sub>3</sub>): 174.9 (C=O), 170.0 (C=O), 39.9 (C<sub>α</sub>), 29.3 (C<sub>2</sub>'), 21.3 (Me), 9.63 (C<sub>3</sub>');  **$m/z$**  (ES<sup>+</sup>): 146.1 [M<sup>+</sup>]

#### 4-methylumbelliferyl-N-propionyl alanine, **69**



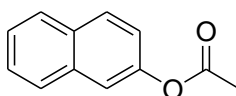
**62** (150 mg, 0.45 mmol) was dissolved in dry DCM (2 ml) and TFA (2 ml) was added. This was left to stir for 30 minutes and after this time the solvents were removed under reduced pressure to yield a colourless oil. This was redissolved in dry DCM (2 ml) and DIPEA (0.09 ml, 1.0 eq) was added. The resulting solution was left to stir for 30 minutes. DIC (0.08 ml, 1.1 eq), DMAP (4 mg, 0.1 eq) and propionic acid (0.03 ml, 1.0 eq) were added and the solution was left to stir overnight. The solution was taken up into water (2 x 20 ml) and the organic layer was collected. The combined organic layers were washed with saturated sodium hydrogen carbonate (20 ml), brine (20 ml) and dried using MgSO<sub>4</sub>. The solvent was removed under reduced pressure to yield a white solid. Purified by flash column chromatography (45% EtOAc:petroleum ether) to yield **69** (40 mg, 29%) as a white solid. **m.p.** 123 - 125 °C;  **$\delta_{\text{H}}$**  (400 MHz, CDCl<sub>3</sub>): 7.61 (1H, d <sup>3</sup>J 8, H<sub>5</sub>), 7.13 (1H, d <sup>4</sup>J 2, H<sub>8</sub>), 7.09 (1H, dd <sup>3</sup>J 8 and <sup>4</sup>J 2, H<sub>6</sub>), 6.28 (1H, d <sup>4</sup>J 1, H<sub>3</sub>), 5.94 (1H, br s, NH), 4.84 (1H, quint <sup>3</sup>J 8 H<sub>2</sub>'), 2.44 (3H, d <sup>4</sup>J 1, C<sub>4</sub>-Me), 2.29 (2H, q <sup>3</sup>J 8, H<sub>5</sub>'), 1.60 (3H, d <sup>3</sup>J 8, C<sub>2</sub>'-Me), 1.20 (3H, t <sup>3</sup>J 8, H<sub>6</sub>');  **$\delta_{\text{C}}$**  (100 MHz, CDCl<sub>3</sub>): 174.8 (C=O), 168.9 (C=O), 160.7 (C=O), 154.3 (QC), 152.7 (C<sub>7</sub>), 152.2 (QC), 125.9 (C<sub>5</sub>), 118.3 (C<sub>6</sub>), 118.0 (C<sub>4</sub>), 114.9 (C<sub>3</sub>), 110.2 (C<sub>8</sub>), 40.8 (C<sub>2</sub>'), 29.7 (C<sub>4</sub>-Me), 18.9 (C<sub>5</sub>'), 18.4 (C<sub>2</sub>'-Me), 9.9 (C<sub>6</sub>');  **$m/z$**  (ES<sup>+</sup>): 303.6 [M<sup>+</sup>]

### 1-naphthyl acetate, 73



1-naphthol (300 mg, 2.08 mmol), Et<sub>3</sub>N (0.58 ml, 2.0 eq) and DMAP (20 mg, 0.1 eq) were dissolved in dry DCM (5 ml) and cooled to 0°C. The solution was left to stir for 20 minutes. Acetyl chloride (0.27 ml, 1.8 eq) was added dropwise upon which an orange precipitate formed. This was warmed to rt and left to stir for 3 hours, after which time the reaction mixture had become a dark orange colour. The solution was added to saturated sodium hydrogen carbonate (2 x 30 ml) and the organic layers were collected and combined. To these were added brine (30 ml) and the organic layer dried using MgSO<sub>4</sub>. The solvent was removed under reduced pressure to yield **73** (248 mg, 64%) as a dark orange oil.  $\nu_{\max}$  (ATR)/cm<sup>-1</sup>: 1754 (s) C=O;  $\lambda_{\max}$  (DCM)/nm:  $\lambda_{\text{ex}}$  277,  $\lambda_{\text{em}}$  345;  $\delta_{\text{H}}$  (500 MHz, CDCl<sub>3</sub>): 7.86 – 7.88 (2H, m, H7 and H8), 7.74 (1H, d <sup>3</sup>J 8, H2), 7.44 – 7.53 (3H, m, H3, H4 and H6), 7.25 (1H, d <sup>3</sup>J 8, H5), 2.45 (3H, s, CH<sub>3</sub>);  $\delta_{\text{C}}$  (125 MHz, CDCl<sub>3</sub>): 169.6 (C=O), 146.8 (C1), 134.8 (QC), 128.2 (C7), 127.0 (C4), 126.6 (C6), 126.2 (C2), 125.5 (C3), 121.3 (C8), 118.2 (C5), 21.1 (Me);  $m/z$  (ES<sup>+</sup>): 187.1 [M+H]<sup>+</sup>

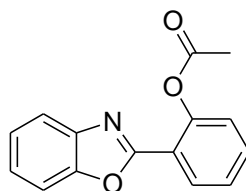
### 2-naphthyl acetate, 74



2-naphthol (300 mg, 2.08 mmol), Et<sub>3</sub>N (0.58 ml, 2.0 eq) and DMAP (20.4 mg, 0.1 eq) were dissolved in dry DCM (5 ml) and cooled to 0°C. The solution was left to stir for 20 minutes. Acetyl chloride (0.27 ml, 1.8 eq) was added dropwise upon which an orange precipitate formed. This was warmed to rt and left to stir for 3 hours, after which time the reaction mixture had become a dark orange colour. The solution was added to saturated sodium hydrogen carbonate (2 x 30 ml) and the organic layers were collected and combined. To these were added brine (30 ml) and the organic layer dried using MgSO<sub>4</sub>. The solvent was removed under reduced pressure to yield a dark orange oil. The oil was triturated using EtOAc/Petroleum ether (60:40) to yield **74** (337 mg, 87%) as an off white solid. **m.p.** 64 – 66 °C;  $\nu_{\max}$  (ATR)/cm<sup>-1</sup>: 1752 (s) C=O;  $\lambda_{\max}$  (DCM)/nm:  $\lambda_{\text{ex}}$

275,  $\lambda_{em}$  340;  $\delta_H$  (500 MHz,  $CDCl_3$ ): 7.80 - 7.87 (3H, m, H4, H7 and H8), 7.56 (1H, d  $^4J$  2, H1), 7.44 - 7.52 (2H, m, H5 and H6), 7.24 (1H, dd  $^3J$  8 and  $^4J$  2, H3), 2.36 (3H, s, Me);  $\delta_C$  (126 MHz,  $CDCl_3$ ): 169.8 (C=O), 148.5 (C2), 133.9 (QC), 131.6 (QC), 129.5 (C4), 127.9 and 127.8 (C7 and C8), 126.7 (C5), 125.8 (C6), 121.3 (C3), 118.7 (C1), 21.3 (Me);  $m/z$  (ES<sup>+</sup>): 186.2 [M<sup>+</sup>]

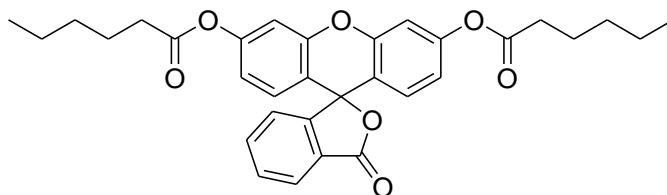
**2-(2-hydroxyphenyl)benzoxazole acetate, 75<sup>250</sup>**



2-(2-hydroxyphenyl)benzoxazole (300 mg, 1.42 mmol),  $Et_3N$  (0.28 ml, 2.0 eq) and DMAP (14 mg, 0.1 eq) were dissolved in dry DCM (5 ml) and cooled to 0°C. The solution was left to stir for 20 minutes. Acetyl chloride (0.18 ml, 1.8 eq) was added dropwise upon which an orange precipitate formed. This was warmed to rt and left to stir for 3 hours, after which time the reaction mixture had become a dark orange colour. The solution was added to saturated sodium hydrogen carbonate (2 x 30 ml) and the organic layers were collected and combined. To these were added brine (30 ml) and the organic layer dried using  $MgSO_4$ . The solvent was removed under reduced pressure to yield a dark orange oil. The oil was triturated using EtOAc/Petroleum ether (60:40) to yield **75** (359 mg, 99%) as an off white solid. **m.p.** 70 - 72 °C (Lit. value 72 °C);  $\nu_{max}$  (ATR)/ $cm^{-1}$ : 1752 (s) C=O, 1640 C=N;  $\lambda_{max}$  (DCM)/nm: 320;  $\delta_H$  (500 MHz,  $CDCl_3$ ): 8.30 (1H, dd  $^3J$  8 and  $^4J$  1, H3'), 7.73 - 7.78 (1H, m, H4), 7.54 - 7.59 (2H, m, H6 and H5'), 7.43 (1H, td  $^3J$  8 and  $^4J$  1, H4'), 7.33 - 7.40 (2H, m, H5 and H7), 7.25 (1H, dd  $^3J$  8 and  $^4J$  1, H6'), 2.49 (3H, s, CH<sub>3</sub>);  $\delta_C$  (125 MHz,  $CDCl_3$ ): 170.0 (C=O), 159.9 (C2'), 150.3 (C2), 149.4 (C1'), 142.1 (QC), 132.5 (C5'), 130.4 (C3'), 126.6 (C4'), 125.5 and 124.7 (C5 and C7), 124.2 (C6'), 120.6 (QC), 120.5 (C4), 110.6 (C6), 21.4 (Me);  $m/z$  (ES<sup>+</sup>): 254.1 [M+H]<sup>+</sup>

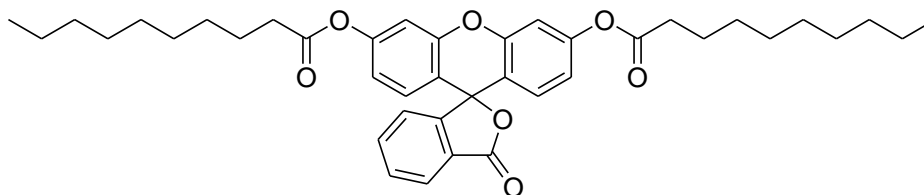


### Fluorescein dihexanoate, **78**



To a solution of fluorescein (300 mg, 0.90 mmol) in pyridine (5 ml) was added hexanoyl chloride (0.63 ml, 5.0 eq). A red-orange precipitate formed and this was stirred for 4 hours. The suspension was poured onto ice and the resulting orange precipitate was taken up into chloroform. The solvent was removed under reduced pressure to yield a deep orange oil. Flash column chromatography (25% EtOAc:Petroleum ether) gave **78** (320 mg, 67%) as a pale yellow oil.  $\lambda_{\text{max}}$  (DCM)/ $\text{cm}^{-1}$ :  $\lambda_{\text{ex}}$  490,  $\lambda_{\text{em}}$  520;  $\nu_{\text{max}}$  (ATR)/ $\text{cm}^{-1}$ : 1611 (s), 1767 (s), 2959 (m);  $\delta_{\text{H}}$  (400 MHz,  $\text{CDCl}_3$ ): 8.03 (1H, d  $^3J$  7, H9), 7.61 – 7.70 (2H, m, H10 and H11), 7.18 (1H, d  $^3J$  7, H12), 7.08 (2H, d  $^4J$  2, H4 and H5), 6.78 – 6.83 (4H, m, H1, H2, H7 and H8), 2.56 (4H, t  $^3J$  8, H2'), 1.72 – 1.79 (4H, m, H3'), 1.37 – 1.41 (8H, m, H4' and H5'), 0.91 – 0.95 (6H, t  $^3J$  8, H6');  $\delta_{\text{C}}$  (126 MHz,  $\text{CDCl}_3$ ): 171.9 (C=O), 169.3 (C=O), 153.1 (C9a), 152.3 (C3 and C6), 151.7 (C4a and C5a), 135.4 (C11), 130.2 (C10), 129.1 (C1 and C8), 126.2 (C12a), 125.3 (C9), 124.2 (C12), 117.9 (C2 and C7), 116.4 (C1a and C8a), 110.5 (C4 and C5), 81.9 (spiroC), 34.5 (C2'), 29.5 ( $\text{sp}^3\text{C}$ ), 29.4 ( $\text{sp}^3\text{C}$ ), 29.2 ( $\text{sp}^3\text{C}$ ), 25.0 (C3');  $m/z$  (ES<sup>+</sup>): 529.2 [M+H]<sup>+</sup>

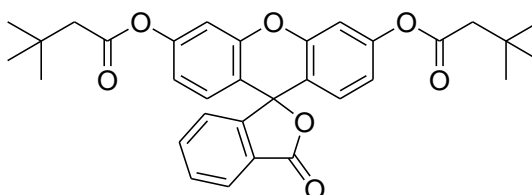
### Fluorescein didecanoate, **79**



To a solution of fluorescein (300 mg, 0.90 mmol) in pyridine (5 ml) was added decanoyl chloride (0.94 ml, 5.0 eq). An orange precipitate formed and this was stirred for 4 hours. The suspension was poured onto ice and the resulting orange precipitate was taken up into chloroform. The solvent was removed under reduced pressure to yield an orange oil. Flash column chromatography, gradient elution (25% EtOAc/petroleum ether to 100% EtOAc) gave **79** (431 mg, 75%) as a pale yellow oil.  $\nu_{\text{max}}$  (ATR)/ $\text{cm}^{-1}$ : 1611 (s), 1767 (s), 2959 (m);  $\delta_{\text{H}}$  (500 MHz,  $\text{CDCl}_3$ ): 8.03 (1H, d  $^3J$  8, H9), 7.62 – 7.70 (2H, m, H10 and

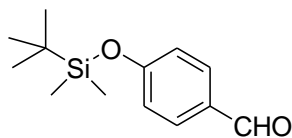
H11), 7.18 (1H, d <sup>3</sup>J 8, H12), 7.08 (2H, d <sup>4</sup>J 2, H4 and H5), 6.78 – 6.84 (4H, m, H1, H2, H7 and H8), 2.56 (4H, t <sup>3</sup>J 8, H2'), 1.74 (4H, quin <sup>3</sup>J 8, H3'), 1.27 – 1.42 (28H, m, H4' – H9'), 0.88 (6H, t <sup>3</sup>J 8, H10');  $\delta_{\text{C}}$  (126 MHz, CDCl<sub>3</sub>): 171.9 (C1'), 169.3 (C=O), 153.1 (C9a), 152.3 (C3 and C6), 151.7 (C4a and C5a), 135.4 (C11), 130.2 (C10), 129.1 (C1 and C8), 126.2 (C12a), 125.3 (C9), 124.2 (C12), 117.9 (C2 and C7), 116.4 (C1a and C8a), 110.5 (C4 and C5), 81.9 (spiroC), 34.5 (C2'), 32.0 (C8'), 29.5 (sp<sup>3</sup>C), 29.4 (sp<sup>3</sup>C), 29.4 (sp<sup>3</sup>C), 29.2 (sp<sup>3</sup>C), 25.0 (C3'), 22.8 (C9'), 14.2 (C10');  $m/z$  (ES<sup>+</sup>): 641.3 [M+H]<sup>+</sup>

### Fluorescein di(3,3-dimethyl)butanoate, **80**



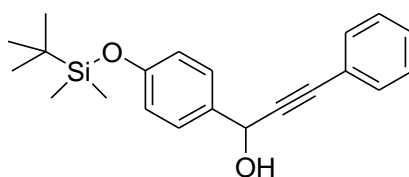
To a solution of fluorescein (300 mg, 0.90 mmol) in pyridine (5 ml) was added 3,3-dimethylbutanoyl chloride (0.63 ml, 5.0 eq). An orange precipitate formed and this was stirred for 4 hours. The suspension was poured onto ice and the resulting orange precipitate was taken up into chloroform. The solvent was removed under reduced pressure to yield an orange oil. Flash column chromatography, gradient elution (25% EtOAc/petroleum ether to 100% EtOAc) gave **80** (370 mg, 78%) as a yellow oil.  $\nu_{\text{max}}$  (ATR)/cm<sup>-1</sup>: 1611 (s), 1767 (s), 2959 (m);  $\delta_{\text{H}}$  (500 MHz, CDCl<sub>3</sub>): 8.03 (1H, d <sup>3</sup>J 8, H9), 7.61 – 7.69 (2H, m, H10 and H11), 7.17 (1H, d <sup>3</sup>J 8, H12), 7.07 (2H, d <sup>4</sup>J 2, H4 and H5), 6.78 – 6.84 (4H, m, H1, H2, H7 and H8), 2.44 (4H, s, H2'), 1.12 (18H, s, *t*Bu);  $\delta_{\text{C}}$  (126 MHz, CDCl<sub>3</sub>): 170.3 (C1'), 169.3 (C=O), 153.1 (C9a), 152.1 (C3 and C6), 151.6 (C4a and C5a), 135.4 (C11), 130.1 (C10), 129.0 (C1 and C8), 126.2 (C12a), 125.3 (C9), 124.2 (C12), 118.0 (C2 and C7), 116.4 (C1a and C8a), 110.5 (C4 and C5), 81.8 (spiroC), 47.8 (C2'), 31.3 (C3'), 29.7 (*t*Bu);  $m/z$  (ES<sup>+</sup>): 529.3 (94%) [M+H]<sup>+</sup>, 551.3 (100) [M+Na]<sup>+</sup>

#### 4-(*tert*-butyldimethylsilyloxy)benzaldehyde, **89**



To a solution of 4-hydroxybenzaldehyde (500 mg, 4.10 mmol) in DCM (10 ml) at 0 °C was added DMAP (50 mg, 0.1 eq), Et<sub>3</sub>N (0.68 ml, 1.2 eq) and TBDMSCl (649 mg, 1.05 eq). The resulting solution was allowed to warm to rt and stirred for 2 hours. Saturated aqueous sodium hydrogen carbonate (20 ml) was added, followed by brine (20 ml). The aqueous layer was separated and extracted with DCM (3 x 20 ml). The combined organic extracts were dried over MgSO<sub>4</sub>, filtered and concentrated under reduced pressure to yield a yellow oil. Flash column chromatography (30% EtOAc:Petroleum ether) gave **89** (600 mg, 65%) as a very pale yellow oil.  $\nu_{\max}$  (ATR)/cm<sup>-1</sup>: 1722 (s) C=O, 1252 (s) Si-C;  $\delta_{\text{H}}$  (500 MHz, CDCl<sub>3</sub>): 9.86 (1H, s, CHO), 7.76 (2H, m, AA' part of the AA'XX' system, H2 and H6), 6.92 (2H, m, XX' part of the AA'XX' system, H3 and H5), 0.97 (9H, s, *t*Bu), 0.22 (6H, s, 2 x Me);  $\delta_{\text{C}}$  (126 MHz, CDCl<sub>3</sub>): 190.9 (C=O), 161.6 (C1), 132.0 (C2 and C6), 130.5 (C4), 120.5 (C3 and C5), 25.6 (*t*Bu), 18.3 (QC), -4.3 (Me);  $m/z$  (ES<sup>+</sup>): 237.1304 ([M+H]<sup>+</sup>, C<sub>13</sub>H<sub>21</sub>O<sub>2</sub>Si requires 237.1305).

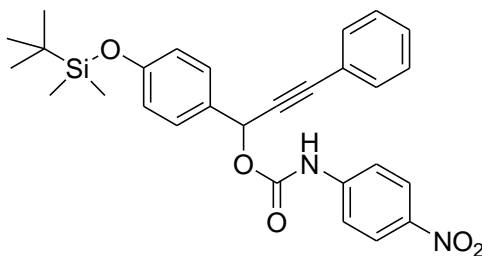
#### 1-(4-(*tert*-butyldimethylsilyloxy)phenyl)-3-phenylprop-2-yn-1-ol, **90**



*n*-Butyllithium (1.6 M solution in hexane, 0.79 ml, 1.27 mmol) was added to a stirred solution of phenylacetylene (0.13 ml, 1.17 mmol) in THF (5 ml) at -78 °C. The resulting solution was left to stir for 15 minutes. **89** (250 mg, 1.06 mmol) was added and was allowed to warm to rt. This was left to stir for 1 hour. Saturated ammonium chloride solution (20 ml) was added. The aqueous layer was separated and extracted with ether (2 x 20 ml). The combined organic extracts were dried over MgSO<sub>4</sub>, filtered and concentrated under reduced pressure to yield a yellow oil. Flash column chromatography, gradient elution (100% petroleum ether to 100% EtOAc) gave **90** (57 mg, 16%) as a pale yellow oil.  $\nu_{\max}$  (ATR)/cm<sup>-1</sup>: 3310 (alkyne C-H), 2194 (C≡C), 1250 (s) Si-C;  $\delta_{\text{H}}$  (500 MHz, CDCl<sub>3</sub>): 7.47 - 7.49 (4H, m, H2, H6 and ArH), 7.32 - 7.33 (3H, m,

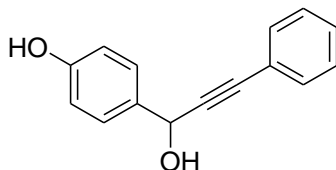
ArH), 6.86 (2H, m, AA' part of the AA'XX' system, H3 and H5), 5.62 (1H, d <sup>3</sup>J 7, H1'), 2.24 (1H, d <sup>3</sup>J 7, OH), 0.99 (9H, s, *t*Bu), 0.21 (6H, s, 2 x Me);  $\delta_c$  (126 MHz, CDCl<sub>3</sub>): 156.1 (C1), 133.6 (ArC), 131.8 (C2 and C6), 128.7 (ArC), 128.4 (C4), 128.3 (ArC), 122.6 (C4'), 120.3 (C3 and C5), 89.0 (C2'), 86.6 (C3'), 64.9 (C1'), 25.8 (*t*Bu), 18.4 (QC), -4.3 (Me);  $m/z$  (ES<sup>+</sup>): 321.1669 ([M-OH<sub>2</sub>]<sup>+</sup>, C<sub>21</sub>H<sub>25</sub>OSi requires 321.1669).

**1-(4-(*tert*-butyldimethylsilyloxy)phenyl)-3-phenylprop-2-ynyl 4-nitrophenylcarbamate, 91**



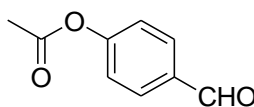
To a solution of **89** (50 mg, 0.15 mmol) in DCM (1 ml) was added Et<sub>3</sub>N (2  $\mu$ L, 0.1 eq) and the mixture was allowed to stir for 15 mins. *p*-Nitrophenylisocyanate (26 mg, 1.1 eq) was added and the reaction was allowed to stir for 1 hour. Saturated ammonium chloride solution (10 ml) was added. The aqueous layer was separated and extracted with DCM (2 x 20 ml). The combined organic extracts were dried over MgSO<sub>4</sub>, filtered and concentrated under reduced pressure to yield a yellow oil. Flash column chromatography (3:1 DCM: Petroleum ether) gave **91** (26 mg, 35%) as a dark yellow oil.  $\lambda_{max}$  (DCM)/nm: 371;  $\delta_H$  (500 MHz, CDCl<sub>3</sub>): 8.12 - 8.15 (2H, m, A<sub>1</sub>A<sub>1</sub>' part of the A<sub>1</sub>A<sub>1</sub>'X<sub>1</sub>X<sub>1</sub>' system, H3'' and H5''), 7.48 - 7.50 (2H, m, AA' part of the AA'XX' system, H2 and H6), 7.40 - 7.44 (2H, m, ArH), 7.38 - 7.44 (3H, m, ArH), 6.88 - 6.90 (2H, m, XX' part of the AA'XX' system, H3 and H5), 6.73 - 6.75 (2H, m, X<sub>1</sub>X<sub>1</sub>' part of the A<sub>1</sub>A<sub>1</sub>'X<sub>1</sub>X<sub>1</sub>' system, H2'' and H6''), 5.52 (1H, d <sup>5</sup>J 0.5, H1'), 4.83 (1H, br s, NH), 0.99 (9H, s, *t*Bu), 0.22 (6H, s, 2 x Me);  $\delta_c$  (126 MHz, CDCl<sub>3</sub>): 156.3 (C1), 151.6 (C1''), 139.1 (C4''), 131.9 (ArC), 130.7 (C4), 128.9 (C4'), 128.7 (ArC), 128.5 (C2 and C6), 126.3 (C3'' and C5''), 120.7 (C3 and C5), 112.5 (C2'' and C6''), 86.8 (C2'), 85.8 (C3'), 49.7 (C1'), 25.8 (*t*Bu), 18.4 (QC), -4.2 (Me);  $m/z$  (ES<sup>+</sup>): 502.1918 ([M<sup>+</sup>], C<sub>28</sub>H<sub>30</sub>N<sub>2</sub>O<sub>5</sub>Si requires 502.1924).

#### 4-(1-hydroxy-3-phenylprop-2-ynyl)phenol, 94



*n*BuLi (1.6 M in hexane, 2.3 ml, 3.69 mmol) was added to a solution of 4-hydroxybenzaldehyde (500 mg, 4.1 mmol) in THF (10 ml) at -78 °C and left to stir for 5 minutes. A solution of phenylacetylene (0.54 ml, 4.92 mmol) and *n*BuLi (1.6 M in hexane, 3.1 ml, 4.92 mmol) was added and the reaction was warmed to rt and left to stir for 90 minutes. Saturated ammonium chloride solution (20 ml) was added. The aqueous layer was separated and extracted with diethyl ether (2 x 10 ml). The combined organic extracts were dried over MgSO<sub>4</sub>, filtered and concentrated under reduced pressure to yield an orange oil. Flash column chromatography, (30% EtOAc/petroleum ether) gave **94** (320 mg, 35%) as an off-white solid.  $\nu_{\max}$  (ATR)/cm<sup>-1</sup>: 3341 (alkyne C-H), 3149 (OH), 2231 (C≡C);  $\delta_{\text{H}}$  (500 MHz, CDCl<sub>3</sub>): 8.57 (1H, s, ArOH), 7.39 - 7.41 (5H, m, H<sub>2</sub>, H<sub>6</sub> and ArH), 7.25 - 7.27 (2H, m, ArH), 6.80 - 6.82 (2H, m XX' part of AA'XX' system, H<sub>3</sub> and H<sub>5</sub>), 5.53 (1H, d <sup>3</sup>J 7, H<sub>1</sub>'), 3.99 - 4.00 (1H, d <sup>3</sup>J 7, OH);  $\delta_{\text{C}}$  (126 MHz, CDCl<sub>3</sub>): 157.1 (C<sub>1</sub>), 132.3 (C<sub>4</sub>), 131.6 (ArC), 128.3 (C<sub>2</sub> and C<sub>6</sub>), 128.2 (ArC), 122.8 (ArC), 115.5 (C<sub>3</sub> and C<sub>5</sub>), 89.9 (C<sub>2</sub>'), 85.6 (C<sub>3</sub>'), 64.4 (C<sub>1</sub>'); *m/z* (ES<sup>+</sup>): 207.1 [M-(H<sub>2</sub>O)+H]<sup>+</sup>

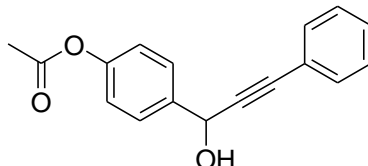
#### 4-Acetoxybenzaldehyde, 97



4-Hydroxybenzaldehyde (500 mg, 4.1 mmol), Et<sub>3</sub>N (0.75 ml, 8.2 mmol) and DMAP (50 mg, 0.41 mmol) were dissolved in DCM (10 ml) and stirred at rt for 20 minutes. The reaction was cooled to 0 °C and acetyl chloride (0.52 ml, 7.4 mmol) was added dropwise. A yellow-orange precipitate formed and this mixture was warmed to rt and left to stir for 45 minutes. Saturated aqueous sodium hydrogen carbonate (20 ml) was added, followed by brine (10 ml). The aqueous layer was separated and extracted with DCM (3 x 20 ml). The combined organic extracts were dried over MgSO<sub>4</sub>, filtered and concentrated under reduced pressure to yield **97** (670 mg, 99%) as a dark orange oil. This was used without further purification.  $\delta_{\text{H}}$  (500 MHz, CDCl<sub>3</sub>): 9.99 (1H, s, CHO),

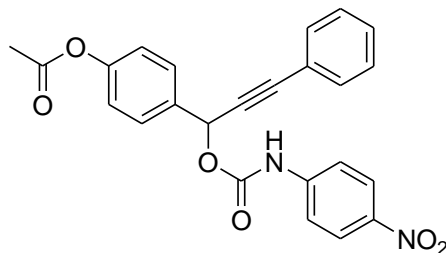
7.91 - 7.93 (2H, m, AA' part of the AA'XX' system, H2 and H6), 7.27 - 7.28 (2H, m, XX' part of the AA'XX' system, H3 and H5), 2.33 (3H, s, Me);  $\delta_c$  (126 MHz, CDCl<sub>3</sub>): 191.1 (aldehyde C=O), 168.9 (ester C=O), 155.5 (C4), 134.1 (C1), 131.3 (C2 and C6), 122.5 (C3 and C5), 21.3 (Me);  $m/z$  (ES<sup>+</sup>): 180.2 [M+H]<sup>+</sup>

#### 4-(1-hydroxy-3-phenylprop-2-ynyl)phenyl acetate, 98



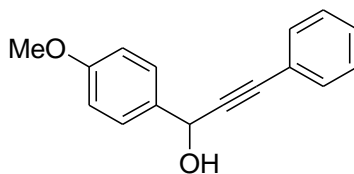
**95** (250 mg, mmol) and Et<sub>3</sub>N ( ml, mmol) were dissolved in DCM (5 ml) and stirred at 0 °C for 10 minutes. Acetyl chloride ( ml, mmol) was added dropwise. A pale yellow precipitate formed and this mixture was left to stir at 0 °C for 15 minutes. Saturated aqueous sodium hydrogen carbonate (10 ml) was added, followed by brine (5 ml). The aqueous layer was separated and extracted with DCM (3 x 10 ml). The combined organic extracts were dried over MgSO<sub>4</sub>, filtered and concentrated under reduced pressure to yield a yellow oil. Flash column chromatography (20% EtOAc:Petroleum ether) gave **98** (212 mg, 71%) as a yellow oil.  $\nu_{\max}$  (ATR)/cm<sup>-1</sup>: 3337 (alkyne C-H), 3150 (OH), 2230 (C≡C), 1744 (C=O);  $\delta_H$  (500 MHz, CDCl<sub>3</sub>): 7.60 - 7.62 (2H, m AA' part of AA'XX' system, H2 and H6), 7.46 - 7.48 (2H, m, ArH), 7.27 - 7.33 (3H, m, ArH), 7.11 - 7.13 (2H, m XX' part of AA'XX' system, H3 and H5), 6.69 (1H, s, H1'), 2.30 (3H, s, Me);  $\delta_c$  (126 MHz, CDCl<sub>3</sub>): 169.9 (C=O), 151.0 (C4), 138.7 (C1), 132.1 (ArC), 129.1 (ArC), 128.7 (ArC), 128.3 (C2 and C6), 122.7 (ArC), 122.1 (C3 and C5), 88.9 (C2'), 87.2 (C3'), 64.9 (C1'), 21.5 (Me);  $m/z$  (ES<sup>+</sup>): 249.1 [(M-H<sub>2</sub>O)+Na]<sup>+</sup>

#### 4-(1-(4-nitrophenylcarbamoyloxy)-3-phenylprop-2-ynyl)phenyl acetate, **96**



To a solution of **99** (170 mg, 0.62 mmol) in DCM (5 ml) was added Et<sub>3</sub>N (0.1 ml, 0.1 eq) and the mixture was allowed to stir for 15 mins. *p*-Nitrophenylisocyanate (111 mg, 1.1 eq) was added and the reaction was allowed to stir for 1 hour. Saturated ammonium chloride solution (10 ml) was added. The aqueous layer was separated and extracted with DCM (2 x 20 ml). The combined organic extracts were dried over MgSO<sub>4</sub>, filtered and concentrated under reduced pressure to yield a yellow oil. Flash column chromatography (20% EtOAc: Petroleum ether) gave **96** (173 mg, 65%) as a yellow solid.  $\lambda_{\text{max}}$  (DCM)/nm: 331;  $\delta_{\text{H}}$  (500 MHz, CDCl<sub>3</sub>): 8.13 – 8.15 (2H, m, A<sub>1</sub>A<sub>1</sub>' part of the A<sub>1</sub>A<sub>1</sub>'X<sub>1</sub>X<sub>1</sub>' system, H3'' and H5''), 7.62 – 7.64 (3H, m, H2, H6 and NH), 7.53 – 7.55 (2H, m, XX' part of the AA'XX' system, H3 and H5), 7.45 – 7.47 (2H, m, ArH), 7.29 – 7.36 (3H, m, ArH), 7.12 – 7.14 (2H, m, X<sub>1</sub>X<sub>1</sub>' part of the A<sub>1</sub>A<sub>1</sub>'X<sub>1</sub>X<sub>1</sub>' system, H2'' and H6''), 6.71 (1H, s, H1'), 2.31 (3H, s, Me);  $\delta_{\text{C}}$  (126 MHz, CDCl<sub>3</sub>): 151.9 (C=O), 151.3 (C=O), 143.9 (C1''), 143.1 (C4''), 134.3 (C1), 132.0 (ArC), 129.3 (C2 and C6), 129.2 (ArC), 128.5 (ArC), 125.2 (C3'' and C5''), 122.1 (C3 and C5), 121.7 (ArC), 118.0 (C2'' and C6''), 88.2 (C3'), 84.7 (C2'), 67.2 (C1'), 21.2 (Me);  $m/z$  (ES<sup>+</sup>): 431.2 [M+H]<sup>+</sup>

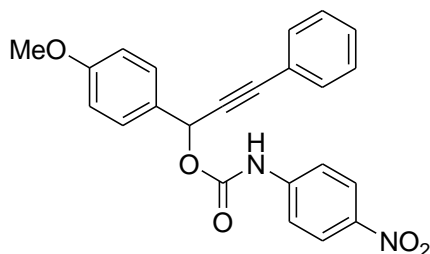
#### 1-(4-methoxyphenyl)-3-phenylprop-2-yn-1-ol, **106**



*n*-Butyllithium (1.6 M solution in hexane, 2.76 ml, 4.41 mmol) was added to a stirred solution of phenylacetylene (0.48 ml, 4.41 mmol) in THF (10 ml) at -78 °C. The resulting solution was left to stir for 15 minutes. *p*-anisaldehyde (0.45 ml, 3.68 mmol) was added and allowed to warm to rt. This was left to stir for 1 hour. Saturated ammonium chloride solution (20 ml) was added. The aqueous layer was separated and extracted

with ether (2 x 20 ml). The combined organic extracts were dried over MgSO<sub>4</sub>, filtered and concentrated under reduced pressure to yield a yellow oil. Flash column chromatography (25% EtOAc/petroleum ether) gave **106** (429 mg, 49%) as a cream solid.  $\nu_{\max}$  (ATR)/cm<sup>-1</sup>: 3334 (alkyne C-H), 2254 (C≡C);  $\delta_{\text{H}}$  (500 MHz, CDCl<sub>3</sub>): 7.54 - 7.56 (2H, m, AA' part of the AA'XX' system, H2 and H6), 7.47 - 7.49 (2H, m, ArH), 7.32 - 7.33 (3H, m, ArH), 6.92 - 6.94 (2H, m, XX' part of the AA'XX' system, H3 and H5), 5.64 (1H, d <sup>3</sup>J 7, H1'), 3.82 (3H, s, Me), 2.30 (1H, d <sup>3</sup>J 7, OH);  $\delta_{\text{C}}$  (126 MHz, CDCl<sub>3</sub>): 159.8 (C4), 133.1 (C1), 131.9 (ArC), 128.7 (ArC), 128.4 (C2 and C6), 128.3 (ArC), 122.6 (C4'), 114.1 (C3 and C5), 89.0 (C2'), 86.6 (C3'), 64.9 (C1'), 55.5 (Me);  $m/z$  (ES<sup>+</sup>): 221.1 [M-H<sub>2</sub>O]<sup>+</sup>

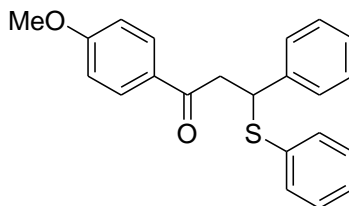
### 1-(4-methoxyphenyl)-3-phenylprop-2-ynyl 4-nitrophenylcarbamate, **105**



Et<sub>3</sub>N (0.01 ml, 0.1 mmol) was added to a stirring solution of **106** (250 mg, 1.04 mmol) in DCM (2 ml) and the resulting reaction was stirred for 10 minutes. *p*-Nitrophenylisocyanate (189 mg, 1.15 mmol) was added and stirring was continued for 1 hour. Saturated ammonium chloride solution (20 ml) was added. The aqueous layer was separated and extracted with DCM (2 x 10 ml). The combined organic extracts were dried over MgSO<sub>4</sub>, filtered and concentrated under reduced pressure to yield a yellow solid. Flash column chromatography, (3:1 DCM:hexane) gave **105** (195 mg, 47%) as a yellow solid.  $\lambda_{\max}$  (DCM)/nm: 369;  $\delta_{\text{H}}$  (500 MHz, CDCl<sub>3</sub>): 8.12 - 8.14 (2H, m A<sub>1</sub>A<sub>1</sub>' part of the A<sub>1</sub>A<sub>1</sub>'X<sub>1</sub>X<sub>1</sub>' system, H3'' and H5''), 7.54 - 7.56 (2H, m AA' part of the AA'XX' system, H2 and H6), 7.41 - 7.43 (2H, m, ArH), 7.30 - 7.33 (3H, m, ArH), 6.95 - 6.97 (2H, m XX' part of the AA'XX' system, H3 and H5), 6.73 - 6.74 (2H, m X<sub>1</sub>X<sub>1</sub>' part of the A<sub>1</sub>A<sub>1</sub>'X<sub>1</sub>X<sub>1</sub>' system, H2'' and H6''), 5.54 (1H, d <sup>5</sup>J 6, H1'), 4.86 (1H, d <sup>5</sup>J 6, NH), 3.84 (3H, s, Me);  $\delta_{\text{C}}$  (126 MHz, CDCl<sub>3</sub>): 160.0 (C4), 151.6 (C1''), 139.2 (C4''), 131.9 (ArC), 130.2 (C1), 128.9 (ArC), 128.7 (ArC), 128.5 (C2 and C6), 126.3 (C3'' and C5''), 122.3 (C4'), 114.6 (C3 and C5), 112.5 (C2'' and C6''), 86.8 (C2'), 85.9 (C3'), 55.5 (Me), 49.7 (C1');  $m/z$  (ES<sup>+</sup>): 403.1 [M+H]<sup>+</sup>

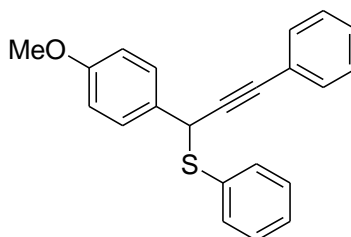


### 1-(4-methoxyphenyl)-3-phenyl-3-(phenylthio)propan-1-one, 107



**105** (150 mg, 0.37 mmol), thiophenol (0.03 ml, 0.37 mmol), KF (2 mg, 0.04 mmol) and NMP (0.5 ml) were heated to 100 °C for 1 hour, during which time the solution became a deep orange colour. The reaction was allowed to cool to rt and adjusted to pH 14 with 5% aqueous NaOH (5 ml). The aqueous layer was separated and extracted with diethyl ether (3 x 5 ml). The combined aqueous extracts were acidified in an ice bath with 6 M HCl (2 ml) and extracted with diethyl ether (3 x 5 ml). The combined organic extracts were washed with brine (5 ml), dried over MgSO<sub>4</sub>, filtered and concentrated under reduced pressure to yield a yellow oil. Flash column chromatography (25% EtOAc/Petroleum ether) gave **107** (14 mg, 49%) as a yellow solid.  $\nu_{\max}$  (ATR)/cm<sup>-1</sup>: 2972w, 1668s (C=O), 1599s;  $\lambda_{\max}$  (CDCl<sub>3</sub>)/nm:  $\lambda_{\text{ex}}$  371,  $\lambda_{\text{em}}$  440;  $\delta_{\text{H}}$  (500 MHz, CDCl<sub>3</sub>): 7.86 – 7.88 (2H, m, AA' part of the AA'XX' system, H2 and H6), 7.31 – 7.34 (4H, m, ArH), 7.21 – 7.25 (6H, m, ArH), 6.89 – 6.91 (2H, m, XX' part of the AA'XX' system, H3 and H5), 4.94 (1H, dd <sup>3</sup>J 9 and <sup>3</sup>J 6, H3'), 3.85 (3H, s, OMe), 3.50 (1H, dd <sup>3</sup>J 9 and <sup>3</sup>J 6, H2'), 3.59 (1H, dd <sup>3</sup>J 9 and <sup>3</sup>J 6, H2');  $\delta_{\text{C}}$  (126 MHz, CDCl<sub>3</sub>): 195.6 (C=O), 163.7 (C4), 141.4 (ArC), 134.5 (ArC), 132.8 (ArC), 130.5 (C2 and C6), 130.0 (C1), 129.0 (ArC), 128.6 (ArC), 127.9 (ArC), 127.6 (ArC), 127.5 (ArC), 113.9 (C3 and C5), 55.6 (OMe), 48.5 (C3'), 44.4 (C2');  $m/z$  (ES<sup>+</sup>): 349.1257 ([M+H]<sup>+</sup>, C<sub>22</sub>H<sub>21</sub>O<sub>2</sub>S requires 349.1257)

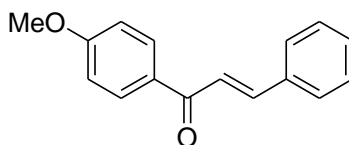
### (1-(4-methoxyphenyl)-3-phenylprop-2-ynyl)phenylsulfane, 108



**105** (39 mg, 0.1 mmol), thiophenol (0.01 ml, 0.1 mmol), KF (1 mg, 0.01 mmol) and NMP (0.5 ml) were stirred at rt for 1 hour. The reaction was adjusted to pH 14 with 5% aqueous NaOH (5 ml). The aqueous layer was separated and extracted with diethyl

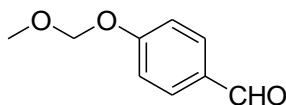
ether (3 x 5 ml). The combined aqueous extracts were acidified in an ice bath with 6 M HCl (2 ml) and extracted with diethyl ether (3 x 5 ml). The combined organic extracts were washed with brine (5 ml), dried over MgSO<sub>4</sub>, filtered and concentrated under reduced pressure to yield a yellow oil. Flash column chromatography (20% EtOAc/petroleum ether) gave **108** (17 mg, 52%) as a yellow oil.  $\nu_{\max}$  (ATR)/cm<sup>-1</sup>: 2233 (C≡C);  $\delta_{\text{H}}$  (500 MHz, CDCl<sub>3</sub>): 7.49 – 7.51 (4H, m, ArH), 7.37 – 7.39 (4H, m, ArH and AA' part of the AA'XX' system, H2 and H6), 7.30 – 7.32 (4H, m, ArH), 6.85 – 6.87 (2H, m, XX' part of the AA'XX' system, H3 and H5), 5.21 (1H, s, H1'), 3.81 (3H, s, OMe);  $\delta_{\text{C}}$  (126 MHz, CDCl<sub>3</sub>): 159.4 (C4), 137.2 (ArC), 134.5 (ArC), 130.2 (C1), 129.4 (C2 and C6), 128.8 (ArC), 128.4 (ArC), 127.6 (ArC), 127.3 (ArC), 114.0 (C3 and C5), 87.8 (C2'), 86.8 (C3'), 55.5 (OMe), 43.9 (C1');  $m/z$  (ES<sup>+</sup>): 331.1153 ([M+H]<sup>+</sup>, C<sub>22</sub>H<sub>19</sub>OS requires 331.1151)

**(E)-1-(4-methoxyphenyl)-3-phenylprop-2-en-1-one, 109**



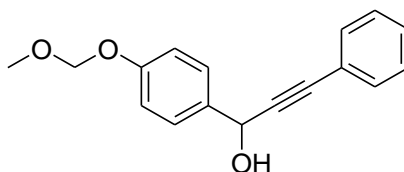
BBr<sub>3</sub> (0.02 ml, 0.12 mmol) in DCM (0.5 ml) was added to a solution of **105** (50 mg, 0.12 mmol) in DCM (1 ml) at -78 °C. The solution was allowed to slowly warm up to rt and left to stir for 16 hours. Water (5 ml) was added. The aqueous layer was separated and extracted with diethyl ether (2 x 20 ml). The combined organic extracts were dried over MgSO<sub>4</sub>, filtered and concentrated under reduced pressure to yield a yellow oil. Flash column chromatography (20% EtOAc: Petroleum ether) gave **109** (14mg, 49%) as a yellow oil.  $\delta_{\text{H}}$  (500 MHz, CDCl<sub>3</sub>): 7.89 – 7.90 (2H, m, ArH), 7.72 (1H, d <sup>3</sup>J 15, H2'), 7.53 – 7.55 (2H, m, AA' part of the AA'XX' system, H2 and H6), 7.42 – 7.45 (3H, m, ArH), 7.35 (1H, d <sup>3</sup>J 15, H3'), 6.86 – 6.89 (2H, m, XX' part of the AA'XX' system, H3 and H5), 3.79 (3H, s, OMe);  $\delta_{\text{C}}$  (126 MHz, CDCl<sub>3</sub>): 190.8 (C=O), 161.8 (C4), 144.9 (ArC), 138.7 (ArC), 132.1 (ArC), 130.4 (C2 and C6), 128.7 (C1), 128.6 (ArC), 114.6 (C3 and C5), 55.6 (OMe), 41.5 (C2'), 38.9 (C3');  $m/z$  (ES<sup>+</sup>): 239.2 [M+H]<sup>+</sup>

#### 4-(methoxymethyl)benzaldehyde, **110**



To a solution of 4-hydroxybenzaldehyde (1 g, 8.20 mmol) in DCM (10 ml) was added diisopropylamine (1.57 ml, 9.84 mmol) and the resulting solution was stirred for 10 minutes at 0 °C. MOMCl was added dropwise over a period of 5 minutes and stirred for a further 2 hours. Saturated aqueous sodium hydrogen carbonate (20 ml) was added, followed by brine (20 ml). The aqueous layer was separated and extracted with DCM (3 x 20 ml). The combined organic extracts were dried over MgSO<sub>4</sub>, filtered and concentrated under reduced pressure to yield **110** (1.34 g, 99%) as a very pale yellow oil. This was used without further purification.  $\delta_{\text{H}}$  (500 MHz, CDCl<sub>3</sub>): 9.89 (1H, s, CHO), 7.82 – 7.83 (2H, m, AA' part of the AA'XX' system, H2 and H6), 7.12 – 7.14 (2H, m, XX' part of the AA'XX' system, H3 and H5), 5.24 (2H, s, CH<sub>2</sub>), 3.48 (3H, s, CH<sub>3</sub>);  $\delta_{\text{C}}$  (126 MHz, CDCl<sub>3</sub>): 191.0 (C=O), 162.0 (C4), 132.0 (C2 and C6), 130.8 (C1), 116.4 (C3 and C5), 94.2 (CH<sub>2</sub>), 56.5 (CH<sub>3</sub>);  $m/z$  (ES<sup>+</sup>): 167.0703 ([M+H]<sup>+</sup>, C<sub>9</sub>H<sub>11</sub>O<sub>3</sub> requires 167.0703)

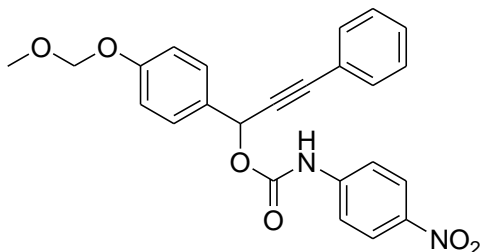
#### 1-(4-methoxymethylphenyl)-3-phenylprop-2-yn-1-ol, **111**



Phenylacetylene (0.78 ml, 6.63 mmol) and *n*BuLi (2.5 M in hexane, 2.89 ml, 7.23 mmol) were stirred in THF (10 ml) at -78 °C for 15 minutes. **110** (1 g, 6.02 mmol) was added as a solution in THF (5 ml) and this was left to stir for 1 hour. Saturated ammonium chloride solution (20 ml) was added. The aqueous layer was separated and extracted with diethyl ether (3 x 20 ml). The combined organic extracts were dried over MgSO<sub>4</sub>, filtered and concentrated under reduced pressure to yield **111** (1.55 g, 96%) as a yellow oil. This was used without further purification.  $\delta_{\text{H}}$  (500 MHz, CDCl<sub>3</sub>): 7.53 – 7.55 (2H, m, AA' part of the AA'XX' system, H2 and H6), 7.46 – 7.54 (2H, m, ArH), 7.31 – 7.33 (3H, m, ArH), 7.06 – 7.08 (2H, m, XX' part of the AA'XX' system, H3 and H5), 5.64 (1H, s, H1'), 5.24 (2H, s, CH<sub>2</sub>), 3.48 (3H, s, CH<sub>3</sub>), 2.60 (1H, br s, OH);  $\delta_{\text{C}}$  (126 MHz, CDCl<sub>3</sub>): 157.4 (C4), 134.3 (C1), 131.8 (ArC), 128.7 (ArC), 128.4 (ArC), 128.3 (C2 and C6), 122.6

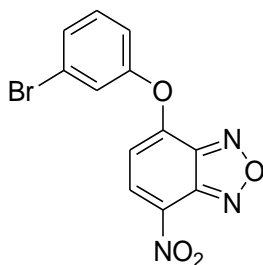
(ArC), 116.4 (C3 and C5), 94.6 (CH<sub>2</sub>), 89.0 (C3'), 86.6 (C2'), 64.7 (C1'), 56.5 (CH<sub>3</sub>); *m/z* (ES<sup>+</sup>): 251.1068 [(M-H<sub>2</sub>O)+H]<sup>+</sup>, C<sub>17</sub>H<sub>15</sub>O<sub>2</sub> requires 251.1067)

### 1-(4-(methoxymethyl)phenyl)-3-phenylprop-2-ynyl 4-nitrophenylcarbamate, **112**



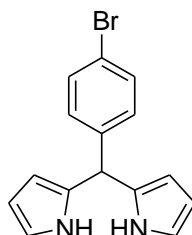
**111** (1 g, 3.73 mmol) and Et<sub>3</sub>N (0.05 ml, 0.37 ml) was stirred in DCM (4 ml) for 10 minutes. *p*-Nitrophenylisocyanate (673 mg, 4.10 mmol) was added and the reaction was stirred for 1 hour. Saturated ammonium chloride solution (5 ml) was added. The aqueous layer was separated and extracted with DCM (3 x 10 ml). The combined organic extracts were dried over MgSO<sub>4</sub>, filtered and concentrated under reduced pressure to yield an orange oil. Flash column chromatography (20% EtOAc: Petroleum ether) gave **112** (558 mg, 35%) as a yellow oil.  $\lambda_{\max}$  (CHCl<sub>3</sub>)/nm: 364;  $\delta_{\text{H}}$  (400 MHz, CDCl<sub>3</sub>): 8.11 - 8.13 (2H, m, AA' part of the AA'XX' system, H3'' and H5''), 7.54 - 7.56 (2H, m, AA' part of the AA'XX' system, H2 and H6), 7.41 - 7.43 (2H, m, ArH), 7.30 - 7.33 (3H, m, ArH), 7.09 - 7.11 (2H, m, XX' part of the AA'XX' system, H3 and H5), 6.71 - 6.74 (2H, m, XX' part of the AA'XX' system, H2'' and H6''), 5.54 (1H, d <sup>5</sup>J 8, H1'), 5.20 (2H, s, CH<sub>2</sub>), 4.95 (1H, d <sup>5</sup>J 8, NH), 3.49 (3H, s, CH<sub>3</sub>);  $\delta_{\text{C}}$  (126 MHz, CDCl<sub>3</sub>): 157.9 (C4), 151.8 (C1''), 139.1 (C4''), 132.0 (ArC), 131.2 (C1), 128.7 (ArC), 128.4 (ArC), 128.3 (C2 and C6), 126.6 (C3'' and C5''), 122.4 (C4'), 116.9 (C3 and C5), 112.9 (C2'' and C6''), 94.5 (CH<sub>2</sub>), 86.1 (C3'), 87.3 (C2'), 56.4 (Me), 49.5 (C1'); *m/z* (ES<sup>+</sup>): 433.3 [M+H]<sup>+</sup>

#### 4-Nitro-7-(3'-bromophenoxy) benzofurazan, **113**



To a solution of NaOH (30 mg, 0.75 mmol) in THF:H<sub>2</sub>O (5 ml) at 0 °C was added 3-bromophenol (1.3 g, 15.0 eq). The resulting solution was stirred for 10 mins, during which time a white colour developed. NBD-Cl (150 mg, 1.0 eq) was added, upon which the solution became orange, and this was stirred for 2 hours. Saturated aqueous sodium hydrogen carbonate (20 ml) was added. The aqueous layer was separated and extracted with ether (2 x 20 ml). The combined organic extracts were dried over MgSO<sub>4</sub>, filtered and concentrated under reduced pressure to yield an orange oil. Flash column chromatography (75% DCM:Petroleum ether) gave **113** (159 mg, 32%) as a yellow solid. **m.p.** 110 – 113 °C;  $\delta_{\text{H}}$  (500 MHz, CDCl<sub>3</sub>): 8.45 (1H, d <sup>3</sup>J 8, H5), 7.54 – 7.55 (2H, m, ArH), 7.41 – 7.45 (1H, m, ArH), 7.22 – 7.24 (1H, m, ArH), 6.60 (1H, d <sup>3</sup>J 8, H6);  $\delta_{\text{C}}$  (126 MHz, CDCl<sub>3</sub>): 152.7 (QC), 153.4 (QC), 145.2 (QC), 144.3 (QC), 133.2 (QC), 132.0 (C5), 131.3 (ArC), 130.7 (ArC), 124.5 (ArC), 123.8 (ArC), 119.8 (ArC), 108.3 (C6).

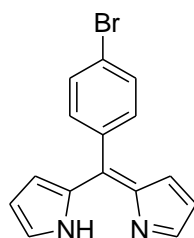
#### 8-(4'-bromophenyl)-dipyrromethane, **120**<sup>174</sup>



TFA (0.02 ml, 0.27 mmol) was added to a stirred solution of 4-bromobenzaldehyde (500 mg, 2.70 mmol) in pyrrole (4.72 ml, 67.6 mmol) with the evolution of a white gas. The resulting solution was stirred for 10 minutes. 0.1 M NaOH (30 ml) was added and the aqueous layer separated and extracted with EtOAc (2 x 30 ml). The combined organic extracts were dried over MgSO<sub>4</sub>, filtered and concentrated under reduced pressure to yield a brown oil. Flash column chromatography, gradient elution (100%

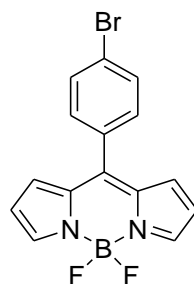
Petrol 40/60 to 50% EtOAc/petrol 40/60) gave **120** (465 mg, 58%) as a pale brown solid. **m.p.** 138 – 141 °C;  $\delta_{\text{H}}$  (500 MHz,  $\text{CDCl}_3$ ): 7.90 (2H, br s, NH), 7.43 – 7.45 (2H, m AA' part of AA'XX' system, H3' and H5'), 7.08 – 7.10 (2H, m XX' part of AA'XX' system, H2' and H6'), 6.70 – 6.71 (2H, m, pyH), 6.16 – 6.18 (2H, m, pyH), 5.89 – 5.90 (2H, m, pyH), 5.43 (1H, s, H8);  $\delta_{\text{C}}$  (126 MHz,  $\text{CDCl}_3$ ): 141.3 (C1'), 132.0 (pyC), 131.8 (C3' and C5'), 130.3 (C2' and C6'), 121.0 (pyC), 117.6 (pyC), 108.7 (pyC), 107.8 (pyC), 43.6 (C8);  $m/z$  (ES+): 300.8  $[\text{M}+\text{H}]^+$

#### 8-(4-bromophenyl)-dipyrromethene, **121**<sup>172</sup>



A suspension of *p*-chloranil (1.50 mmol, 369 mg) in DCM was added to a solution of **120** (1.50 mmol, 455 mg) in DCM (6 ml) and left to stir for 1 hour. The solvent was removed under reduced pressure to yield a brown solid. Flash column chromatography, gradient elution (100% Petrol 40/60 to 100% EtOAc) gave **121** (54 mg, 12%) as a brown oil.  $\delta_{\text{H}}$  (500 MHz,  $\text{CDCl}_3$ ): 7.66 – 7.66 (2H, m, pyH), 7.58 – 7.60 (2H, m AA' part of AA'XX' system, H3' and H5'), 7.35 – 7.38 (2H, m XX' part of AA'XX' system, H2' and H6'), 6.56 – 6.58 (2H, dd  $^3J$  4 and  $^4J$  1, pyH), 6.40 – 6.42 (2H, dd  $^3J$  4 and  $^4J$  2, pyH);  $m/z$  (ES+): 299.5  $[\text{M}+\text{H}]^+$

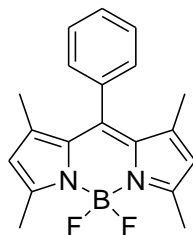
#### 4,4-difluoro-8-(4-bromophenyl)-4-bora-3a,4a-diaza-s-indacene, **116**



4-bromobenzaldehyde (500 mg, 2.70 mmol) and pyrrole (362 mg, 5.40 mmol) were dissolved in DCM (15 ml). One drop of TFA was added and the reaction stirred for 2

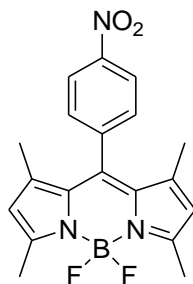
hours. A suspension of DDQ (610 mg, 2.70 mmol) in DCM was added and the stirring was continued for 15 minutes. DIPEA (0.71 ml, 4.05 mmol) and  $\text{BF}_3 \cdot \text{OEt}_2$  (0.86 ml, 5.40 mmol) was added and the reaction was stirred for 30 minutes. The reaction mixture was washed with water (20 ml), dried over  $\text{MgSO}_4$ , filtered and concentrated under reduced pressure to yield a black solid. Flash column chromatography (50% DCM/hexane) gave **116** (9 mg, 2%) as a brown solid. **m.p.** 194 - 197 °C;  $\lambda_{\text{max}}$  ( $\text{CHCl}_3$ )/nm:  $\lambda_{\text{ex}}$  504,  $\lambda_{\text{em}}$  520;  $\delta_{\text{H}}$  (500 MHz,  $\text{CDCl}_3$ ): 7.96 (2H, s, H3 and H5), 7.68 - 7.69 (2H, m AA' part of AA'XX' system, H3' and H5'), 7.44 - 7.46 (2H, m XX' part of AA'XX' system, H2' and H6'), 6.91 (2H, d  $^3J$  4, H2 and H6), 6.56 (2H, d  $^3J$  4, H1 and H7);  $\delta_{\text{F}}$  (376 MHz,  $\text{CDCl}_3$ ): -145.3 - -145.6 (m);  $m/z$  (ES<sup>+</sup>): 347.4 [M+H]<sup>+</sup>

#### 4,4-difluoro-1,3,5,7-tetramethyl-8-phenyl-4-bora-3a,4a-diaza-s-indacene, **122**



Benzoyl chloride (200 mg, 1.42 mmol) and 2,4-dimethylpyrrole (0.29 ml, 2.84 mmol) were dissolved in DCM (10 ml) and refluxed for 3 hours, after which time the solution became deep red. After cooling to rt  $\text{Et}_3\text{N}$  (0.36 ml, 2.56 mmol) and  $\text{BF}_3 \cdot \text{OEt}_2$  (0.49 ml, 3.84 mmol) were added and the reaction stirred for 3 hours. Water (20 ml) was added and the aqueous layer was separated and extracted with DCM (2 x 20 ml). The combined organic extracts were dried over  $\text{MgSO}_4$ , filtered and concentrated under reduced pressure to yield an orange solid. Flash column chromatography (50% DCM/hexane) followed by recrystallisation ( $\text{CHCl}_3$ /hexane) gave **122** (78 mg, 17%) as a crystalline orange solid. **m.p.** 150 - 152 °C;  $\nu_{\text{max}}$  (ATR)/ $\text{cm}^{-1}$ : 1465m (B-F);  $\lambda_{\text{max}}$  (acetone)/nm:  $\lambda_{\text{ex}}$  498,  $\lambda_{\text{em}}$  508;  $\delta_{\text{H}}$  (500 MHz,  $\text{CDCl}_3$ ): 7.46 - 7.48 (3H, m, ArH), 7.27 - 7.28 (2H, m, ArH), 5.97 (2H, s, H2 and H6), 2.55 (6H, s, C3Me and C5Me), 1.36 (6H, s, C1Me and C7Me);  $\delta_{\text{C}}$  (126 MHz,  $\text{CDCl}_3$ ): 155.5 (C3 and C5), 143.3 (C1 and C7), 141.8 (C8), 135.1 (C1'), 131.5 (C1a and C7a), 129.2 (ArC), 129.0 (ArC), 128.4 (ArC), 128.2 (ArC), 128.0 (ArC), 121.3 (C2 and C6), 14.7 (C1Me and C7Me), 14.4 (C3Me and C5Me);  $\delta_{\text{F}}$  (376 MHz,  $\text{CDCl}_3$ ): -146.8 - -146.4 (m);  $\delta_{\text{B}}$  (128 MHz,  $\text{CDCl}_3$ ): 0.78 (t,  $J_{\text{B-F}}$  31);  $m/z$  (ES<sup>+</sup>): 325.16787 (20%) ([M+H]<sup>+</sup>,  $\text{C}_{19}\text{H}_{20}\text{N}_2\text{BF}_2$  requires 325.16821), 347.1497 (100) ([M+Na]<sup>+</sup>,  $\text{C}_{19}\text{H}_{19}\text{N}_2\text{BF}_2\text{Na}$  requires 347.1501).

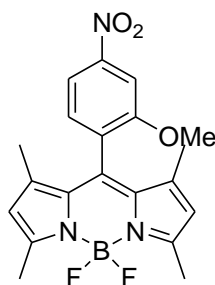
**4,4-difluoro-1,3,5,7-tetramethyl-8-(4-nitrophenyl)-4-bora-3a,4a-diaza-s-indacene, 126**



4-Nitrobenzoyl chloride (300 mg, 1.62 mmol) and 2,4-dimethylpyrrole (0.38 ml, 3.23 mmol) were dissolved in DCM (10 ml) and refluxed for 4 hours, after which time the solution became deep red. After cooling to rt Et<sub>3</sub>N (0.36 ml, 2.56 mmol) and BF<sub>3</sub>·OEt<sub>2</sub> (0.49 ml, 3.84 mmol) were added and the reaction stirred for 16 hours. Water (20 ml) was added and the aqueous layer was separated and extracted with DCM (2 x 20 ml). The combined organic extracts were dried over MgSO<sub>4</sub>, filtered and concentrated under reduced pressure to yield an orange solid. Flash column chromatography (50% DCM/hexane) followed by recrystallisation (CHCl<sub>3</sub>/hexane) gave **126** (179 mg, 30%) as a crystalline red solid. **m.p.** 169 – 170 °C;  $\lambda_{\text{max}}$  (acetone)/nm: 502;  $\nu_{\text{max}}$  (ATR)/cm<sup>-1</sup>: 1516s and 1343s (NO<sub>2</sub>), 1468m (B-F); Found: C, 55.82 H, 4.52 N, 10.19; Calc. for C<sub>19</sub>H<sub>18</sub>BF<sub>2</sub>N<sub>3</sub>O<sub>2</sub>·0.4CHCl<sub>3</sub>: C, 55.82 H, 4.44 N, 10.06;  $\delta_{\text{H}}$  (500 MHz, CDCl<sub>3</sub>): 8.38 – 8.40 (2H, m, AA' part of the AA'XX' system, H3' and H5'), 7.53 – 7.55 (2H, m, XX' part of the AA'XX' system, H2' and H6'), 6.02 (2H, s, H2 and H6), 2.56 (6H, s, C3Me and C5Me), 1.34 (6H, s, C1Me and C7Me);  $\delta_{\text{C}}$  (126 MHz, CDCl<sub>3</sub>): 156.8 (C5 and C3), 148.5 (C4'), 142.7 (C7 and C1), 142.1 (C8), 138.5 (C1'), 130.8 (C1a and C7a), 129.8 (C2' and C6'), 124.5 (C3' and C5'), 122.0 (C2 and C6), 14.9 (C3Me and C5Me), 14.8 (C1Me and C7);  $\delta_{\text{F}}$  (376 MHz, CDCl<sub>3</sub>): -146.8 – -146.5 (m);  $\delta_{\text{B}}$  (128 MHz, CDCl<sub>3</sub>): 0.70 (t,  $J_{\text{B-F}}$  31);  $m/z$  (ES<sup>+</sup>): 370.1529 (M+H<sup>+</sup>, requires 370.15329) (M<sup>+</sup>, C<sub>22</sub>H<sub>21</sub>O<sub>2</sub>S requires 349.1257)

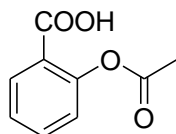


**4,4-difluoro-1,3,5,7-tetramethyl-8-(2-methoxy-4-nitrophenyl)-4-bora-3a,4a-diaza-s-indacene, 127**



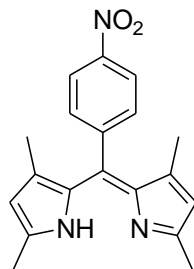
To a stirring solution of 2-methoxy-4-nitrobenzoic acid (300 mg, 1.52 mmol) in DCM (10 ml) was added oxalyl chloride (0.52 ml, 6.09 mmol) and 2 drops of DMF. This was left to stir until no more effervescence was seen. Oxalyl chloride and the solvent were removed under reduced pressure to afford a pale yellow solid. This was redissolved in DCM (10 ml) and 2,4-dimethylpyrrole (0.31 ml, 3.04 mmol) was added and the resulting solution refluxed for 3 hours, after which time the solution became deep red. After cooling to rt Et<sub>3</sub>N (0.38 ml, 2.74 mmol) and BF<sub>3</sub>•OEt<sub>2</sub> (0.52 ml, 4.11 mmol) were added and the reaction stirred for 3 hours. Water (20 ml) was added and the aqueous layer was separated and extracted with DCM (2 x 20 ml). The combined organic extracts were dried over MgSO<sub>4</sub>, filtered and concentrated under reduced pressure to yield an orange solid. Flash column chromatography (50% DCM/hexane) followed by recrystallisation (CHCl<sub>3</sub>/hexane) gave **127** (133 mg, 22%) as a crystalline orange solid.  $\lambda_{\max}$  (acetone)/nm: 502;  $\nu_{\max}$  (ATR)/cm<sup>-1</sup>: 1518s and 1346s (NO<sub>2</sub>), 1468m (B-F);  $\delta_{\text{H}}$  (500 MHz, CDCl<sub>3</sub>): 8.00 (1H, dd <sup>3</sup>J 8 and <sup>4</sup>J 2, H5'), 7.86 (1H, d <sup>4</sup>J 2, H3'), 7.38 (1H, d, <sup>3</sup>J 8, H6'), 5.99 (2H, s, H2 and H6), 3.90 (3H, s, OMe), 2.56 (6H, s, C3Me and C5Me), 1.42 (6H, s, C1Me and C7Me);  $\delta_{\text{C}}$  (126 MHz, CDCl<sub>3</sub>): 157.9 (C2'), 156.5 (C3 and C5), 150.1 (C4'), 142.4 (C1 and C7), 136.0 (C8), 131.3 (C6'), 131.1 (C1a and C7a), 131.0 (C1'), 121.8 (C2 and C6), 117.0 (C5'), 106.6 (C3'), 56.8 (OMe), 15.1 (C3Me and C5Me), 14.5 (C1Me and C7Me);  $\delta_{\text{B}}$  (128 MHz, CDCl<sub>3</sub>): 0.74 (t, J<sub>B-F</sub> 31);  $\delta_{\text{F}}$  (376 MHz, CDCl<sub>3</sub>): -146.8 - -147.1 (m); *m/z* (ES<sup>+</sup>): 400.1633 ([M+H]<sup>+</sup>, C<sub>20</sub>H<sub>21</sub>N<sub>3</sub>O<sub>3</sub> BF<sub>2</sub> requires 400.1639).

## 2-acetoxybenzoic acid, **134**



Salicylic acid (200 mg, 1.45 mmol) was dissolved in acetic anhydride (2 ml). 3 drops of phosphoric acid was added and the resulting solution was stirred for 10 minutes at 60 °C. Water (8 ml) was slowly added. The reaction was cooled in an ice bath which yielded **134** (217 mg, 83%) as white crystals. **m.p.** 134 - 135 °C;  $\nu_{\max}$  (ATR)/cm<sup>-1</sup>: 2950(s) OH, 1750(s) ester C=O, 1700(s) acid C=O; Found: C, 59.73 H, 4.47; Calc. for C<sub>9</sub>H<sub>8</sub>O<sub>4</sub>: C, 60.00 H, 4.48;  $\delta_{\text{H}}$  (500 MHz, CDCl<sub>3</sub>): 8.12 (1H, dd <sup>3</sup>J 8 and <sup>4</sup>J 2, H6), 7.62 (1H, td <sup>3</sup>J 8 and <sup>4</sup>J 1, H4), 7.36 (1H, td <sup>3</sup>J 8 and <sup>4</sup>J 1, H5), 7.14 (1H, dd <sup>3</sup>J 8 and <sup>4</sup>J 2, H3), 2.35 (3H, s, Me);  $\delta_{\text{C}}$  (126 MHz, CDCl<sub>3</sub>): 170.1 (C=O), 169.9 (C=O), 151.4 (C2), 135.1 (C4), 132.7 (C6), 126.3 (C5), 124.2 (C3), 122.3 (C1), 21.2 (Me); HRMS (ES<sup>-</sup>): 179.0350 (95%) ([M-H]<sup>-</sup>, C<sub>9</sub>H<sub>7</sub>O<sub>4</sub> requires 179.0350), 137.0244 (5) ([M-Ac]<sup>-</sup>, C<sub>7</sub>H<sub>5</sub>O<sub>3</sub> requires 137.0244)

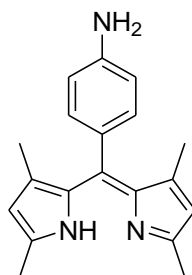
## 1,3,5,7-tetramethyl-8-(4-nitrophenyl)-dipyrromethene, **136**



4-Nitrobenzoyl chloride (500 mg, 2.69 mmol) and 2,4-dimethylpyrrole (0.55 ml, 5.39 mmol) were dissolved in DCM (10 ml) and refluxed for 4 hours, after which time the solution became deep red. Water (20 ml) was added and the aqueous layer was separated and extracted with DCM (3 x 20 ml). The combined organic extracts were dried over MgSO<sub>4</sub>, filtered and concentrated under reduced pressure to yield a brown solid. Flash column chromatography (DCM, alumina) followed by recrystallisation (CHCl<sub>3</sub>/hexane) gave **136** (125 mg, 15%) as a brown solid. Found: C, 70.44 H, 6.19 N, 12.39; Calc. for C<sub>19</sub>H<sub>19</sub>N<sub>3</sub>O<sub>2</sub>·0.03 CHCl<sub>3</sub>: C, 70.45 H, 5.91 N, 12.95;  $\nu_{\max}$  (ATR)/cm<sup>-1</sup>: 1512(s) and 1350(s) NO<sub>2</sub>;  $\delta_{\text{H}}$  (500 MHz, CDCl<sub>3</sub>): 8.33 - 8.35 (2H, m, AA' part of the AA'XX' system, H3' and H5'), 7.51 - 7.53 (2H, m, XX' part of the AA'XX' system, H2'

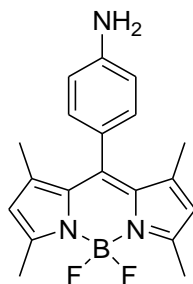
and H6'), 5.90 (2H, s, H2 and H6), 2.35 (6H, s, C3Me and C5Me), 1.27 (6H, s, C1Me and C7Me);  $\delta_C$  (126 MHz, CDCl<sub>3</sub>): 152.6 (C5 and C3), 148.0 (C4'), 145.3 (C7 and C1), 139.7 (C8), 135.7 (C1'), 135.5 (C1a and C7a), 130.8 (C2' and C6'), 123.9 (C3' and C5'), 120.4 (C2 and C6), 16.2 (C3Me and C5Me), 15.0 (C1Me and C7Me);  $m/z$  (ES<sup>+</sup>): 322.1551 ([M+H]<sup>+</sup>, C<sub>19</sub>H<sub>19</sub>N<sub>3</sub>O<sub>2</sub>BF<sub>2</sub> requires 322.1550).

### 1,3,5,7-tetramethyl-8-(4-aminophenyl)-dipyrrromethene, 137



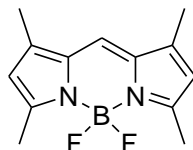
**136** (100 mg, 0.31 mmol) was dissolved in DCM which had been saturated with concentrated HCl and stirred for 30 minutes at 0 °C. SnCl<sub>2</sub>·2H<sub>2</sub>O (1.4 g, 6.23 mmol) was added and the reaction was warmed to rt and left to stir for 16 hours. 2M NaOH (10 ml) was added and the aqueous layer separated and extracted with DCM (2 x 20 ml). The combined organic extracts were dried over MgSO<sub>4</sub>, filtered and concentrated under reduced pressure to yield a dark orange oil. Flash column chromatography (DCM) gave **137** (32 mg, 35%) as an orange oil.  $\delta_H$  (400 MHz, CDCl<sub>3</sub>): 7.03 – 7.05 (2H, m, AA' part of the AA'XX' system, H2' and H6'), 6.72 – 6.74 (2H, m, XX' part of the AA'XX' system, H3' and H5'), 5.91 (2H, s, H2 and H6), 3.82 (2H, br s, NH<sub>2</sub>), 2.36 (6H, s, C3Me and C5Me), 1.42 (6H, s, C1Me and C7Me);  $\delta_C$  (126 MHz, CDCl<sub>3</sub>): 154.9 (C5 and C3), 147.1 (C4'), 143.3 (C7 and C1), 129.1 (C8), 124.9 (C1'), 121.1 (C1a and C7a), 115.9 (C2' and C6'), 124.2 (C3' and C5'), 120.6 (C2 and C6), 14.9 (C3Me and C5Me), 14.7 (C1Me and C7Me);  $m/z$  (ES<sup>+</sup>): 292.1809 ([M+H]<sup>+</sup>, C<sub>19</sub>H<sub>22</sub>N<sub>3</sub> requires 292.1808).

#### 4,4-difluoro-1,3,5,7-tetramethyl-8-(4-aminophenyl)-4-bora-3a,4a-diaza-s-indacene, 135



DIPEA (0.5 ml) was added to a solution of **137** (32 mg, 0.11 mmol) in DCM (10 ml) and this was stirred for 10 minutes.  $\text{BF}_3 \cdot \text{OEt}_2$  (0.5 ml) was added and the reaction was left to stir for 45 minutes. A mixture of water and 2M NaOH (30 ml 1:1) was added and the aqueous layer separated and extracted with DCM (2 x 20 ml). The combined organic extracts were dried over  $\text{MgSO}_4$ , filtered and concentrated under reduced pressure to yield a dark orange oil. Flash column chromatography (DCM, alumina) gave **135** (12 mg, 32%) as an orange solid.  $\lambda_{\text{max}}$  (acetone)/nm:  $\lambda_{\text{ex}}$  502,  $\lambda_{\text{em}}$  512;  $\delta_{\text{H}}$  (500 MHz,  $\text{CDCl}_3$ ): 7.00 – 7.02 (2H, m, AA' part of the AA'XX' system, H2' and H6'), 6.77 – 6.79 (2H, m, XX' part of the AA'XX' system, H3' and H5'), 5.98 (2H, s, H2 and H6), 2.54 (6H, s, C3Me and C5Me), 1.49 (6H, s, C1Me and C7Me);  $\delta_{\text{C}}$  (126 MHz,  $\text{CDCl}_3$ ): 155.1 (C5 and C3), 147.1 (C4'), 143.3 (C7 and C1), 129.1 (C8), 124.9 (C1'), 121.1 (C1a and C7a), 115.6 (C2' and C6'), 123.9 (C3' and C5'), 120.4 (C2 and C6), 14.8 (C3Me and C5Me), 14.7 (C1Me and C7Me);  $\delta_{\text{F}}$  (376 MHz,  $\text{CDCl}_3$ ): -146.9 – -146.7 (m);  $\delta_{\text{B}}$  (128 MHz,  $\text{CDCl}_3$ ): 0.79 (t,  $J_{\text{B-F}}$  31);  $m/z$  ( $\text{ES}^+$ ): 340.1787 ( $[\text{M}+\text{H}]^+$   $\text{C}_{19}\text{H}_{21}\text{N}_3\text{BF}_2$  requires 340.1791).

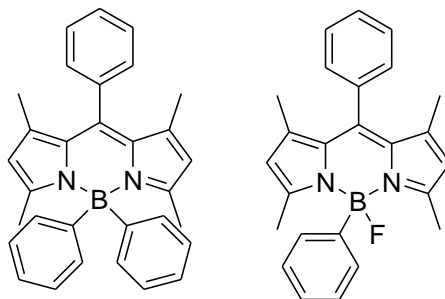
#### 4,4-difluoro-1,3,5,7-tetramethyl-4-bora-3a,4a-diaza-s-indacene, 153



2,4-Dimethylpyrrole (0.21 ml, 2.10 mmol) and formic acid (0.04 ml, 1.05 mmol) were dissolved in DCM (2 ml). To this was added a drop of TFA and the resulting solution was stirred for 2 hours.  $\text{Et}_3\text{N}$  (0.27 ml, 2.84 mmol) and  $\text{BF}_3 \cdot \text{OEt}_2$  (0.36 ml, 2.84 mmol) were added and stirring was continued for 1 hour. Water (10 ml) was added and the aqueous layer separated and extracted with DCM (2 x 10 ml). The combined organic extracts were dried over  $\text{MgSO}_4$ , filtered and concentrated under reduced pressure to

yield a dark orange oil. Flash column chromatography (DCM, silica) gave **153** (2 mg, 0.01%) as an orange solid.  $\lambda_{\max}$  (acetone)/nm:  $\lambda_{\text{ex}}$  503,  $\lambda_{\text{em}}$  508;  $m/z$  (ES<sup>+</sup>): 248.2 [M+H]<sup>+</sup>

**4,4-diphenyl-1,3,5,7-tetramethyl-8-(4-phenyl)-4-bora-3a,4a-diaza-s-indacene, 154** and **4-fluoro-4-phenyl-1,3,5,7-tetramethyl-8-(4-phenyl)-4-bora-3a,4a-diaza-s-indacene, 155**

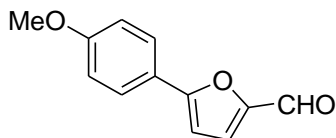


To a stirring solution of **122** (150 mg, 0.46 mmol) in THF (5 ml) was added PhMgBr (2 eq) and the resulting solution was left to stir for 1 hour. Water (10 ml) was added and the aqueous layer separated and extracted with diethyl ether (2 x 20 ml). The combined organic extracts were dried over MgSO<sub>4</sub>, filtered and concentrated under reduced pressure to yield a brown solid. Flash column chromatography (CHCl<sub>3</sub>) gave **154** (35 mg, 8%) as an orange oil and **155** (29 mg, 8%) as an orange oil. Data for **154**:  $\lambda_{\max}$  (acetone)/nm:  $\lambda_{\text{ex}}$  502,  $\lambda_{\text{em}}$  523;  $\delta_{\text{H}}$  (500 MHz, CDCl<sub>3</sub>): 7.59 – 7.61 (3H, m, ArH), 7.43 – 7.48 (4H, m, ArH), 7.32 – 7.34 (5H, m, ArH), 7.19 – 7.24 (3H, m, ArH), 5.92 (2H, s, H2 and H6), 1.78 (6H, s, C3Me and C5Me), 1.39 (6H, s, C1Me and C7Me);  $\delta_{\text{C}}$  (126 MHz, CDCl<sub>3</sub>): 154.7 (C3 and C5), 142.5 (C1 and C7), 141.4 (C8), 140.4 (ArC), 136.2 (ArC), 134.0 (ArC), 131.6 (C1a and C7a), 129.0 (ArC), 128.9 (ArC), 128.9 (ArC), 128.7 (ArC), 128.6 (ArC), 127.4 (ArC), 127.3 (ArC), 127.2 (ArC), 125.8 (ArC), 122.1 (C2 and C6), 17.1 (C1Me and C7Me), 14.9 (C3Me and C5Me);  $\delta_{\text{B}}$  (128 MHz, CDCl<sub>3</sub>): -0.01 (s);  $m/z$  (ES<sup>+</sup>): 440.3 [M+H]<sup>+</sup> (5%), 363.3 [M-Ph]<sup>+</sup> (100).

Data for **155**:  $\lambda_{\max}$  (acetone)/nm:  $\lambda_{\text{ex}}$  503,  $\lambda_{\text{em}}$  523;  $\delta_{\text{H}}$  (700 MHz, CDCl<sub>3</sub>): 7.35 – 7.55 (8H, m, ArH), 7.16 – 7.23 (2H, m, ArH), 5.88 (2H, s, H2 and H6), 2.20 (6H, s, C3Me and C5Me), 1.40 (6H, s, C1Me and C7Me);  $\delta_{\text{C}}$  (176 MHz, CDCl<sub>3</sub>): 155.6 (C3 and C5), 142.1 (C1a and C7a), 141.9 (C1 and C7), 133.2 (ArC), 132.0 (ArC), 131.1 (C8), 129.24 (ArC), 129.18 (ArC), 129.0 (ArC), 128.4 (ArC), 128.3 (ArC), 127.4 (ArC), 127.1 (ArC), 126.3 (ArC), 121.5 (C2 and C6), 15.4 (C1Me and C7Me), 14.6 (C3Me and C5Me);  $\delta_{\text{F}}$  (376 MHz,

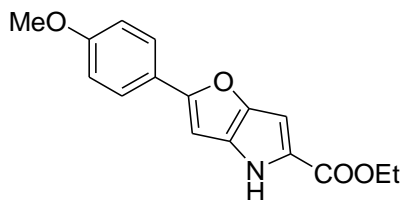
CDCl<sub>3</sub>): -147.4 (br s);  $\delta_B$  (128 MHz, CDCl<sub>3</sub>): 2.96 (br s);  $m/z$  (ES<sup>+</sup>): 382.2 [M+H]<sup>+</sup> (100%), 363.2 [M-HF]<sup>+</sup> (30)

#### 5-(4-Methoxyphenyl)-furan-2-carbaldehyde, **157**



5-Bromo-2-furaldehyde (0.53 g, 3.03 mmol) and 4-methoxyphenylboronic acid (0.46 g, 3.03 mmol) was dissolved in toluene (18 ml), ethanol (4.5 ml) and 2M sodium carbonate (3 ml) and the resulting solution was degassed using the freeze-pump-thaw method. Pd(dppf)<sub>2</sub>Cl<sub>2</sub>.DCM (14 mg, 3% by mass of boronic acid) was added and the reaction mixture heated to 110 °C for 13 hours. This was left to cool to rt, water (30 ml) was added and the aqueous layer separated and extracted with toluene (2 x 30 ml). The combined organic extracts were dried over MgSO<sub>4</sub>, filtered and concentrated under reduced pressure to yield an orange oil. Flash column chromatography, gradient elution (95% hexane/EtOAc to 70% hexane/EtOAc) gave **157** (0.48 g, 80%) as an orange oil.  $\delta_H$  (700 MHz, CDCl<sub>3</sub>): 9.59 (1H, s, CHO), 7.75 - 7.76 (2H, m, AA' part of the AA'XX' system, H2' and H6'), 7.29 (1H, d <sup>3</sup>J 4, furan H), 6.95 - 6.96 (2H, m, XX' part of the AA'XX' system, H3' and H5'), 6.70 (1H, d <sup>3</sup>J 4, furan H), 3.85 (3H, s, OMe);  $\delta_C$  (175 MHz, CDCl<sub>3</sub>): 177.0 (CHO), 161.0 (C4'), 159.9 (C5), 151.8 (C2), 127.1 (C2' and C6'), 121.9 (C1'), 114.6 (C3' and C5'), 106.4 (furan C), 55.5 (OMe);  $m/z$  (ES<sup>+</sup>): 203.0703 ([M+H]<sup>+</sup>, C<sub>12</sub>H<sub>11</sub>O<sub>3</sub> requires 203.0703)

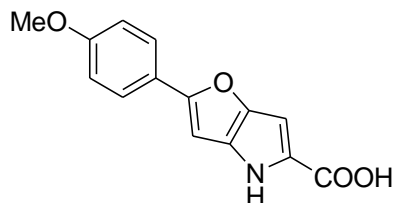
#### Ethyl 2-(4-Methoxyphenyl)-4H-furo[3,2-b]pyrrole-5-carboxylate, **158**



**157** (920 mg, 4.56 mmol) and ethyl azidoacetate (2.4 g, 18.2 mmol) were dissolved in anhydrous EtOH (30 ml) and stirred at 0 °C. A solution of sodium ethoxide (20% weight in EtOH, 1.24 g, 18.2 mmol) was added dropwise and the resulting solution was stirred for 2 hours. Saturated ammonium chloride solution (50 ml) was added and the

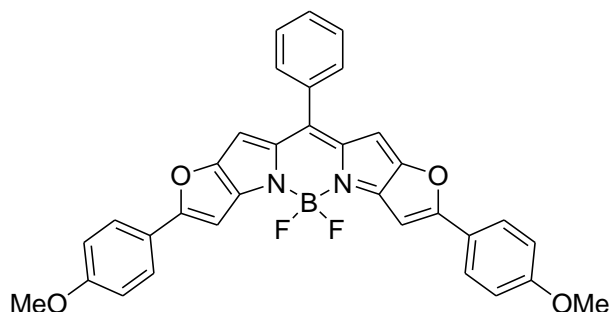
yellow precipitate that formed was collected by centrifugation. This was washed with water and dried. The yellow solid was redissolved in toluene (15 ml) and heated to reflux for 90 minutes. The reaction was cooled to rt and the solvent was removed under reduced pressure to yield an orange oil. Flash column chromatography (25% EtOAc/petroleum ether) gave **158** (342 mg, 26%) as an orange solid. Found: C, 67.80 H, 5.19 N, 4.60; Calc. for C<sub>16</sub>H<sub>15</sub>NO<sub>4</sub>: C, 67.36 H, 5.26 N, 4.91;  $\delta_{\text{H}}$  (500 MHz, CDCl<sub>3</sub>): 9.86 (1H, br s, NH), 7.54 - 7.56 (2H, m, AA' part of the AA'XX' system, H2' and H6'), 6.82 - 6.84 (2H, m, XX' part of the AA'XX' system, H3' and H5'), 6.67 (1H, d <sup>4</sup>J 0.5, H6), 6.49 (1H, s, H3), 4.25 (2H, q <sup>3</sup>J 7, CH<sub>2</sub>), 3.74 (3H, s, OMe), 1.29 (3H, t <sup>3</sup>J 7, CH<sub>3</sub>);  $\delta_{\text{C}}$  (125 MHz, CDCl<sub>3</sub>): 162.0 (C=O), 159.7 (C2), 159.4 (C4'), 147.1 (QC), 130.9 (QC), 125.3 (C2' and C6'), 124.1 (C1'), 123.3 (C5), 114.1 (C3' and C5'), 96.3 (C6), 92.3 (C3), 60.1 (CH<sub>2</sub>), 55.2 (OMe), 14.4 (CH<sub>3</sub>); *m/z* (ES<sup>-</sup>): 284.0926 (M-H<sup>-</sup>, C<sub>16</sub>H<sub>14</sub>NO<sub>4</sub> requires 284.0928)

### 2-(4-Methoxyphenyl)-4H-furo[3,2-*b*]pyrrole-5-carboxylic acid, **159**



**158** (150 mg, 0.53 mmol) was dissolved in EtOH (5 ml). NaOH (316 mg, 7.89 mmol) in water (5 ml) was added and the reaction stirred at reflux for 1.5 hours. The solution was cooled to rt and acidified to pH 1 with HCl. The resulting purple precipitate was collected by centrifugation, washed with water (5 ml), dried and gave **159** (135 mg, 99%) as a grey-purple solid.  $\delta_{\text{H}}$  (500 MHz, d<sup>6</sup>-DMSO): 12.3 (1H, br s, OH), 11.6 (1H, br s, NH), 7.72 - 7.74 (2H, m, AA' part of the AA'XX' system, H2' and H6'), 6.97 - 7.01 (2H, m, XX' part of the AA'XX' system, H3' and H5'), 6.96 (1H, d <sup>4</sup>J 1, H3), 6.70 (1H, dd <sup>4</sup>J 1 and <sup>5</sup>J 0.5, H6), 3.79 (3H, s, OMe);  $\delta_{\text{C}}$  (125 MHz, CDCl<sub>3</sub>): 163.2 (C=O), 159.8 (C4'), 159.4 (C2), 147.1 (QC), 131.3 (QC), 125.9 (C2' and C6'), 124.6 (C5), 124.4 (C1'), 115.1 (C3' and C5'), 96.4 (C6), 94.0 (C3), 55.9 (OMe); *m/z* (ES<sup>-</sup>): 257.1 [M-H]<sup>-</sup>

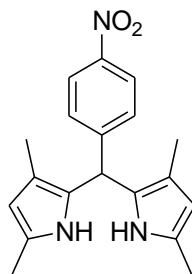
**4,4-difluoro-di(4-methoxyphenyl)-difuro[2,3-*b*]-[3,2-*g*]-8-(4-phenyl)-4-bora-3a,4a-diaza-*s*-indacene, 160**



**159** (200 mg, 0.94 mmol) and benzoyl chloride (88 mg, 0.47 mmol) were stirred in DCM (10 ml) for 2 hours. Et<sub>3</sub>N (0.24 ml, 1.69 mmol) and BF<sub>3</sub>·OEt<sub>2</sub> (0.32 ml, 2.54 mmol) were added and the reaction stirred for 1 hour. Water (20 ml) was added and the aqueous layer was separated and extracted with DCM (2 x 20 ml). The combined organic extracts were dried over MgSO<sub>4</sub>, filtered and concentrated under reduced pressure to yield a green oil. Flash column chromatography (50% DCM/hexane) gave **160** (179 mg, 30%) as a green oil.  $\lambda_{\max}$  (CHCl<sub>3</sub>)/nm:  $\lambda_{\text{ex}}$  678,  $\lambda_{\text{em}}$  687;  $\delta_{\text{H}}$  (500 MHz, CDCl<sub>3</sub>): 7.75 – 7.77 (4H, m AA' part of AA'XX' system, H2' and H6'), 7.56– 7.59 (2H, m, ArH), 7.51 – 7.55 (3H, m, ArH), 6.97 – 6.99 (4H, m XX' part of AA'XX' system, H3' and H5'), 6.87 (2H, s, H6), 6.25 (2H, s, H3), 3.88 (6H, s, OMe);  $\delta_{\text{C}}$  (126 MHz, CDCl<sub>3</sub>): 168.0 (C4'), 161.5 (QC), 149.8 (QC), 145.3 (QC), 131.1 (QC), 130.8 (QC), 129.8 (ArC), 129.3 (ArC), 129.0 (ArC), 128.4 (ArC), 127.3 (C2' and C6'), 126.7 (ArC), 122.8 (C1'), 118.6 (QC), 114.7 (C3' and C5'), 103.1 (C6), 94.2 (C3), 55.6 (OMe);  $\delta_{\text{F}}$  (376 MHz, CDCl<sub>3</sub>): -146.9 - -146.7 (m);  $m/z$  (ES<sup>+</sup>): 561.3 [M+H]<sup>+</sup>



## 1,3,5,7-tetramethyl-8-(4-nitrophenyl)-dipyrromethane, **162**



TFA (0.27 mmol, 0.02 ml) was added to a stirred solution of 4-nitrobenzaldehyde (300 mg, 1.99 mmol) and 2,4-dimethylpyrrole (0.42 ml, 4.17 mmol) in DCM (10 ml). The resulting solution was stirred for 10 minutes. Water (20 ml) was added and the aqueous layer separated and extracted with DCM (2 x 20 ml). The combined organic extracts were dried over MgSO<sub>4</sub>, filtered and concentrated under reduced pressure to yield a brown oil. Flash column chromatography (DCM) gave **162** (410 mg, 64%) as a brown solid.  $\delta_{\text{H}}$  (500 MHz, CDCl<sub>3</sub>): 8.13 – 8.15 (2H, m, AA' part of the AA'XX' system, H3' and H5'), 7.32 – 7.34 (2H, m, XX' part of the AA'XX' system, H2' and H6'), 5.75 (2H, s, H2 and H6), 5.55 (2H, s, NH), 2.19 (6H, s, Me), 1.83 (6H, s, Me);  $\delta_{\text{C}}$  (126 MHz, CDCl<sub>3</sub>): 152.6 (C5 and C3), 148.0 (C4'), 145.3 (C7 and C1), 139.7 (C8), 135.7 (C1'), 135.5 (C1a and C7a), 130.8 (C2' and C6'), 123.9 (C3' and C5'), 120.4 (C2 and C6), 16.2 (C3Me and C5Me), 15.0 (C1Me and C7Me);  $m/z$  (ES<sup>+</sup>): 324.4 [M+H]<sup>+</sup>

## 7.2 Biology

### 7.2.1 General Procedures

#### Flow Cytometry

Flow cytometric analysis and sorting was conducted using a Beckman Coulter MoFlo multi-laser flow cytometer operating at 60 psi and a 70  $\mu\text{m}$  nozzle. Samples were interrogated with a 100 mW, 488 nm solid state laser. Fluorescence signals were detected and collected through the FL1 (530/40) and FL2 (580/30) interference filter in logarithmic mode. The data were analysed using Summit v4.3 (Beckman Coulter) software.

## **Confocal Microscopy**

The samples were observed using a Zeiss 510 inverted confocal microscope, with an Argon/Krypton laser, equipped with a Plan-Neofluor 40x 1.3 oil immersion objective. 127 fluorescence was imaged using excitation with a 488 nm laser, coupled with a 505–530 nm band pass filter and mCherry fusions were imaged using a 543 nm laser with a 650-nm-long pass filter. For each fluorophore combination, controls lacking each fluorophore in turn confirmed negligible channel crosstalk and autofluorescence (except from chloroplasts). Images were edited with Zeiss LSM Image Browser.

## **FlashScan Kinetic Analysis**

Enzymatic kinetic analysis was performed using a FlashScan 550 (Analytik Jena AG). The data were analysed using WinFLASH (Analytik Jena AG) software.

## **Site-Directed Mutagenesis and Error-prone Polymerase Chain Reaction**

All PCR reactions were undertaken in a ThermoHybaid PCR Sprint thermocycler (Thermo Scientific) or an Eppendorf Mastercycler Gradient using standard PCR tubes.

## **Primer Design and DNA Sequencing**

Primers were supplied by MWG Biotech, Ebersberg, Germany and sequencing was performed by DBS Genomics, Durham, UK or GATC Biotech AG, Konstanz, Germany.

## **Protein analysis *via* SDS-PAGE**

SDS-PAGE gels were ran using a Mini-PROTEAN® 3 cell system (BioRad) and analysed using fluorescent imaging on a Gel Doc™ EQ system (BioRad), using Quantity One® 1-D Analysis software.

## 7.2.2 Experimental detail

### Isolation of protoplasts from *Arabidopsis thaliana* leaves

Driselase from *Basidiomycetes* sp. (100 mg), cellulase from *Aspergillus niger* (30 mg), pectinase from *Rhizopus* sp. (20 mg),  $\text{CaCl}_2 \cdot 2\text{H}_2\text{O}$  (7.5 mg) and sucrose (1.75 g) were dissolved in  $\text{dH}_2\text{O}$  (10 ml). Small leaves were removed from an *At* plant, using a scalpel, approximately 2 months after seeding. Plant material (~200 mg) was placed into above enzyme solution (2.5 ml) and left at rt for 24 hours. The enzyme solution was removed and placed into an eppendorf tube. The contents were allowed to settle for 30 minutes during which time the protoplasts floated to the top. These were drawn off and placed into an eppendorf tube containing 10 mM sucrose. This was repeated and the concentration of protoplasts determined using a haemocytometer. Concentrations were typically in the range of  $3 \times 10^5$  protoplasts/ml

### Isolation of protoplasts from *Arabidopsis thaliana* cell cultures

Driselase from *Basidiomycetes* sp. (100 mg), cellulase from *Aspergillus niger* (30 mg), pectinase from *Rhizopus* sp. (20 mg),  $\text{CaCl}_2 \cdot 2\text{H}_2\text{O}$  (7.5 mg) and sucrose (1.75 g) were dissolved in  $\text{dH}_2\text{O}$  (10 ml). Protoplasts were harvested from *At* 5 days after being subcultured. The cell culture suspension was filtered through nylon mesh, washed with distilled water and dried to form a yellow powder. This was placed in the above enzyme solution (2.5 ml) and left at rt for 24 hours. The enzyme solution was removed and placed into an eppendorf tube. The contents were allowed to settle for 30 minutes during which time the protoplasts floated to the top. These were drawn off and placed into an eppendorf tube containing 10 mM sucrose. This was repeated and the concentration of protoplasts determined using a haemocytometer. Concentrations were typically in the range of  $3 \times 10^5$  protoplasts/ml

### Protein extraction from *Arabidopsis thaliana*

5 g of *At* leaves were ground to a fine powder in a pestle and mortar containing liquid  $\text{N}_2$  and sand. A cold solution of Tris buffer (20 ml, 0.1 M, pH 7.4), EDTA (200  $\mu\text{L}$ , 5 mM), DTT (40  $\mu\text{L}$ , 2mM) and PVPP (1 g) was added and the leaves were further ground up. The suspension was sieved through fabric filter paper to remove large debris and the resulting suspension was centrifuged (10 minutes, 10,000 RCF). The



The remainder of the construct was synthesised using the high-fidelity DNA polymerase Phusion (Finnzymes). The PCR mixture consisted of 250 ng megaprimer, 500 ng *AtCXE12* template, 0.25  $\mu$ M each dNTP, 5  $\mu$ L *Pfu* buffer, sterile dH<sub>2</sub>O up to a final volume of 50  $\mu$ L and 1  $\mu$ L Phusion. The cycling parameters were 95 °C for 2 mins, 26 cycles of 95 °C for 35 sec, 55 °C for 40 sec and 69 °C for 6 mins. Mutants obtained by PCR were purified with a QIAquick PCR purification kit (Qiagen). DpnI digestion was undertaken on 20  $\mu$ L of the purified PCR mixture, with the addition of 1  $\mu$ L DpnI, 3  $\mu$ L Tango buffer and 6  $\mu$ L sterile dH<sub>2</sub>O. This mixture was incubated at 37 °C for 4 hours. The resulting mutated plasmid library was isolated from *E. coli* XL10 (Stratagene) cells.

### **Bacterial transformation**

Amplification of plasmid DNA was achieved by transforming competent *E. coli* XL-10 ultracompetent cells (Stratagene). 1  $\mu$ L of the appropriate plasmid was added to 20  $\mu$ L of competent cells and incubated on ice for 5 mins. The cells were then heat shocked for 30 secs at 42 °C and placed back on ice for 2 mins. 80  $\mu$ L LB media was added and cells were incubated at 37 °C with shaking at 270 rpm, for 1 hour. Competent cells were plated onto agar plates containing the appropriate antibiotic and incubated overnight at 37 °C.

### **Protein expression**

Following transformation of *E. coli* tuner(DE3)pRARE cells (Novagen) cultures were grown to an OD (measured at 600 nm) of 0.6 at 37 °C, then cooled to 10 °C prior to induction with IPTG (100  $\mu$ L, 1 mM). Following growth at 37 °C for 2 hours, bacteria were pelleted and resuspended in a solution of 20 mM Tris/0.5 M NaCl/20 mM imidazole (5 ml) and sonicated for 30 secs. Recombinant His-tagged proteins were then purified by nickel-chelate affinity chromatography.<sup>92</sup>

### **Site-directed mutagenesis**

The *atcx12* gene contained in the pET24d vector was isolated from *E. coli* XL10 (Stratagene) ultracompetent cells using the QIAprep Spin Miniprep kit (Qiagen) and used as a template for site-directed mutagenesis with the *Pfu* ultra DNA polymerase (Stratagene). All reactions were carried out with the primer pair Y198AF (5'-GGAATCATCTTGCTTCATCCTGCCTTCTGGTCGAAAACA-3') and Y198AR (5'-

GGTGTTCGACCAGAAGGCAGGATGAAGCAAGATGATTCC-3'). The cycling parameters were 95 °C for 1 mins, 17 cycles of 95 °C for 50 sec, 60 °C for 50 sec and 68 °C for 6 mins 10 secs and a final cycle of 95 °C for 50 sec, 60 °C for 50 sec and 68 °C for 7 mins. The *Pfu* ultra PCR mixture contained 0.25 µM each dNTP, 50 ng *atcxe12* template, 5 µL 10x reaction buffer, 100 ng of each primer, sterile dH<sub>2</sub>O up to a final volume of 50 µL and 1 µL of *Pfu* ultra. DpnI digestion was undertaken on 20 µL of the PCR mixture, with the addition of 0.5 µL DpnI. This mixture was incubated at 37 °C for 1 hour. The resulting mutated plasmid was isolated from Top 10 (Invitrogen) competent cells.

### **DNA Cloning - Digestion and Ligation**

DNA fragments to be ligated were prepared by digestion with the appropriate restriction enzyme (1 µL) at 37 °C for 2.5 hours. Fragments were separated by electrophoresis and following excision from the gel were purified using the QIAquick Gel Extraction kit (QIAGEN).

### ***Agrobacterium tumefaciens* transformation and infiltration**

Amplification of plasmid DNA was achieved by transforming *Agrobacterium* cells. 1 µL of the appropriate plasmid was added to 20 µL of *Agrobacterium* cells. The cells were electroporated (2400 V, Gene Pulser Xcell, Bio-Rad) and 250 µL prechilled LB media was immediately added. Cells were incubated at 28 °C for 2 hours. 100 µL was plated onto agar plates containing kanamycin, rifampicin and gentamycin and incubated at 28 °C for 2 days.

A single colony was incubated overnight in LB media at 28 °C. Cultures were mixed 1:1 with similarly prepared cultures containing the construct 35S:p19, to provide co-expression of the tomato bushy stunt virus p19 protein. The resulting suspension was centrifuged (3 minutes, 10,000 RCF) and the pellet resuspended in dH<sub>2</sub>O. Underside of *Nicotiana benthamiana* leaves were infiltrated using a 1 mL syringe filled with solution. Transformed leaf tissue were harvested 4 days later and used immediately for imaging. For co-localization studies, similar *A. tumefaciens* cultures containing the constructs px-rk for labelling of peroxisomes<sup>206</sup>, were co-infiltrated with **127**. This construct expressed the red fluorescent protein mCherry, with a C-terminal SKL motif added for peroxisomal targeting. 1 hour prior to imaging, transformed leaves were infiltrated

with a solution of **127** (5  $\mu\text{M}$  in  $\text{dH}_2\text{O}$ ) and subsequently analysed by confocal microscopy.

---

## 8 REFERENCES

- <sup>1</sup> Eijsink V. G. H., Gåseidnes S., Borchert T. V. and van den Burg B., *Biomolecular Engineering*, 2005, **23**, 21 – 30
- <sup>2</sup> Alexeeva M., Carr R. and Turner N. J., *Org. Biomol. Chem.*, 2003, **1**, 4133 – 4137
- <sup>3</sup> Reetz M. T., Brunner B., Schneider T., Schulz F., Clouthier C. M. and Kayser M. M., *Angew. Chem., Int. Ed.*, 2004, **43**, 4075 – 4078
- <sup>4</sup> Reetz M. T., *Tetrahedron*, 2002, **58**, 6595 – 6602
- <sup>5</sup> Peters M. W., Meinhold P., Glieder A. and Arnold F. H., *J. Am. Chem. Soc.*, 2003, **125**, 13442 – 13450
- <sup>6</sup> Cline J., Braman J. C. and Hogrefe H. H., *Nuc. Acid Res.*, 1996, **24**, 3546 – 3551
- <sup>7</sup> Zaccolo M., Williams D. M., Brown D. M. and Gheradi E., *J. Mol. Biol.*, 1996, **225**, 589 – 603
- <sup>8</sup> Shafikhani S., Siegel R. A., Ferrari E. and Schellenberger V., *Biotechniques*, 1997, **23**, 304 – 310
- <sup>9</sup> Hogrefe H. H. and Cline J. M., *US Pat.* 6 803 216, 2002
- <sup>10</sup> Liebeton K., Zonta A., Schimossek K., Nardini M., Lang D., Dijkstra B. W., Reetz M. T. and Jaeger K-E., *Chem. Biol.*, 2000, **7**, 709 – 718
- <sup>11</sup> Zha D., Wilensek S., Hermes M., Jaeger K-E. and Reetz M. T., *Chem. Commun.*, 2001, 2664 – 2665
- <sup>12</sup> (a) Stemmer W. P., *Nature*, 1994, **370**, 389 – 391; (b) Stemmer W. P., *Proc. Natl. Acad. Sci. USA*, 1994, **91**, 10747 – 10751
- <sup>13</sup> Shao Z. Zhao H., Giver L. and Arnold F. H., *Nucleic Acid Res.*, 1998, **26**, 681 – 684
- <sup>14</sup> Otten L. G. and Quax W. J., *Biomolecular Engineering*, 2005, **22**, 1 – 9
- <sup>15</sup> Zhao H., Giver L., Shao Z., Affholter J. A. and Arnold F. H., *Nat. Biotech.*, 1998, **16**, 258 – 261
- <sup>16</sup> Coco W. M., Levinson W. E., Crist M. J., Hektor H. J., Darzins A., Pienkos P. T., Squires C. H. and Monticello D. J., *Nat. Biotech.*, 2001, **19**, 354 – 359
- <sup>17</sup> Ostermeier M., Shim J. H. and Benkovic S. J., *Nat. Biotech.*, 1999, **17**, 1205 – 1209
- <sup>18</sup> Sieber V., Martinez C. A. and Arnold F. H., *Nat. Biotech.*, 2001, **19**, 456 – 460
- <sup>19</sup> Hiraga K. and Arnold F. H., *J. Mol. Biol.*, 2003, **330**, 287 – 296
- <sup>20</sup> Berquist P. L., Reeves R. A. and Moreland M. D., *Biomolecular Engineering*, 2005, **22**, 63 – 72



- 
- <sup>21</sup> Gibbs M. D., Nevalainen K. M. H. and Bergquist P. L., *Gene*, 2001, **271**, 13 – 20
- <sup>22</sup> Abécassis V., Pompon D. and Truan G., *Nuc. Acid. Res.*, 2000, **28**, e88
- <sup>23</sup> Ness J. E., Kim S., Gottman A., Pak R., Krebber A., Borchert T. V., Govindarajan S., Mundorff E. C. and Minshull J., *Nat. Biotech.*, 2002, **20**, 1251 – 1255
- <sup>24</sup> Zhao H. and Arnold F. H., *Curr. Opin. Struct. Biol.*, 1997, **7**, 480 – 485
- <sup>25</sup> Bornscheuer U. T., Altenbuchner J. and Meyer H. H., *Bioorg. & Med. Chem.*, 1999, **7**, 2169 – 2173
- <sup>26</sup> Zocher F., Enzelberger M. M., Bornscheuer U. T., Hauer B. and Schmid R. D., *Anal. Chim. Acta*, 1999, **391**, 345 – 351
- <sup>27</sup> Copeland G. T. and Miller S. J., *J. Am. Chem. Soc.*, 1999, **121**, 4306 – 4307
- <sup>28</sup> Janes L. E. and Kazlauskas R. J., *J. Org. Chem.*, 1997, **62**, 4560 – 4561
- <sup>29</sup> Reetz M. T., Zonta A., Schimossek K. and Jaeger K-E., *Angew. Chem. Int. Ed.*, 1997, **36**, 2830 – 2832
- <sup>30</sup> Holzwarth A., Schmidt H-W. and Maier W. F., *Angew. Chem. Int. Ed.*, 1998, **37**, 2644 – 2647
- <sup>31</sup> Reetz M. T., Becker M. H., Kühling K. M. and Holzwarth A., *Angew. Chem. Int. Ed.*, 1998, **37**, 2647 – 2650
- <sup>32</sup> Horswill A. R., Savinov S. N. and Benkovic S. J., *Proc. Natl. Acad. Sci.*, 2004, **101**, 15591 – 15596
- <sup>33</sup> Lin H., Abida W. M., Sauer R. T. and Cornish V. W., *J. Am. Chem. Soc.*, 2000, **122**, 4247 – 4248
- <sup>34</sup> Baker K., Bleczinski C., Lin H., Salazar-Jimenez G., Sengupta D., Krane S. and Cornish V. W., *Proc. Natl. Am. Soc.*, 2002, **99**, 16537 – 16542
- <sup>35</sup> Lin H., Tao H. and Cornish V. W., *J. Am. Chem. Soc.*, 2004, **126**, 15051 – 15059
- <sup>36</sup> Practical Flow Cytometry, 4th Ed., Shapiro H. M., Wiley-Liss, 2003, 1
- <sup>37</sup> Van Antwerp J. J. and Wittrup K. D., *Biotechnol. Prog.*, 2000, **16**, 31 – 37
- <sup>38</sup> Boder E. T., Midelfort K. S. and Wittrup K. D., *Proc. Natl. Acad. Sci.*, 2000, **97**, 10701 – 10705
- <sup>39</sup> Farinas E. T., Bulter T. and Arnold F. H., *Curr. Opin. Biotech.*, 2001, **12**, 545 – 55
- <sup>40</sup> Griffiths A. D. And Tawfik D. S., *EMBO J.*, 2003, **22**, 24 – 35
- <sup>41</sup> Chen I. and Dubnau D., *Nat. Rev. Microbiol.*, 2004, **2**, 241 – 249
- <sup>42</sup> Sheen J., *Plant Physiol.*, 2001, **127**, 1466 – 1475
- <sup>43</sup> Yoo S-D., Cho Y-H. and Sheen J., *Nature Protocols*, 2007, **2**, 1565 – 1572
- <sup>44</sup> Cocking E. C., *Nature*, 1970, **187**, 927 – 929
- <sup>45</sup> Abel S. and Theologis A., *Plant Physiol.*, 1996, **111**, 9 – 17

- 
- 46 Hamilton D. W., Hills A., Kohler B. and Blatt M. R., *Proc. Natl. Acad. Sci. USA*, 2000, **97**, 4967 – 4972
- 47 Bethke P. C. and Jones R. I., *Plant J.*, 2001, **25**, 19 – 29
- 48 Kao K. N., Keller W. A. and Miller R. A., *Exp. Cell. Res.*, 1970, **62**, 338 – 340
- 49 Ruiz-Díez B., *J. Appl. Microbiol.*, 2002, **92**, 189 – 195
- 50 Lindsey K. and Jones M. G. K., *Physiol. Plant.*, 1990, **79**, 168 – 172
- 51 Negrutiu I., Shillito R., Potrykus I., Biasini G. and Sala F., *Plant Mol. Biol.*, 1987, **8**, 363 – 373
- 52 Karesch H., Bilanz O., Scheld O. M. and Potrykus I., *Plant Cell Rep.*, 1991, **9**, 571 – 574
- 53 Köhler F., Cardon G., Pöhlman M., Gill R. and Schieder O., *Plant Mol. Biol.*, 1989, **12**, 189 – 199
- 54 Radchuk V. V., Ryschka U., Schumann G. and Klocke E., *Physiol. Plant.*, 2002, **114**, 429 – 438
- 55 Tiwari V. K., Zhang J., Golds T. J., Cocking E. C., Davey M. R. and Power J. B., *Biologia Plantarum*, 2001, **44**, 25 – 31
- 56 Meyer V., Mueller D., Strowig T. and Stahl U., 2003, *Curr. Genet.*, **43**, 371 – 377
- 57 Fromm M. E., Taylor L. P. and Walbot W., *Nature*, 1987, **319**, 791 – 793
- 58 Sanford J. C., *Physiol. Plant.*, 1990, **79**, 206 – 209
- 59 Wang Y. C., Klein T. M., Fromm M. Cao J. and Sanford J. C., *Plant Mol. Biol.*, 1988, **11**, 433 – 439
- 60 Christou P., McCabe D. E. and Swain W. F., *Plant Physiol.*, 1988, **87**, 671 – 674
- 61 Smith E. F. and Townsend C. D., *Science*, 1907, **25**, 671 – 673
- 62 de la Riva G. A., González-Cabrera J., Vázquez-Padrón R. and Ayra-Pardo C., *Electronic J. Biotech.*, 1998, **1**, 118 – 133
- 63 Torisky R. S., Kovacs L., Avdiushko S., Newman J. D., Hunt A. G. and Collins G. B., *Plant Cell Reports*, 1997, **17**, 102 – 108
- 64 Evans M. J. and Cravatt B. F., *Chem. Rev.*, 2006, **106**, 3279 – 3301
- 65 Dijkstra H. P., Sprong H., Aerts B. N. H., Kruithof C. A., Egmond M. R. and Klein Gebbink R. J. M., *Org. Biomol. Chem.*, 2008, **6**, 523 – 531
- 66 Greenbaum D., Medzihradzsky K. F., Burlingame A. and Bogyo M., *Chem. Biol.*, 2000, **7**, 569 – 581
- 67 Thornberry N. A., Peterson E. P., Zhao J. J., Howard A. D., Griffin P. R. and Chapman K. T., *Biochem.*, 1994, **33**, 3934 – 3940
- 68 Kurogochi M., Nishimura S. and Lee Y. C., *J. Biol. Chem.*, 2004, **279**, 44704 – 44712

- 
- <sup>69</sup> Chan E. W. S., Chattopadhyaya S., Panicker R. C., Huang X. and Yao S. Q., *J. Am. Chem. Soc.*, 2004, **126**, 14435 - 14446
- <sup>70</sup> Jeffery D. A. and Bogyo M., *Curr. Opin. Biotech.*, 2003, **14**, 87 - 95
- <sup>71</sup> Liau M-L., Panicker R. C. and Yao S. Q., *Tet. Lett.*, 2003, **44**, 1043 - 1046
- <sup>72</sup> Meyer Y., Richard J-A., Massonneau M., Renard P-Y. and Romleu A., *Org. Lett.*, 2008, **10**, 1517 - 1520
- <sup>73</sup> Kessler B. M., Tortorella D., Altun M., Kisselev A. F., Fiebiger E., Hekking B. G., Ploegh H. L. and Overkleeft H. S., *Chem. Biol.*, 2001, **8**, 913 - 929
- <sup>74</sup> Matthews C. M. E. *Phys. Med. Biol.*, 1960, **5**, 45 - 47
- <sup>75</sup> Wilchek M. and Bayer E. A., *Methods Enzymol.*, 1990, **184**, 5 - 13
- <sup>76</sup> Liu Y., Patricelli M. P. and Cravatt B. F., 1999, *Proc. Natl. Acad. Sci. USA*, **96**, 14694 - 14699
- <sup>77</sup> Borodovsky A., Ovaia H., Kolli N., Gan-Erdene T., Wilkinson K. D., Ploegh H. L. and Kessler B. M., *Chem. Biol.*, 2002, **9**, 1149 - 1159
- <sup>78</sup> Sadaghiani A. M., Verhelst S. H. L. and Bogyo M., *Curr. Opin. Chem. Biol.*, 2007, **11**, 20 - 28
- <sup>79</sup> Greenbaum D., Baruch A., Hayrapetian L., Darula Z., Burlingame A., Medzihradszky K. F. and Bogyo M., *Mol. Cell. Proteomics*, 2002, **1**, 60 - 68
- <sup>80</sup> Patricelli M. P., Giang D. K., Stamp L. M. and Burbaum J. J., *Proteomics*, 2001, **1**, 1067 - 1071
- <sup>81</sup> Adam G. C., Sorensen E. J. and Cravatt B. F., *Mol. Cell. Proteomics*, 2002, **1**, 828 - 835
- <sup>82</sup> Kolb H. C., Finn M. G. and Sharpless K. B., *Angew. Chem. Int. Ed.*, 2001, **40**, 2004 - 2021
- <sup>83</sup> Speers A. E., Adam G. C. and Cravatt B. F., *J. Am. Chem. Soc.*, 2003, **125**, 4686 - 4687
- <sup>84</sup> Cummins I., Steel P. G. and Edwards R., *Plant Biotech. J.*, 2007, **5**, 354 - 359
- <sup>85</sup> Cummins I., McAuley K., Fordham-Skelton A., Schwoerer R., Steel P. G., Davis B. P. and Edwards R., *J. Mol. Biol.*, 2006, **359**, 422 - 432
- <sup>86</sup> Hanson A. D., Gage D. A. and Shachar-Hill Y., *Trends Plant Sci.*, 2000, **5**, 206-213
- <sup>87</sup> Hell R. and Bergmann L., *Planta*, 1990, **180**, 603 - 612
- <sup>88</sup> Marrs K. A., *Annu. Rev. Plant Physiol. Plant Mol. Biol.*, 1996, **47**, 127-158
- <sup>89</sup> Xiang C., Werner B. L., Christensen E. M. and Oliver D. J., *Plant Physiology*, 2001, **126**, 564-574
- <sup>90</sup> Uotila L., *Hum. Hered.*, 1984, **34**, 273 - 277
- <sup>91</sup> Harms N., Ras J., Reijnders W. N. M., van Spanning R. J. M. and Stouthamer A. H., *J. Bacteriol.*, 1996, **178**, 6296 - 6299
- <sup>92</sup> Kordic S., Cummins I. and Edwards R., *Arch. Biochem. Biophys.*, 2002, **399**, 232-238

- 
- <sup>93</sup> Uotila L. and Koivusalo M., *J. Biol. Chem.*, 1974, **249**, 7664 – 7672
- <sup>94</sup> McAuley K. E. and Fordham-Skelton A. P., CLRC, Daresbury Library
- <sup>95</sup> Cummins I., Landrum M., Steel P. G. and Edwards R., 2007, *Phytochemistry*, **68**, 811 – 818
- <sup>96</sup> *Organic Chemistry*, Clayden J., Greeves N., Warren S. and Wothers P., OUP, 2001, 669
- <sup>97</sup> Snieckus V., *Chem. Rev.*, 1990, **90**, 879 - 933
- <sup>98</sup> Pfeffer P. E., Silbert L. S. and Chirinko J. M., *J. Org. Chem.*, 1972, **37**, 451-458
- <sup>99</sup> Foder P. J., Price V. E. and Greenstein J. P., *J. Biol. Chem.*, 1950, **182**, 467 – 470
- <sup>100</sup> Walter C. and Frieden E., *Adv. Enzymol. Relat. Areas Mol. Biol.*, 1963, **25**, 167 – 274
- <sup>101</sup> Van den Ende W. and Van Laere A., *New Phytol.*, 1993, **123**, 31 – 37
- <sup>102</sup> Redinbo M. R. and Potter P. M., *Drug Discovery Today*, 2005, **71**, 178 – 189
- <sup>103</sup> Heikinheimo P., Goldman A., Jeffries C. and Ollis D. L., *Structure*, 1999, **7**, R141 – R146
- <sup>104</sup> Provencher L. and Jones J. B., *J. Org. Chem.*, 1994, **59**, 2729 – 2732
- <sup>105</sup> Aubin J. B., *J. Histochem. Cytochem.*, 1979, **27**, 36 – 43
- <sup>106</sup> Rotman B. and Papermaster B. W., *Biochem.*, 1965, **55**, 134 – 141
- <sup>107</sup> Kitahata N., Nakano T., Kuchitsu K., Yoshida S. and Asami T., *Bioorg. Med. Chem.*, 2005, **13**, 3351 – 3358
- <sup>108</sup> Kadota Y., Watanabe T., Fujii S., Higashi K., Sano T., Nagata T., Hasezawa S. and Kuchitsu K., *Plant J.*, 2004, **40**, 131 – 142
- <sup>109</sup> Alberti S., Parks D. R. and Herzenberg L. A., *Cytometry*, 1987, **8**, 114 – 119
- <sup>110</sup> Ollis D. L., Cheah E., Cygler M., Dijkstra B., Frolow F., Franken S. M., Harel M., Remington S. J., Silman I., Schrag J., Sussman J. L., Verschueren K. H. G. and Goldman A., *Protein Eng.*, 1992, **5**, 197 – 211
- <sup>111</sup> Marshall S. D. G., Putterill J. J., Plummer K. M. and Newcomb R. D., *J. Mol. Evol.*, 2003, **57**, 487 – 500
- <sup>112</sup> Bukowska B., Kopka A., Michałowicz J. and Duda W., *Environ. Toxicol. Pharmacol.*, 2006, **22**, 189 – 193
- <sup>113</sup> Gershater M. C., Cummins I. and Edwards R., *J. Biol. Chem.*, 2007, **282**, 21460 – 21466
- <sup>114</sup> Wei Y., Contreras J. A., Sheffield P., Osterlund T., Derewenda U., Kneusel R. E., Matern U., Holm C. and Derewenda Z. S., *Nature Structural Biol.*, 1999, **6**, 340 – 345
- <sup>115</sup> Østerland T., Danielsson B., Degerman E., Contreras J. A., Edgren G., David R. C., Schotz M. C. and Holm C., *Biochem. J.*, 1996, **319**, 411 – 420
- <sup>116</sup> <http://scratch.proteomics.ics.uci.edu/>
- <sup>117</sup> Biles B. D. and Connolly B. A., *Nuc. Acid Res.*, 2004, **32**, e176
- <sup>118</sup> Kong H., Kucers R. B. and Jack W. E., *J. Biol. Chem.*, 1993, **268**, 1965 – 1975

- 
- <sup>119</sup> Franklin M. C., Wang J. and Steitz T. A., *Cell*, 2001, **105**, 657 - 667
- <sup>120</sup> Evans S. J., Fogg M. J., Mamone A., Davis M., Pearl L. H. and Connolly B. A., *Nuc. Acids Res.*, 2000, **28**, 1059 - 1066
- <sup>121</sup> Sagner G., Rüger R. and Kessler C., *Gene*, 1991, **97**, 119 - 123
- <sup>122</sup> Provost G. S., Kretz P. L., Hamner R. T., Matthews C. D., Rogers B. J., Lundberg K. S., Dyaico M. J. and Short J. M., *Mutat. Res.*, 1993, **288**, 133 - 149
- <sup>123</sup> Kunkel T. A. and Bebenek K., *Annu. Rev. Biochem.*, 2000, **69**, 497 - 529
- <sup>124</sup> Kunkel T. A., *J. Biol. Chem.*, 2004, **279**, 16895 - 16898
- <sup>125</sup> Senn A. M. and Wolosiuk R. A., *Anal. Biochem.*, 2005, **339**, 150 - 156
- <sup>126</sup> Taekda A., Sugiyama K., Nagano H., Mori M., Kaido M., Mise K., Tsuda S. and Okuno T., *FEBS Letters*, 2002, **532**, 75 - 79 (and references therein)
- <sup>127</sup> Li H., Li W. X. and Ding S. W., *Science*, 2002, **296**, 1319 - 1321
- <sup>128</sup> Tsai C-S., Li Y-K. and Lo L-C., *Org. Lett.*, 2002, **4**, 3607 - 3610
- <sup>129</sup> Lo L-C., Lo C-H. L., Janda K. D., Kassel D. B. and Raushel F. M., *Bioorg. & Med. Chem. Lett.*, 1996, **6**, 2117 - 2120
- <sup>130</sup> Zhu Q., Huang X., Chen G. Y. J. and Yao S. Q., *Tet. Lett.*, 2003, **44**, 2669 - 2672
- <sup>131</sup> Komatsu T., Kikuchi K., Takakusa H., Hanaoka K., Ueno T., Kamiya M., Urano Y. and Nagano T., *J. Am. Chem. Soc.*, 2006, **128**, 15946 - 15947
- <sup>132</sup> Blum G., Mullins S. R., Keren K., Fonovič M., Jedeszko C., Rice M. J., Sloane B. F. and Bogyo M., *Nat. Chem. Biol.*, 2005, **1**, 203 - 209
- <sup>133</sup> Blum G., von Degenfeld G., Merchant M. J., Blau H. M. and Bogyo M., *Nat. Chem. Biol.*, 2007, **3**, 668 - 677
- <sup>134</sup> Lah T. T., Čerček M., Blejec A., Kos J., Gorodetsky E., Somers R. and Daskal I., *Clin. Cancer Res.*, 2000, **6**, 578 - 584
- <sup>135</sup> a) Boyall D., Frantz D. E. and Carreira E. M., *Org. Lett.*, 2002, **4**, 2605 - 2606; b) Frantz D. E., Fassler R. and Carreira E. M., *J. Am. Chem. Soc.*, 2000, **122**, 1806 - 1807; c) Anand N. K. and Carreira E. M., *J. Am. Chem. Soc.*, 2001, **123**, 9687 - 9688; d) Knöpfel T. F., Zarotti P., Ichikawa T. and Carreira E. M., *J. Am. Chem. Soc.*, 2005, **127**, 9682 - 9683
- <sup>136</sup> Vestling M. M., Murphy C. M. and Fenselau C., *Anal. Chem.*, 1990, **62**, 2391 - 2394
- <sup>137</sup> Wang H., Wahi M. S. and Rokita S. E., *Angew. Chem. Int. Ed.*, 2008, **47**, 1291 - 1293
- <sup>138</sup> Weinert E. E., Dondi R., Colloredo-Melz S., Frankenfield K. M., Mitchell C. H., Freccero M. and Rokita S. E., *J. Am. Chem. Soc.*, 2006, **128**, 11940 - 11947
- <sup>139</sup> Zhou Q. and Turnbull K. D., *J. Org. Chem.*, 2001, **66**, 7072 - 7077
- <sup>140</sup> Tracy T. S., Marra C., Wrighton S. A., Gonzalez F. J. and Korzekwa K. R., *Eur. J. Clin. Pharmacol.*, 1997, **52**, 293 - 298

- 
- <sup>141</sup> Stresser D. M. and Kupper D., *Drug Metab. Dispos.*, 1998, **26**, 868 – 874
- <sup>142</sup> Mathijssen R. H. J. and van Schaik R. H. N., *Eur. J. Cancer*, 2006, **42**, 141 – 148
- <sup>143</sup> Kumar G. N., Rodrigues A. D., Buko A. M. and Denissen J. F., *J. Pharmacol. Exp. Ther.*, 1996, **277**, 423 – 431
- <sup>144</sup> Kim D. and Guengerich F. P., *Arch. Biochem. Biophys.*, 2004, **432**, 102 – 108
- <sup>145</sup> Ortiz de Montellano P. R. and De Voss J. J., *Nat. Prod. Res.*, 2002, **19**, 477 – 493
- <sup>146</sup> McOmie J. F. W., Watts M. L. and West D. E., *Tetrahedron*, 1968, **24**, 2289 – 2292
- <sup>147</sup> Majetich G., Zhang Y. and Wheless K., *Tet. Lett.*, 1994, **35**, 8727 – 8730
- <sup>148</sup> a) Chakraborti A. K., Sharma L. and Nayak M. K., *J. Org. Chem.*, 2002, **67**, 2541 – 2547;  
b) Nayak M. K. and Chakraborti A. K., *Chem. Lett.*, 1998, **27**, 297 – 298
- <sup>149</sup> a) Auerbach J. and Weinreb S. M., *J. Chem. Soc., Chem. Commun.*, 1974, 298 – 299; b) Meyers A. I., Durandetta J. L. and Munavu R., *J. Org. Chem.*, 1975, **40**, 2025 – 2029
- <sup>150</sup> Stork G. and Takahashi T., *J. Am. Chem. Soc.*, 1977, **99**, 1275 – 1276
- <sup>151</sup> Porter T. D. and Coon M. J., *J. Biol. Chem.*, 1991, **266**, 13469 – 13472
- <sup>152</sup> Chefson A. and Auclair K., *Mol. Biosyst.*, 2006, **2**, 462 – 469
- <sup>153</sup> Bernhardt B., *J. Biotechnol.*, 2006, **124**, 128 – 145
- <sup>154</sup> Oliver C. F., Modi S., Sutcliffe M. J., Primrose W. U., Lian L-Y. and Roberts G. C. K., *Biochemistry*, 1997, **36**, 1567 – 1572
- <sup>155</sup> Entz O., Li Q-S., Schwaneberg U., Lutz-Wahl S., Fischer P and Schmid R. D., *J. Mol. Catal. B: Enzym.*, 2001, **15**, 123 – 133
- <sup>156</sup> Bell S. G., Sowden R. J. and Wong L-L., *Chem. Commun.*, 2001, 635 – 636
- <sup>157</sup> Bell S. G., Chen X., Sowden R. J., Xu F., Williams N. J., Wong L-L. and Rao Z., *J. Am. Chem. Soc.*, 2003, **125**, 705 – 714
- <sup>158</sup> <http://drnelson.utmem.edu/CytochromeP450.html>, accessed on 18 Aug 2008
- <sup>159</sup> Samuel K., Yin W., Stearns R. A., Tang Y. S., Chaudhary A. G., Jewell J. P., Lanza Jr T., Lin L. S., Hagmann W. K., Evans D. C. and Kumar S., *J. Mass Spectrom.*, 2003, **38**, 211 – 221
- <sup>160</sup> Okamoto M., *J. Phys. Chem A.*, 2000, **104**, 7518 – 7524
- <sup>161</sup> Crampton M. R., Pearce L. M. and Rabbitt L. C., *J. Chem. Soc., Perkin Trans 2*, 2002, 257 – 261
- <sup>162</sup> Parhi A. K., Kung M-P., Ploessl K. and Kung H. F., *Tet. Lett.*, 2008, **49**, 3395 – 3399
- <sup>163</sup> Sun Z-N., Liu F-Q., Chen Y., Tam P. K. H. and Yang D., *Org. Lett.*, 2008, **10**, 2171 – 2174
- <sup>164</sup> Gabe Y., Urano Y., Kikuchi K., Kojima H. and Nagano T., *J. Am. Chem. Soc.*, 2004, **126**, 3357 – 3367

- 
- <sup>165</sup> Matsumoto T., Urano Y., Shoda T., Kojima H. and Nagano T., *Org. Lett.*, 2007, **9**, 3375 – 3377
- <sup>166</sup> Baruah M., Qin W., Vallée R. A. L., Beijonne D., Rohand T., Dehaen W. and Boens N., *Org. Lett.*, 2005, **7**, 4377 – 4380
- <sup>167</sup> Ekmekcki Z., Yilmaz M. D. and Akkaya E. U., *Org. Lett.*, 2008, **10**, 461 – 464
- <sup>168</sup> Ziesel R., Goze C., Ulrich G., Césarío M., Retailleau P., Harriman A. and Rostron J. P., *Chem. Eur. J.*, 2005, **11**, 7366 – 7378
- <sup>169</sup> Zhang X., Xiao Y. and Qian X., *Org. Lett.*, 2008, **10**, 29 – 32
- <sup>170</sup> Galletta M., Campagna S., Quesada M., Ulrich G. and Ziesel R., *Chem. Commun.*, 2005, 4222 – 4223
- <sup>171</sup> Jones G., Kumar S., Klueva O. and Pacheco D., *J. Phys. Chem. A*, 2003, **107**, 8429 – 8434
- <sup>172</sup> Baruah M., Qin W., Basarić N., De Borggraeve W. M. and Boens N., *J. Org. Chem.*, 2005, **70**, 4152 – 4157
- <sup>173</sup> Kollmannsberger M., Rurack K., Resch-Genger U. and Daub J., *J. Phys. Chem. A*, 1998, **102**, 10211 – 10220
- <sup>174</sup> Littler B. J., Miller M. A., Hung C-H., Wagner R. W., O'Shea D. F., Boyle P. D. and Lindsey J. S., *J. Org. Chem.*, 1999, **64**, 1391 – 1396
- <sup>175</sup> Chen J., Burghart A., Derecskei-Kovacs A. and Burgess K., *J. Org. Chem.*, 2000, **65**, 2900 – 2906
- <sup>176</sup> Ulrich G., Ziesel R. and Harriman A., *Angew. Chem. Int. Ed.*, 2008, **47**, 1184 – 1201
- <sup>177</sup> de Silva A. P., Gunarante H. Q. N., Gunnlaugsson T., Huxley A. J. M., McCoy C. P., Rademacher J. T. and Rice T. E., *Chem Rev.*, 1997, **97**, 1500 – 1566
- <sup>178</sup> Tanaka K., Miura T., Umezawa N., Urano Y., Kikuchi K., Higuchi T. and Nagano T., *J. Am. Chem. Soc.*, 2001, **123**, 2530 – 2536
- <sup>179</sup> a) Kee H. K., Kirmaier C., Yu L., Thamyongkit P., Youngblood W. J., Calder M. E., Ramos L., Noll B. C., Bocian D. F., Scheidt W. R., Birge R. R., Lindsey J. S. and Holten D., *J. Phys. Chem. B.*, 2005, **109**, 20433 – 20443; b) Ziesel R., Bonardi L., Retailleau P. and Ulrich G., *J. Org. Chem.*, 2006, **71**, 3093 – 3102
- <sup>180</sup> Ueno T., Urano Y., Setsukinai K., Takakusa H., Kojima H., Kikuchi K., Ohkubo K., Fukuzumi S. and Nagano T., *J. Am. Chem. Soc.*, 2004, **126**, 14079 – 14085
- <sup>181</sup> Gaussian 03, Revision C.02, Frisch M. J., Trucks G. W., Schlegel H. B., Scuseria G. E., Robb M. A., Cheeseman J. R., Montgomery Jr. J. A., Vreven T., Kudin K. N., Burant J. C., Millam J. M., Iyengar S. S., Tomasi J., Barone V., Mennucci B., Cossi M., Scalmani G., Rega N., Petersson G. A., Nakatsuji H., Hada M., Ehara M., Toyota K., Fukuda R., Hasegawa J., Ishida M., Nakajima T., Honda Y., Kitao O., Nakai H., Klene M., Li X.,

- 
- Knox J. E., Hratchian H. P., Cross J. B., Adamo C., Jaramillo J., Gomperts R., Stratmann R. E., Yazyev O., Austin A. J., Cammi R., Pomelli C., Ochterski J. W., Ayala P. Y., Morokuma K., Voth G. A., Salvador P., Dannenberg J. J., Zakrzewski V. G., Dapprich S., Daniels A. D., Strain M. C., Farkas O., Malick D. K., Rabuck A. D., Raghavachari K., Foresman J. B., Ortiz J. V., Cui Q., Baboul A. G., Clifford S., Cioslowski J., Stefanov B. B., Liu G., Liashenko A., Piskorz P., Komaromi I., Martin R. L., Fox D. J., Keith T., Al-Laham M. A., Peng C. Y., Nanayakkara A., Challacombe M., Gill P. M. W., Johnson B., Chen W., Wong M. W., Gonzalez C. and Pople J. A., Gaussian, Inc., Wallingford CT, 2004.
- <sup>182</sup> Li L., Han J., Nguyen B and Burgess K., *J. Org. Chem.*, 2008, **73**, 1963 – 1970
- <sup>183</sup> Ortiz de Montellano P. R. and Mathews J. M., *Biochem. J.*, 1981, **195**, 761 – 764
- <sup>184</sup> Woodcroft K. J., Webb C. D., Yao M., Weedon A. C. and Bend J. R., *Chem. Res. Toxicol.*, 1997, **10**, 589 – 599
- <sup>185</sup> Colby H. D., Abbott B., Cachovic M., Debolt K. M. and Mico B. A., *Biochem. Pharmacol.*, 1995, **49**, 1057 – 1062
- <sup>186</sup> Takeyama K., Mori N, and Osakabe M., *Appl. Entomol. Zool.*, 2006, **41**, 487 – 491
- <sup>187</sup> Song W. C. and Brash A. R., *Science*, 1991, **252**, 781 – 782
- <sup>188</sup> Chapple C., *Annu. Rev. Plant Physiol. Plant Mol. Biol.*, 1998, **49**, 311 – 343
- <sup>189</sup> Oh K. and Murofushi N., *Bioorg. Med. Chem.*, 2002, **10**, 3707 - 3713
- <sup>190</sup> Li M., Wang H., Zhang X. and Zhang H., *Spectrochimica Acta.*, 2004, **60**, 987 – 993
- <sup>191</sup> Miškinienė V., Šarlauskas J., Jacquot J-P. and Čėnas N., *Biochim. Biophys. Acta*, 1998, **1366**, 275 – 283
- <sup>192</sup> Misecičienė L., Anusevičius Ž., Šarlauskas J. and Čėnas N., *Acta Biochim. Pol.*, 2006, **53**, 569 – 576
- <sup>193</sup> Arnér E. S. J., Björnstedt M. and Holmgren A., *J. Biol. Chem.*, 1995, **270**, 3479 – 3482
- <sup>194</sup> Nakajima Y., Yoshida S. and Ono T., *Plant Cell Physiol.*, 1996, **37**, 673 – 680
- <sup>195</sup> Zhao W. and Carriera E. M., *Chem. Eur. J.*, 2006, **12**, 7254 – 7263
- <sup>196</sup> Schrader M. and Fahimi H. D., *Histochem. Cell Biol.*, 2004, **122**, 383 – 393
- <sup>197</sup> Wiemer E. A., Wenzel T., Deerinck, T. J., Ellisman M. H. and Subramani S., *J. Cell Biol.*, 1997, **136**, 71 – 80
- <sup>198</sup> Olsen L. J., *Plant Mol. Biol.*, 1998, **38**, 163
- <sup>199</sup> Lopez-Huertas E., Charlton W. L., Johnston B., Graham L. A. and Baker A., *EMBO J.*, 2000, **19**, 6770 – 6777
- <sup>200</sup> Titorenko V. I. and Rachubinski R. A., *Nat. Rev. Mol. Cell Biol.*, 2001, **2**, 357 – 368



- 
- <sup>201</sup> Hsu M. H., Savas U., Griffin K. J. and Johnson E.F., *J. Biol. Chem.*, 2001, **276**, 27950 – 27958
- <sup>202</sup> Blaauboer B. J., van Holsteijn C. W., Bleumink R., Mennes W. C., van Pelt F. N., Yap S. H., van Pelt J. F., van Iersel A. A., Timmerman A. and Schmid B. P., *Biochem. Pharmacol.*, 1990, **40**, 521 – 528
- <sup>203</sup> Fahimi H. D. and Baumgart E., *J. Histochem. Cytochem.*, 1999, **47**, 1219 – 1232
- <sup>204</sup> Colton H. M., Falls J. G., Ni H., Kwanyuen P., Creech D., McNeil E., Casey W. M., Hamilton G. and Cariello N. F., *Toxicol. Sci.*, 2004, **80**, 183 – 192
- <sup>205</sup> Gould S. J., Keller G-A., Hosken N., Wilkinson J. and Subramani S., *J. Cell. Biol.*, 1989, **108**, 1657 – 1664
- <sup>206</sup> Nelson B. K., Cai X. and Nebenführ A., *Plant J.*, 2007, **51**, 1126 – 1136
- <sup>207</sup> Dansen T. B., Pap E. H. W., Wanders R. J. A. and Wirtz K. W. A., *Histochem. J.*, 2001, **33**, 65 – 69
- <sup>208</sup> Pap E. H. W., Dansen T. B. and Wirtz K. W. A., *Trends Cell Biol.*, 2001, **11**, 10 – 13
- <sup>209</sup> Pap E. H. W., Dansen T. B., van Summeren R. and Wirtz K. W. A., *Exp. Cell Res.*, 2001, **265**, 288 – 293
- <sup>210</sup> Banbury D. N., Oakley J. D., Sessions R. B. and Banting G., *J. Biol. Chem.*, 2003, **278**, 12022 – 12028
- <sup>211</sup> Aniento F. and Robinson D. G., *Protoplasma*, 2005, **226**, 3 – 11
- <sup>212</sup> Klausner R. D., Donaldson J. G. and Lippincott-Schwartz J., *J. Cell. Biol.*, 1992, **116**, 1071 – 1080
- <sup>213</sup> Oda K., Hirose S., Takami N., Misumi A., Takatsuki A. and Ikehara Y., *FEBS Lett.*, 1987, **214**, 135 – 138
- <sup>214</sup> Lippincott-Schwartz J., Yuan L. C., Bonifacino J. S. and Klausner R. D., *Cell*, 1989, **56**, 801 – 813
- <sup>215</sup> Wymann M. P., Bulgarelli-Leva G., Zvelebil M. J., Pirola L., Vanhaesebroeck B., Waterfield M. D. and Panayotou G., *Mol. Cell. Biol.*, 1996, **16**, 1722 – 1733
- <sup>216</sup> Emans N., Zimmermann S. and Fischer R., *Plant Cell*, 2002, **14**, 71 – 86
- <sup>217</sup> Oikawa K., Kasahara M., Kiyosuo T., Kagawa T., Suetsugu N., Takahashi F., Kanegae T., Niwa Y., Kadota A. and Wada M., *Plant Cell*, 2003, **15**, 2805 – 2815
- <sup>218</sup> Lundgren B., Meijer J. and DePierre J. W., *Biochem. Pharmacol.*, 1987, **36**, 815 – 821
- <sup>219</sup> Vainio H., Nickels J. and Linnainmaa K., *Scand. J. Work Environ. Health*, 1999, **8**, 70 – 3
- <sup>220</sup> Boitier E., Gautier J-C. and Roberts R., *Comp. Hepatol.*, 2003, **2**, 3 – 18
- <sup>221</sup> Vamecq J. and Latruffe N., *Lancet*, 1999, **354**, 141 – 148

- 
- 222 Willson T. M., Brown P. J., Sternbach D. D., and Henke B. R., *J. Med. Chem.*, 2000, **43**, 527 – 550
- 223 Nila A. G., Sandalio L. M., López M. G., Gómez M., del Rio L., A. and Gómez-lim M. A., *Planta*, 2006, **224**, 569 – 581
- 224 Palma J. M., Garrido M., Rodriguez-Garcia M. I. and del Rio L. A., *Arch. Biochem. Biophys.*, 1991, **287**, 68 – 74
- 225 Halliwell B. and Whiteman M., *Br. J. Pharmacol.*, 2004, **142**, 231 – 255
- 226 Khan N., Wilmot C. M., Rosen G. M., Demidenko E., Sun J., Joseph J., O'Hara J., Kalyanaraman B. and Swartz H. M., *Free Radic. Biol. Med.*, 2003, **34**, 1473 – 1481
- 227 Dizdaroglu M., Jaruga P., Birincioglu M. and Rodriguez H., *Free Radic. Biol. Med.*, 2002, **32**, 1102 – 1115
- 228 Levine R. L., Berlett B. S., Moskovitz J., Mosoni L. and Stadtman E. R., *Mech. Ageing Dev.*, 1999, **107**, 323 – 332
- 229 Hempel S. L., Buettner G. R., O'Malley Y. Q., Wessels D. A. and Flaherty D. M., *Free Radic. Biol. Med.*, 1999, **27**, 146 – 159
- 230 Heyne B., Ahmed S. and Scaiano J. C., *Org. Biomol. Chem.*, 2008, **6**, 354 – 358
- 231 Shreck R., Albermann K. and Bauerle P. A., *Free Radical Res. Commun.*, 1992, **17**, 221 – 237
- 232 Rao G. N., Lessegue B., Griendling K. K. and Alexander R. W., *Oncogene*, 1993, **8**, 2759 – 2764
- 233 Halliwell B. and Arouma O. I., *FEBS Lett.*, 1991, **281**, 9 – 19
- 234 Headlam H. A. and Davies M. J., *Free Radical Biol. Med.*, 2003, **34**, 44 – 55
- 235 Noguchi N., Takahashi M., Tsuchiya J., Yamashita H., Komouro E. and Niki E., *Biochem. Pharmacol.*, 1998, **55**, 785 – 791
- 236 Tatla S., Woodhead V., Foreman J. C. and Chain B. M., *Free Radical Biol. Med.*, 1999, **26**, 14 – 24
- 237 Az-ma T., Saeki N. and Yuge O., *Br. J. Pharmacol.*, 1999, **126**, 1462 – 1470
- 238 Wiseman H. and Halliwell B., *Biochem. J.*, 1996, **313**, 17 – 29
- 239 King P. A., Anderson V. E., Edwards J. O., Gustafson G., Plumb R. C. and Suggs J. W., *J. Am. Chem. Soc.*, 1992, **114**, 5430 – 5432
- 240 Deby C. and Goutier R., *Biochem. Pharmacol.*, 1990, **312**, 159 – 164
- 241 Goze C., Ulrich G., Mallon L. J., Allen B. D., Harriman A. and Ziessel R., *J. Am. Chem. Soc.*, 2006, **128**, 10231 – 10239
- 242 Loudet A. and Burgess K., *Chem. Rev.*, 2007, **107**, 4891 – 4932

- 
- <sup>243</sup> Kietaro U., Nakamura Y., Makino H., Citterio D. and Suzuki K., *J. Am. Chem. Soc.*, 2008, **130**, 1550 – 1551
- <sup>244</sup> Umezawa K., Matsui A., Nakamura Y., Citterio D. and Suzuki K., *Chem. Eur. J.*, 2009, **15**, 1096 – 1106
- <sup>245</sup> Kee H. L., Kirmaier C., Yu L., Thamyongkiy P., Youngblood W. J., Calder M. E., Ramos L., Noll B. C., Bocian D. F., Scheidt W. R., Birge R. R., Lindsey J. S. and Holten D., *J. Phys. Chem. B*, 2005, **109**, 20433 – 20443
- <sup>246</sup> Maeda H., Hasegawa M., Hashimoto T., Kakimoto T., Nishio S. and Nakanishi T., *J. Am. Chem. Soc.*, 2006, **128**, 10024 – 10025
- <sup>247</sup> Yu L., Muthukumaran K., Sazanovich I. V., Kirmaier C., Hindin E., Diers J. R., Boyle P. D., Bocian D. F., Holten D. and Lindsey J. S., *Inorg. Chem.*, 2003, **42**, 6629 – 6647
- <sup>248</sup> Brückner C., Zhang Y., Rettig S. J. and Dolphin D., *Inorg. Chim. Acta*, 1997, **263**, 279 – 286
- <sup>249</sup> Sigma Aldrich Catalogue #M0083
- <sup>250</sup> Brewster K., Chittenden R. A., Harrison J. M., Inch T. D. and Brown C., *J. Chem. Soc. Perkin I.*, 1976, 1291 – 6